

AD-A048 659

IIT RESEARCH INST CHICAGO ILL
BIAxIAL TESTING OF GRAPHITE/EPOXY COMPOSITES CONTAINING STRESS --ETC(U)
JUN 77 I M DANIEL

F/G 11/4

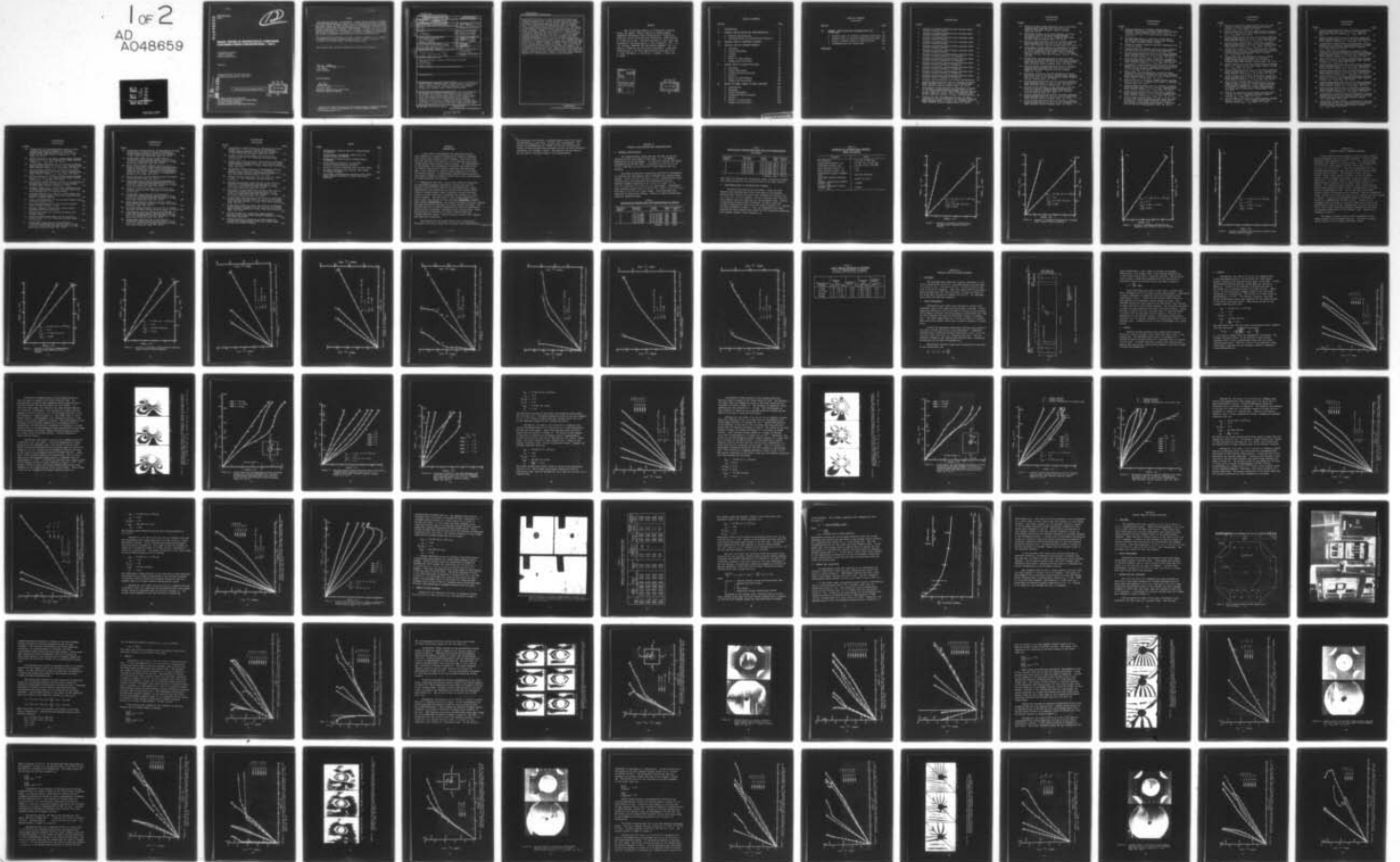
F33615-76-C-5162

UNCLASSIFIED

AFML-TR-76-244-PT-2

NL

1 of 2
AD
AO48659



AD A 0 48659

AFML-TR-76-244
Part II

BS

**BIAXIAL TESTING OF GRAPHITE/EPOXY COMPOSITES
CONTAINING STRESS CONCENTRATIONS — Part II**

*IIT RESEARCH INSTITUTE
10 WEST 35th STREET
CHICAGO, ILLINOIS 60616*

JUNE 1977

TECHNICAL REPORT AFML-TR-76-244, PART II
Final Report for Period April 1976 — March 1977

AD NO. —
DDC FILE COPY

Approved for public release; distribution unlimited.

DDC
RECEIVED
JAN 17 1978
D

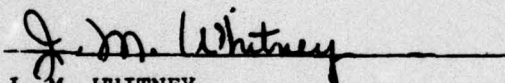
AIR FORCE MATERIALS LABORATORY
AIR FORCE WRIGHT AERONAUTICAL LABORATORIES
AIR FORCE SYSTEMS COMMAND
WRIGHT-PATTERSON AIR FORCE BASE, OHIO 45433

NOTICE

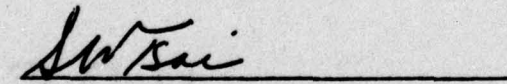
When Government drawings, specifications, or other data are used for any purpose other than in connection with a definitely related Government procurement operation, the United States Government thereby incurs no responsibility nor any obligation whatsoever; and the fact that the government may have formulated, furnished, or in any way supplied the said drawings, specifications, or other data, is not to be regarded by implication or otherwise as in any manner licensing the holder or any other person or corporation, or conveying any rights or permission to manufacture, use, or sell any patented invention that may in any way be related thereto.

This report has been reviewed by the Information Office (ASD/OIP) and is releasable to the National Technical Information Service (NTIS). At NTIS, it will be releasable to the general public, including foreign nations.

This technical report has been reviewed and is approved for publication.


J. M. WHITNEY
Project Engineer

FOR THE DIRECTOR


S. W. TSAI, Chief
Mechanics & Surface Interactions Branch
Nonmetallic Materials Division

Copies of this report should not be returned unless return is required by security considerations, contractual obligations, or notice on a specific document.

A041490

UNCLASSIFIED

SECURITY CLASSIFICATION OF THIS PAGE (When Data Entered)

18. (19) REPORT DOCUMENTATION PAGE		READ INSTRUCTIONS BEFORE COMPLETING FORM	
1. REPORT NUMBER	2. GOVT ACCESSION NO.	3. RECIPIENT'S CATALOG NUMBER	
AFML-TR-76-244 - Final P7-2			
4. TITLE (and Subtitle)		5. TYPE OF REPORT & PERIOD COVERED	
BIAXIAL TESTING OF GRAPHITE/EPOXY COMPOSITES CONTAINING STRESS CONCENTRATIONS Part II		Final Report April, 1976-March, 1977	
6. PERFORMING ORG. REPORT NUMBER		7. AUTHOR(s)	
		I.M./Daniel	
8. CONTRACT OR GRANT NUMBER(s)		9. PROGRAM ELEMENT, PROJECT, TASK AREA & WORK UNIT NUMBERS	
F33615-76-C-5162		7340398 (17) 03	
10. PERFORMING ORGANIZATION NAME AND ADDRESS		11. CONTROLLING OFFICE NAME AND ADDRESS	
IIT Research Institute 10 W. 35th Street Chicago, Illinois		Air Force Materials Laboratory (AFML/MBM) Air Force Wright Aeronautical Laboratories Wright-Patterson AFB, Ohio 45433	
12. REPORT DATE		13. NUMBER OF PAGES	
June 1977		166	
14. MONITORING AGENCY NAME & ADDRESS (if different from Controlling Office)		15. SECURITY CLASS. (of this report)	
Final rept. 1 Apr 76 - 31 Mar 77		Unclassified	
16. DISTRIBUTION STATEMENT (of this Report)		15a. DECLASSIFICATION/DOWNGRADING SCHEDULE	
Approved for public release, distribution unlimited (12) 172p.			
17. DISTRIBUTION STATEMENT (of the abstract entered in Block 20, if different from Report)			
18. SUPPLEMENTARY NOTES			
19. KEY WORDS (Continue on reverse side if necessary and identify by block number) Graphite/epoxy composites, holes, cracks, stress concentrations, biaxial testing, failure modes, failure criteria, notch size effect, crack extension, strength reduction, strain gages, photoelastic coatings, moiré, strain distributions.			
20. ABSTRACT (Continue on reverse side if necessary and identify by block number) An experimental program was conducted to study the deformation and failure under uniaxial and biaxial tensile loading of [0/+45/90] _s and [02/+45] _s graphite/epoxy plates with circular holes and through-the-thickness cracks and to determine the influence of notch size. Experimental stress analysis techniques used were strain gages, photoelastic coatings and moiré grids. In the case of uniaxially loaded [02/+45] _s plates with holes appreciable stress and strain redistribution takes			

62102F

DD FORM 1 JAN 73 1473

EDITION OF 1 NOV 65 IS OBSOLETE

UNCLASSIFIED

SECURITY CLASSIFICATION OF THIS PAGE (When Data Entered)

175350

LB

UNCLASSIFIED

SECURITY CLASSIFICATION OF THIS PAGE(When Data Entered)

place around the hole as a result of nonlinear response and compressive failure near the hole boundary around the 0-deg. location (loading axis). In the case of larger holes failure initiates at points approximately 72-deg. from the loading axis. For smaller holes the predominant mode is separation of the outer 0-degree plies near the vertical axis. The effect of hole diameter was satisfactorily described using the average stress criterion. There is a critical hole diameter below which the laminate becomes notch insensitive. Biaxial testing of $[0_2/+45]_s$ laminates with holes under 2:1 tensile biaxiality revealed two basic patterns of failure: a) nearly horizontal cracking initiating at points off the horizontal axis with extensive delamination and b) vertical cracking accompanied by delamination of the outer 0-degree plies. The strength reduction ratios for 2:1 biaxial loading are approximately 16 percent lower than those for uniaxial loading, although in the latter case the stress concentration is appreciably higher. This is attributed to interaction of failure modes around the hole boundary. In $[0/+45/90]_s$ laminates with cracks under biaxial stress fields it was found that the normal stress component in the crack direction tends to decrease the crack opening displacement appreciably but decreases the strength only slightly. The shear stress component, however, has a more pronounced contribution on failure.

UNCLASSIFIED

SECURITY CLASSIFICATION OF THIS PAGE(When Data Entered)

PREFACE

This is the Final Report on IIT Research Institute Project No. D6119, "Biaxial Testing of Graphite/Epoxy Composites Containing Stress Concentrations," prepared by IITRI for the Air Force Materials Laboratory, under Contract No. F33615-76-C-5162. The work described in this report was conducted in the period April 1, 1976 to March 31, 1977. Dr. J.M. Whitney, AFML/MBM, was the project engineer. Dr. I.M. Daniel of IITRI was the principal investigator. Additional contributions to the work reported herein were made by Dr. T. Liber and Messrs. W. Hartrick, R. LaBedz, T. Niuro and B. Nowak.

ACCESSION for	
NTIS	White Section <input checked="" type="checkbox"/>
DDC	Buff Section <input type="checkbox"/>
UNANNOUNCED	<input type="checkbox"/>
JUSTIFICATION.....	
BY.....	
DISTRIBUTION/AVAILABILITY CODES	
Dist.	AVAIL. and/or SPECIAL
A	

DDC
RECEIVED
JAN 17 1978
D

TABLE OF CONTENTS

SECTION	PAGE
I INTRODUCTION	1
II MATERIAL QUALIFICATION AND CHARACTERIZATION	3
1. Material Qualification	3
2. Characterization of Unidirectional Material	4
III UNIAXIAL TESTS OF UNNOTCHED LAMINATE	10
IV UNIAXIAL TESTS OF NOTCHED LAMINATE	20
1. Specimens	20
2. Strain Measurement	20
3. Loading	22
4. Results	23
5. Effect of Hole Diameter	43
6. Summary and Conclusions	47
V BIAXIAL TESTS OF PLATES WITH HOLES	50
1. Specimens	50
2. Strain Measurement	50
3. Loading and Data Recording	50
4. Results	54
5. Effect of Hole Diameter	98
6. Summary and Conclusions	106
VI EFFECT OF NORMAL STRESS IN CRACK DIRECTION	108
1. Introduction	108
2. Specimens	111
3. Strain Measurement	112
4. Loading and Data Recording	112
5. Results	112
6. Effect of Crack Length	145
7. Summary and Conclusions	148

TABLE OF CONTENTS
(Continued)

SECTION		PAGE
VII	SUMMARY, CONCLUSIONS AND RECOMMENDATIONS FOR FUTURE WORK	150
	1. Uniaxial Tests of $[0_2/+45]_s$ Laminates With Holes	150
	2. Biaxial Tests of $[0_2/+45]_s$ Laminates With Holes	151
	3. Effect of Normal Stress in Crack Direction	153
	4. Recommendations for Future Work	154
	REFERENCES	156

ILLUSTRATIONS

FIGURE		PAGE
1	Strains in 0-Degree Unidirectional Specimen Under Uniaxial Tensile Loading	6
2	Strains in 0-Degree Unidirectional Specimen Under Uniaxial Tensile Loading	7
3	Strains in 90-Degree Unidirectional Specimen Under Uniaxial Tensile Loading	8
4	Strains in 90-Degree Unidirectional Specimen Under Uniaxial Tensile Loading	9
5	Strains in $[0_2/+45]_s$ Graphite/Epoxy Specimen Under Uniaxial Tensile Loading	11
6	Strains in $[0_2/+45]_s$ Graphite/Epoxy Specimen Under Uniaxial Tensile Loading	12
7	Strains in $[0_2/+45]_s$ Graphite/Epoxy Specimen Under Uniaxial Tensile Loading at 22.5-Degrees	13
8	Strains in $[0_2/+45]_s$ Graphite/Epoxy Specimen Under Uniaxial Tensile Loading at 22.5-Degrees	14
9	Strains in $[0_2/+45]_s$ Graphite/Epoxy Specimen Under Uniaxial Tensile Loading at 45-Degrees	15
10	Strains in $[0_2/+45]_s$ Graphite/Epoxy Specimen Under Uniaxial Tensile Loading at 45-Degrees	16
11	Strains in $[0_2/+45]_s$ Graphite/Epoxy Specimen Under Uniaxial Tensile Loading at 90-Degrees	17
12	Strains in $[0_2/+45]_s$ Graphite/Epoxy Specimen Under Uniaxial Tensile Loading at 90-Degrees	18
13	Uniaxial Tensile Specimen with Stress Concentration	21
14	Strains Along Horizontal Axis of $[0_2/+45]_s$ Graphite/Epoxy Specimen With 2.54 cm (1 in.) Circular Hole Under Uniaxial Tensile Loading (Spec. No. 4A-1)	24
15	Isochromatic Fringe Patterns in Photoelastic Coating of $[0_2/+45]_s$ Graphite/Epoxy Specimen With 2.54 cm (1 in.) Diameter Circular Hole Under Uniaxial Tensile Loading (Spec. No. 4A-1) a) $\sigma_{xx} = 276$ MPa (40 ksi), b) $\sigma_{xx} = 345$ MPa (50 ksi), c) $\sigma_{xx} = 414$ MPa (60 ksi)	26
16	Fringe Order and Circumferential Strain at Three Locations on the Hole Boundary for $[0_2/+45]_s$ Graphite/Epoxy Specimen With 2.54 cm (1 in.) Circular Hole Under Uniaxial Tensile Loading (Spec. No. 4A-1)	27

ILLUSTRATIONS

(Continued)

FIGURE		PAGE
17	Vertical Strains Along Horizontal Axis of $[0_2/+45]_s$ Graphite/Epoxy Specimen With 2.54 cm (1 in.) Diameter Hole Under Uniaxial Tensile Loading (Spec. No. 4A-2)	28
18	Horizontal Strains on the Hole Boundary and Along Horizontal Axis of $[0_2/+45]_s$ Graphite/Epoxy Specimen With 2.54 cm (1 in.) Diameter Hole Under Uniaxial Tensile Loading (Spec. No. 4A-2)	29
19	Strains Along Horizontal Axis of $[0_2/+45]_s$ Graphite/Epoxy Specimen With 1.91 cm (0.75 in.) Circular Hole Under Uniaxial Tensile Loading (Spec. No. 4A-3)	31
20	Isochromatic Fringe Patterns in Photoelastic Coating of $[0_2/+45]_s$ Graphite/Epoxy Specimen With 1.91 cm (0.75 in.) Diameter Circular Hole Under Uniaxial Tensile Loading (Spec. No. 4A-3) a) $\sigma_{xx} = 207$ MPa (30 ksi), b) $\sigma_{xx} = 276$ MPa (40 ksi), c) $\sigma_{xx} = 345$ MPa (50 ksi)	33
21	Fringe Order and Circumferential Strain at Three Locations on the Hole Boundary for $[0_2/+45]_s$ Graphite/Epoxy Specimen With 1.91 cm (0.75 in.) Circular Hole Under Uniaxial Tensile Loading (Spec. No. 4A-3)	34
22	Vertical Strains Along Horizontal Axis of $[0_2/+45]_s$ Graphite/Epoxy Specimen With 1.91 cm (0.75 in.) Diameter Hole Under Uniaxial Tensile Loading (Spec. No. 4A-4)	35
23	Horizontal Strains on the Hole Boundary and Along Horizontal Axis of $[0_2/+45]_s$ Graphite/Epoxy Specimen With 1.91 cm (0.75 in.) Diameter Hole Under Uniaxial Tensile Loading (Spec. No. 4A-4)	36
24	Strains Along Horizontal Axis of $[0_2/+45]_s$ Graphite/Epoxy Specimen With 1.27 cm (0.5 in.) Circular Hole Under Uniaxial Tensile Loading (Spec. No. 4A-5)	38
25	Strains on the Boundary of the Hole and in the Far Field of $[0_2/+45]_s$ Graphite/Epoxy Specimen With 1.27 cm (0.50 in.) Diameter Hole Under Uniaxial Tensile Loading (Spec. No. 4A-6)	39
26	Strains Along Horizontal Axis of $[0_2/+45]_s$ Graphite/Epoxy Specimen With 0.64 cm (0.25 in.) Circular Hole Under Uniaxial Tensile Loading (Spec. No. 4A-7)	41
27	Strains Along Horizontal Axis of $[0_2/+45]_s$ Graphite/Epoxy Specimen With 0.64 cm (0.25 in.) Diameter Hole Under Uniaxial Tensile Loading (Spec. No. 4A-8)	42

ILLUSTRATIONS

(Continued)

FIGURE		PAGE
28	Failure Patterns in $[0_2/+45]_s$ Graphite/Epoxy Specimens With Holes of Various Sizes Under Uniaxial Tension. (Hole Diameters are 2.54 cm (1 in.), 1.91 cm (0.75 in.), 1.27 cm (0.50 in.) and 0.64 cm (0.25 in.))	44
29	Strength Reduction as a Function of Hole Radius for $[0_2/+45]_s$ Graphite/Epoxy Plates With Circular Holes Under Uniaxial Tensile Loading	48
30	Sketch of Biaxial Composite Specimen (Dimensions are in mm and inches)	51
31	Loading Frame for Biaxial Testing of Flat Laminates and Associated Strain Recording Instrumentation	52
32	Strains Along Horizontal Axis of $[0_2/+45]_s$ Graphite/Epoxy Specimen With 2.54 cm (1.00 in.) Diameter Hole Under Biaxial Loading $\sigma_{yy} = 2\sigma_{xx}$ (Spec. No. 6A-1)	55
33	Strains Along Vertical Axis of $[0_2/+45]_s$ Graphite/Epoxy Specimen With 2.54 cm (1.00 in.) Diameter Hole Under Biaxial Loading $\sigma_{yy} = 2\sigma_{xx}$ (Spec. No. 6A-1)	56
34	Isochromatic Fringe Patterns in Photoelastic Coating Around 2.54 cm (1.00 in.) Diameter Hole in $[0_2/+45]_s$ Graphite/Epoxy Specimen Under Biaxial Loading $\sigma_{yy} = 2\sigma_{xx}$ (Spec. No. 6A-1)	58
35	Fringe Order and Circumferential Strain at Three Locations on the Hole Boundary of $[0_2/+45]_s$ Graphite/Epoxy Specimen With 2.54 cm (1.00 in.) Diameter Hole Under Biaxial Loading (Spec. No. 6A-1)	59
36	Failure Pattern in $[0_2/+45]_s$ Graphite/Epoxy Specimen With 2.54 cm (1 in.) Diameter Hole Under 2:1 Biaxial Loading (Spec. No. 6A-1)	60
37	Strains Along Horizontal Axis of $[0_2/+45]_s$ Graphite/Epoxy Specimen With 2.54 cm (1.00 in.) Diameter Hole Under Biaxial Loading $\sigma_{yy} = 2\sigma_{xx}$ (Spec. No. 6A-2)	61
38	Strains Along Vertical Axis of $[0_2/+45]_s$ Graphite/Epoxy Specimen With 2.54 cm (1.00 in.) Diameter Hole Under Biaxial Loading $\sigma_{yy} = 2\sigma_{xx}$ (Spec. No. 6A-2)	62
39	Moiré Fringe Patterns Around 2.54 cm (1.00 in.) Hole in $[0_2/+45]_s$ Graphite/Epoxy Specimen Under Biaxial Loading $\sigma_{yy} = 2\sigma_{xx}$ (Right-Hand Part of Pattern Corresponds to Horizontal Displacements, Left-Hand Part to Vertical Displacements; Spec. No. 6A-2)	64

ILLUSTRATIONS

(Continued)

FIGURE		PAGE
40	Strains in $[0_2/+45]_s$ Graphite/Epoxy Specimen With 2.54 cm (1.00 in.) Diameter Hole Under Biaxial Loading $\sigma_{yy} = 2\sigma_{xx}$ (Spec. No. 6A-2)	65
41	Failure Pattern of $[0_2/+45]_s$ Graphite/Epoxy Specimen With 2.54 cm (1.00 in.) Hole Under Biaxial Loading $\sigma_{yy} = 2\sigma_{xx}$ (Spec. No. 6A-2)	66
42	Strains Along Horizontal Axis of $[0_2/+45]_s$ Graphite/Epoxy Specimen With 1.91 cm (0.75 in.) Diameter Hole Under Biaxial Loading $\sigma_{yy} = 2\sigma_{xx}$ (Spec. No. 6A-3)	68
43	Strains Along Vertical Axis of $[0_2/+45]_s$ Graphite/Epoxy Specimen With 1.91 cm (0.75 in.) Diameter Hole Under Biaxial Loading $\sigma_{yy} = 2\sigma_{xx}$ (Spec. No. 6A-3)	69
44	Isochromatic Fringe Patterns in Photoelastic Coating Around 1.91 cm (0.75 in.) Diameter Hole in $[0_2/+45]_s$ Graphite/Epoxy Specimen Under Biaxial Loading $\sigma_{yy} = 2\sigma_{xx}$ (Spec. No. 6A-3)	70
45	Fringe Order and Circumferential Strain at Three Locations on the Hole Boundary of $[0_2/+45]_s$ Graphite/Epoxy Specimen With 1.91 cm (0.75 in.) Diameter Hole Under Biaxial Loading (Spec. No. 6A-3)	71
46	Failure Pattern of $[0_2/+45]_s$ Graphite/Epoxy Specimen With a 1.91 cm (0.75 in.) Hole Under Biaxial Loading $\sigma_{yy} = 2\sigma_{xx}$ (Spec. No. 6A-3)	72
47	Strains Along Horizontal Axis of $[0_2/+45]_s$ Graphite/Epoxy Specimen With 1.91 cm (0.75 in.) Diameter Hole Under Biaxial Loading $\sigma_{yy} = 2\sigma_{xx}$ (Spec. No. 6A-4)	74
48	Strains Along Vertical Axis of $[0_2/+45]_s$ Graphite/Epoxy Specimen With 1.91 cm (0.75 in.) Diameter Hole Under Biaxial Loading $\sigma_{yy} = 2\sigma_{xx}$ (Spec. No. 6A-4)	75
49	Moiré Fringe Patterns Around 1.91 cm (0.75 in.) Diameter Hole in $[0_2/+45]_s$ Graphite/Epoxy Specimen Under Biaxial Loading $\sigma_{yy} = 2\sigma_{xx}$ (Right-hand part of pattern corresponds to vertical displacements, left-hand part to horizontal displacements; Spec. No. 6A-4)	76
50	Strains in $[0_2/+45]_s$ Graphite/Epoxy Specimen With 1.91 cm (0.75 in.) Diameter Hole Under Biaxial Loading $\sigma_{yy} = 2\sigma_{xx}$ (Spec. No. 6A-4)	77
51	Failure Pattern of $[0_2/+45]_s$ Graphite/Epoxy Specimen With a 1.91 cm (0.75 in.) Diameter Hole Under Biaxial Loading $\sigma_{yy} = 2\sigma_{xx}$ (Spec. No. 6A-4)	78

ILLUSTRATIONS

(Continued)

FIGURE		PAGE
52	Strains Along Horizontal Axis of $[0_2/+45]_s$ Graphite/Epoxy Specimen With 1.27 cm (0.50 in.) Diameter Hole Under Biaxial Loading $\sigma_{yy} = 2\sigma_{xx}$ (Spec. No. 6A-5)	79
53	Strains Along Vertical Axis of $[0_2/+45]_s$ Graphite/Epoxy Specimen With 1.27 cm (0.50 in.) Diameter Hole Under Biaxial Loading $\sigma_{yy} = 2\sigma_{xx}$ (Spec. No. 6A-5)	80
54	Isochromatic Fringe Patterns in Photoelastic Coating Around 1.27 cm (0.50 in.) Diameter Hole in $[0_2/+45]_s$ Graphite/Epoxy Specimen Under Biaxial Loading $\sigma_{yy} = 2\sigma_{xx}$ (Spec. No. 6A-5)	82
55	Fringe Order and Circumferential Strain at Three Locations on the Hole Boundary of $[0_2/+45]_s$ Graphite/Epoxy Specimen With 1.27 cm (0.50 in.) Diameter Hole Under Biaxial Loading $\sigma_{yy} = 2\sigma_{xx}$ (Spec. No. 6A-5)	83
56	Failure Pattern of $[0_2/+45]_s$ Graphite/Epoxy Specimen With 1.27 cm (0.50 in.) Diameter Hole Under Biaxial Loading $\sigma_{yy} = 2\sigma_{xx}$ (Spec. No. 6A-5)	84
57	Strains Along Horizontal Axis of $[0_2/+45]_s$ Graphite/Epoxy Specimen With 1.27 cm (0.50 in.) Diameter Hole Under Biaxial Loading $\sigma_{yy} = 2\sigma_{xx}$ (Spec. No. 6A-6)	85
58	Strains Along Vertical Axis of $[0_2/+45]_s$ Graphite/Epoxy Specimen With 1.27 cm (0.50 in.) Diameter Hole Under Biaxial Loading $\sigma_{yy} = 2\sigma_{xx}$ (Spec. No. 6A-6)	86
59	Failure Pattern of $[0_2/+45]_s$ Graphite/Epoxy Specimen With 1.27 cm (0.50 in.) Diameter Hole Under Biaxial Loading $\sigma_{yy} = 2\sigma_{xx}$ (Spec. No. 6A-6)	88
60	Strains Along Horizontal Axis of $[0_2/+45]_s$ Graphite/Epoxy Specimen With 0.64 cm (0.25 in.) Diameter Hole Under Biaxial Loading $\sigma_{yy} = 2\sigma_{xx}$ (Spec. No. 6A-7)	89
61	Strains Along Vertical Axis of $[0_2/+45]_s$ Graphite/Epoxy Specimen With 0.64 cm (0.25 in.) Diameter Hole Under Biaxial Loading $\sigma_{yy} = 2\sigma_{xx}$ (Spec. No. 6A-7)	90
62	Isochromatic Fringe Patterns in Photoelastic Coating Around 0.64 cm (0.25 in.) Diameter Hole in $[0_2/+45]_s$ Graphite/Epoxy Specimen Under Biaxial Loading $\sigma_{yy} = 2\sigma_{xx}$ (Spec. No. 6A-7)	91
63	Isochromatic Fringe Patterns in Photoelastic Coating Around 0.64 cm (0.25 in.) Diameter Hole in $[0_2/+45]_s$ Graphite/Epoxy Specimen Under Biaxial Loading $\sigma_{yy} = 2\sigma_{xx}$ (Spec. No. 6A-7)	92

ILLUSTRATIONS

(Continued)

FIGURE		PAGE
64	Fringe Order and Circumferential Strain at Three Locations on the Hole Boundary of $[0_2/+45]_s$ Graphite/Epoxy Specimen With 0.64 cm (0.25 in.) Diameter Hole Under Biaxial Loading $\sigma_{yy} = 2\sigma_{xx}$ (Spec. No. 6A-7)	94
65	Failure Pattern of $[0_2/+45]_s$ Graphite/Epoxy Specimen With 0.64 cm (0.25 in.) Diameter Hole Under Biaxial Loading $\sigma_{yy} = 2\sigma_{xx}$ (Spec. No. 6A-7)	95
66	Strains Along Horizontal Axis of $[0_2/+45]_s$ Graphite/Epoxy Specimen With 0.64 cm (0.25 in.) Diameter Hole Under Biaxial Loading $\sigma_{yy} = 2\sigma_{xx}$ (Spec. No. 6A-8)	96
67	Strains Along Vertical Axis of $[0_2/+45]_s$ Graphite/Epoxy Specimen With 0.64 cm (0.25 in.) Diameter Hole Under Biaxial Loading $\sigma_{yy} = 2\sigma_{xx}$ (Spec. No. 6A-8)	97
68	Failure Pattern of $[0_2/+45]_s$ Graphite/Epoxy Specimen With 0.64 cm (0.25 in.) Diameter Hole Under Biaxial Loading $\sigma_{yy} = 2\sigma_{xx}$ (Spec. No. 6A-8)	99
69	Distribution Around Boundary of Hole of Circumferential Strength and Stress for $[0_2/+45]_s$ Graphite/Epoxy Specimen Under Biaxial Loading $\sigma_{yy} = 2\sigma_{xx}$	102
70	Strength Reduction as a Function of Hole Radius for $[0_2/+45]_s$ Graphite/Epoxy Plates With Circular Holes Under Uniaxial and 2:1 Biaxial Loading	103
71	Strength Reduction as a Function of Hole Radius for $[0_2/+45]_s$ Graphite/Epoxy Plates With Circular Holes Under 2:1 Biaxial Loading	105
72	Stress Transformations of the Far-Field Biaxial State of Stress Around a Crack	109
73	Stress Transformations of the Far-Field Uniaxial State of Stress Around a Crack	110
74	Uniaxial Loading of $[0/+45/90]_s$ Graphite/Epoxy Specimens With Inclined Cracks	113
75	Typical Gage Layout for Uniaxial Specimens With Inclined Cracks	114
76	Closeup of Gage Layout Near 2.54 cm (1.00 in.) Crack of Spec. No. 5A-1 (Smallest Division Shown in 0.01 in.)	116
77	Strains Near Crack Tip and in Far Field in $[0/+45/90]_s$ Graphite/Epoxy Specimen With 2.54 cm (1.00 in.) Crack Under Uniaxial Loading at 71-deg. With Crack Direction (Spec. No. 5A-1)	117

ILLUSTRATIONS

(Continued)

FIGURE		PAGE
78	Isochromatic Fringe Patterns in Photoelastic Coating Around 2.54 cm (1.00 in.) Crack in $[0/+45/90]_s$ Graphite/Epoxy Specimen Under Uniaxial Loading at 71-deg. With Crack Direction (Spec. No. 5A-1)	118
79	Strains Near Crack Tip and in Far Field in $[0/+45/90]_s$ Graphite/Epoxy Specimen With 2.54 cm (1.00 in.) Crack Under Uniaxial Loading at 71-deg. With Crack Direction (Spec. No. 5A-2)	120
80	Moiré Fringe Patterns Around 2.54 cm (1.00 in.) Crack in $[0/+45/90]_s$ Graphite/Epoxy Specimen Under Uniaxial Loading at 71-deg. With Crack Direction. (left part of pattern corresponds to displacements normal to the crack, right part to displacements parallel to it; Spec. No. 5A-2)	121
81	Far Field Strains Around Crack Obtained from Moiré Fringe Patterns (Spec. No. 5A-2)	122
82	Crack Opening and Crack Shearing Displacement in $[0/+45/90]_s$ Graphite/Epoxy Specimen With 2.54 cm (1.00 in.) Crack Under Uniaxial Loading at 71-deg. With Crack Direction (Spec. No. 5A-2)	123
83	Closeup of Gage Layout Near 1.91 cm (0.75 in.) Crack of Spec. No. 5A-3 (Smallest Division Shown is 0.01 in.)	125
84	Strains Near Crack Tip and in Far Field in $[0/+45/90]_s$ Graphite/Epoxy Specimen With 1.91 cm (0.75 in.) Crack Under Uniaxial Loading at 71-deg. With Crack Direction (Spec. No. 5A-3)	126
85	Moiré Fringe Patterns Around 1.91 cm (0.75 in.) Crack Under Uniaxial Loading at 71-deg. With Crack Direction (Spec. No. 5A-3)	127
86	Far Field Strains Around 1.91 cm (0.75 in.) Crack Obtained from Moiré Fringe Patterns (Spec. No. 5A-3)	128
87	Crack Opening and Crack Shearing Displacements in $[0/+45/90]_s$ Graphite/Epoxy Specimen With 1.91 cm (0.75 in.) Crack Under Uniaxial Loading at 71-deg. With Crack Direction (Spec. No. 5A-3)	129
88	Strains Near Crack Tip and in Far Field in $[0/+45/90]_s$ Graphite/Epoxy Specimen With 1.91 cm (0.75 in.) Crack Under Uniaxial Loading at 71-deg. With Crack Direction (Spec. No. 5A-4)	131

ILLUSTRATIONS

(Continued)

FIGURE		PAGE
89	Isochromatic Fringe Patterns in Photoelastic Coating Around 1.91 cm (0.75 in.) Crack in $[0/+45/90]_s$ Graphite/Epoxy Specimen Under Uniaxial Loading at 71-deg. With Crack Direction (Spec. No. 5A-4)	132
90	Closeup of Gage Layout Near 1.27 cm (0.50 in.) Crack of Spec. No. 5A-5 (Smallest Division Shown is 0.01 in.)	134
91	Strains Near Crack Tip and in Far Field in $[0/+45/90]_s$ Graphite/Epoxy Specimen With 1.27 cm (0.50 in.) Crack Under Uniaxial Loading at 71-deg. With Crack Direction (Spec. No. 5A-5)	135
92	Isochromatic Fringe Patterns in Photoelastic Coating Around 1.27 cm (0.50 in.) Crack in $[0/+45/90]_s$ Graphite/Epoxy Specimen Under Uniaxial Loading at 71-deg. With Crack Direction (Spec. No. 5A-5)	136
93	Closeup of Gage Layout Near 1.27 cm (0.50 in.) Crack of Spec. No. 5A-6 (Smallest Division Shown in 0.01 in.)	137
94	Vertical Strains Near Crack Tip and in Far Field in $[0/+45/90]_s$ Graphite/Epoxy Specimen With 1.27 cm (0.50 in.) Crack Under Uniaxial Loading at 71-deg. With Crack Direction (Spec. No. 5A-6)	138
95	Horizontal Strains Near Crack Tip and in Far Field in $[0/+45/90]_s$ Graphite/Epoxy Specimen With 1.27 cm (0.50 in.) Crack Under Uniaxial Loading at 71-deg. With Crack Direction (Spec. No. 5A-6)	139
96	Strains Near Crack Tip and in Far-Field in $[0/+45/90]_s$ Graphite/Epoxy Specimen With 0.64 cm (0.25 in.) Crack Under Uniaxial Loading at 71-deg. With Crack Direction (Spec. No. 5A-7)	141
97	Strains Near Crack Tip and in Far-Field in $[0/+45/90]_s$ Graphite/Epoxy Specimen With 0.64 cm (0.25 in.) Crack Under Uniaxial Loading at 71-deg. With Crack Direction (Spec. No. 5A-8)	143
98	Failure Patterns in $[0/+45/90]_s$ Graphite/Epoxy Specimens With Cracks Under Uniaxial Loading at 71-deg. With Crack Direction	144
99	Strength Ratios as a Function of Crack Length for $[0/+45/90]_s$ Graphite/Epoxy Plates With Cracks Under Uniaxial and Biaxial Loading	147

TABLES

TABLE		PAGE
1	Qualification Flexure Tests for Graphite/Epoxy SP-286T300	3
2	Qualification Interlaminar Shear Tests for Graphite/Epoxy SP-286T300	4
3	Properties of Unidirectional Graphite/Epoxy, SP-286T300	5
4	Static Tensile Properties of Unnotched [0 ₂ /+45] _s Graphite/Epoxy Laminates	19
5	Uniaxial [0 ₂ /+45] _s Laminates With Circular Holes	45
6	[0 ₂ /+45] _s Laminates With Circular Holes Under 2:1 Biaxial Loading	100
7	[0/+45/90] _s Graphite/Epoxy Laminates With Cracks Under Uniaxial Loading at 71-deg. With Crack Direction	146

SECTION I
INTRODUCTION

A great deal of experimental and analytical work has been conducted to evaluate the behavior of composite laminates with cutouts under uniaxial tensile loading. Very little work has been reported on the behavior of such laminates with stress concentrations under biaxial states of stress. The inhomogeneity of the material, the nonlinearity of response near failure and the complex interaction of failure modes near discontinuities make it very difficult to predict biaxial behavior on the basis of uniaxial response. An experimental approach dealing directly with biaxial loading of composite plates with stress concentrations was deemed important and necessary.

Recognizing this need, the Air Force Materials Laboratory has sponsored a two-phase experimental program with the IIT Research Institute. The objective of the program was to study experimentally the deformation and failure under biaxial tensile loading of graphite/epoxy plates containing circular holes and cracks of various sizes and to determine the influence of notch size on failure. The first phase of this program described in a recent report was limited to quasi-isotropic ~~10/145/90~~ graphite/epoxy laminates (Reference 1). The program consisted of testing uniaxial unnotched and notched specimens and biaxial notched specimens. The approach used was to measure deformations by means of experimental strain analysis techniques, determine strain concentrations, strain distributions and variations to failure, failure modes and strength reduction ratios. Whenever possible results were compared with analytical predictions.

The objective of the second phase of this investigation described in this final report was to further study experimentally

the deformation and failure of graphite/epoxy plates with stress concentrations. A new layup, $[0_2/+45]_s$ was investigated. The program included testing of uniaxial notched and unnotched and biaxial notched and unnotched specimens of both the quasi-isotropic $[0/+45/90]_s$ and $[0_2/+45]_s$ layups. The approach was the same as the one used in the first phase of this investigation.

SECTION II
MATERIAL QUALIFICATION AND CHARACTERIZATION

1. MATERIAL QUALIFICATION

The graphite/epoxy system used was the same as the one selected for the first phase of this work, i.e., SP-286T300 manufactured by the 3M Company. It consists of Thornel 300 fibers impregnated with PR-286 resin. A quantity of 50 lb of 30.5 cm (12 in.) wide and 0.13 mm (0.005 in.) thick prepreg tape was obtained.

The batch of material received was qualified by determining its flexural and interlaminar shear strengths from unidirectional coupons. A 15.2 cm x 15.2 cm (6 in. x 6 in.) unidirectional plate, 15-ply thick, was fabricated for qualification testing. Flexural strength coupons were 10.2 cm (4 in.) long, 1.3 cm (0.5 in.) wide with a 6.3 cm (2.5 in.) span length. Interlaminar shear strength coupons were 1.5 cm (0.6 in.) long, 0.6 cm (0.25 in.) wide with a 1 cm (0.4 in.) span length. These specimens were subjected to three-point bending. Results of these qualification tests are tabulated below.

Table 1
QUALIFICATION FLEXURE TESTS FOR GRAPHITE/EPOXY SP-286T300

Specimen Number	Thickness mm (in)	Width mm (in)	Flexural Strength MPa	Strength (ksi)
1	1.83 (0.072)	12.75 (0.502)	1710	(248)
2	1.75 (0.069)	12.73 (0.501)	1931	(280)
3	1.80 (0.071)	12.75 (0.502)	1789	(259)
4	1.73 (0.068)	12.75 (0.502)	1973	(286)
5	1.75 (0.069)	12.73 (0.501)	2007	(291)
6	1.83 (0.072)	12.78 (0.503)	1717	(249)
Average:			1855	(269)

Table 2
QUALIFICATION INTERLAMINAR SHEAR TESTS FOR GRAPHITE/EPOXY
SP-286T300

Specimen Number	Thickness mm (in)	Width mm(in)	Shear Strength MPa (ksi)
1	1.85 (0.073)	6.27 (0.247)	108.5 (15.7)
2	1.88 (0.074)	6.27 (0.247)	107.6 (15.6)
3	1.85 (0.073)	6.27 (0.247)	108.8 (15.8)
4	1.88 (0.074)	6.35 (0.250)	107.1 (15.5)
5	1.85 (0.073)	6.38 (0.251)	105.3 (15.3)
6	1.90 (0.075)	6.32 (0.249)	110.0 (15.9)
7	1.90 (0.075)	6.30 (0.248)	111.6 (16.1)

Average: 108.4 (15.7)

The values of flexural and interlaminar shear strengths are higher than those obtained for the previous batch of the same material.

2. CHARACTERIZATION OF UNIDIRECTIONAL MATERIAL

Material characterization was minimal, since the same material was characterized in the first phase of the program. Unidirectional tensile properties were obtained by testing 2.54 x 22.9 cm (1 in. x 9 in.) coupons. Six-ply specimens were used for the 0-degree tests and eight-ply for the 90-degree tests. Typical stress-strain curves as well as modulus, Poisson's ratio and strength obtained from these tests are shown in Figures 1-4. Results are also tabulated in Table 3. They are comparable with those obtained for the previous batch except for the transverse properties which appear slightly lower (Reference 1).

Table 3
PROPERTIES OF UNIDIRECTIONAL GRAPHITE/
EPOXY, SP-286T300

Property	Value
Ply Thickness	0.127 mm (0.0050 in.)
Longitudinal Modulus, E_{11}	147 GPa (21.3×10^6 psi)
Transverse Modulus, E_{22}	9.8 GPa (1.42×10^6 psi)
Major Poisson's Ratio, ν_{12}	0.29
Minor Poisson's Ratio, ν_{21}	0.017
Longitudinal Tensile Strength, S_{11T}	1435 MPa (208 ksi)
Transverse Tensile Strength, S_{22T}	48 MPa (7.0 ksi)
Ultimate Longitudinal Tensile Strain, ϵ_{11T}^u	0.00968
Ultimate Transverse Tensile Strain, ϵ_{22T}^u	0.00505

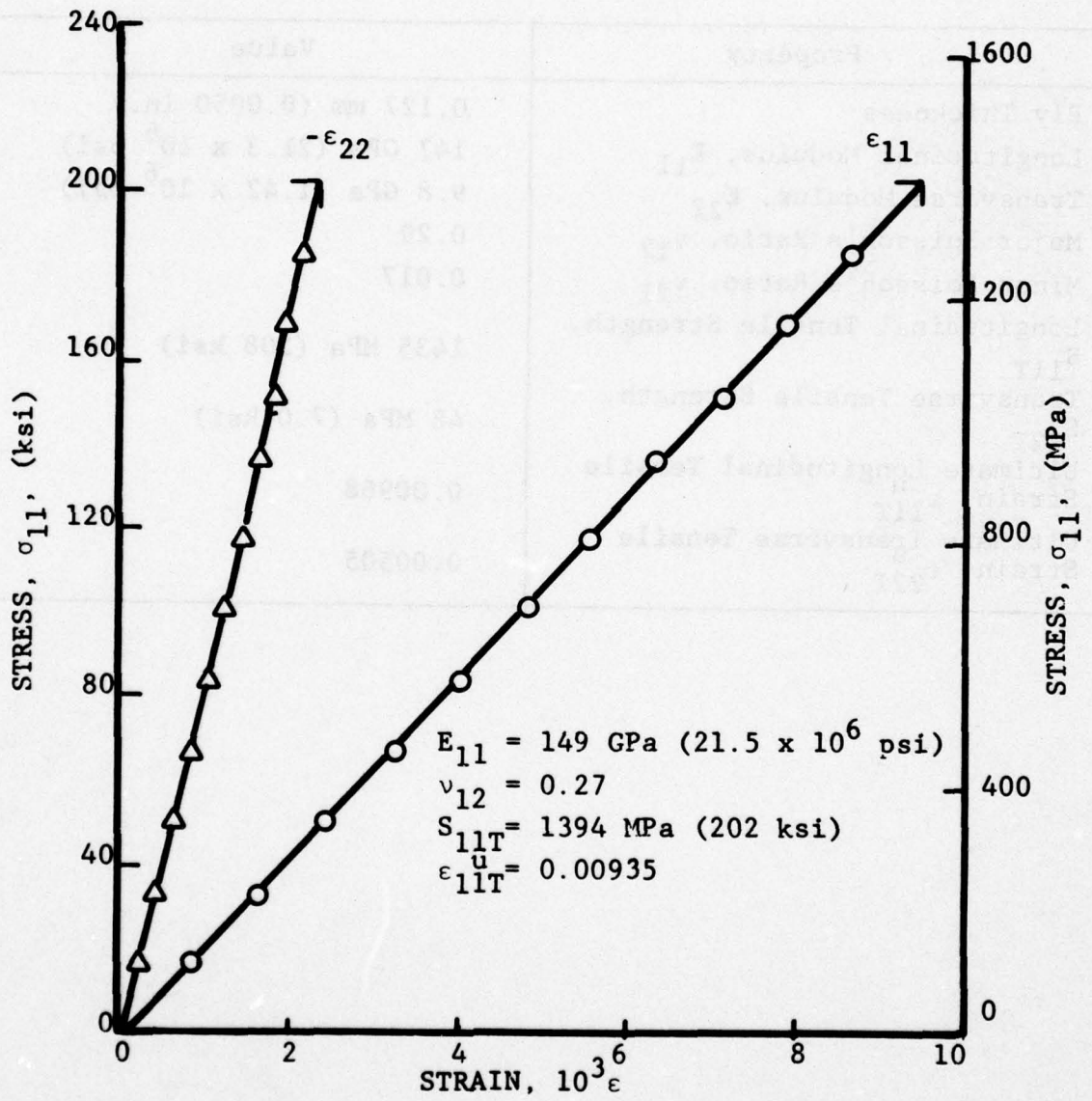


Figure 1. Strains in 0-Degree Unidirectional Specimen Under Uniaxial Tensile Loading

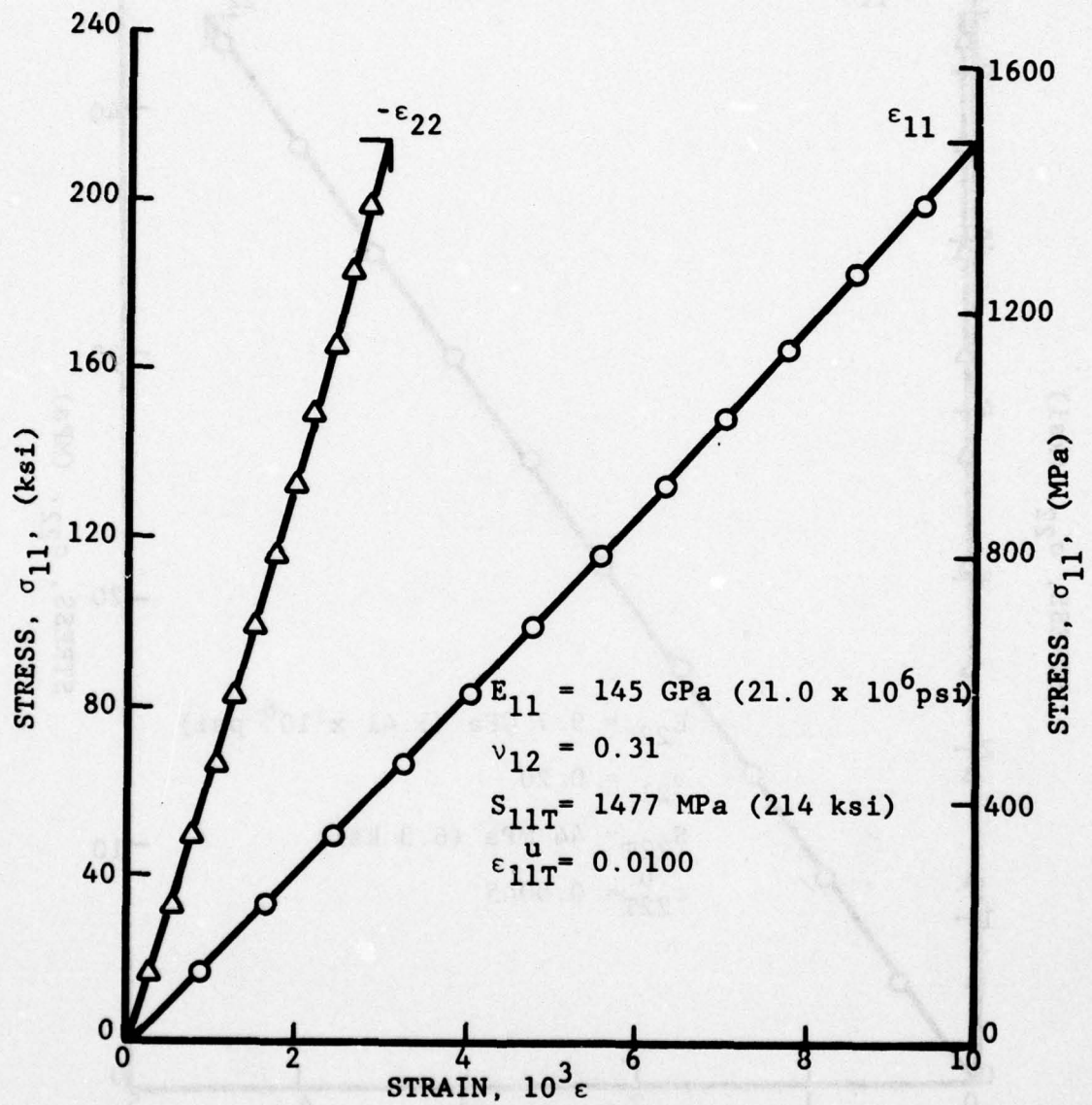


Figure 2. Strains in 0-Degree Unidirectional Specimen Under Uniaxial Tensile Loading

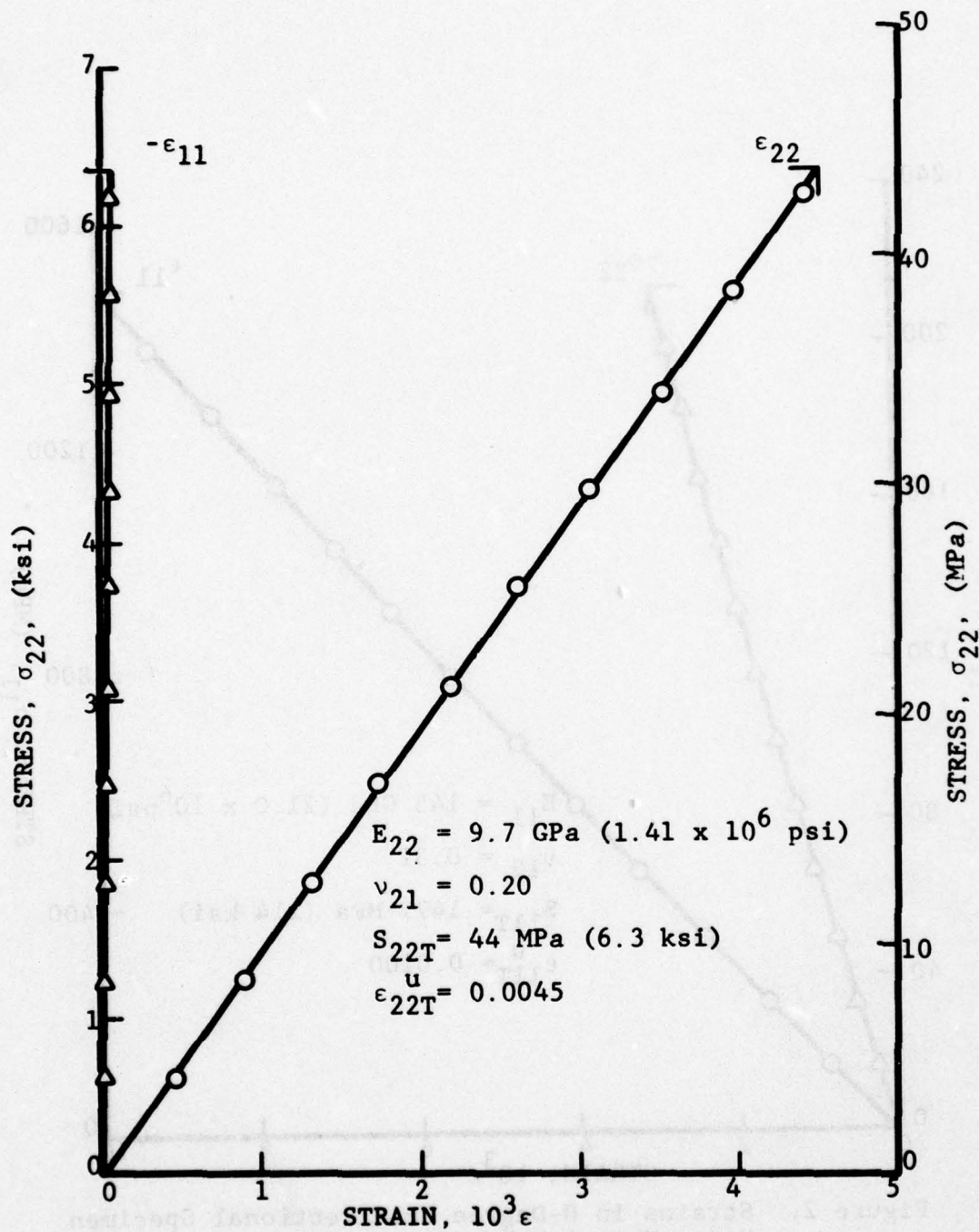


Figure 3. Strains in 90-Degree Unidirectional Specimen Under Uniaxial Tensile Loading

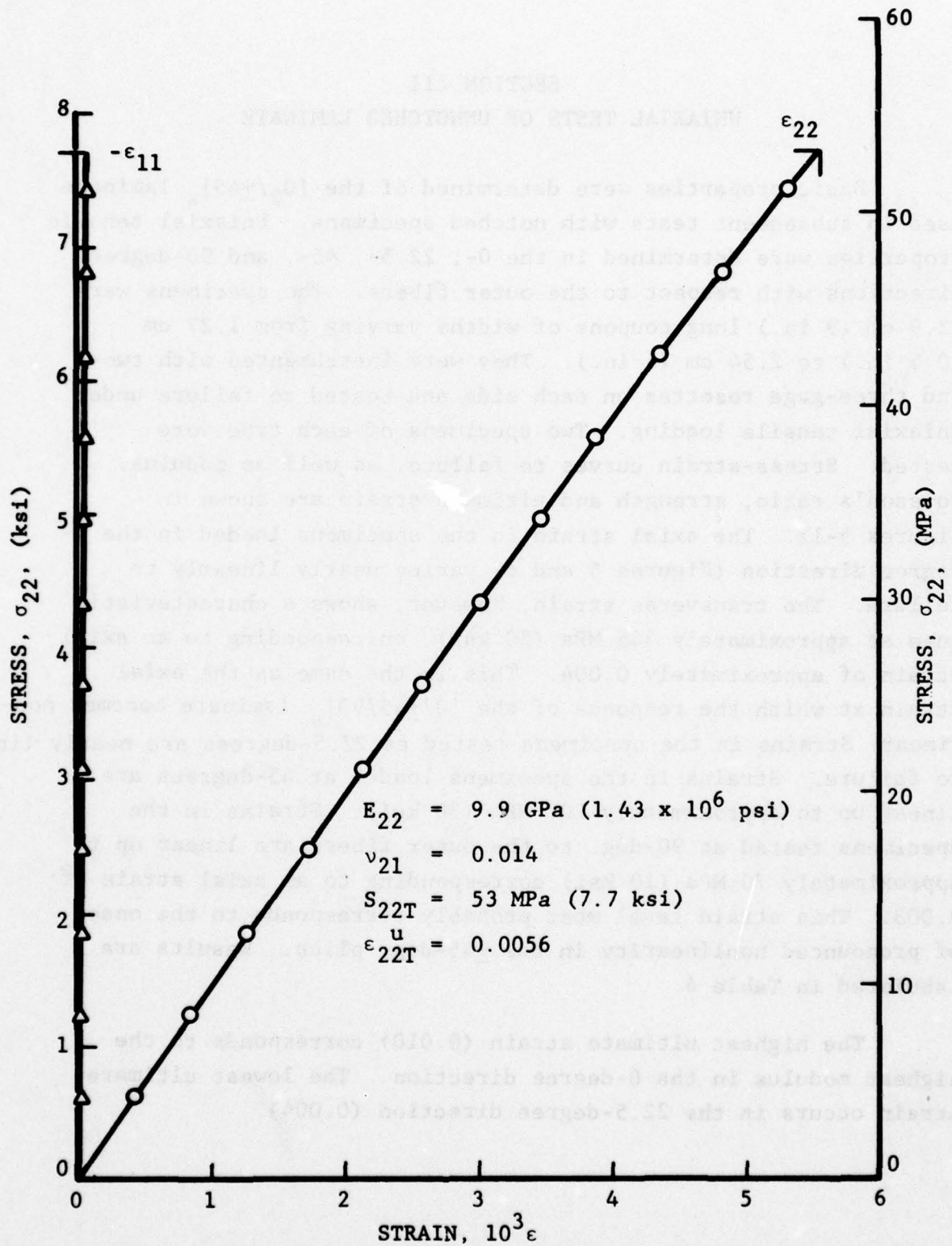


Figure 4. Strains in 90-Degree Unidirectional Specimen Under Uniaxial Tensile Loading

SECTION III
UNIAXIAL TESTS OF UNNOTCHED LAMINATE

Basic properties were determined of the $[0_2/\pm 45]_s$ laminate used in subsequent tests with notched specimens. Uniaxial tensile properties were determined in the 0-, 22.5-, 45-, and 90-degree directions with respect to the outer fibers. The specimens were 22.9 cm (9 in.) long coupons of widths varying from 1.27 cm (0.5 in.) to 2.54 cm (1 in.). They were instrumented with two- and three-gage rosettes on each side and tested to failure under uniaxial tensile loading. Two specimens of each type were tested. Stress-strain curves to failure, as well as modulus, Poisson's ratio, strength and ultimate strain are shown in Figures 5-12. The axial strain in the specimens loaded in the 0-degree direction (Figures 5 and 6) varies nearly linearly to failure. The transverse strain, however, shows a characteristic knee at approximately 345 MPa (50 ksi), corresponding to an axial strain of approximately 0.004. This is the same as the axial strain at which the response of the $[0/\pm 45/90]_s$ laminate becomes non-linear. Strains in the specimens tested at 22.5-degrees are nearly linear to failure. Strains in the specimens loaded at 45-degrees are linear up to approximately 207 MPa (30 ksi). Strains in the specimens tested at 90-deg. to the outer fibers are linear up to approximately 70 MPa (10 ksi) corresponding to an axial strain of 0.003. This strain level most probably corresponds to the onset of pronounced nonlinearity in the ± 45 -deg. plies. Results are tabulated in Table 4.

The highest ultimate strain (0.010) corresponds to the highest modulus in the 0-degree direction. The lowest ultimate strain occurs in the 22.5-degree direction (0.004).

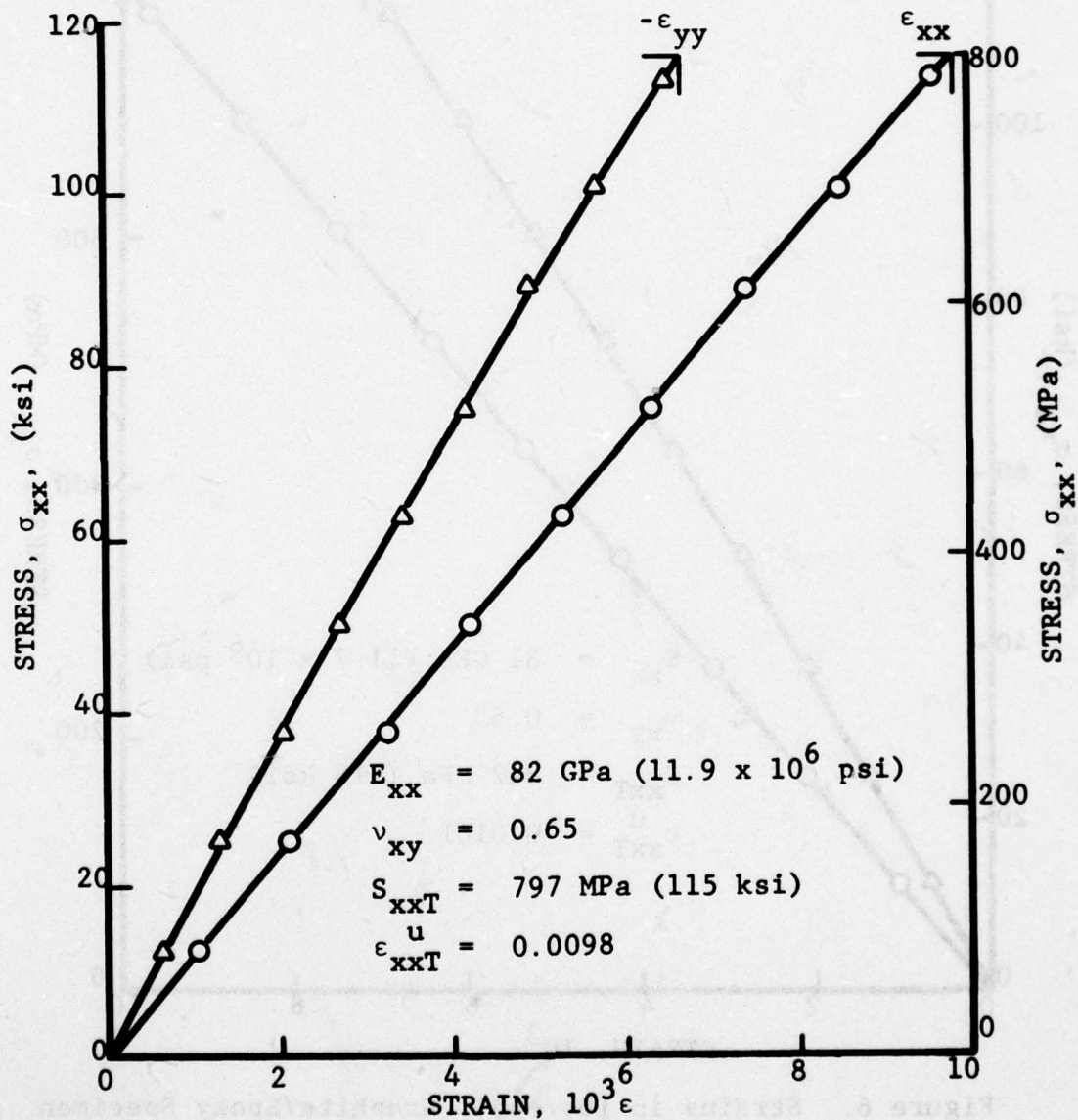


Figure 5. Strains in $[0_2/+45]_s$ Graphite/Epoxy Specimen Under Uniaxial Tensile Loading

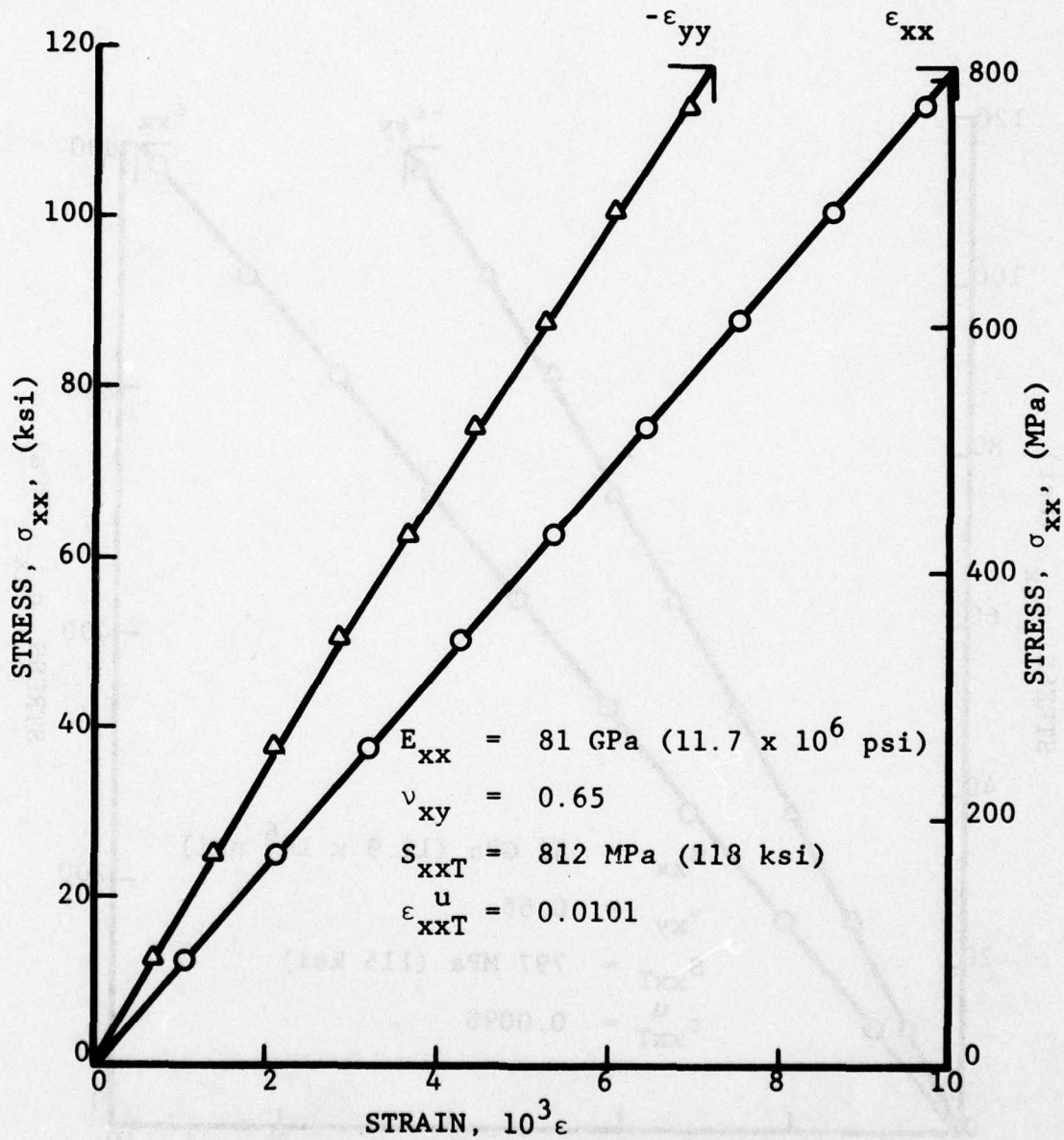


Figure 6. Strains in $[0_2/+45]_s$ Graphite/Epoxy Specimen Under Uniaxial Tensile Loading

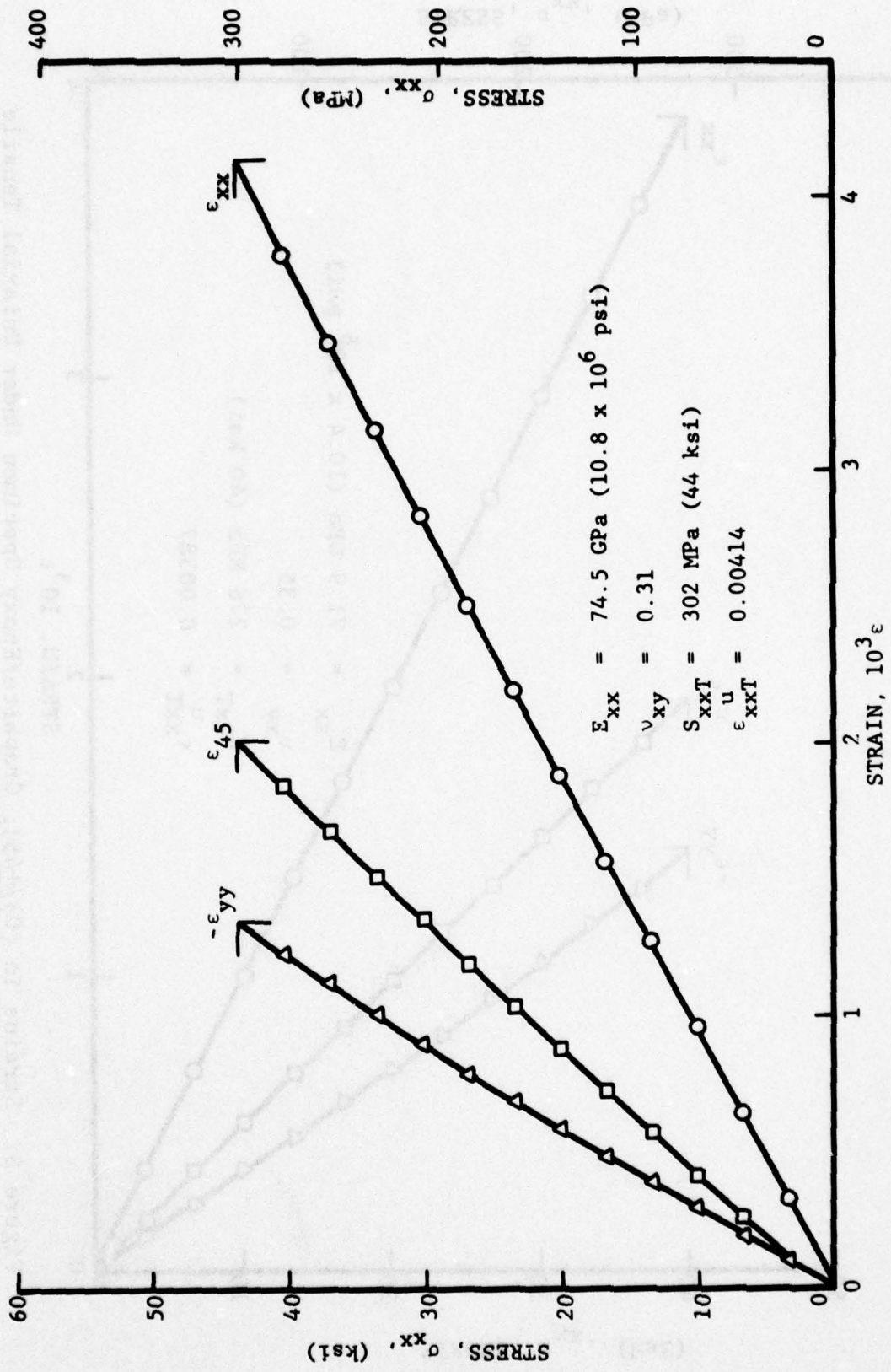


Figure 7. Strains in $[0_2/\pm 45]_s$ Graphite/Epoxy Specimen Under Uniaxial Tensile Loading at 22.5-Degrees

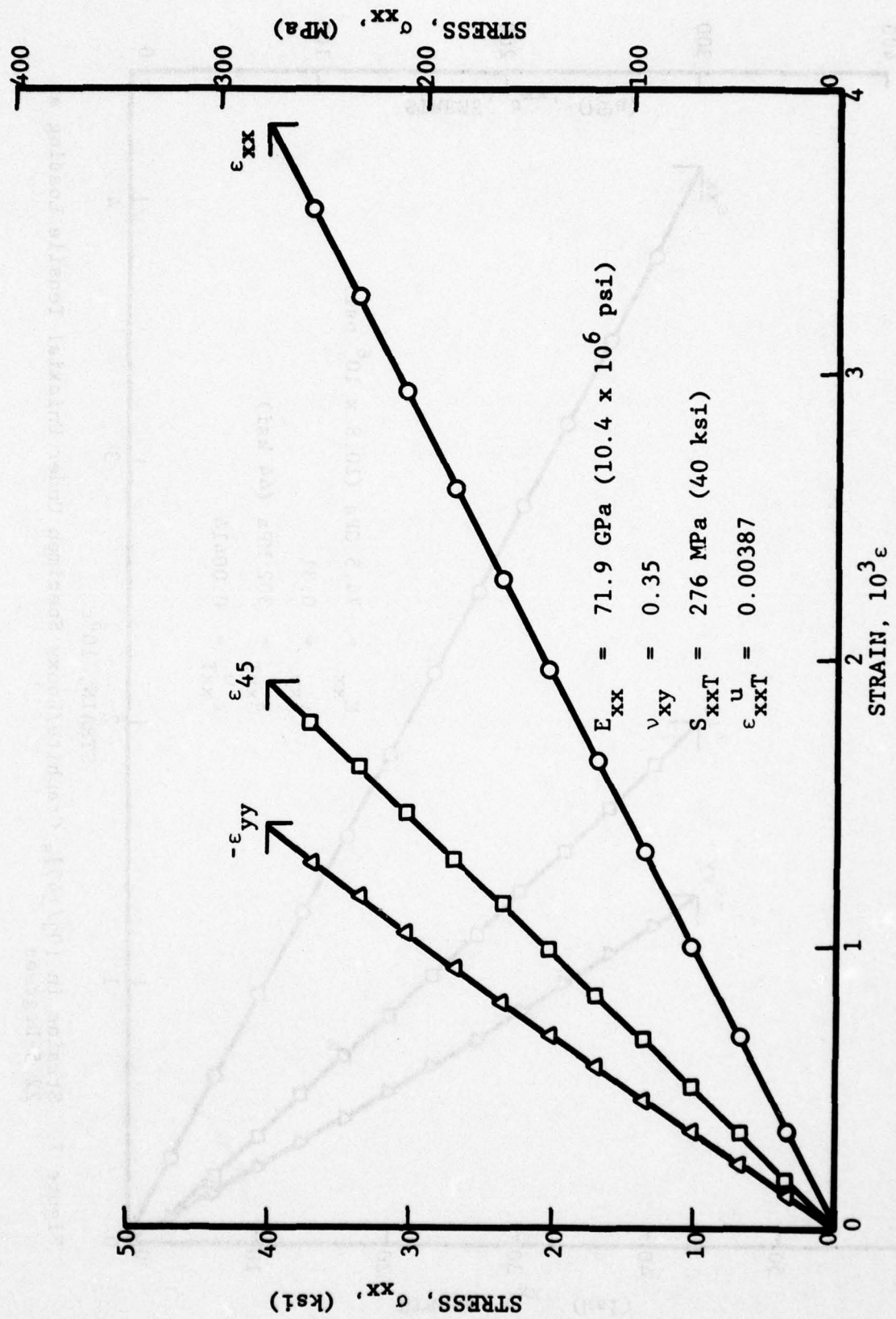


Figure 8. Strains in $[0_2/+45]_s$ Graphite/Epoxy Specimen Under Uniaxial Tensile Loading at 22.5-Degrees

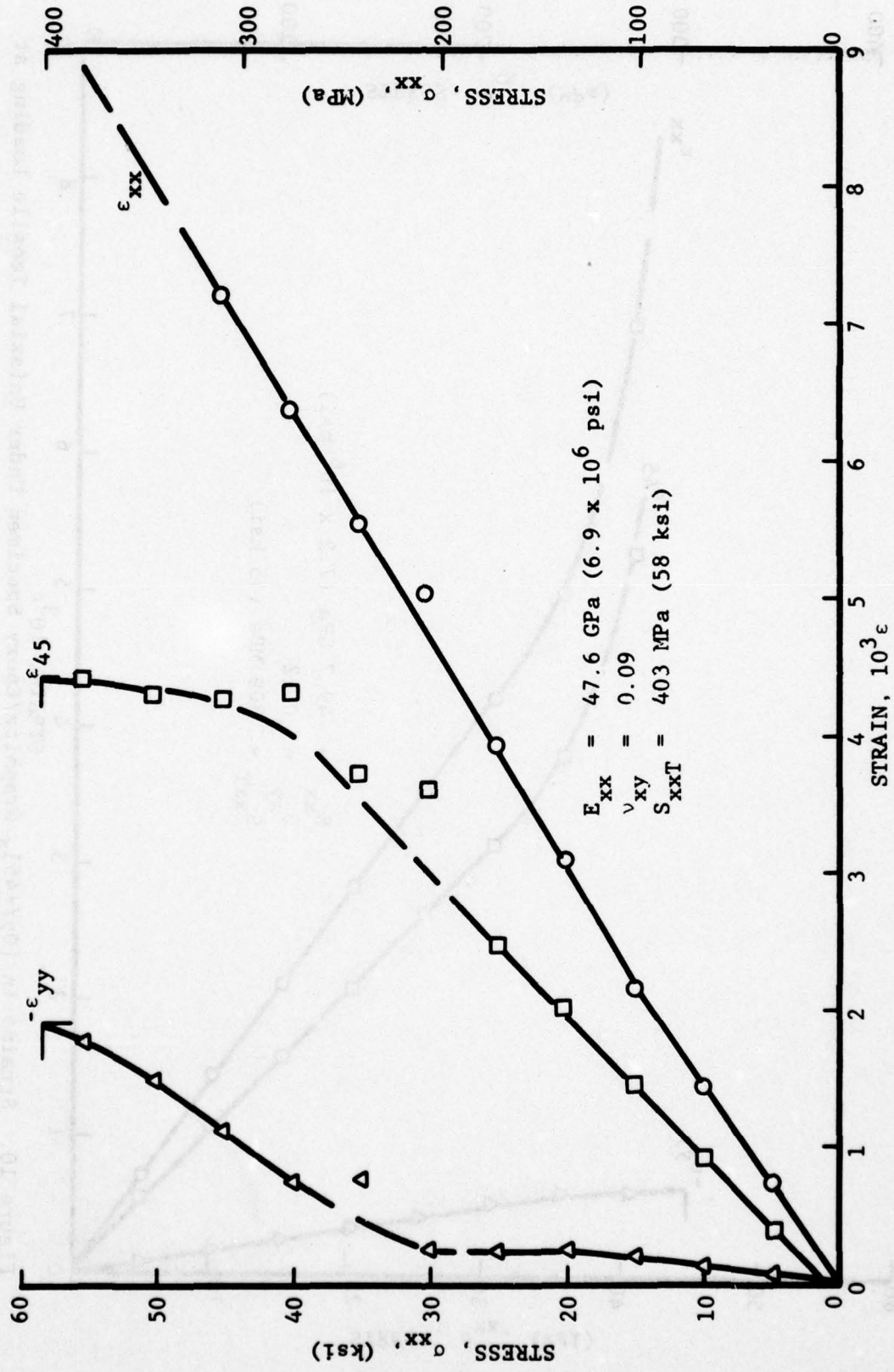


Figure 9. Strains in $[0_2/+45]_s$ Graphite/Epoxy Specimen Under Uniaxial Tensile Loading at 45-Degrees

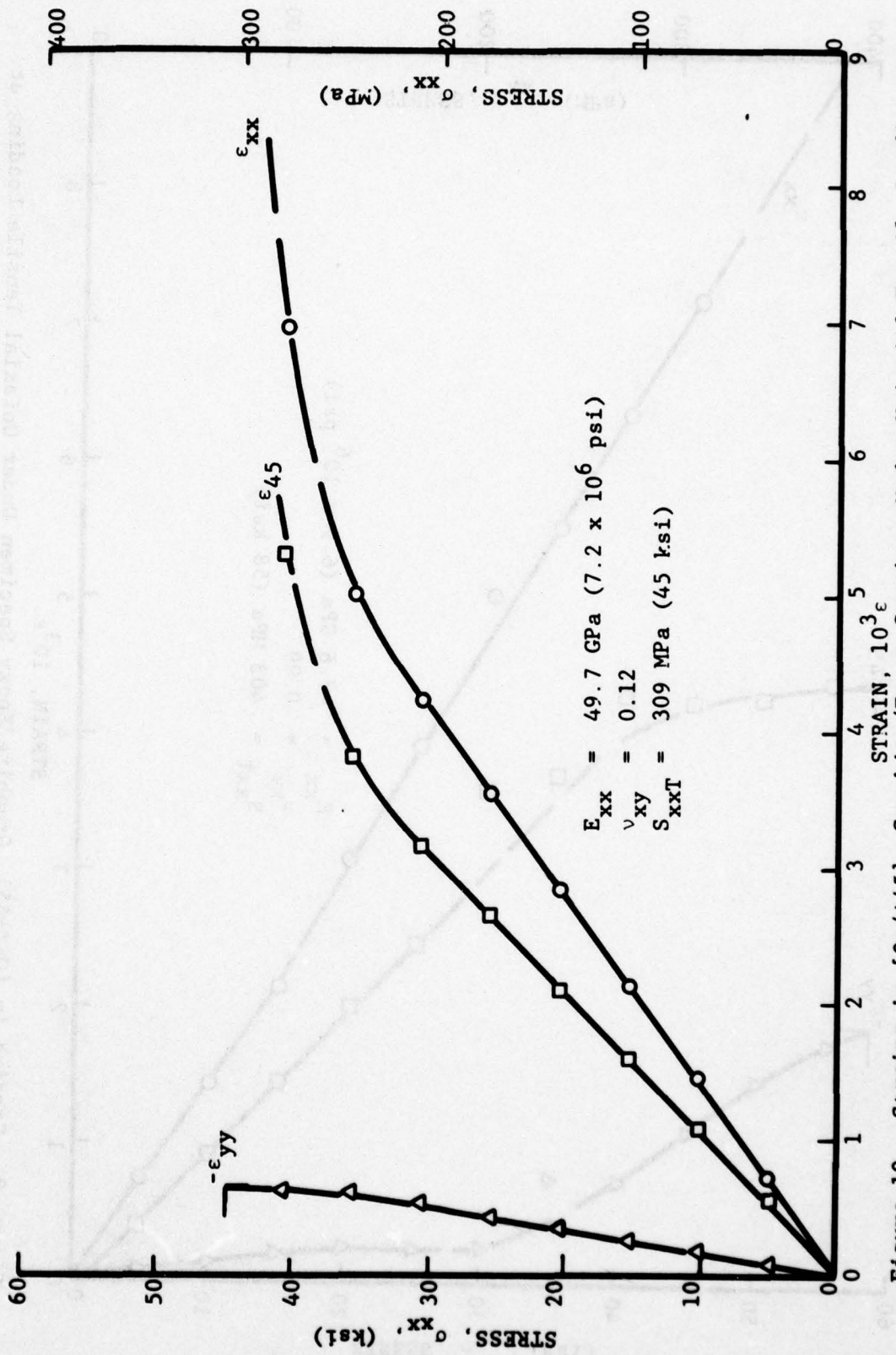


Figure 10. Strains in [0₂/+45]_s Graphite/Epoxy Specimen Under Uniaxial Tensile Loading at 45-Degrees

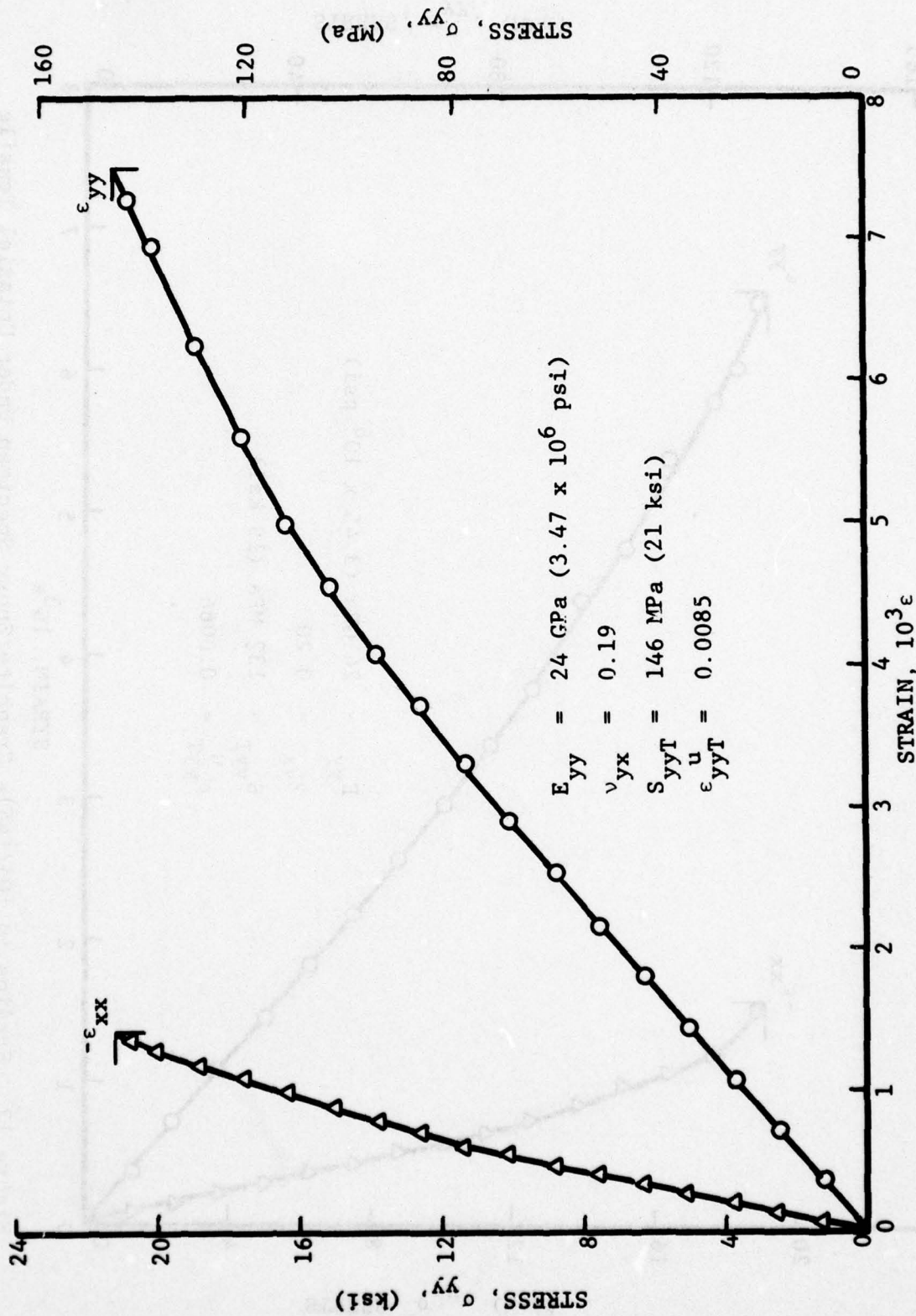


Figure 11. Strains in [0₂/+45]_s Graphite/Epoxy Specimen Under Uniaxial Tensile Loading at 90-Degrees

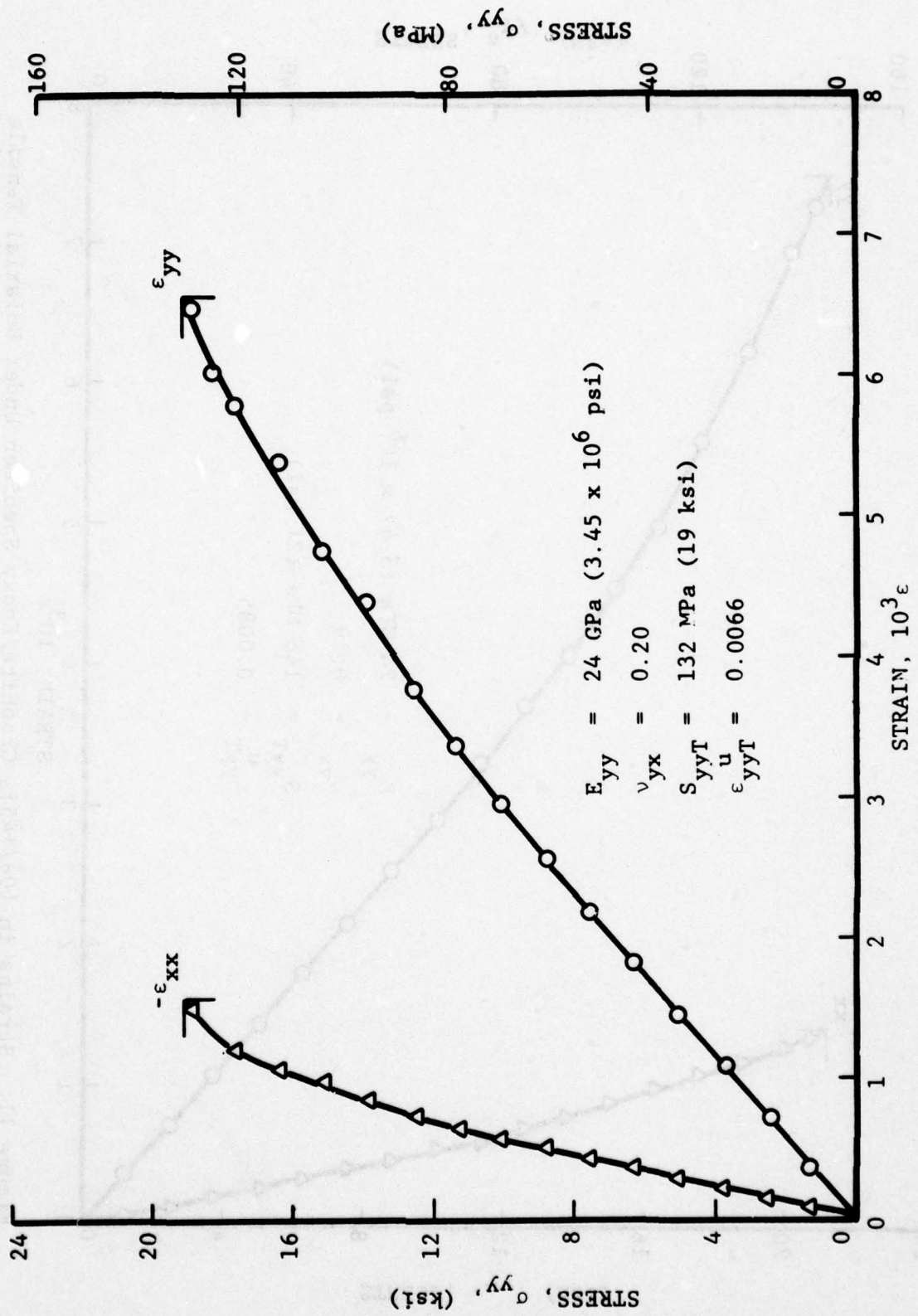


Figure 12. Strains in $[0_2/+45]_s$ Graphite/Epoxy Specimen Under Uniaxial Tensile Loading at 90-Degrees

Table 4
STATIC TENSILE PROPERTIES OF UNNOTCHED
[0₂/+45]_s GRAPHITE/EPOXY LAMINATES

Direction of Loading	Modulus E_{xx} GPa (10^6 psi)	Poisson's Ratio, ν_{xy}	Strength S_{xxT} MPa (ksi)	Ultimate Strain ϵ_{xxT}^u ($10^3 \epsilon$)
0-deg	82 (11.8)	0.65	805 (116)	10.0
22.5-deg	73 (10.6)	0.33	290 (42)	4.0
45-deg	49 (7.1)	0.11	356 (52)	>9.0
90-deg	24 (3.46)	0.20	139 (20)	7.5

SECTION IV
UNIAXIAL TESTS OF NOTCHED LAMINATE

1. SPECIMENS

The specimens were eight-ply $[0_2/+45]_s$ laminates 12.7 cm (5 in.) wide and 56 cm (22 in.) long with central circular holes of 2.54 cm (1 in.), 1.91 cm (0.75 in.), 1.27 cm (0.50 in.) and 0.64 cm (0.25 in.) diameter. They were tabbed with 11-ply glass/epoxy crossply tabs (3M, 1002 Scotchply) as shown in Figure 13. All holes were drilled with diamond core drills. Two specimens were tested for each hole diameter.

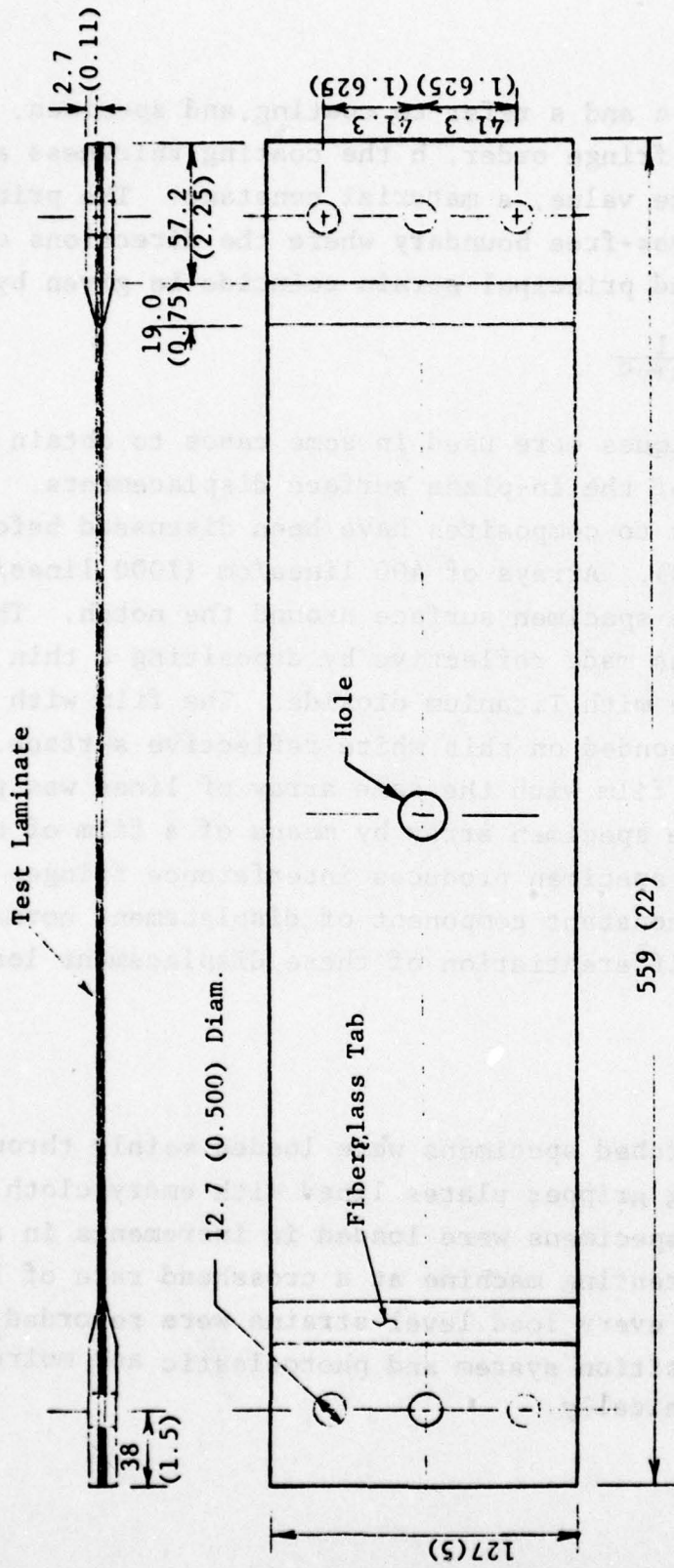
2. STRAIN MEASUREMENT

Deformations and strains were recorded at various load increments using strain gages and birefringent coatings. Strain gages were mounted on the curved edge of the hole at the 0-degree and 90-degree locations (Micro-Measurements EA-06-015DJ-120), near the hole boundary and along the horizontal (normal to loading) axis. The strain gage output was recorded by means of a digital data acquisition system, which gave a printout directly in strain units.

In half the specimens birefringent coatings were bonded to one side to obtain full-field strain information. Commercial coatings with a reflective backing (Photolastic, Inc.) of 0.5 mm (0.02 in.) and 1 mm (0.04 in.) thickness were used. The isochromatic fringes in the coating were observed with a reflection polariscope and recorded photographically.

Photoelastic coating fringes were interpreted on the basis of the strain-optic law

$$\epsilon_1^c - \epsilon_2^c = \epsilon_1^s - \epsilon_2^s = \frac{Nf}{2h} \epsilon$$



Note: Dimensions are in millimeters and inches.

Figure 13. Uniaxial Tensile Specimen with Stress Concentration

where superscripts c and s refer to coating and specimen, respectively, N is fringe order, h the coating thickness and f_{ϵ} the strain fringe value, a material constant. The principal strain along a stress-free boundary where the directions of principal stress and principal strain coincide is given by

$$\epsilon_1^s = \frac{Nf_{\epsilon}}{2h} \cdot \frac{1}{1+\nu^c}$$

Moire' techniques were used in some cases to obtain full-field information of the in-plane surface displacements. Application of these techniques to composites have been discussed before (References 2 and 3). Arrays of 400 lines/cm (1000 lines/in.) were applied to the specimen surface around the notch. The specimen surface was made reflective by depositing a thin coating of epoxy dyed white with Titanium dioxide. The film with the array of lines was then bonded on this white reflective surface. During testing, a similar film with the same array of lines was placed in contact with the specimen array by means of a film of oil. Deformation of the specimen produces interference fringes which represent loci of constant component of displacement normal to the specimen array. Differentiation of these displacement loci yields strains.

3. LOADING

Uniaxial notched specimens were loaded mainly through friction by bolting gripper plates lined with emery cloth to the tabbed ends. The specimens were loaded in increments in a 120,000 lb Riehle testing machine at a crosshead rate of 1 mm/min (0.04 in/min). At every load level strains were recorded with a digital data acquisition system and photoelastic and moire fringes recorded photographically.

4. RESULTS

Specimen No. 4A-1 had a 2.54 cm (1 in.) diameter hole. It was instrumented with a 1.07 mm (0.042 in.) thick photo-elastic coating on one side and strain gages on the other. Strain distributions obtained from the strain gages are plotted in Figure 14. Strains on the boundary of the hole and near it are linear up to an applied stress of 172 MPa (25 ksi). Thereafter, the strain variation changes abruptly with the strain increasing at a reduced rate. This occurs at a strain level of approximately 6.5×10^{-3} . The modulus, Poisson's ratio and strain concentration factor were computed for the linear portion of the strain variation curves. These values as well as the strength reduction ratio are:

$$\begin{aligned} E_{xx} &= 84 \text{ GPa } (12.1 \times 10^6 \text{ psi}) \\ \nu_{xy} &= 0.70 \\ (k_\epsilon)_{90^\circ} &= 3.27 \\ S_{xxT} &= 445 \text{ MPa } (65 \text{ ksi}) \\ k_s &= \frac{65}{116} = 0.555 \end{aligned}$$

The theoretical value for the strain concentration factor computed from the expression

$$(k_\epsilon)_{90^\circ} = 1 + \sqrt{2 \left[\sqrt{\frac{E_{xx}}{E_{yy}} - \nu_{xy}} \right] + \frac{E_{xx}}{G_{xy}}}$$

is 3.44 which is higher than the experimental value above. The strength reduction factor, or the inverse of the strength reduction ratio (1.80) is appreciably lower than the strain concentration factor. This is a result of the nonlinear strain variations at and near the hole boundary related to extensive stress redistribution.

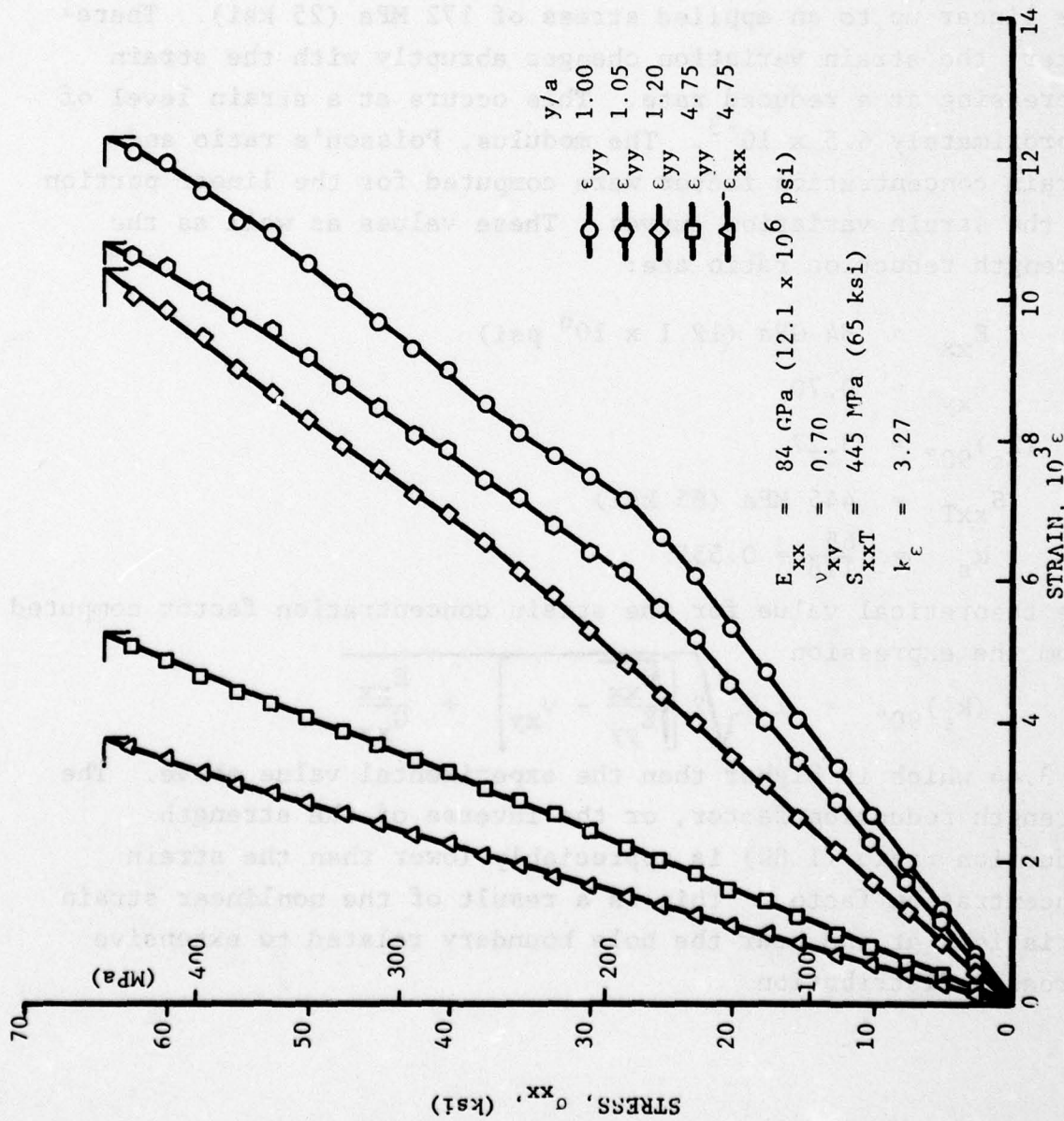
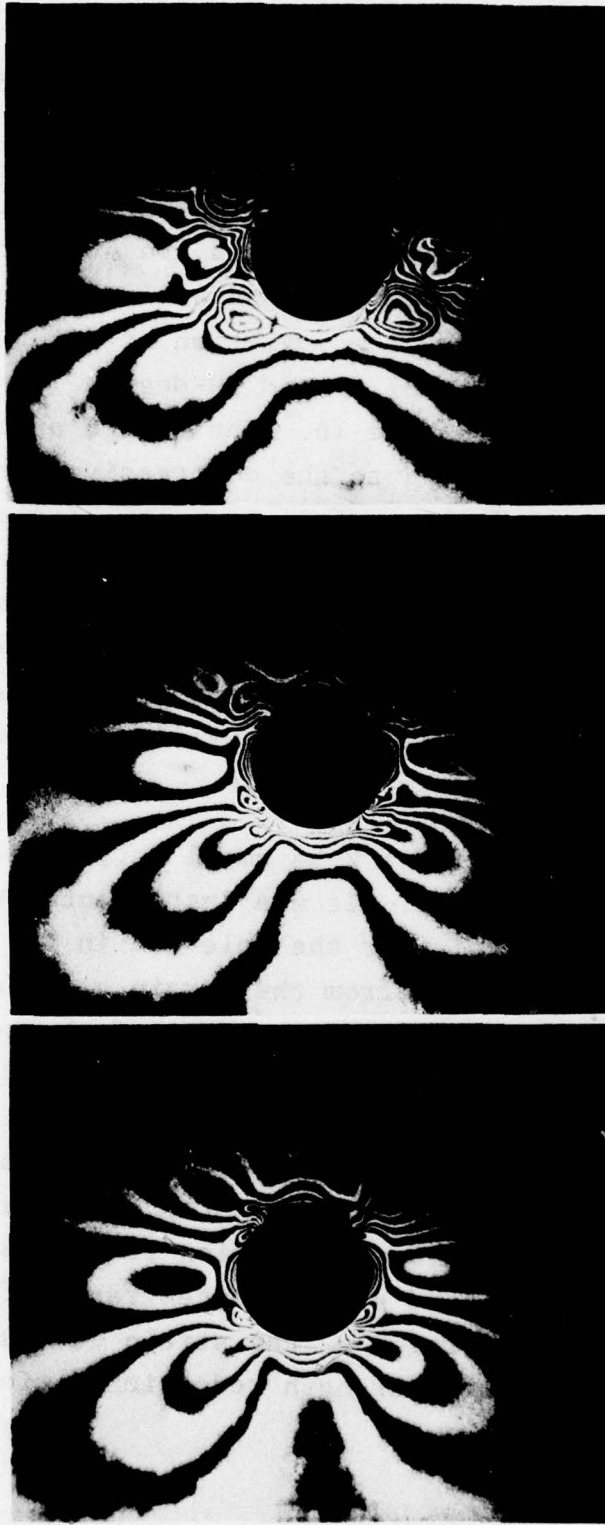


Figure 14. Strains Along Horizontal Axis of [02/+45] Graphite/Epoxy Specimen With 2.54 cm (1 in.) Circular Hole Under Uniaxial Tensile Loading (Spec. No. 4A-1)

Photoelastic fringe patterns in the coating around the hole are shown in Figure 15 for three levels of load. The characteristic points of high tangential strain concentration on the hole boundary off the horizontal axis are evident. In this case these points are located at an angle of approximately 67.5° from the loading axis. The variation of fringe order and tangential strain at the 0-, 67.5- and 90-degree locations on the hole boundary is shown in Figure 16. The fringe order at the 0-degree location, corresponding to the compressive strain at that point, varies nearly linearly to failure. The birefringence at the 90-degree location varies linearly up to an applied stress of approximately 241 MPa (35 ksi), thereafter it increases at a much reduced rate as the corresponding strains obtained from strain gages. The birefringence at the 67.5-degree location becomes nonlinear at a lower stress of 138 MPa (20 ksi). Failure initiated at these off-axis points.

Specimen No. 4A-2 with a 2.54 cm (1 in.) diameter hole was a replicate of No. 4A-1 above. It was instrumented with strain gages on the hole boundary, near the hole and in the far field. Strain distributions obtained from the strain gages are plotted in Figures 17 and 18. Strains on the boundary of the hole and near it are linear up to an applied stress of 138 MPa (20 ksi). Thereafter, these strains increase at a reduced rate. This is due to some stress redistribution taking place at a maximum strain of approximately 6×10^{-3} . It should be noted that the ultimate strain of the laminate in the 22.5-deg. direction is only 4×10^{-3} . The modulus, Poisson's ratio, and strain concentration factors were computed for the linear portion of the strain curves. These values as well as the strength and strength reduction ratio are:



(c)

(b)

(a)

Figure 15. Isochromatic Fringe Patterns in Photoelastic Coating of $[0_2/+45]_s$ Graphite/Epoxy Specimen with 2.54 cm (1 in.) Diameter Circular Hole Under Uniaxial Tensile Loading (Spec. No. 4A-1)

a) $\sigma_{xx} = 276$ MPa (40 ksi), b) $\sigma_{xx} = 345$ MPa (50 ksi), c) $\sigma_{xx} = 414$ MPa (60 ksi)

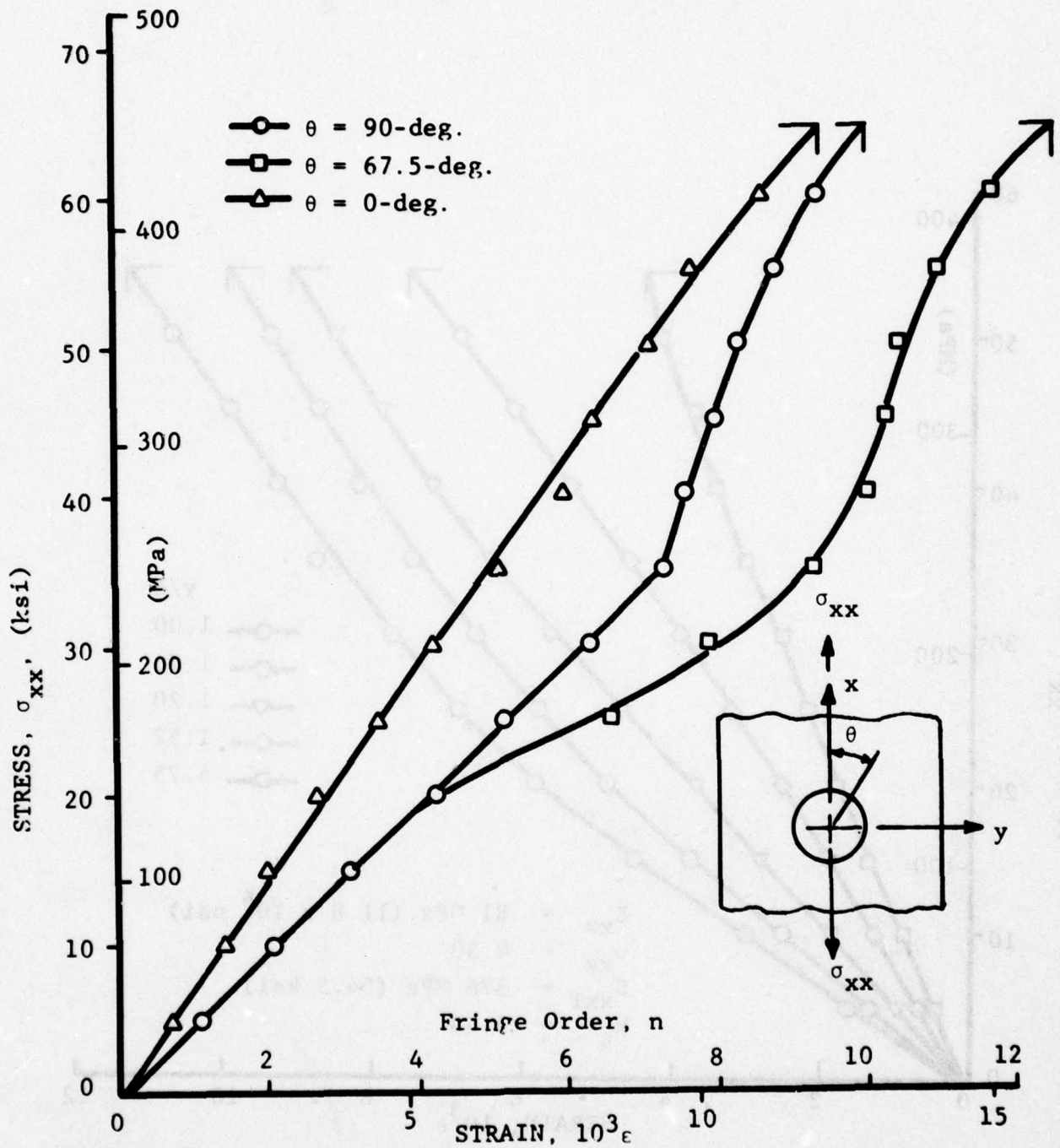


Figure 16. Fringe Order and Circumferential Strain at Three Locations on the Hole Boundary for $[0_2/+45]_8$ Graphite/Epoxy Specimen with 2.54 cm (1 in.) Circular Hole Under Uniaxial Tensile Loading (Spec. No. 4A-1)

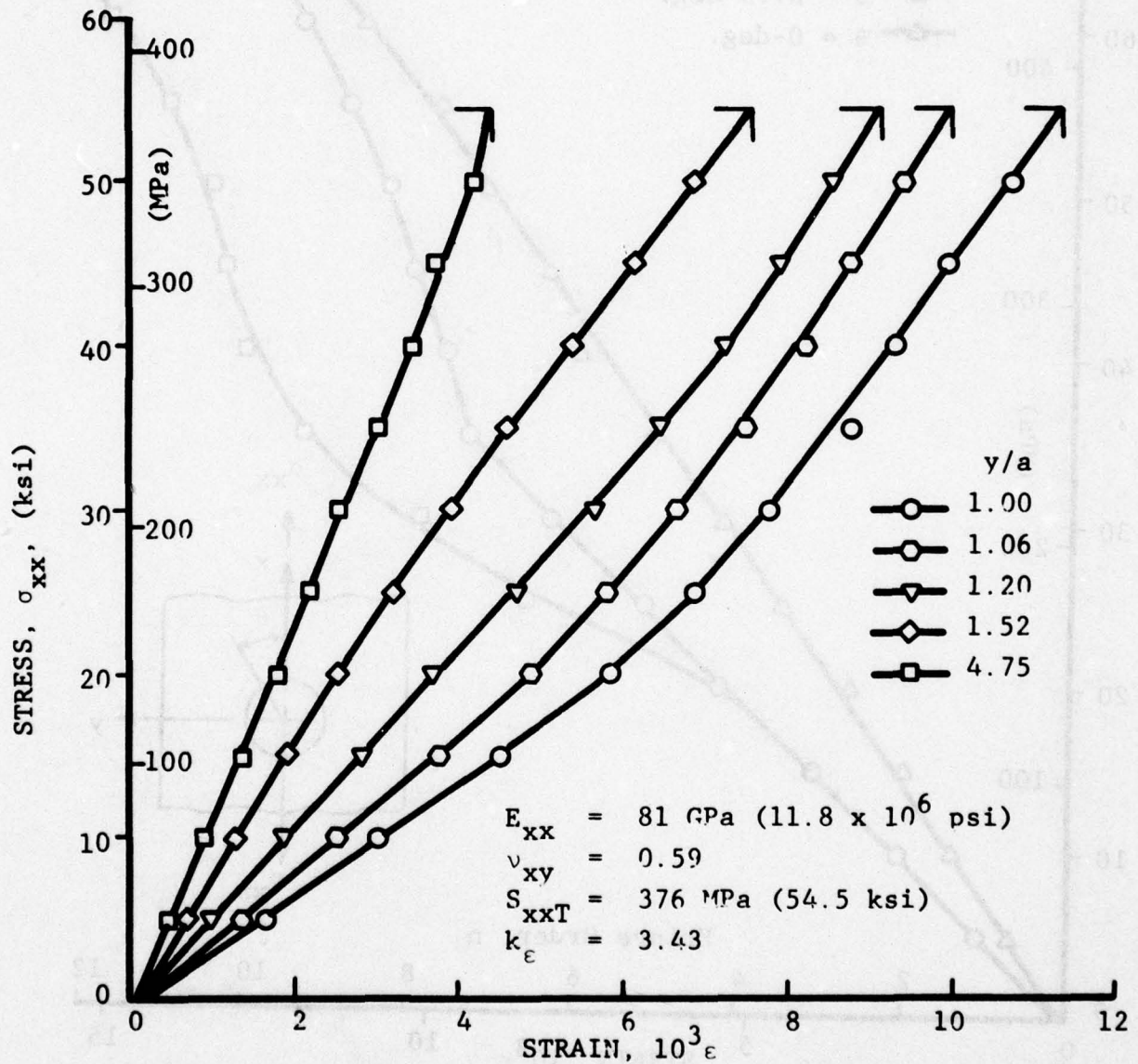


Figure 17. Vertical Strains Along Horizontal Axis of $[0_2/\pm 45]_s$ Graphite/Epoxy Specimen with 2.54 cm (1 in.) Diameter Hole Under Uniaxial Tensile Loading (Spec. No. 4A-2)

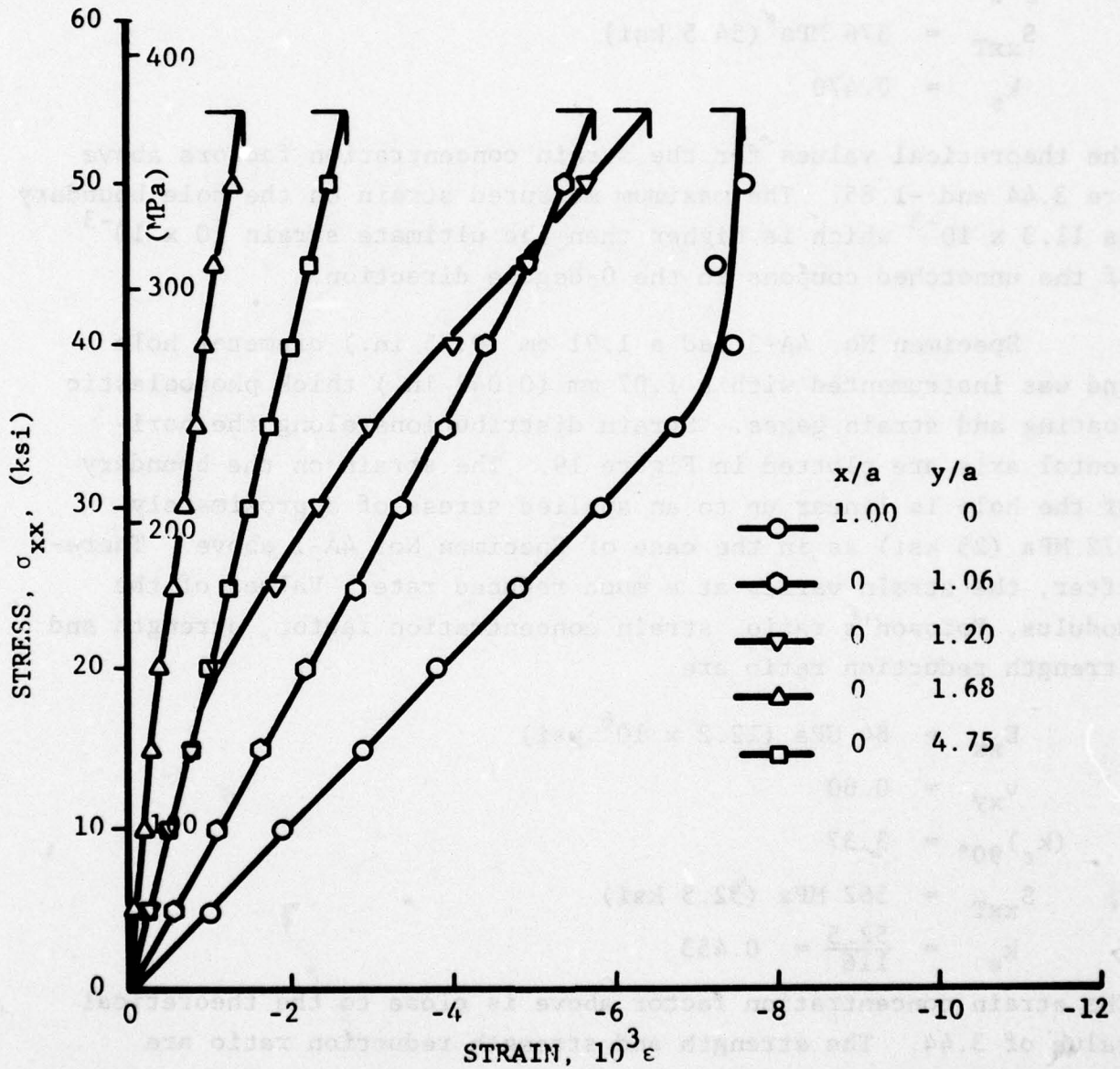


Figure 18. Horizontal Strains on the Hole Boundary and Along Horizontal Axis of $[0_2/+45]_s$ Graphite/Epoxy Specimen with 2.54 cm (1 in.) Diameter Hole Under Uniaxial Tensile Loading (Spec. No. 4A-2)

$$\begin{aligned}
E_{xx} &= 81 \text{ GPa } (11.8 \times 10^6 \text{ psi}) \\
\nu_{xy} &= 0.59 \\
(k_{\epsilon})_{90^\circ} &= 3.43 \\
(k_{\epsilon})_{0^\circ} &= -2.26 \\
S_{xxT} &= 376 \text{ MPa } (54.5 \text{ ksi}) \\
k_s &= 0.470
\end{aligned}$$

The theoretical values for the strain concentration factors above are 3.44 and -1.85. The maximum measured strain on the hole boundary is 11.3×10^{-3} which is higher than the ultimate strain 10×10^{-3} of the unnotched coupons in the 0-degree direction.

Specimen No. 4A-3 had a 1.91 cm (0.75 in.) diameter hole and was instrumented with a 1.07 mm (0.042 in.) thick photoelastic coating and strain gages. Strain distributions along the horizontal axis are plotted in Figure 19. The strain on the boundary of the hole is linear up to an applied stress of approximately 172 MPa (25 ksi) as in the case of Specimen No. 4A-1 above. Thereafter, the strain varies at a much reduced rate. Values of the modulus, Poisson's ratio, strain concentration factor, strength and strength reduction ratio are:

$$\begin{aligned}
E_{xx} &= 84 \text{ GPa } (12.2 \times 10^6 \text{ psi}) \\
\nu_{xy} &= 0.60 \\
(k_{\epsilon})_{90^\circ} &= 3.37 \\
S_{xxT} &= 362 \text{ MPa } (52.5 \text{ ksi}) \\
k_s &= \frac{52.5}{116} = 0.453
\end{aligned}$$

The strain concentration factor above is close to the theoretical value of 3.44. The strength and strength reduction ratio are appreciably lower than for Specimen No. 4A-1 with the 2.54 cm (1 in.) diameter hole.

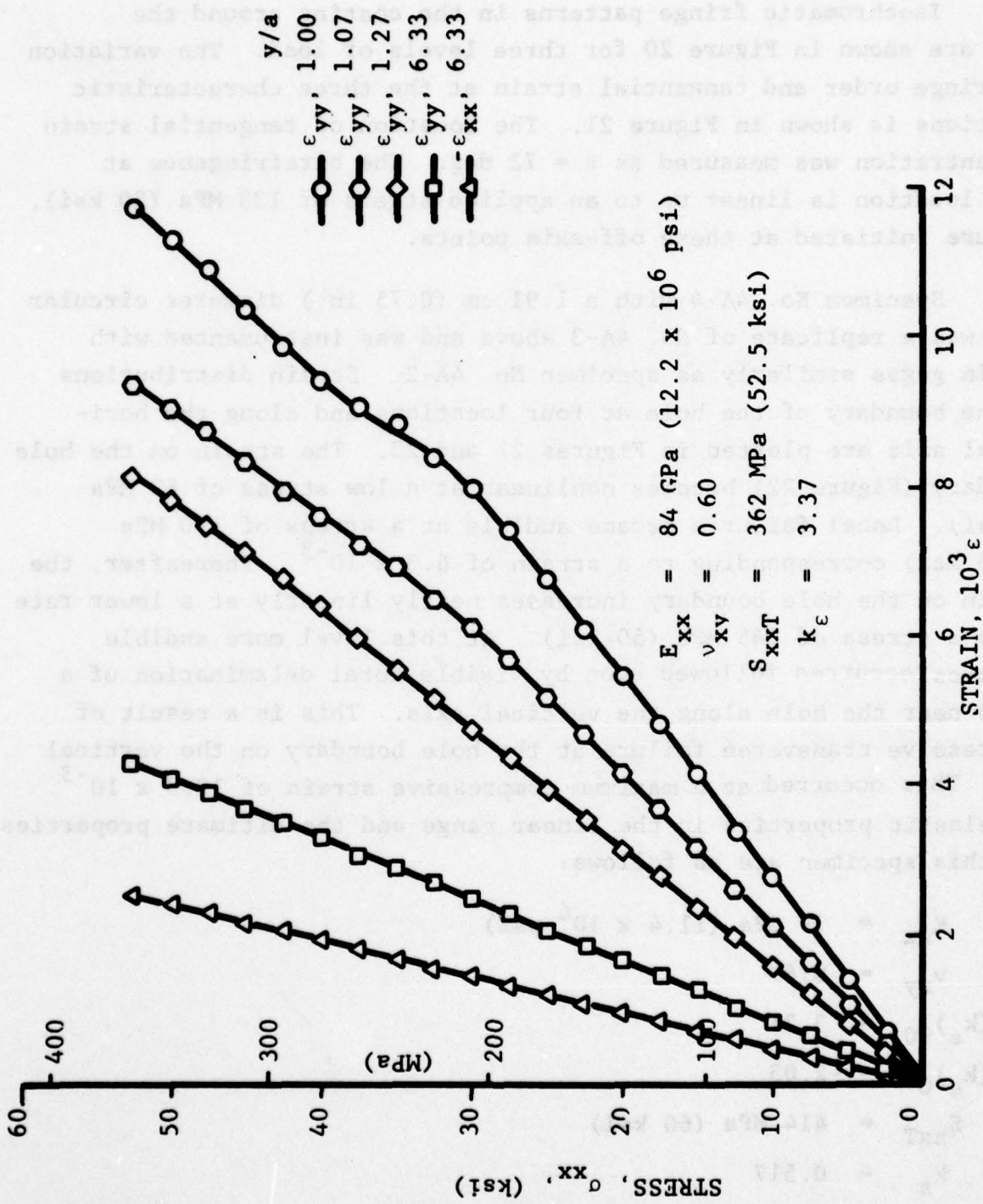


Figure 19. Strains Along Horizontal Axis of [02/+45]s Graphite/Epoxy Specimen with 1.91 cm (0.75 in.) Circular Hole Under Uniaxial Tensile Loading (Spec. No. 4A-3)

Isochromatic fringe patterns in the coating around the hole are shown in Figure 20 for three levels of load. The variation of fringe order and tangential strain at the three characteristic locations is shown in Figure 21. The location of tangential strain concentration was measured as $\theta = 72$ deg. The birefringence at this location is linear up to an applied stress of 138 MPa (20 ksi). Failure initiated at these off-axis points.

Specimen No. 4A-4 with a 1.91 cm (0.75 in.) diameter circular hole was a replicate of No. 4A-3 above and was instrumented with strain gages similarly as specimen No. 4A-2. Strain distributions on the boundary of the hole at four locations and along the horizontal axis are plotted in Figures 22 and 23. The strain on the hole boundary (Figure 22) becomes nonlinear at a low stress of 62 MPa (9 ksi). Local failures became audible at a stress of 190 MPa (27.5 ksi) corresponding to a strain of 6.3×10^{-3} . Thereafter, the strain on the hole boundary increases nearly linearly at a lower rate up to a stress of 345 MPa (50 ksi). At this level more audible failures occurred followed soon by visible total delamination of a strip near the hole along the vertical axis. This is a result of compressive transverse failure at the hole boundary on the vertical axis. This occurred at a maximum compressive strain of 10.3×10^{-3} . The elastic properties in the linear range and the ultimate properties for this specimen are as follows:

$$\begin{aligned}
 E_{xx} &= 79 \text{ GPa } (11.4 \times 10^6 \text{ psi}) \\
 \nu_{xy} &= 0.67 \\
 (k_\epsilon)_{90^\circ} &= 3.31 \\
 (k_\epsilon)_{0^\circ} &= -2.03 \\
 S_{xxT} &= 414 \text{ MPa } (60 \text{ ksi}) \\
 k_s &= 0.517
 \end{aligned}$$

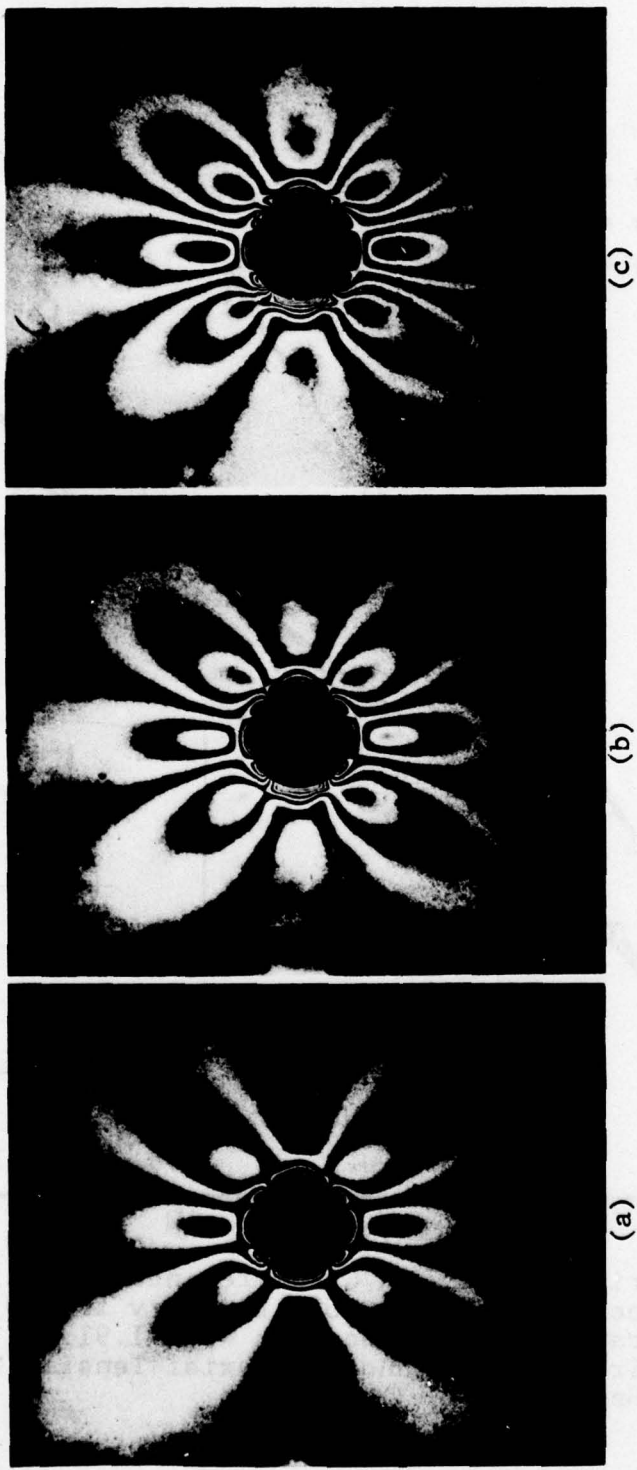


Figure 20. Isochromatic Fringe Patterns in Photoelastic Coating of $[0_2/+45]_s$ Graphite/Epoxy Specimen with 1.91 cm (0.75 in.) Diameter Circular Hole Under Uniaxial Tensile Loading (Spec. No. 4A-3)

a) $\sigma_{xx} = 207$ MPa (30 ksi), b) $\sigma_{xx} = 276$ MPa (40 ksi), c) $\sigma_{xx} = 345$ MPa (50 ksi)

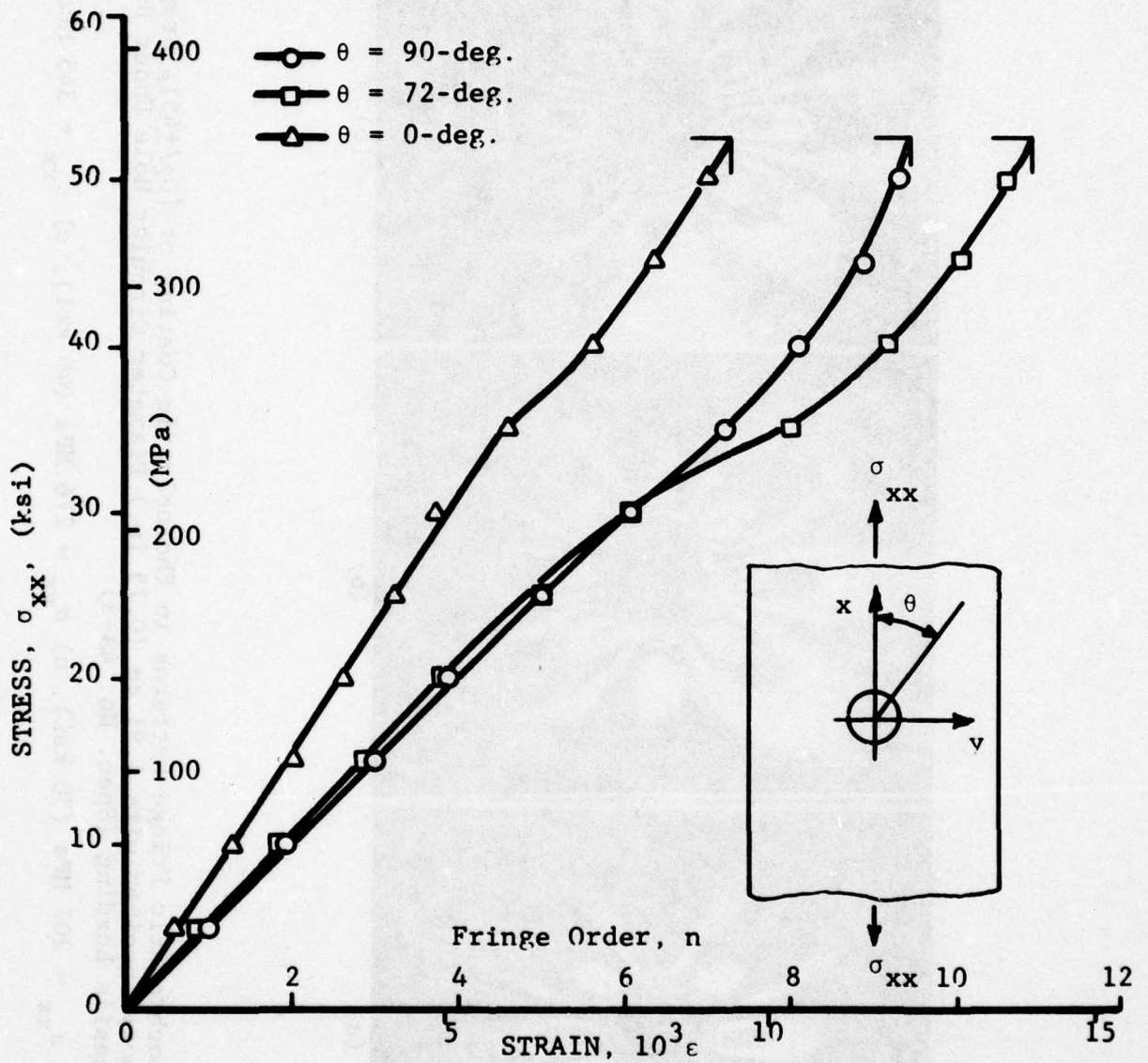


Figure 21. Fringe Order and Circumferential Strain at Three Locations on the Hole Boundary for $[0_2/+45]_s$ Graphite/Epoxy Specimen with 1.91 cm (0.75 in.) Circular Hole Under Uniaxial Tensile Loading (Spec. No. 4A-3)

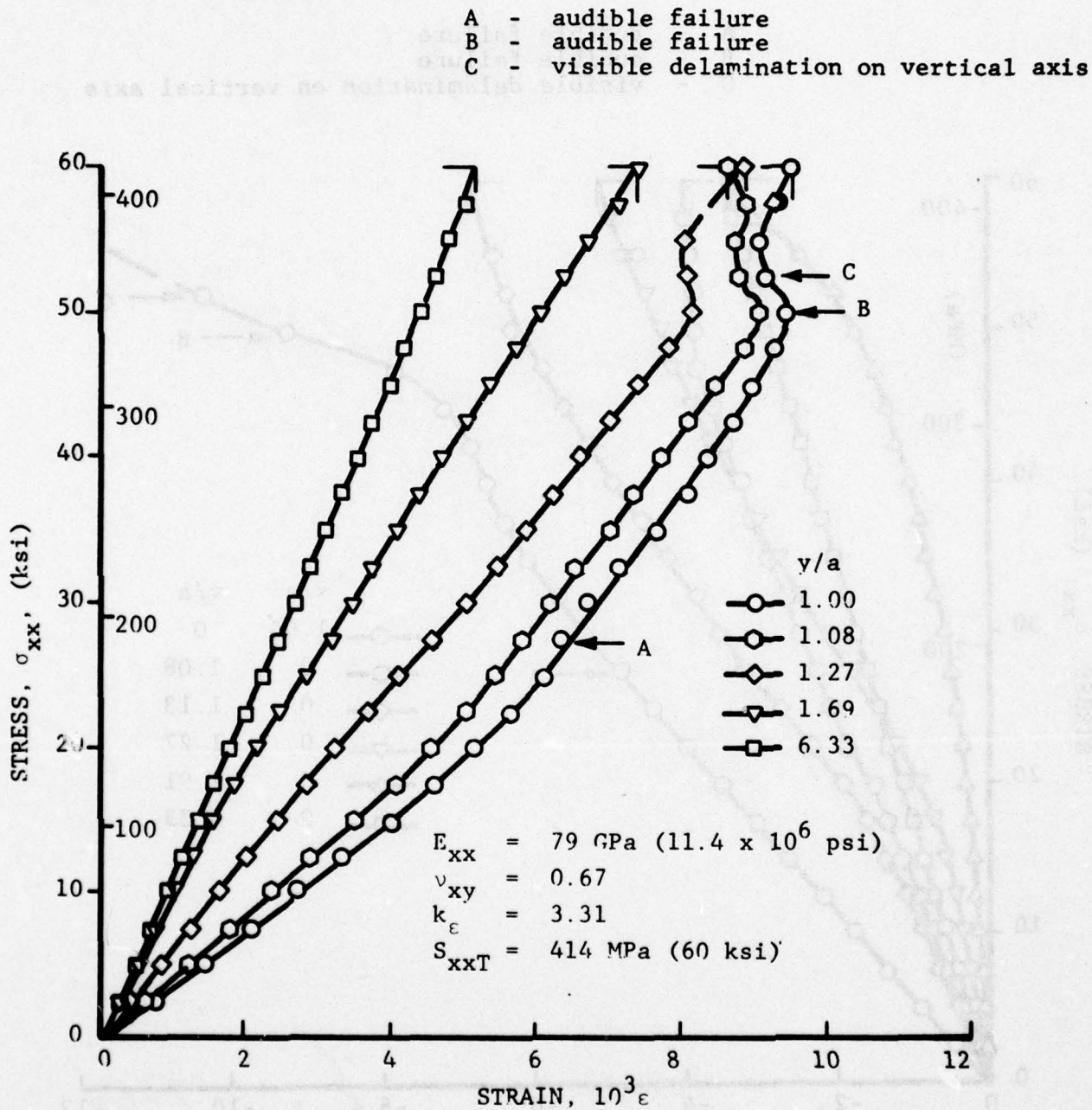


Figure 22. Vertical Strains Along Horizontal Axis of $[0_2/+45]_s$ Graphite/Epoxy Specimen with 1.91 cm (0.75 in.) Diameter Hole Under Uniaxial Tensile Loading (Spec. No. 4A-4)

- A - audible failure
- B - audible failure
- C - visible delamination on vertical axis

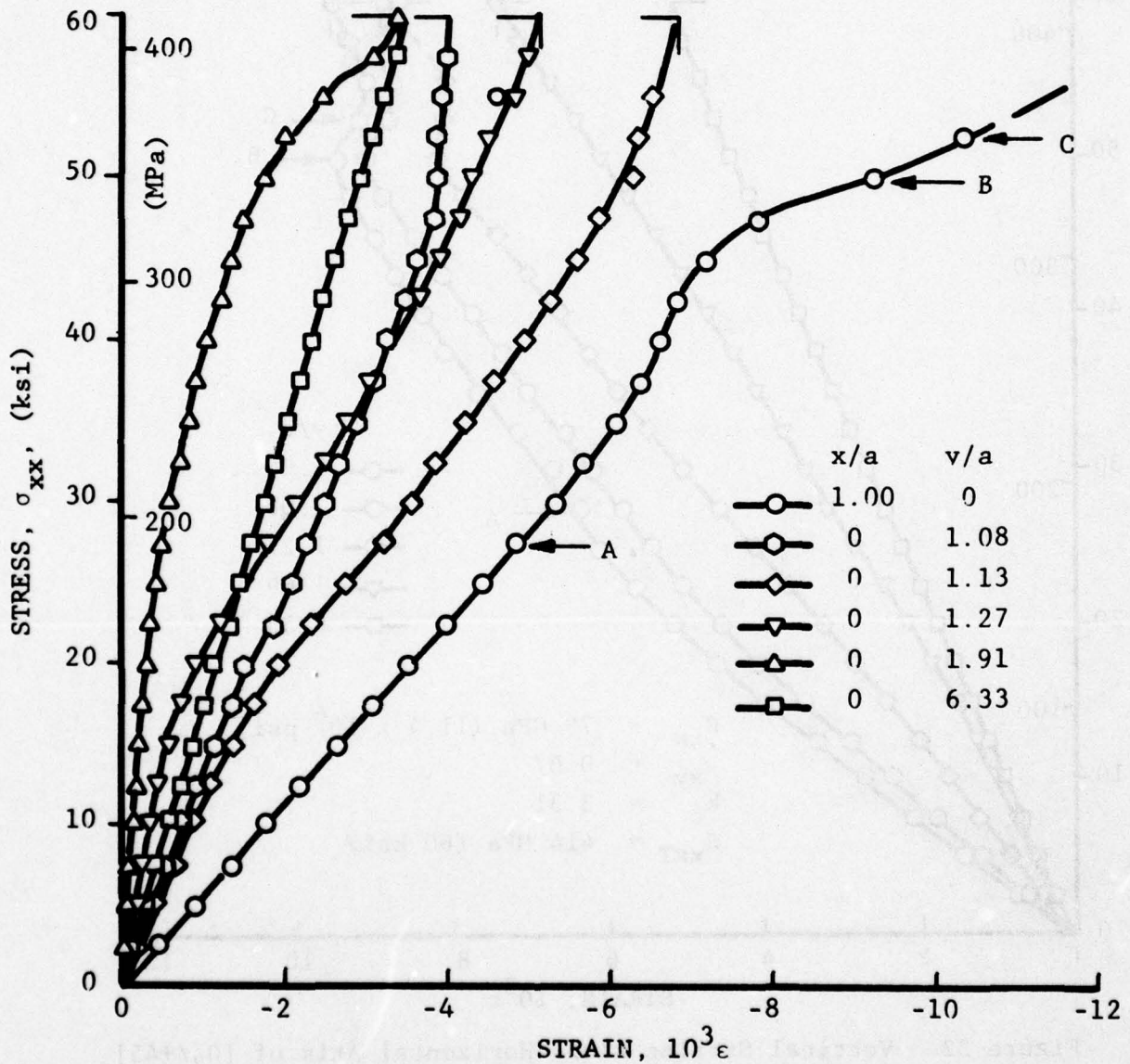


Figure 23. Horizontal Strains on the Hole Boundary and Along Horizontal Axis of $[0_2/+45]_S$ Graphite/Epoxy Specimen with 1.91 cm (0.75 in.) Diameter Hole Under Uniaxial Tensile Loading (Spec. No. 4A-4)

Specimen No. 4A-5 had a 1.27 cm (0.50 in.) diameter hole and was instrumented with strain gages and a 0.61 mm (0.024 in.) thick photoelastic coating. Strain distributions along the horizontal axis are plotted in Figure 24. The strain on the boundary of the hole is linear up to an applied stress of 172 MPa (25 ksi), thereafter it varies at a reduced rate. Values of the modulus, Poisson's ratio, strain concentration factor, strength and strength reduction ratio are:

$$\begin{aligned}
 E_{xx} &= 84 \text{ GPa } (12.2 \times 10^6 \text{ psi}) \\
 \nu_{xy} &= 0.68 \\
 (k_\epsilon)_{90^\circ} &= 3.14 \\
 S_{xxT} &= 414 \text{ MPa } (60 \text{ ksi}) \\
 k_s &= \frac{60}{116} = 0.517
 \end{aligned}$$

The value of the strain concentration factor above is lower than the theoretical value of 3.44. Isochromatic fringe patterns were similar to those obtained for specimens No. 4A-1 and No. 4A-3 before with the characteristic fringe concentrations at the off-axis locations.

Specimen No. 4A-6 with a 1.27 cm (0.50 in.) diameter circular hole was a replicate of No. 4A-5 above and was instrumented with moiré grids of 400 lines/cm (1000 lines/in.) around the hole in the horizontal and vertical directions. Strains on the boundary of the hole and in the far field obtained from moiré fringe patterns are shown in Figure 25. The maximum strain on the boundary of the hole is linear up to a stress of approximately 207 MPa (30 ksi), corresponding to a strain of 10×10^{-3} which is the ultimate strain of the unnotched laminate. Thereafter, the strain increases at a sharply lower rate. The elastic properties in the linear range and the ultimate properties for this specimen are as follows:

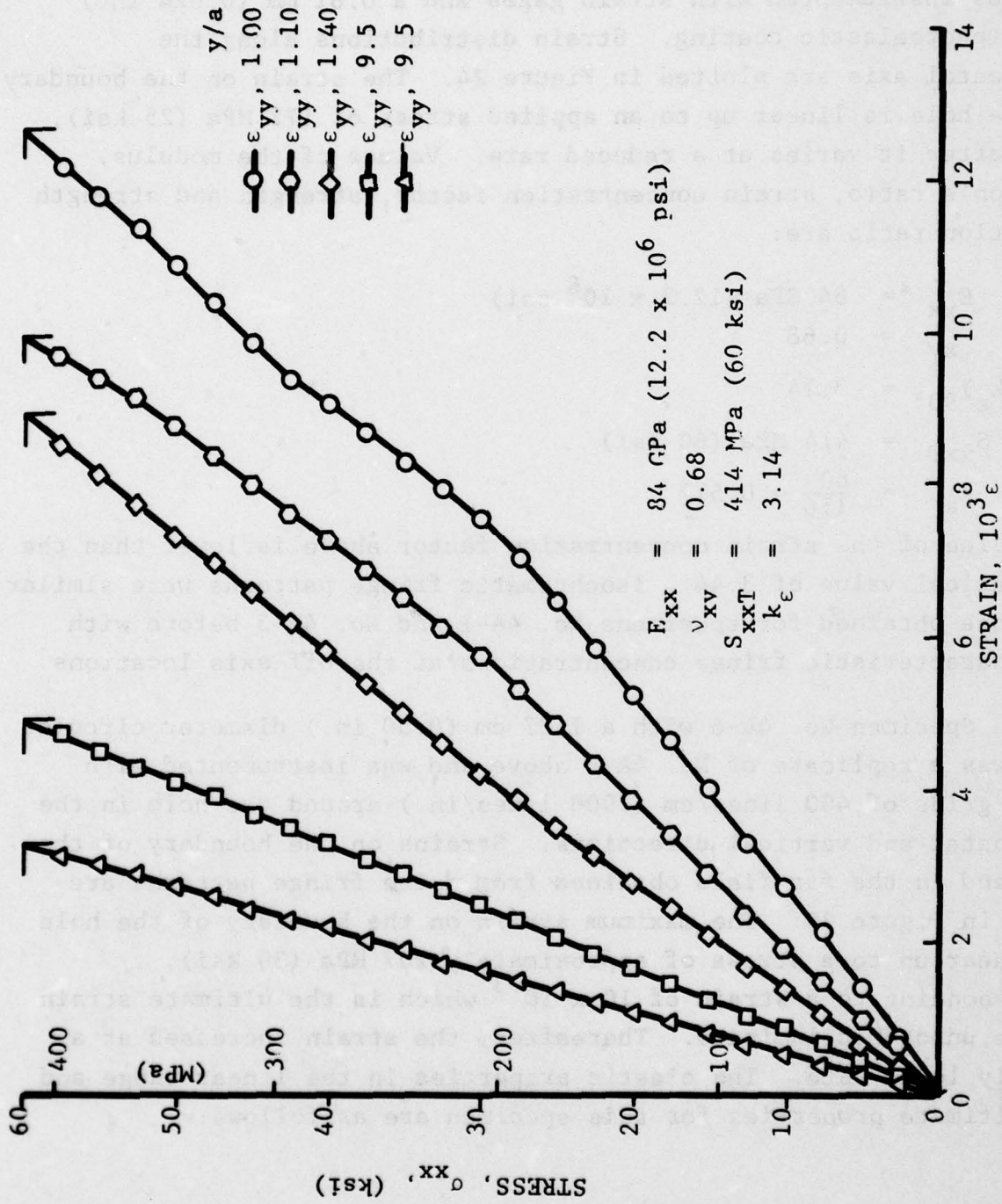


Figure 24. Strains Along Horizontal Axis of [02/+45]_s Graphite/Epoxy Specimen With 1.27 cm (0.5 in.) Circular Hole Under Uniaxial Tensile Loading (Spec. No. 4A-5)

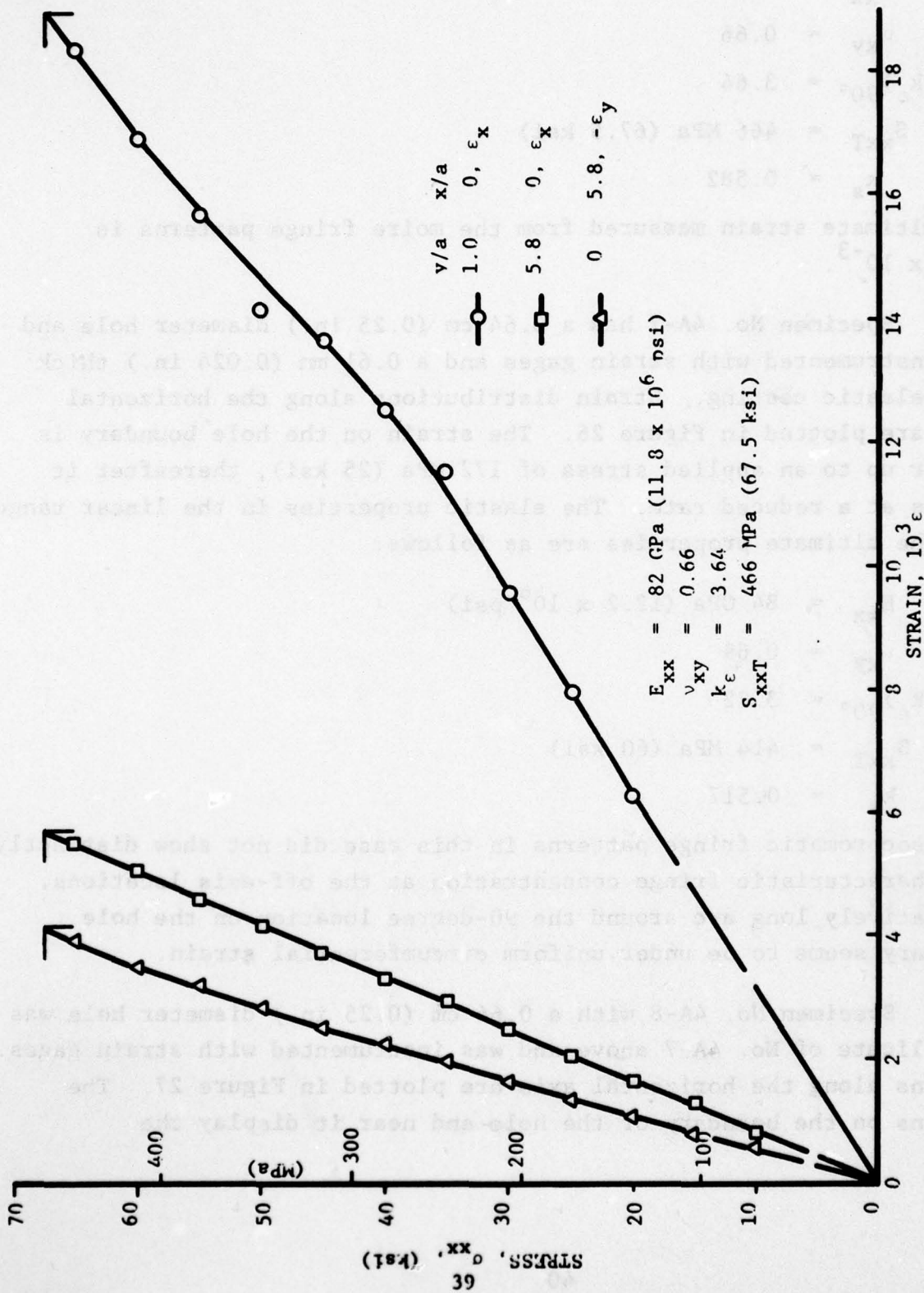


Figure 25. Strains on the Boundary of the Hole and in the Far Field of $[0_2/+45]$ s Graphite/Epoxy Specimen With 1.27 cm (0.50 in.) Diameter Hole Under Uniaxial Tensile Loading (Spec. No. 4A-6)

$$\begin{aligned}
E_{xx} &= 82 \text{ GPa } (11.8 \times 10^6 \text{ psi}) \\
\nu_{xy} &= 0.66 \\
(k_{\epsilon})_{90^{\circ}} &= 3.64 \\
S_{xxT} &= 466 \text{ MPa } (67.5 \text{ ksi}) \\
k_s &= 0.582
\end{aligned}$$

The ultimate strain measured from the moire fringe patterns is 19.5×10^{-3} .

Specimen No. 4A-7 had a 0.64 cm (0.25 in.) diameter hole and was instrumented with strain gages and a 0.61 mm (0.024 in.) thick photoelastic coating. Strain distributions along the horizontal axis are plotted in Figure 26. The strain on the hole boundary is linear up to an applied stress of 172 MPa (25 ksi), thereafter it varies at a reduced rate. The elastic properties in the linear range and the ultimate properties are as follows:

$$\begin{aligned}
E_{xx} &= 84 \text{ GPa } (12.2 \times 10^6 \text{ psi}) \\
\nu_{xy} &= 0.69 \\
(k_{\epsilon})_{90^{\circ}} &= 3.22 \\
S_{xxT} &= 414 \text{ MPa } (60 \text{ ksi}) \\
k_s &= 0.517
\end{aligned}$$

The isochromatic fringe patterns in this case did not show distinctly the characteristic fringe concentration at the off-axis locations. A relatively long arc around the 90-degree location on the hole boundary seems to be under uniform circumferential strain.

Specimen No. 4A-8 with a 0.64 cm (0.25 in.) diameter hole was a replicate of No. 4A-7 above and was instrumented with strain gages. Strains along the horizontal axis are plotted in Figure 27. The strains on the boundary of the hole and near it display the

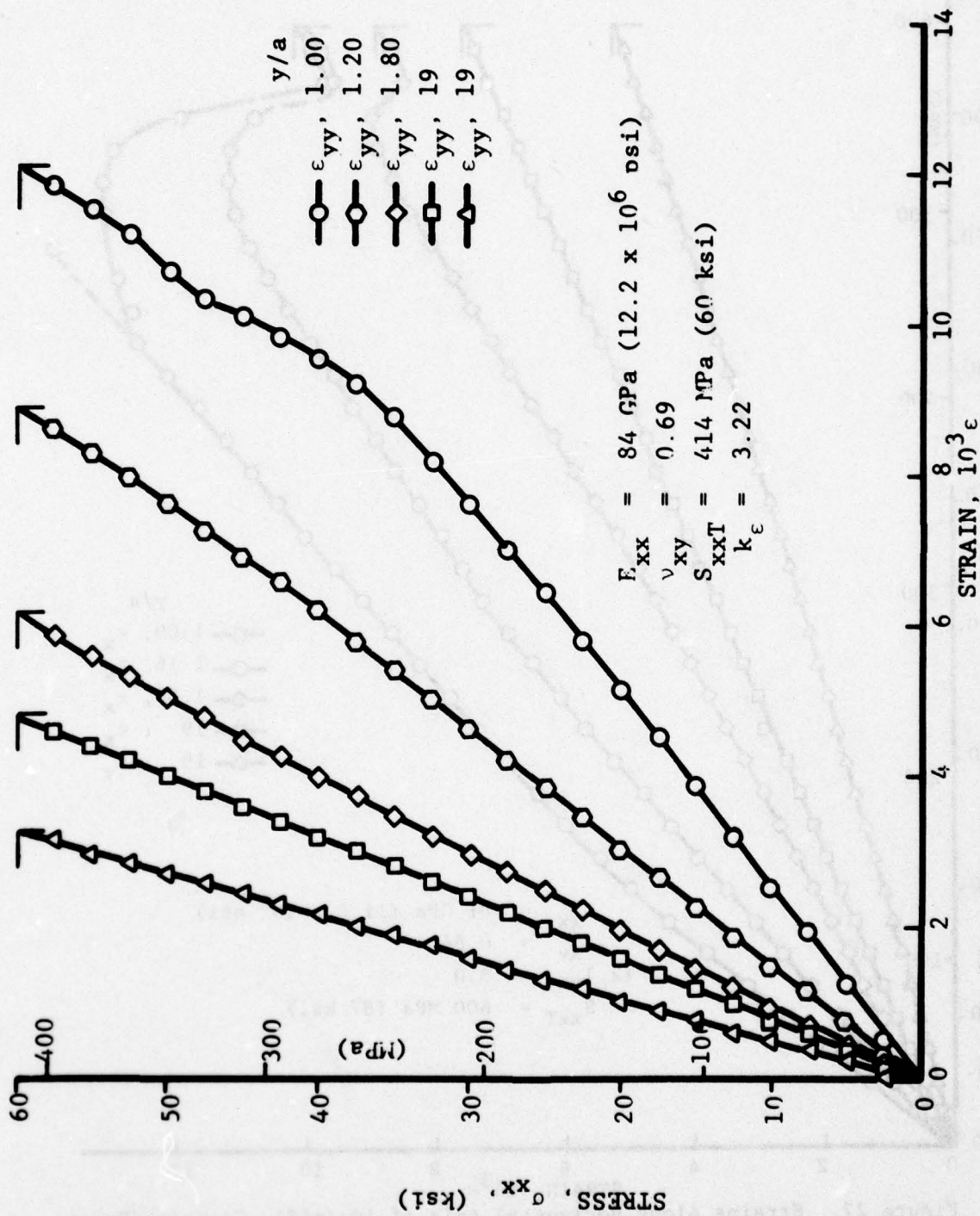


Figure 26. Strains Along Horizontal Axis of $[0_2/+45]_s$ Graphite/Epoxy Specimen With 0.64 cm (0.25 in.) Circular Hole Under Uniaxial Tensile Loading (Spec. No. 4A-7)

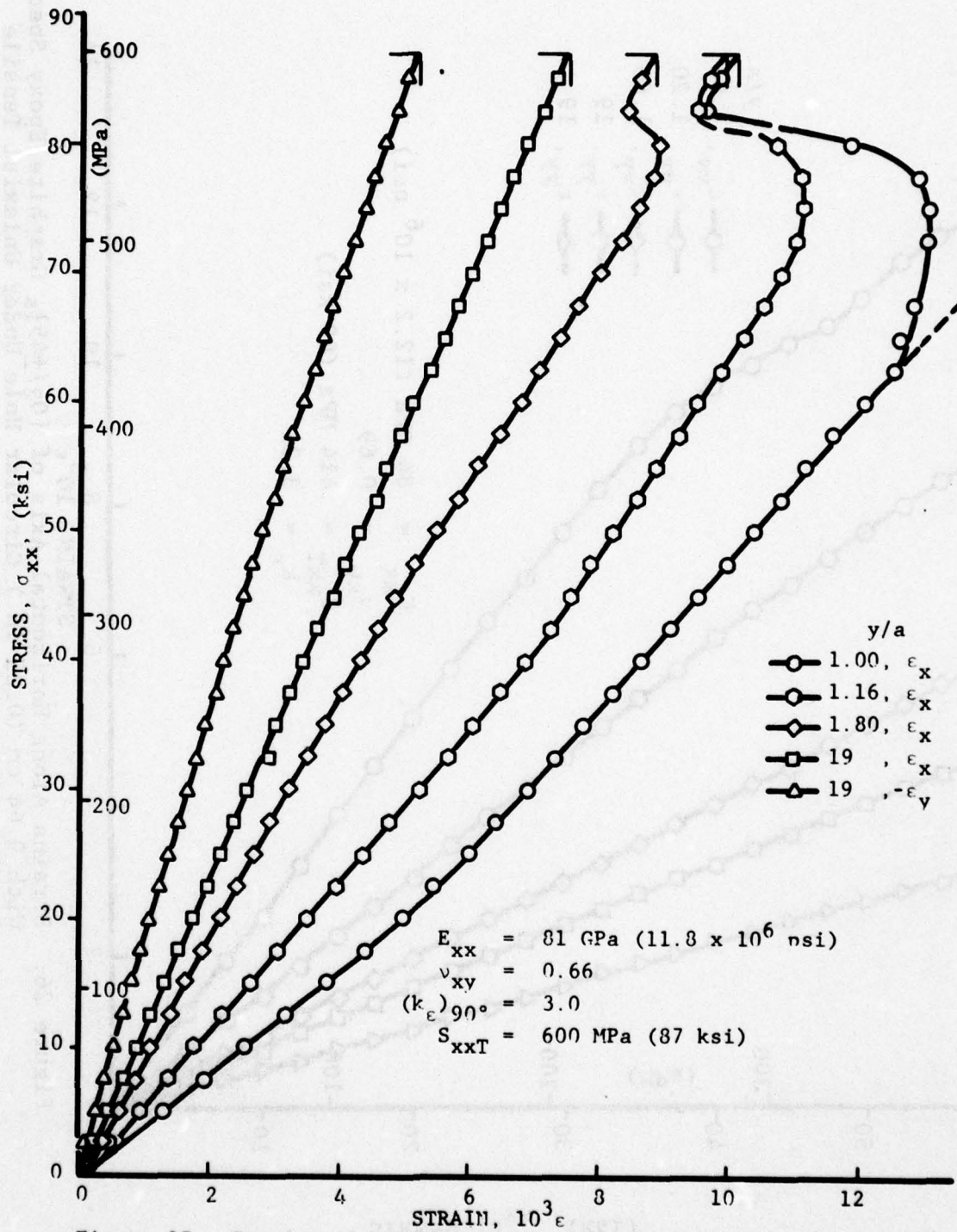


Figure 27. Strains Along Horizontal Axis of $[0_2/+45]_s$ Graphite/Epoxy Specimen With 0.64 cm (0.25 in.) Diameter Hole Under Uniaxial Tensile Loading (Spec. No. 4A-8)

characteristic bilinear behavior. The maximum strain becomes nonlinear first at a stress of 138 MPa (20 ksi), thereafter it increases nearly linearly at a lower rate up to a stress of 431 MPa (62.5 ksi). At this level the outer 0-degree strips along the vertical axis of the specimen through the hole started separating, thereby blunting the strain concentration. Final failure occurred away from the hole after the specimen had separated essentially into two strips. The elastic properties in the linear range and the ultimate properties are as follows:

$$\begin{aligned}E_{xx} &= 81 \text{ GPa } (11.8 \times 10^6 \text{ psi}) \\ \nu_{xy} &= 0.66 \\ (k_\epsilon)_{90^\circ} &= 3.0 \\ S_{xxT} &= 600 \text{ MPa } (87 \text{ ksi}) \\ k_s &= 0.750\end{aligned}$$

Several additional plates of $[0_2/\pm 45]_s$ layup with central circular holes were prepared and tested under uniaxial tensile loading. Typical failure modes are illustrated in Figure 28. Specimens No. 4A-9 through 4A-12 had holes of 2.54 cm (1 in.), 1.91 cm (0.75 in.), 1.27 cm (0.50 in.) and 0.64 cm (0.25 in.) diameter. They were instrumented with strain gages on the boundary of the hole and in the far-field. Additional specimens 2.54 cm (1 in.) wide with holes of diameters 4.76 mm (0.187 in.), 3.17 mm (0.125 in.), 1.57 mm (0.062 in.), and 0.41 mm (0.016 in.) were tested. All specimens with 0.41 mm (0.016 in.) holes and most specimens with 1.57 mm (0.062 in.) diameter holes failed away from the hole, thus indicating a strength reduction ratio of unity.

5. EFFECT OF HOLE DIAMETER

Results for all specimens with holes of diameters between 0.64 cm (0.25 in.) and 2.54 cm (1 in.) are tabulated in Table 5.

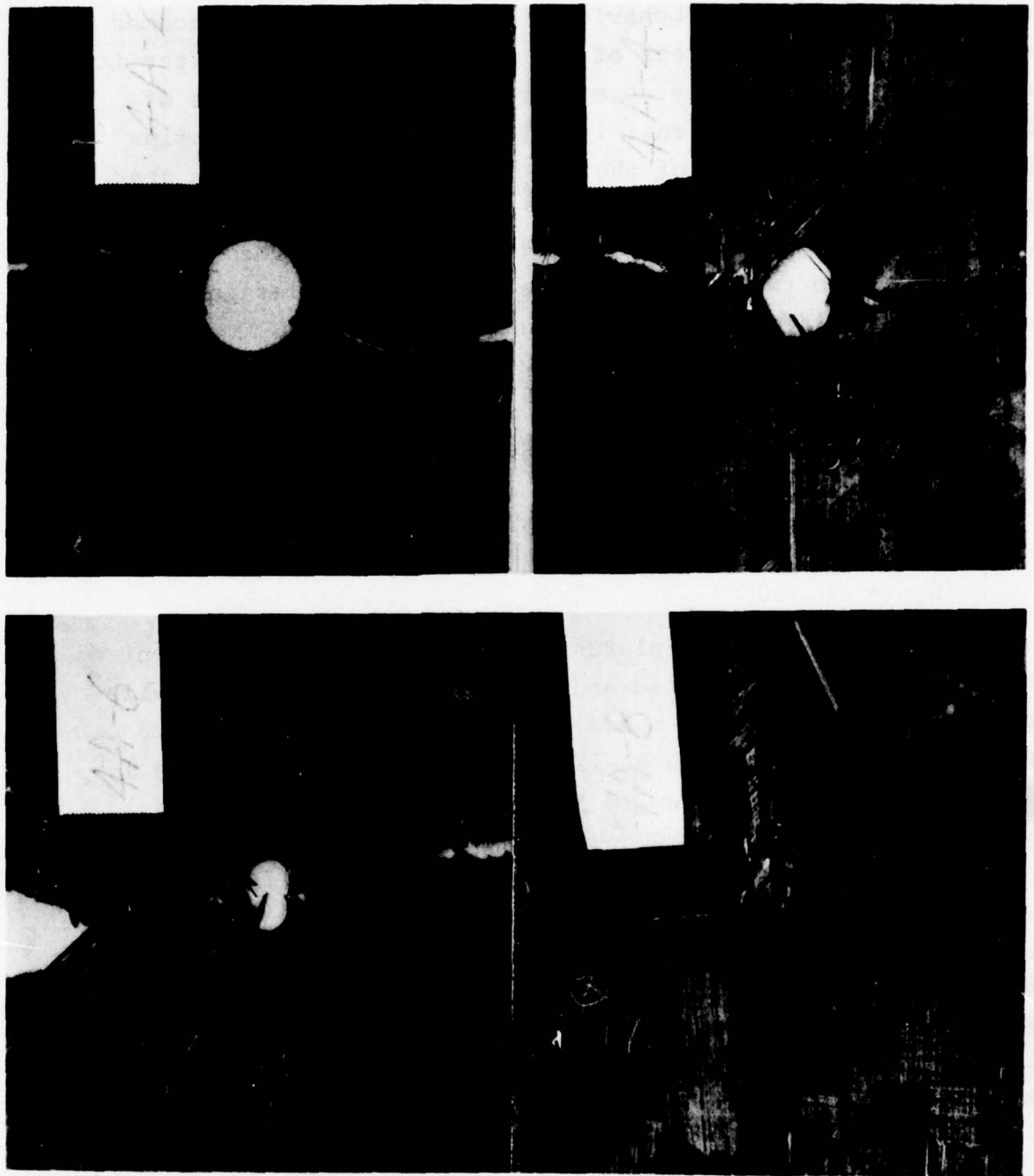


Figure 28. Failure Patterns in $[0_2/+45]_s$ Graphite/Epoxy Specimens With Holes of Various Sizes Under Uniaxial Tension. (Hole Diameters are 2.54 cm (1 in.), 1.91 cm (0.75 in.), 1.27 cm (0.50 in.) and 0.64 cm (0.25 in.)

Table 5
UNIAXIAL $[0_2/+45]_s$ LAMINATES WITH CIRCULAR HOLES

Spec. No.	Hole Diameter $2a$ (in.)	Modulus E_{xx} (10^6 psi)	Poisson's Ratio, ν_{xy}	Strain Concentration Factor		Strength S_{xxT} (ksi)	Maximum Strain at Failure ($10^{-3}\epsilon$)	Strength Reduction Ratio S_{xxT}/S_0
				$(k_\epsilon)_{90^\circ}$	$(k_\epsilon)_{0^\circ}$			
4A-1	2.54 (1.00)	84 (12.1)	0.70	3.27	-	445 (65)	12.3	0.560
4A-2	2.54 (1.00)	81 (11.8)	0.59	3.43	-2.26	376 (55)	11.3	0.470
4A-9	2.54 (1.00)	83 (12.0)	0.62	3.02	-2.22	397 (58)	10.0	0.496
4A-3	1.91 (0.75)	84 (12.2)	0.60	3.37	-	362 (53)	11.8	0.453
4A-4	1.91 (0.75)	79 (11.4)	0.67	3.31	-2.03	414 (60)	9.5	0.517
4A-10	1.91 (0.75)	81 (11.7)	0.62	3.20	-	397 (58)	10.2	0.496
4A-5	1.27 (0.50)	84 (12.2)	0.68	3.14	-	414 (60)	12.7	0.517
4A-6	1.27 (0.50)	82 (11.8)	0.66	3.64	-	466 (68)	-	0.582
4A-11	1.27 (0.50)	82 (11.8)	0.63	3.04	-	486 (71)	12.1	0.608
4A-7	0.64 (0.25)	84 (12.2)	0.69	3.22	-	414 (60)	12.1	0.517
4A-8	0.64 (0.25)	81 (11.8)	0.66	3.00	-	600 (87)	13.1	0.750
4A-12	0.64 (0.25)	81 (11.8)	0.62	-	-	642 (93)	-	0.802

The average values for modulus, Poisson's ratio and strain concentration factors for twelve specimens are:

$$\begin{aligned} E_{xx} &= 82 \text{ GPa } (11.9 \times 10^6 \text{ psi}) \\ \nu_{xy} &= 0.65 \\ (k_\epsilon)_{90^\circ} &= 3.24 \\ (k_\epsilon)_{0^\circ} &= -2.17 \end{aligned}$$

Theoretical values for the strain concentration factors are $(k_\epsilon)_{90^\circ} = 3.44$ and $(k_\epsilon)_{0^\circ} = -1.85$. Values of the strength reduction ratio for these twelve specimens range between 0.470 and 0.802. The maximum strain measured on the hole boundary at failure ranges between 9.5×10^{-3} and 13.1×10^{-3} compared to an ultimate strain of 10×10^{-3} for the unnotched laminate in the 0-deg. direction.

The hole size effect was described using the average stress criterion for the $[0_2/\pm 45]_s$ laminate under uniaxial loading proposed by Whitney and Nuismer (Reference 4) and applied in the case of the $[0/\pm 45/90]_s$ laminate in the first phase of this work (Reference 1). For this purpose, an approximate expression suggested by Konish and Whitney (Reference 5) was used for the stress distribution along the horizontal axis through the hole:

$$\frac{\sigma_y(x,0)}{\sigma_o} \approx \left[1 + \frac{1}{2} \rho^{-2} + \frac{3}{2} \rho^{-4} - \frac{k_\sigma^{-3}}{2} (5\rho^{-6} - 7\rho^{-8}) \right]$$

where

$$\begin{aligned} \sigma_y(x,0) &= \text{vertical (axial) stress along horizontal axis} \\ \sigma_o &= \text{applied far-field stress} \\ \rho &= \frac{x}{a} \\ a &= \text{hole radius} \\ k_\sigma &= \text{anisotropic stress concentration factor} \end{aligned}$$

According to the average stress criterion applied in this case, failure occurs when the axial stress averaged over a distance a_o from the hole boundary equals the unnotched tensile strength

of the laminate. The strength reduction ratio computed for this criterion is

$$k_s = \frac{2}{(1+\xi) [2+\xi^2+(k_o-3)\xi b]}$$

where

$$\xi = \frac{a}{a+a_o}$$

a_o = characteristic length dimension

Experimental results for the strength reduction ratio are in good agreement with theoretical ones based on the average stress criterion for a characteristic length of $a_o = 5$ mm (Figure 29). The only discrepancies occur for very small and large diameter holes. In the former case, the average stress criterion does not predict the fact that there is a critical hole (notch) size below which the laminate becomes insensitive to it. In the case of large holes local buckling in the compressively stressed part of the hole boundary causes more stress redistribution around the hole near the horizontal axis and alters the failure mode.

6. SUMMARY AND CONCLUSIONS

An experimental study was conducted of the deformation and failure of uniaxially loaded $[0_2/+45]_s$ graphite/epoxy plates with holes of various diameters. Experimental methods used were strain gages, birefringent coatings and moiré grids. The hole diameters investigated ranged between 2.54 cm (1 in.) and 0.41 mm (0.016 in.).

In the linear range, the measured stress (strain) concentration factor on the horizontal axis 3.24 is somewhat lower than the theoretical value of 3.44. The compressive strain concentration factor on the vertical axis -2.17 is higher than the theoretical value of -1.85. Strains on the hole boundary on the horizontal axis become nonlinear at an applied stress of approximately 173 MPa (25 ksi) corresponding to a local strain of 0.0065. Thereafter, the maximum strain on the hole boundary increases nearly linearly at a

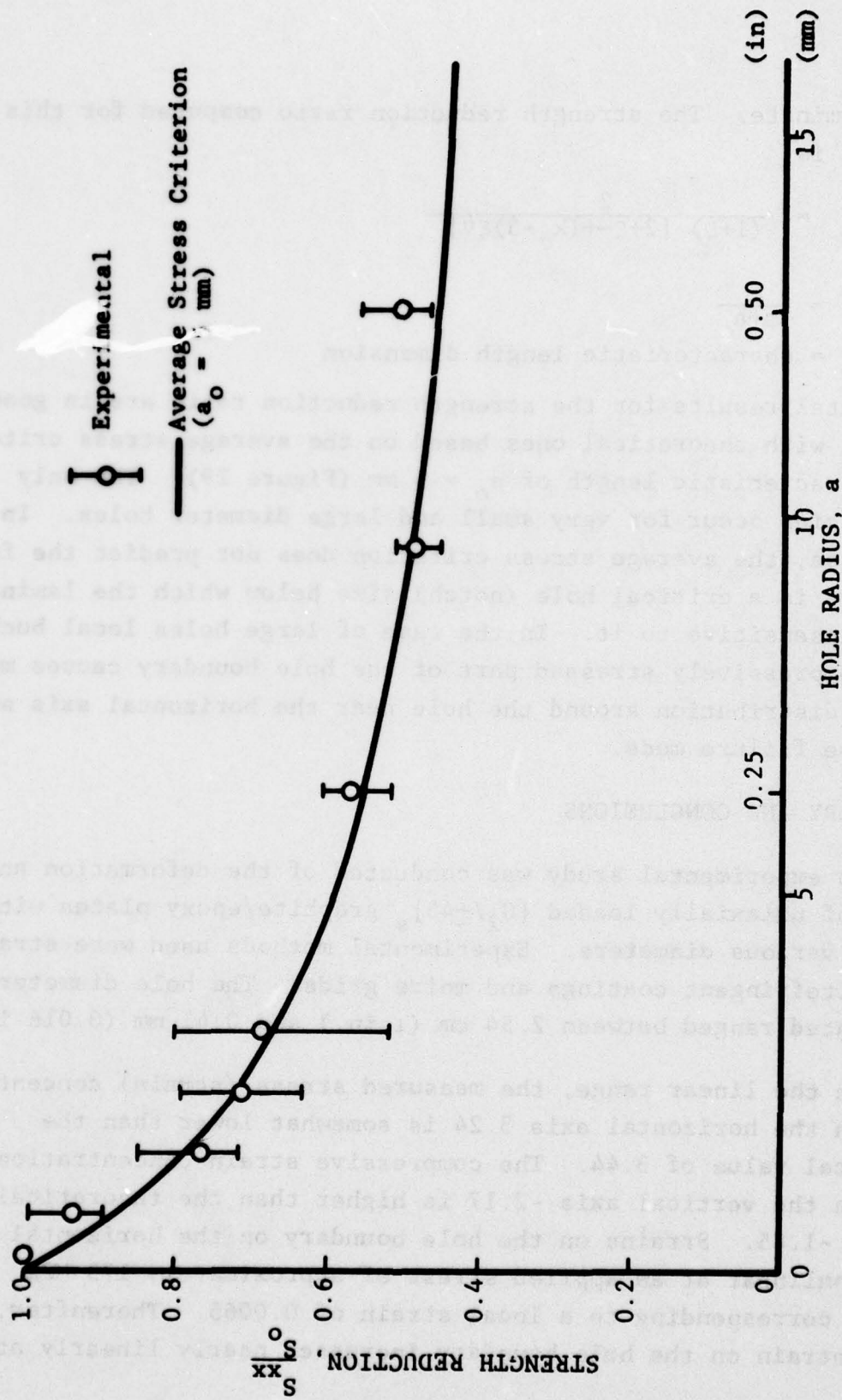


Figure 29. Strength Reduction as a Function of Hole Radius for [02/+45]s Graphite/Epoxy Plates With Circular Holes Under Uniaxial Tensile Loading

much reduced rate. The level of first nonlinearity above corresponds to a strain level of over 0.004 on the hole boundary at the 0-degree location. The strain response of the unnotched $[0_2/+45]_s$ laminate in the 90-degree direction becomes appreciably nonlinear at this strain level (Figures 11 and 12). This material nonlinearity at the 0-degree location on the hole boundary produces a stress redistribution around the hole boundary resulting in nonlinear response at the 90-degree location. A second level of pronounced nonlinearity occurs as a result of stress and strain redistribution produced by localized compressive failure (delamination) on the hole boundary around the vertical axis. Maximum measured strains at failure on the hole boundary are somewhat higher than the ultimate strain of the unnotched laminate.

In the specimens with larger holes failure initiates at locations around the circumference approximately 72-degrees from the load axis, at points of high strain concentration with nonlinear response. In the case of smaller holes the outer 0-degree plies through the hole tend to separate and thus reduce or eliminate the strain concentration at the 90-degree location.

The strength reduction ratio ranges between 0.470 and 0.802 for holes between 2.5 cm and 0.64 cm in diameter. The effect of hole diameter can be described satisfactorily by using the average stress criterion with a characteristic length of $a_0 = 5$ mm. There is a critical hole diameter, approximately 1.57 mm (0.062 in.), below which the laminate becomes insensitive to it, i.e., failure is as likely to occur through the hole as elsewhere.

SECTION V
BIAXIAL TESTS OF PLATES WITH HOLES

1. SPECIMENS

The specimens were 8-ply $[0_2/+45]_s$ 40 cm x 40 cm (16 in. x 16 in.) graphite/epoxy plates. Corners of approximately 5 cm x 5 cm (2 in.) sides were cut off from these plates. These plates were then tabbed with 5-ply crossply glass/epoxy tabs having the outer fibers parallel with the 0-degree fibers of the graphite/epoxy laminate. These tabs had a circular cutout in the center of 20.3 cm (8 in.) diameter. A sketch of this specimen is shown in Figure 30. Central circular holes were drilled in the specimens with diamond core drills. Four hole diameters, 2.54 cm (1 in.), 1.91 cm (0.75 in.), 1.27 cm (0.50 in.) and 0.64 cm (0.25 in.), were investigated. Two specimens were tested for each hole diameter.

2. STRAIN MEASUREMENT

Deformations and strains were measured using strain gages, birefringent coatings and moiré grids. Strain gages were mounted on the hole boundary, near it and in the far field along the horizontal (x-) and vertical (y-) axes of symmetry. In most cases birefringent coatings 0.5 mm (0.02 in.) and 1 mm (0.04 in.) thick were used on one side of the specimen.

3. LOADING AND DATA RECORDING

Four 0.95 cm (0.037 in.) diameter holes were provided on each side of the tabbed specimen for bolting individual pairs of metal grips approximately 5 cm (2 in.) wide and 10 cm (4 in.) long. Loading was introduced by means of four whiffle-tree grip linkages designed to ensure that four equal loads were applied to each side of the specimen. A photograph of a biaxial specimen with the loading grip linkages is shown in Figure 31.

Load was applied by means of two pairs of hydraulic jacks attached to the four sides of a reaction frame. The load was

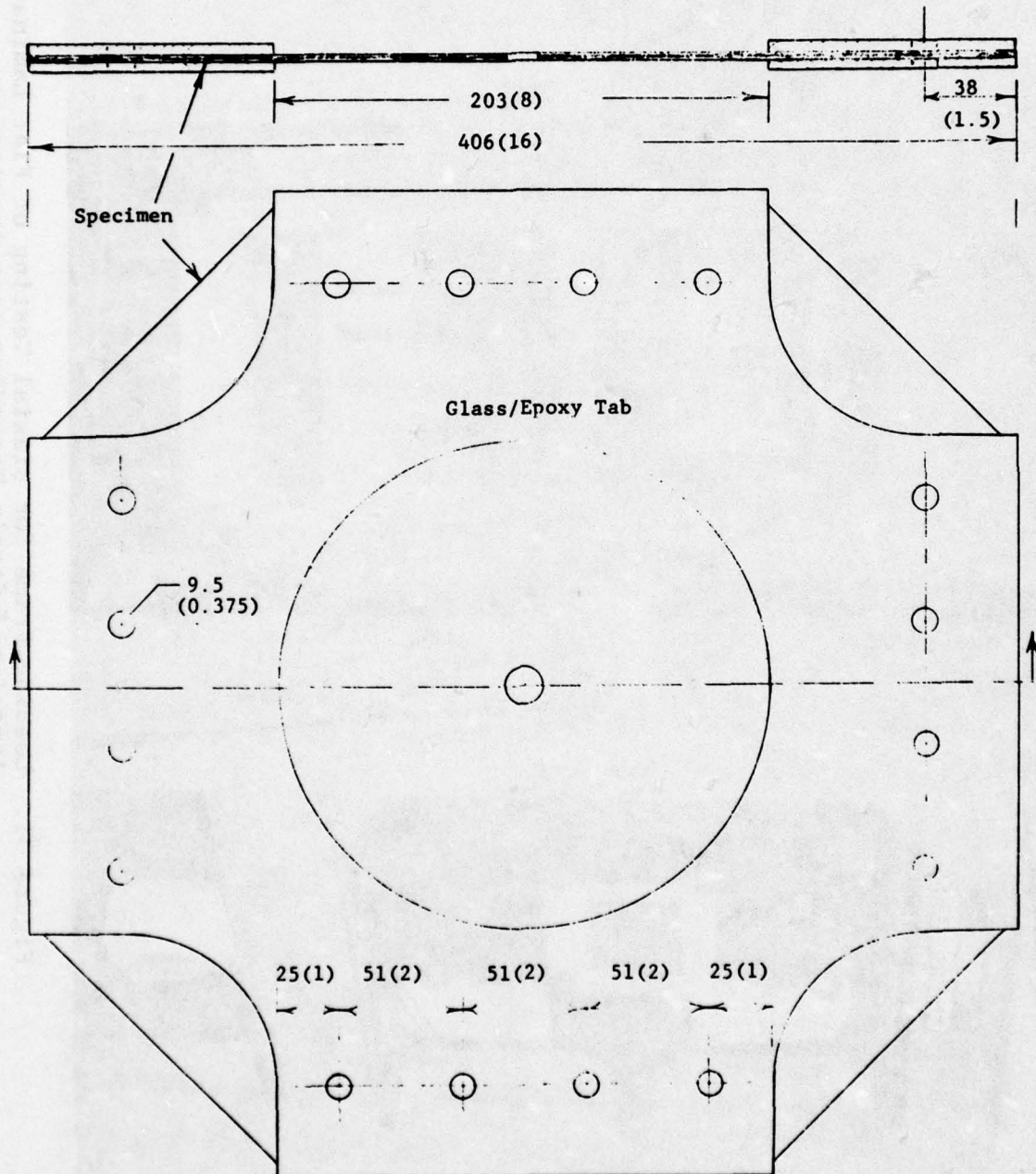


Figure 30. Sketch of Biaxial Composite Specimen (Dimensions are in mm and inches)

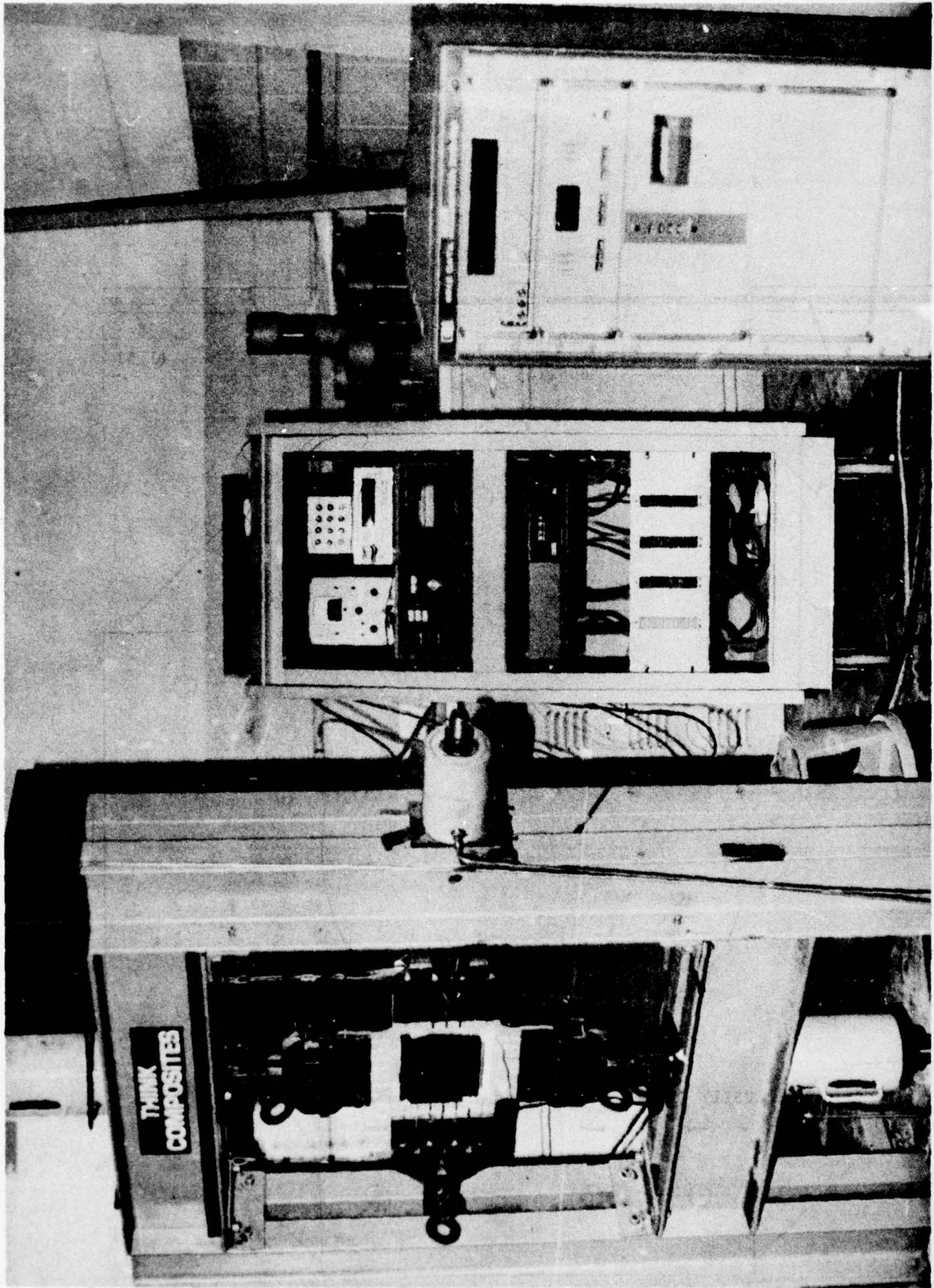


Figure 31. Loading Frame for Biaxial Testing of Flat Laminates and Associated Strain Recording Instrumentation

transmitted from the hydraulic cylinders to the grip linkages through cylindrical rods going through the bore of these cylinders. The rods were instrumented with strain gages and calibrated in a testing machine to establish the exact relationship between loads and strain gage signals. These strain gage readings were used subsequently both for recording the exact loads applied to the specimen and as feedback signals for controlling the pressures by means of the servohydraulic system used.

The specimens were loaded in increments under a 2:1 biaxial tension with the highest load in the direction of the 0-degree fibers. At each load level strains and loads were recorded with a digital data acquisition system and photoelastic and moire fringes recorded photographically.

The relationship between the input loads and the effective stress for the specimen geometry used and stress biaxiality desired was established by preliminary calibration tests. Unnotched specimens of $[0_2/+45]_s$ layup tabbed as described above were instrumented with strain gages at the center and at far-field locations. The principal strains at the center of this unnotched plate are related to the effective stresses σ_{11} and σ_{22} by

$$\epsilon_{11} = S_{11} \sigma_{11} + S_{12} \sigma_{22} = \frac{1}{E_{11}} (\sigma_{11} - \nu_{12} \sigma_{22})$$

$$\epsilon_{22} = S_{12} \sigma_{11} + S_{22} \sigma_{22} = \frac{1}{E_{22}} (\sigma_{22} - \nu_{21} \sigma_{11})$$

where directions 1 and 2 are parallel and normal to the 0-deg. fibers, respectively. Substituting the measured values of the material constants

$$E_{11} = 81 \text{ GPa } (11.8 \times 10^6 \text{ psi})$$

$$E_{22} = 24 \text{ GPa } (3.46 \times 10^6 \text{ psi})$$

$$\nu_{12} = 0.65$$

$$\nu_{21} = 0.20$$

and the desired biaxiality relation $\sigma_{11} = 2\sigma_{22}$, we obtain

$$\epsilon_{22} = 1.52\epsilon_{11}.$$

The input load ratio was adjusted until the desired strain ratio above was obtained at the center of the plate.

4. RESULTS

Specimen No. 6A-1 had a 2.54 cm (1.00 in.) central circular hole. It was instrumented with a 0.5 mm (0.02 in.) photoelastic coating and strain gages on the hole boundary, near it and in the far-field along the horizontal and vertical axes. The specimen was loaded in biaxial tension producing a 2:1 ratio of effective stresses in the vicinity of the hole. The variation of strains with effective far-field vertical stress (in the 0-deg. direction) is shown in Figures 32 and 33. On the horizontal axis, the strain on the hole boundary is linear up to an applied vertical stress of 138 MPa (20 ksi), thereafter this strain as well as vertical strains near it increase at a decreasing rate. This is a result of stress redistribution around the hole boundary caused by fracture initiation at points off the horizontal axis. This phenomenon was more pronounced under uniaxial loading. On the vertical axis the strain on the hole boundary remains linear up to an applied vertical stress of 255 MPa (37 ksi) whereas strains near it become nonlinear earlier at a stress of approximately 159 MPa (23 ksi).

Stress ratios were computed at two locations on the hole boundary for the linear range of response:

$$\left(\frac{\sigma_{\theta\theta}}{\sigma_{yy}}\right)_{\theta=0^\circ} = 0.55$$

$$\left(\frac{\sigma_{\theta\theta}}{\sigma_{yy}}\right)_{\theta=90^\circ} = 2.12$$

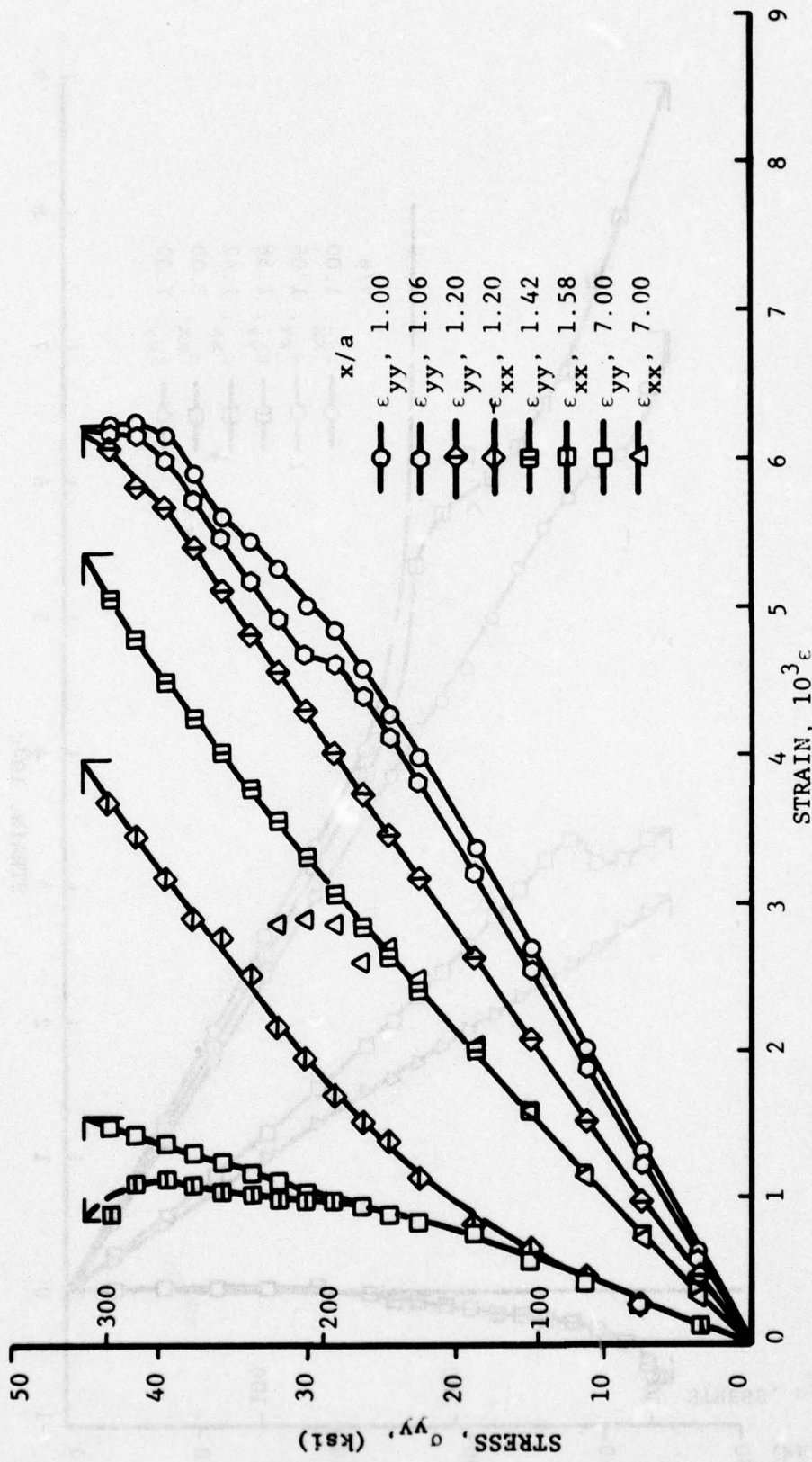


Figure 32. Strains Along Horizontal Axis of $[0_2/+45]_s$ Graphite/Epoxy Specimen With 2.54 cm (1.00 in.) Diameter Hole Under Biaxial Loading $\sigma_{yy} = 2\sigma_{xx}$ (Spec. No. 6A-1)

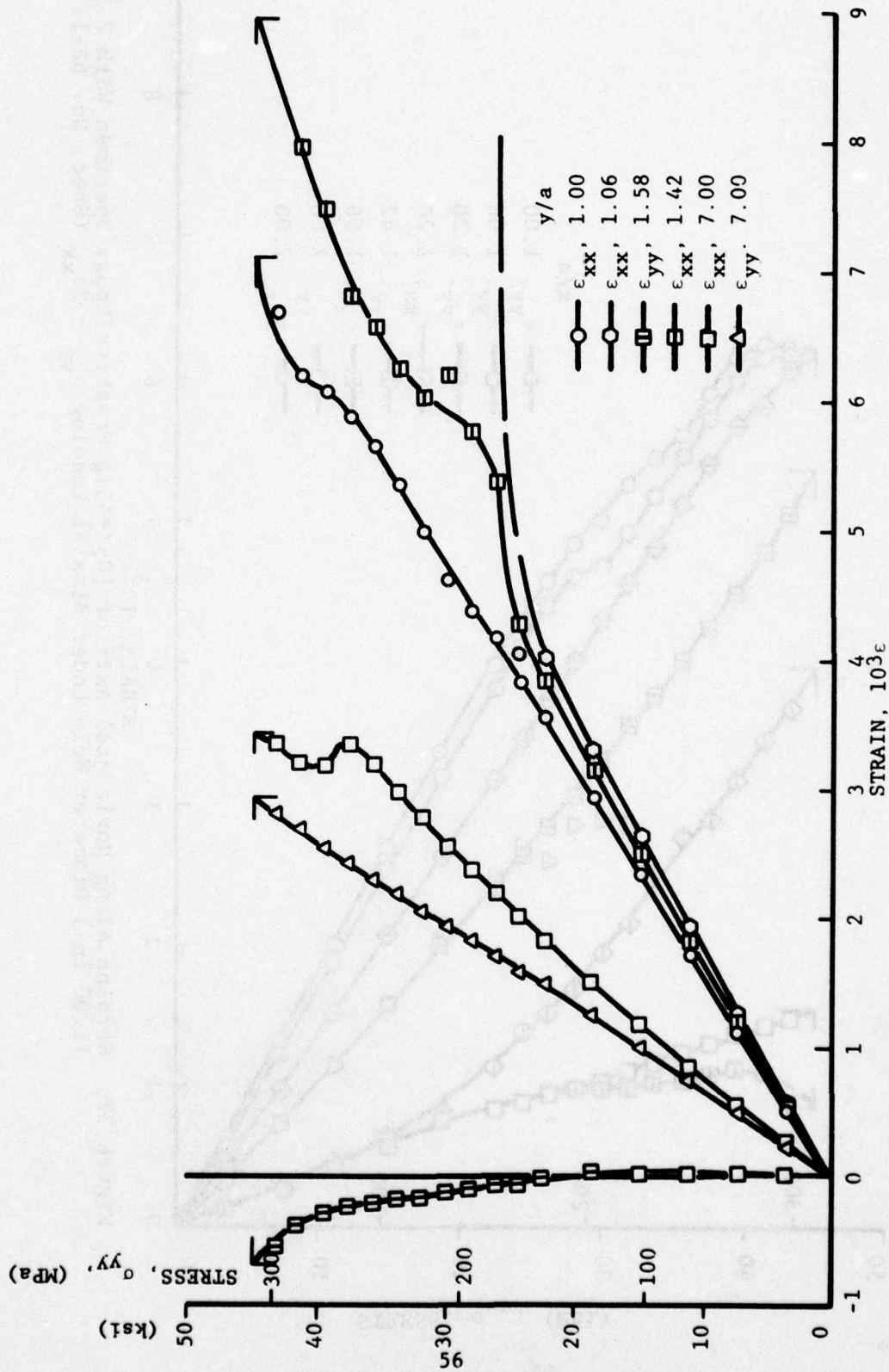


Figure 33. Strains Along Vertical Axis of [02/+45]_s Graphite/Epoxy Specimen With 2.54 cm (1.00 in.) Diameter Hole Under Biaxial Loading $\sigma_{yy} = 2\sigma_{xx}$ (Spec. No. 6A-1)

The corresponding theoretical values for these ratios based on linear anisotropic elasticity are 0.62 and 2.51.

Isochromatic fringe patterns in the photoelastic coating around the hole are shown in Figure 34 for various levels of applied stress σ_{yy} . Characteristic points of birefringence concentration develop at points 22.5-deg. off the horizontal axis only. Visible failure initiated at one of these points at a stress of approximately 276 MPa (40 ksi). The variation of fringe order and strain with stress at the 0-, 67.5- and 90-deg. locations is plotted in Figure 35. The first nonlinear response occurs at the 67.5-deg. location at a stress of approximately 172 MPa (25 ksi). Fracture initiation is followed by localized unloading on the hole boundary around the 90-deg. location.

Failure is preceded by extensive delamination of the outer 0-deg. plies near the vertical axis as shown by the strain readings of Figure 33. This delamination starts early, at around 40 percent of the ultimate load. Ultimate failure took the form of vertical cracks starting at two characteristic points off the horizontal axis (Figure 36). The vertical stress at failure was 311 MPa (45.1 ksi).

Specimen No. 6A-2 with a 2.54 cm (1.00-in.) central circular hole was a replicate of No. 6A-1 above. It was instrumented with strain gages and 400 lines/cm (1000 lpi) moire rulings in the two loading directions. The specimen was loaded in biaxial tension producing a 2:1 ratio of effective stresses in the vicinity of the hole. The variation of strains obtained from strain gages along the two loading axes is shown in Figures 37 and 38. On the horizontal axis the strains on the hole boundary and near it are linear up to an applied vertical stress of 155 MPa (22 ksi), thereafter they increase at a decreasing rate. On the vertical

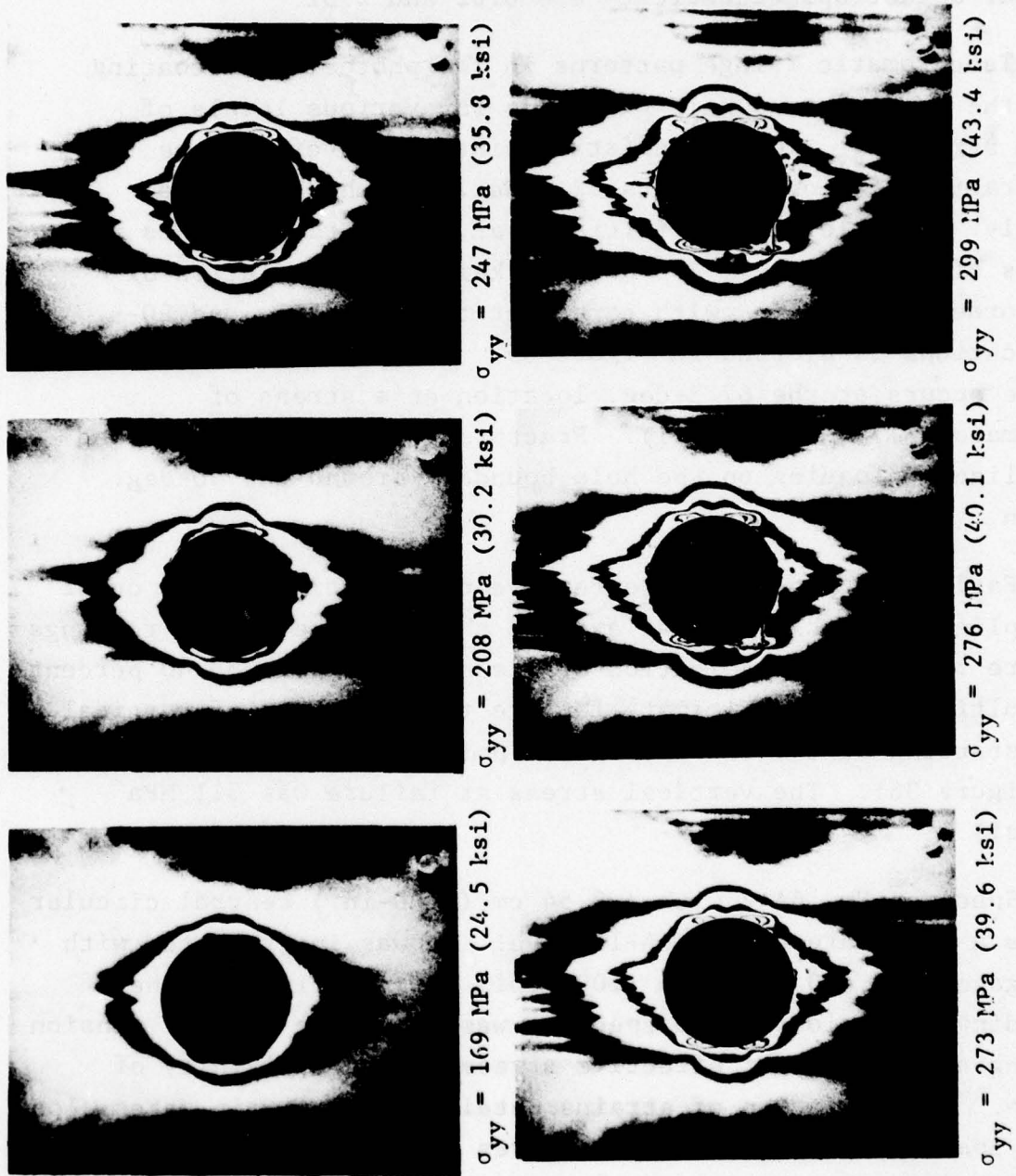


Figure 34. Isochromatic Fringe Patterns in Photoelastic Coating Around 2.54 cm (1.00 in.) Diameter Hole in $[0_2/+45]_s$ Graphite/Epoxy Specimen Under Biaxial Loading $\sigma_{yy} = 2\sigma_{xx}$ (Spec. No. 6A-1)

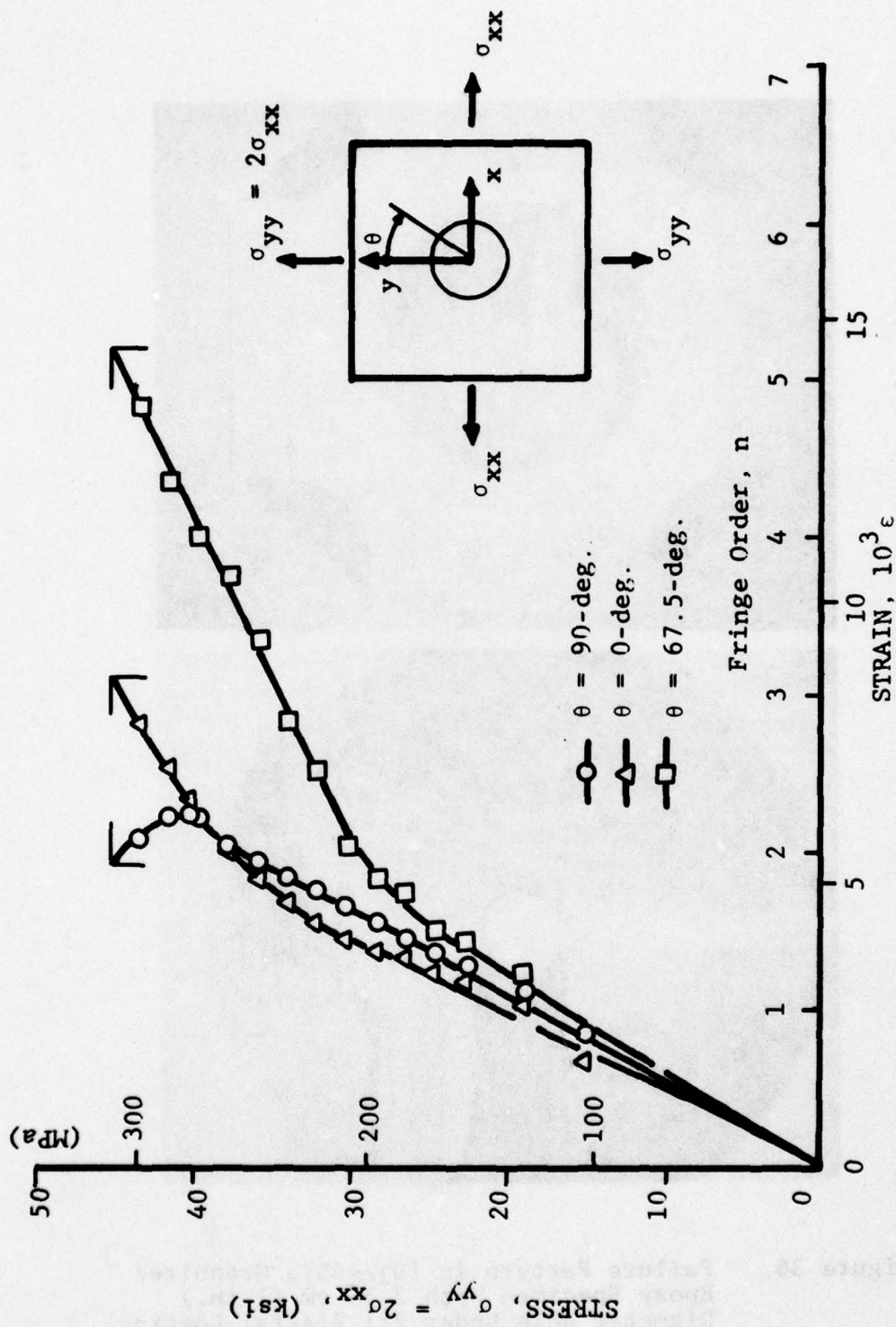


Figure 35. Fringe Order and Circumferential Strain at Three Locations on the Hole Boundary of [0₂/+45] Graphite/Epoxy Specimen With 2.54 cm (1.00 in.) Diameter Hole Under Biaxial Loading (Spec. No. 6A-1)

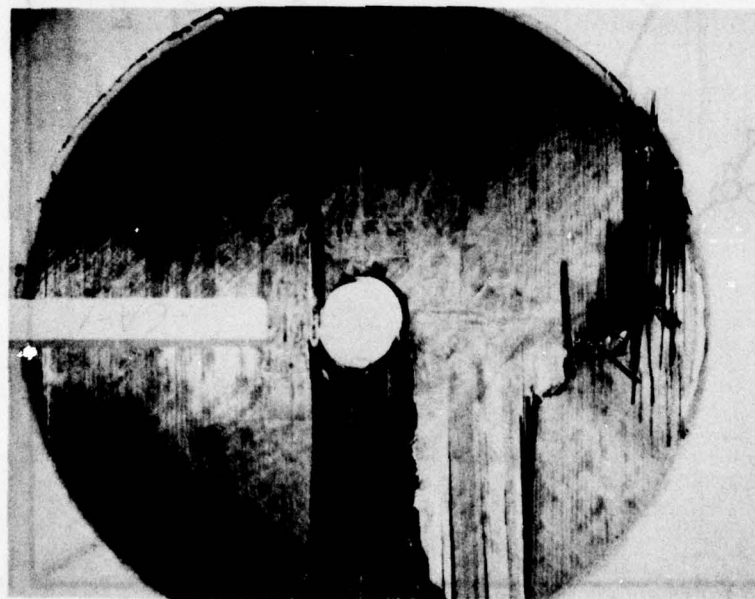
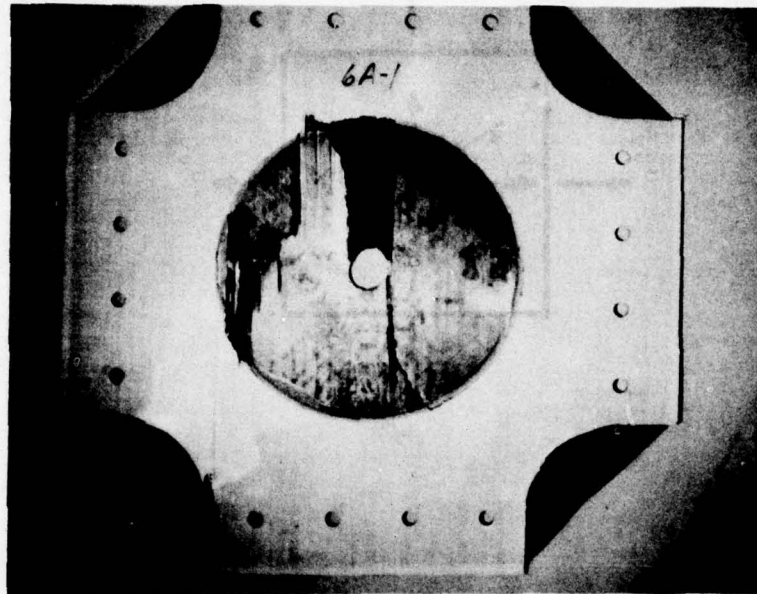


Figure 36. Failure Pattern in $[0_2/+45]_s$ Graphite/
Epoxy Specimen With 2.54 cm (1 in.)
Diameter Hole Under 2:1 Biaxial Loading
(Spec. No. 6A-1)

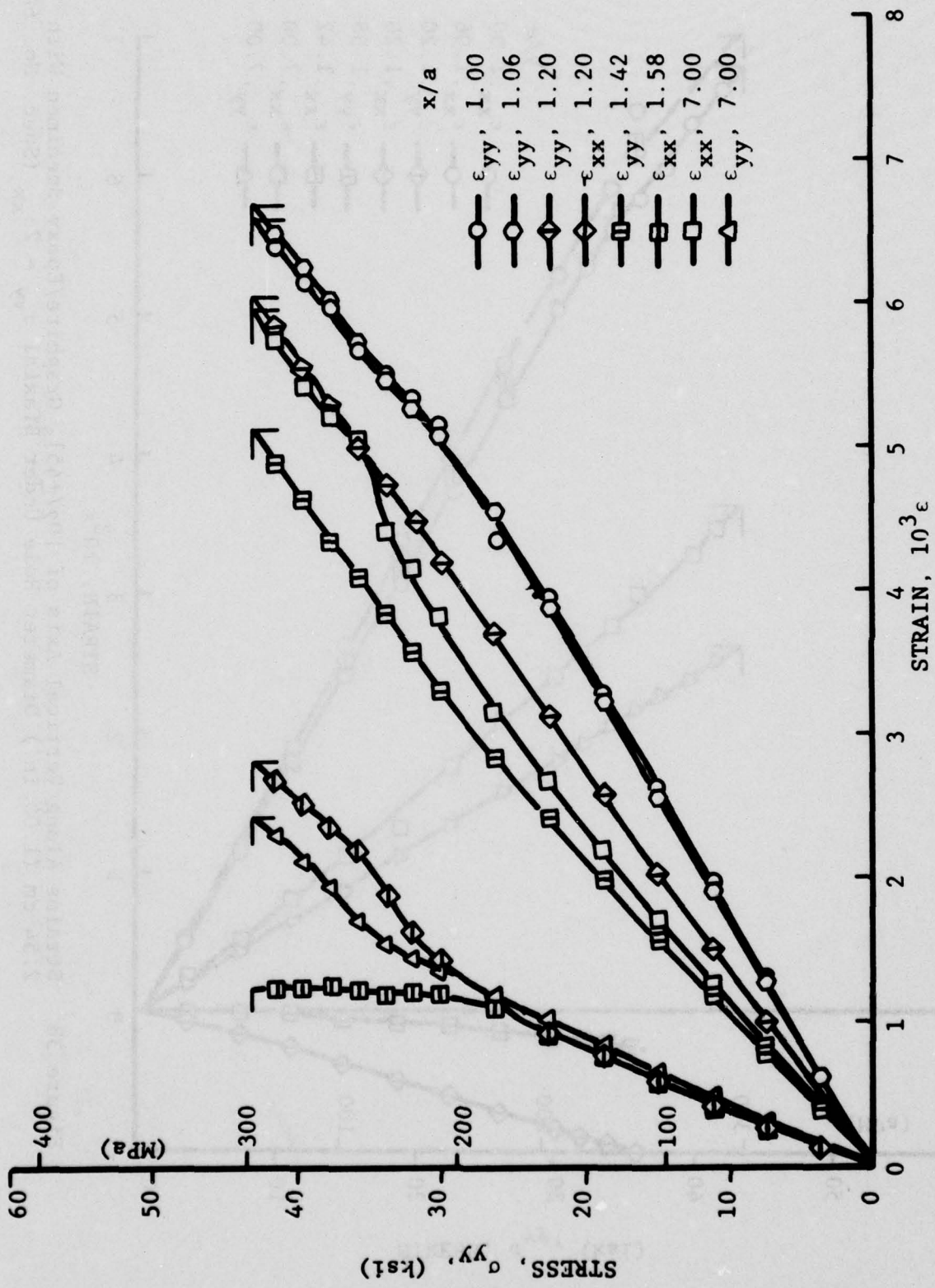


Figure 37. Strains Along Horizontal Axis of $[0_2/+45]_s$ Graphite/Epoxy Specimen With 2.54 cm (1.00 in.) Diameter Hole Under Biaxial Loading $\sigma_{yy} = 2\sigma_{xx}$ (Spec. No. 6A-2)

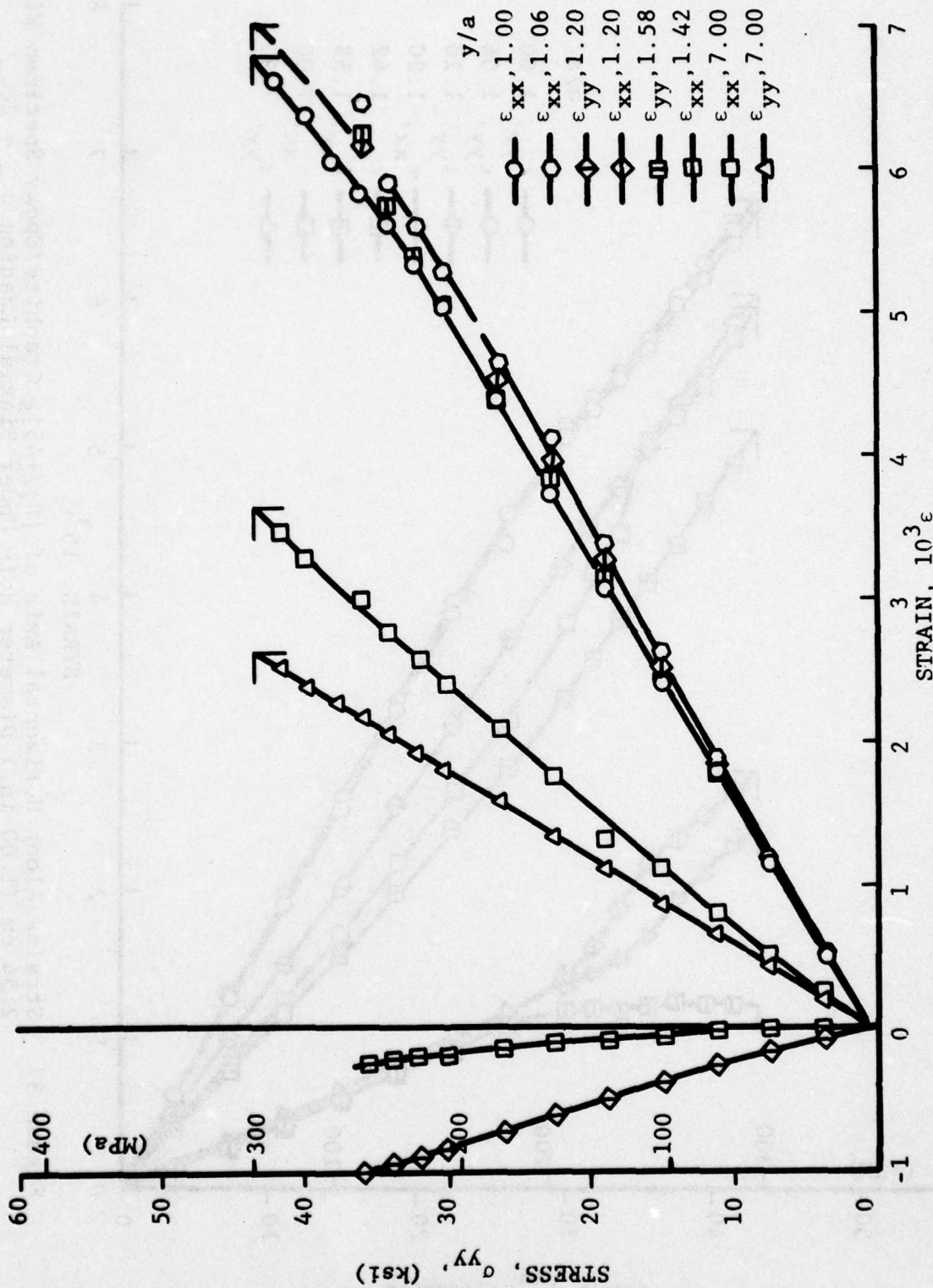


Figure 38. Strains Along Vertical Axis of [02/+45]_s Graphite/Epoxy Specimen With 2.54 cm (1.00 in.) Diameter Hole Under Biaxial $\sigma_{yy} = 2\sigma_{xx}$ (Spec. No. 6A-2)

axis the strain on the hole boundary remains linear up to an applied vertical stress of 225 MPa (33 ksi). The stress ratios computed at two locations on the hole boundary in the linear range are:

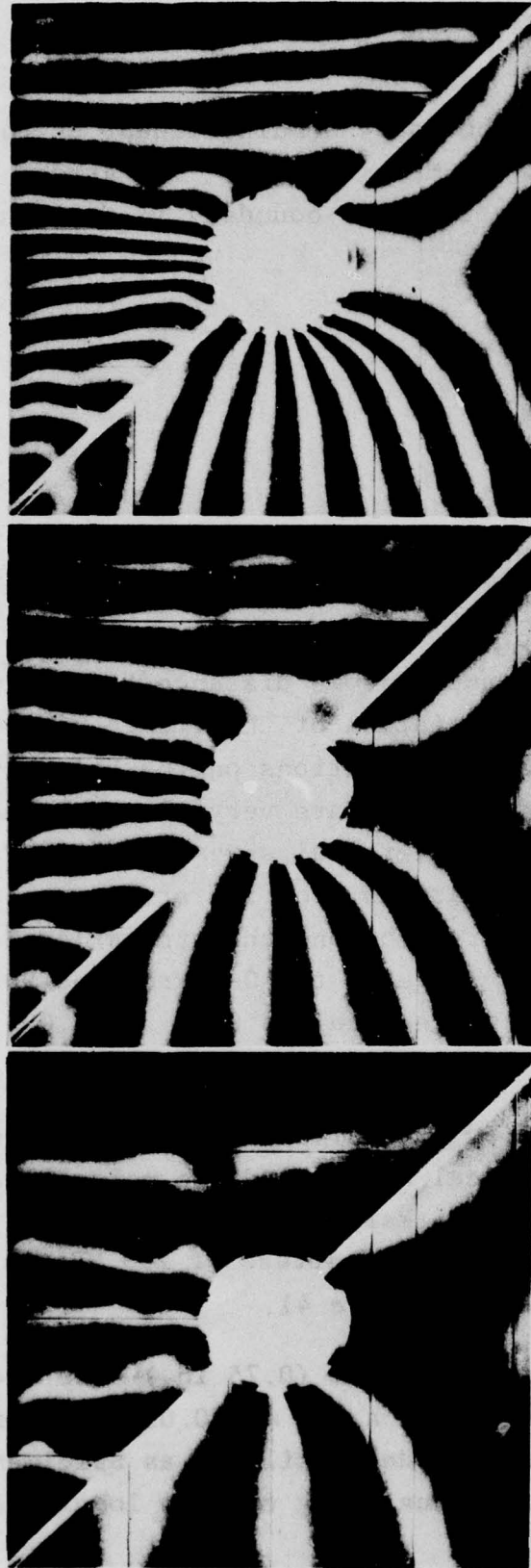
$$\left(\frac{\sigma_{\theta\theta}}{\sigma_{yy}}\right)_{\theta=0^\circ} = 0.59$$

$$\left(\frac{\sigma_{\theta\theta}}{\sigma_{yy}}\right)_{\theta=90^\circ} = 2.09$$

Moire fringe patterns were obtained by superimposing arrays of 400 lines/cm (1000 lpi) in the two loading directions. Fringe patterns for three levels of load are shown in Figure 39. Strains on the boundary of the hole and at some distance from it were obtained by graphical differentiation of the fringe patterns (Figure 40). The strains at two locations on the hole boundary, on the horizontal and vertical axes, are very close to each other and are linear up to an applied vertical stress of 155 MPa (22 ksi). However, contrary to the indications from the strain gages the strains increase at a faster rate beyond the stress level above. Stress ratios for the linear range at the 0-degree and 90-degree locations obtained from the moire data are 0.61 and 2.09, respectively.

Failure was preceded by extensive delamination of the outer 0-degree plies near the vertical axis. Audible noises started at an applied stress of 182 MPa (26 ksi) and continued until final failure which occurred at an applied stress of 299 MPa (43.4 ksi). The failure pattern is shown in Figure 41.

Specimen No. 6A-3 had a 1.91 cm (0.75 in.) hole and was instrumented with strain gages and a 0.5 mm (0.02 in.) thick photoelastic coating. It was loaded similarly as Specimen No. 6A-2 above. The strain variations along the two loading axes are



$\sigma_{yy} = 130 \text{ MPa (18.9 ksi)}$

$\sigma_{yy} = 208 \text{ MPa (30.2 ksi)}$

$\sigma_{yy} = 286 \text{ MPa (41.5 ksi)}$

Figure 39. Moiré Fringe Patterns Around 2.54 cm (1.00 in.) Hole in $[0_2/+45]_s$ Graphite/Epoxy Specimen Under Biaxial Loading $\sigma_{yy} = 2\sigma_{xx}$ (Right-Hand Part of Pattern Corresponds to Horizontal Displacements, Left-Hand Part to Vertical Displacements; Spec. No. 6A-2).

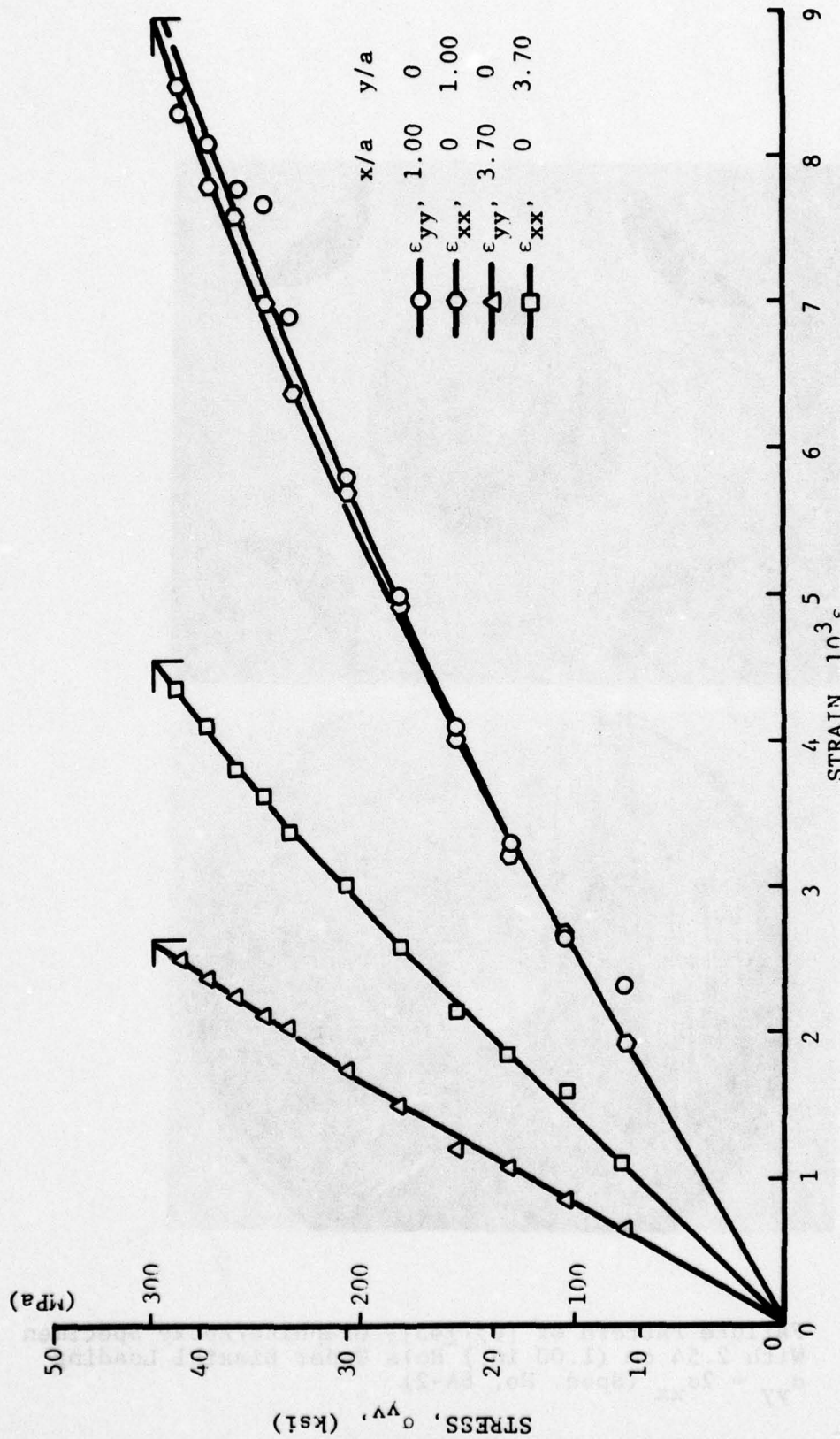


Figure 40. Strains in $[0_2/+45]_s$ Graphite/Epoxy Specimen With 2.54 cm (1.00 in.) Diameter Hole Under Biaxial Loading $\sigma_{yy} = 2\sigma_{xx}$ (Spec. No. 6A-2)

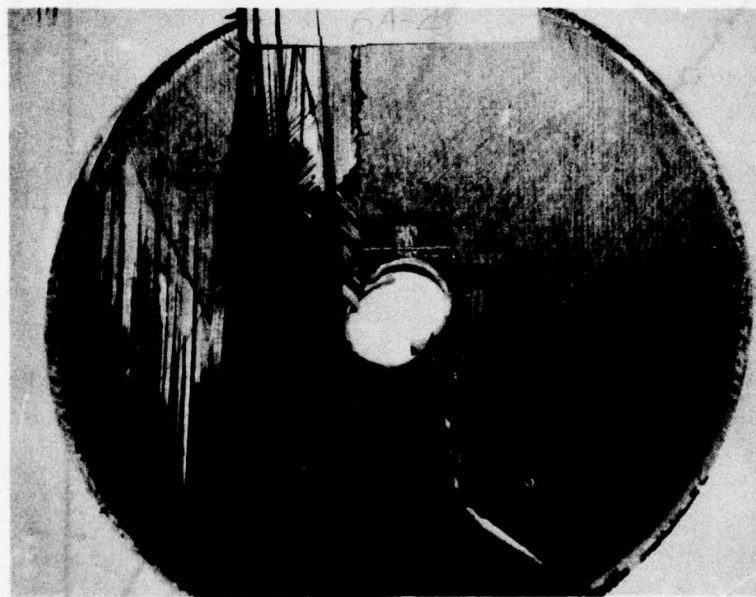
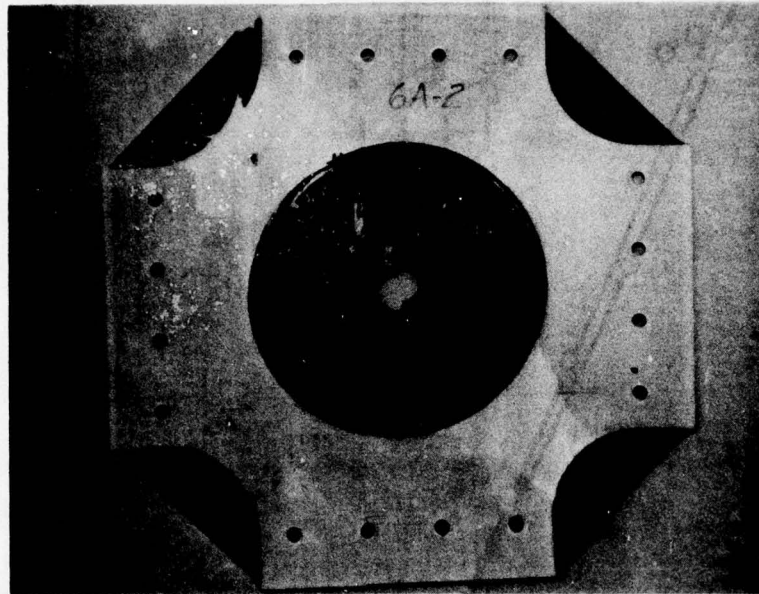


Figure 41. Failure Pattern of $[0_2/+45]_s$ Graphite/Epoxy Specimen
With 2.54 cm (1.00 in.) Hole Under Biaxial Loading
 $\sigma_{yy} = 2\sigma_{xx}$ (Spec. No. 6A-2)

shown in Figures 42 and 43. On the horizontal axis the strain on the boundary is linear up to an applied stress of 159 MPa (23 ksi), thereafter it increases at a reduced rate. The stress ratios at two locations on the hole boundary are:

$$\left(\frac{\sigma_{\theta\theta}}{\sigma_{yy}} \right)_{\theta=0^\circ} = 0.61$$

$$\left(\frac{\sigma_{\theta\theta}}{\sigma_{yy}} \right)_{\theta=90^\circ} = 2.01$$

Isochromatic fringe patterns in the photoelastic coating around the hole are shown in Figure 44 for three levels of applied stress. As observed before, characteristic regions of birefringence concentration develop at points approximately 25-degrees off the horizontal axis. The variation of fringe order and strain at the 0-, 65- and 90-degree locations is plotted in Figure 45. The first nonlinear response occurred at the 65-degree location at a stress of approximately 152 MPa (22 ksi). Fracture initiation was followed by localized strain relief on the hole boundary around the 90-degree location.

The failure mode was the same as for Specimen No. 6A-2 above. The first audible fracture occurred at a stress of 130 MPa (19 ksi). Ultimate failure occurred at 325 MPa (47.1 ksi). The failure pattern is shown in Figure 46.

Specimen No. 6A-4 was a replicate of No. 6A-3 above with a 1.91 cm (0.75 in.) diameter hole and was instrumented with strain gages and 400 lines/cm (1000 lps) moiré rulings in the two loading directions. It was loaded in biaxial tension producing a 2:1 ratio of effective stresses in the vicinity of the hole. The strain variations along the two loading axes are shown in Figures 47 and 48. On the horizontal axis the strain on the hole boundary is linear up to an applied vertical stress of 200 MPa (29 ksi),

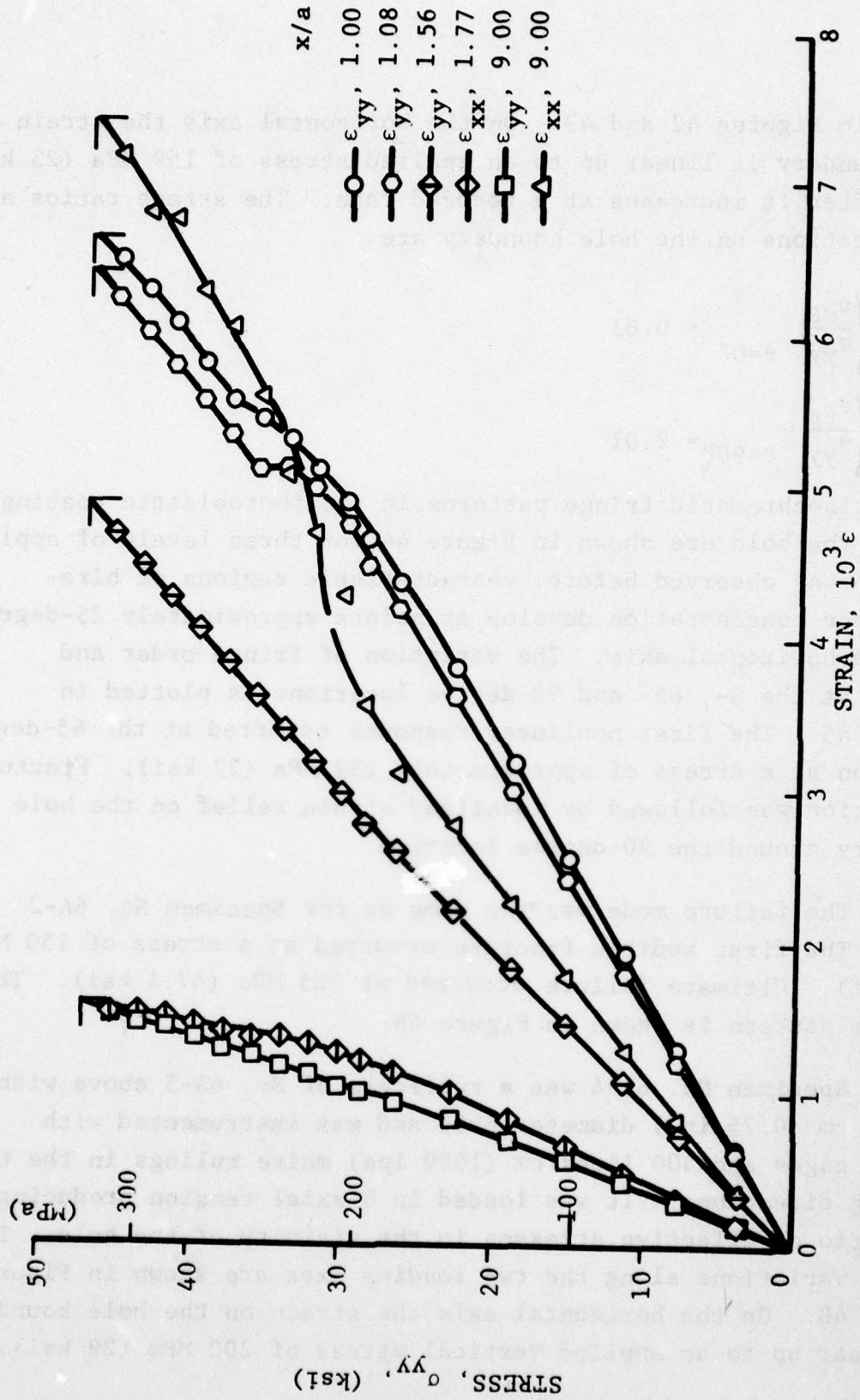


Figure 42. Strains Along Horizontal Axis of $[0_2/+45]_s$ Graphite/Epoxy Specimen With 1.91 cm (0.75 in.) Diameter Hole Under Biaxial Loading $\sigma_{yy} = 2\sigma_{xx}$ (Spec. No. 6A-3)

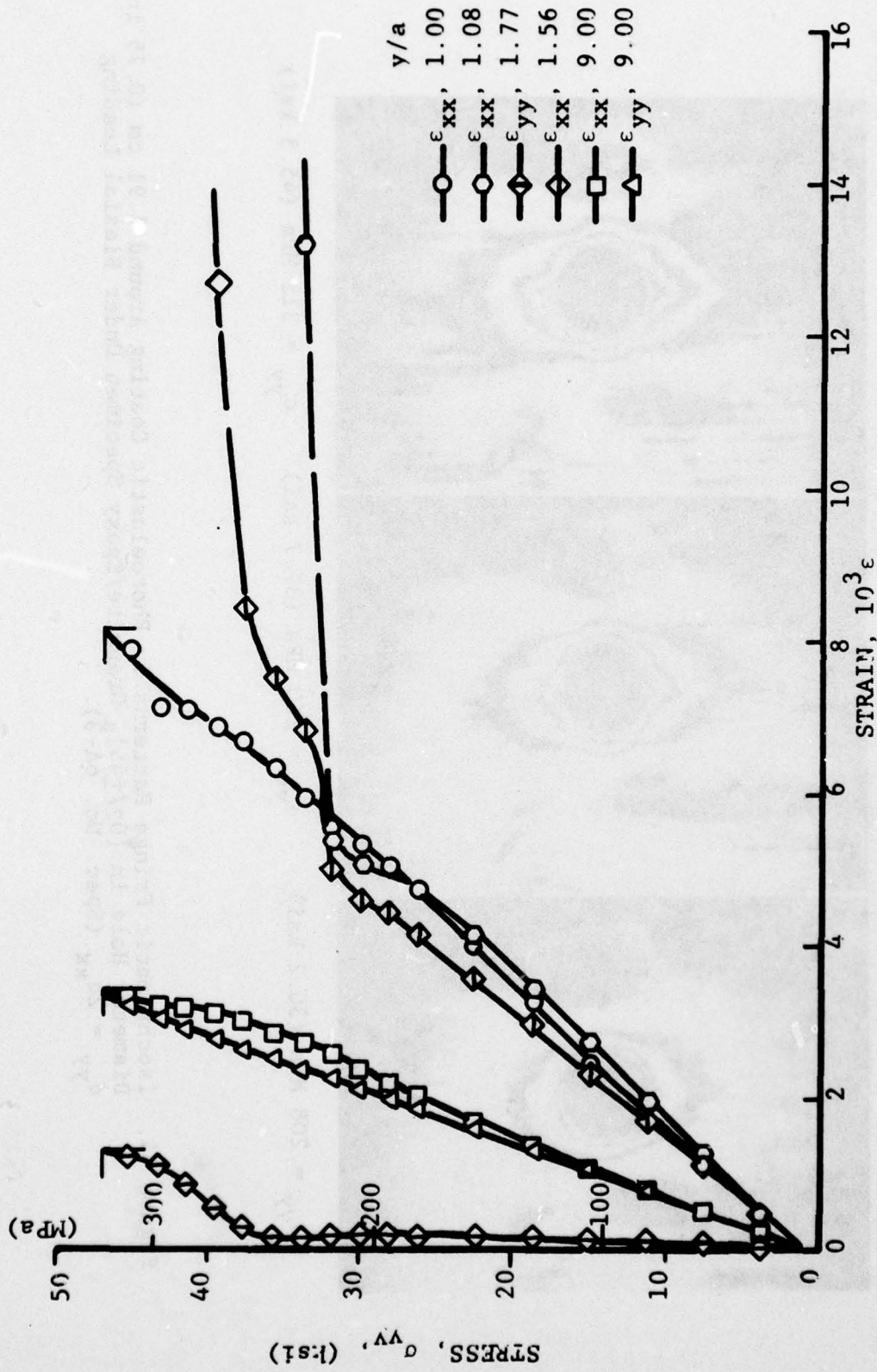
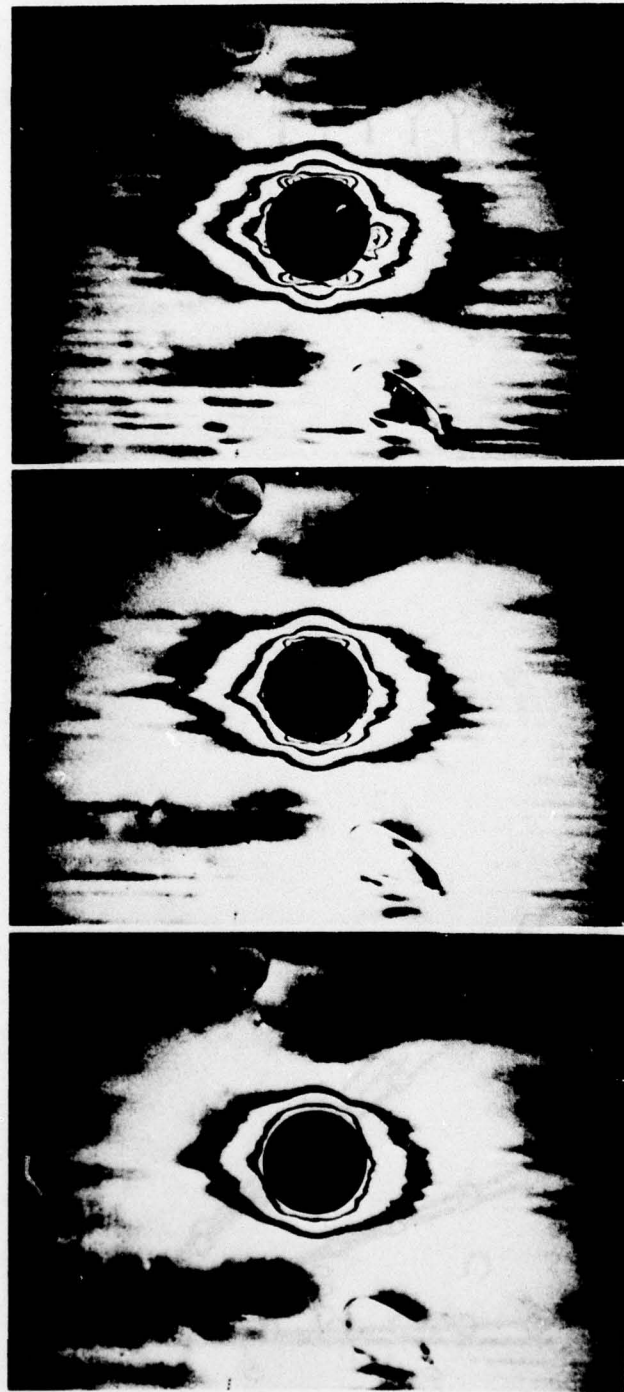


Figure 43. Strains Along Vertical Axis of $[0_2/+45]_s$ Graphite/Epoxy Specimen With 1.91 cm (0.75 in.) Diameter Hole Under Biaxial Loading, $\sigma_{yy} = 2\sigma_{xx}$ (Spec. No. 6A-3)



$\sigma_{yy} = 208 \text{ MPa (30.2 ksi)}$ $\sigma_{yy} = 260 \text{ MPa (37.7 ksi)}$ $\sigma_{yy} = 312 \text{ MPa (45.3 ksi)}$

Figure 44. Isochromatic Fringe Patterns in Photoelastic Coating Around 1.91 cm (0.75 in.) Diameter Hole in $[0_2/+45]_s$ Graphite/Epoxy Specimen Under Biaxial Loading $\sigma_{yy} = 2\sigma_{xx}$ (Spec. No. 6A-3).

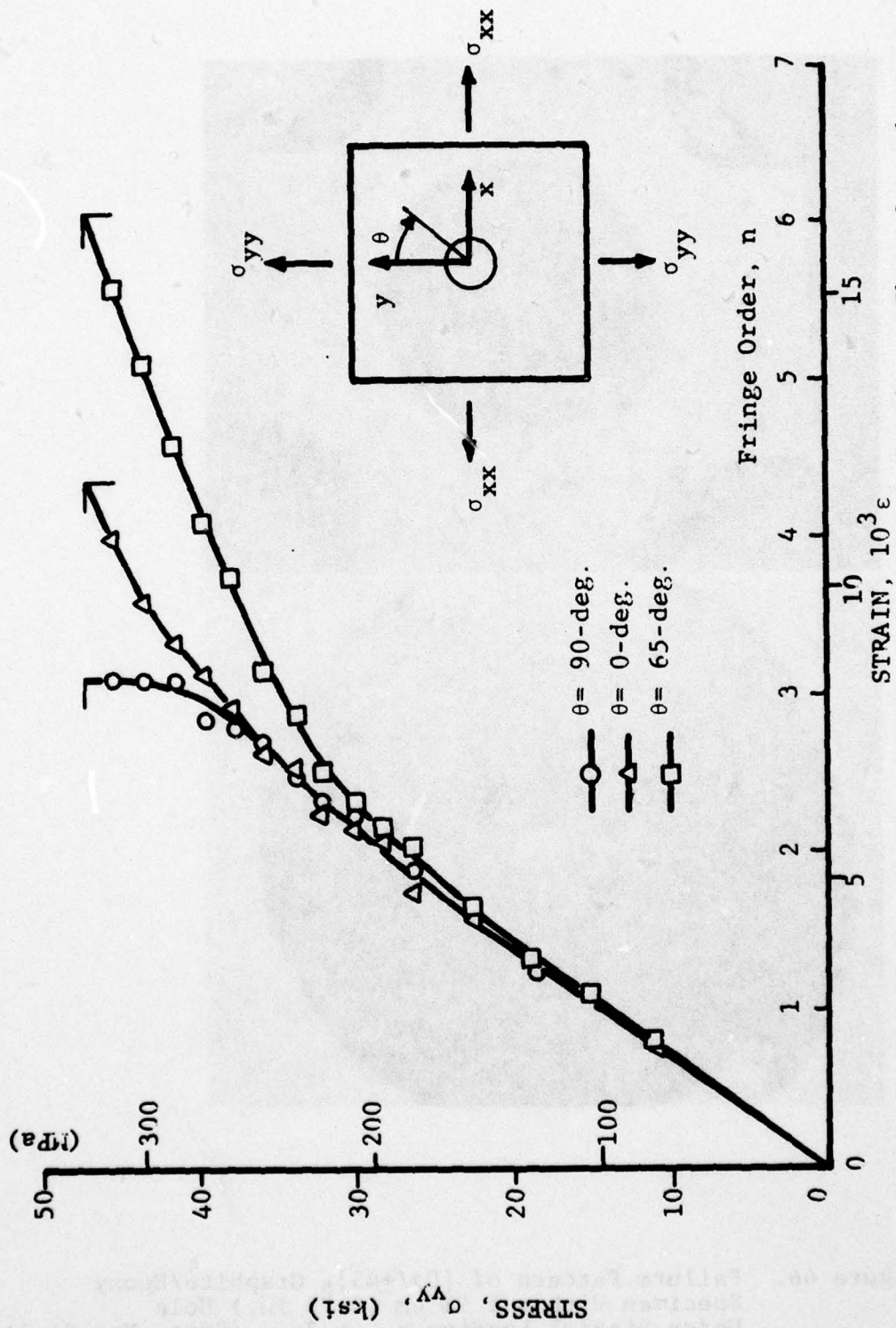


Figure 45. Fringe Order and Circumferential Strain at Three Locations on the Hole Boundary of $[0_2/+45]_s$ Graphite/Epoxy Specimen With 1.91 cm (0.75 in.) Diameter Hole Under Biaxial Loading (Spec. No. 6A-3)

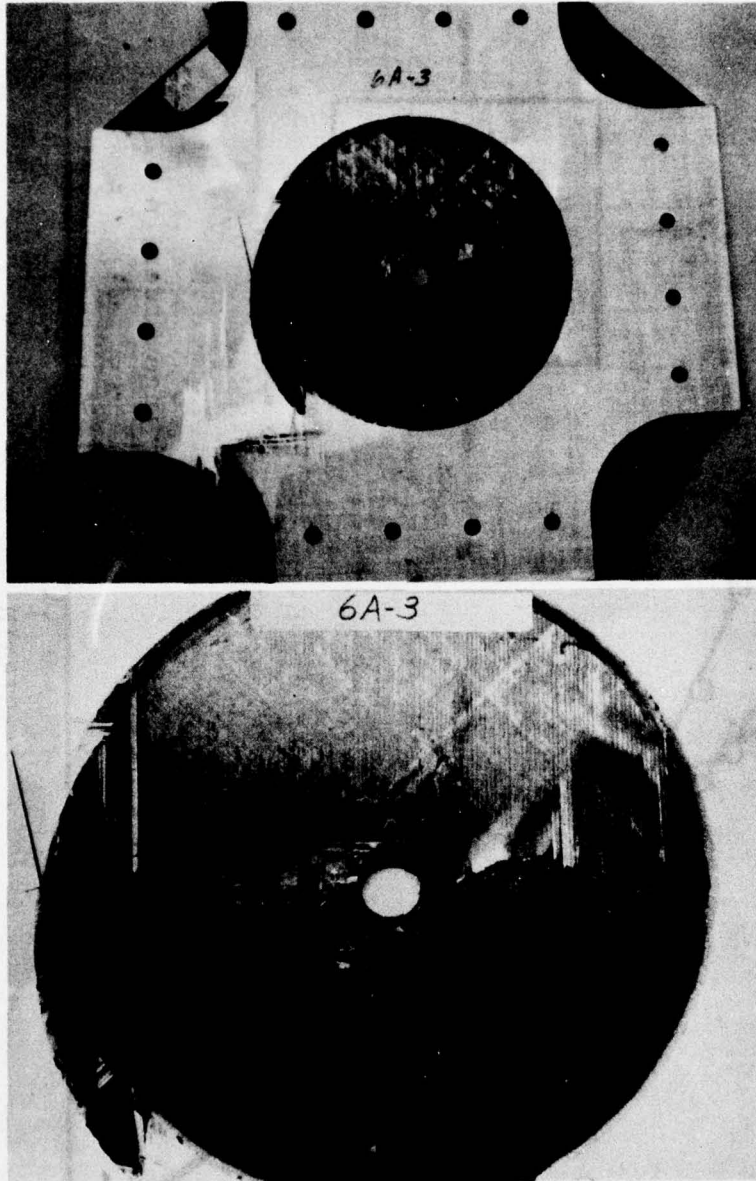


Figure 46. Failure Pattern of $[0_2/+45]_s$ Graphite/Epoxy Specimen With a 1.91 cm (0.75 in.) Hole Under Biaxial Loading $\sigma_{yy} = 2\sigma_{xx}$ (Spec. No. 6A-3)

thereafter it increases at a reduced rate. On the vertical axis the strain on the hole boundary remains linear up to a stress of 248 MPa (36 ksi). The horizontal strains near the hole boundary are slightly larger than that on the boundary (Figure 48). The stress ratios at two locations on the hole boundary in the linear range are:

$$\left(\frac{\sigma_{\theta\theta}}{\sigma_{yy}} \right)_{\theta=0^\circ} = 0.62$$

$$\left(\frac{\sigma_{\theta\theta}}{\sigma_{yy}} \right)_{\theta=90^\circ} = 2.04$$

Moire fringe patterns corresponding to horizontal and vertical deformations around the hole are shown in Figure 49 for three levels of load. Strains on the boundary of the hole and at some distance from it were obtained by graphical differentiation of these patterns (Figure 50). Strains on the hole boundary are linear up to an applied stress of approximately 207 MPa (30 ksi). The stress ratios computed from the moire data in the linear range at the 0-degree and 90-degree locations are 0.56 and 2.53, respectively.

The failure mode was the same as for the specimens discussed before. The first audible fracture occurred at a stress of 156 MPa (23 ksi). Ultimate failure occurred at 325 MPa (47.1 ksi). The failure pattern is shown in Figure 51.

Specimen No. 6A-5 had a 1.27 cm (0.50 in.) diameter hole and was instrumented with strain gages and a 0.61 mm (0.024 in.) thick photoelastic coating. It was loaded similarly as specimen No. 6A-4 above. The strain variations along the two loading axes are shown in Figures 52 and 53. On the horizontal axis the strain on the hole boundary is linear up to an applied stress of 166 MPa (24 ksi), thereafter it increases at a reduced rate as seen in all

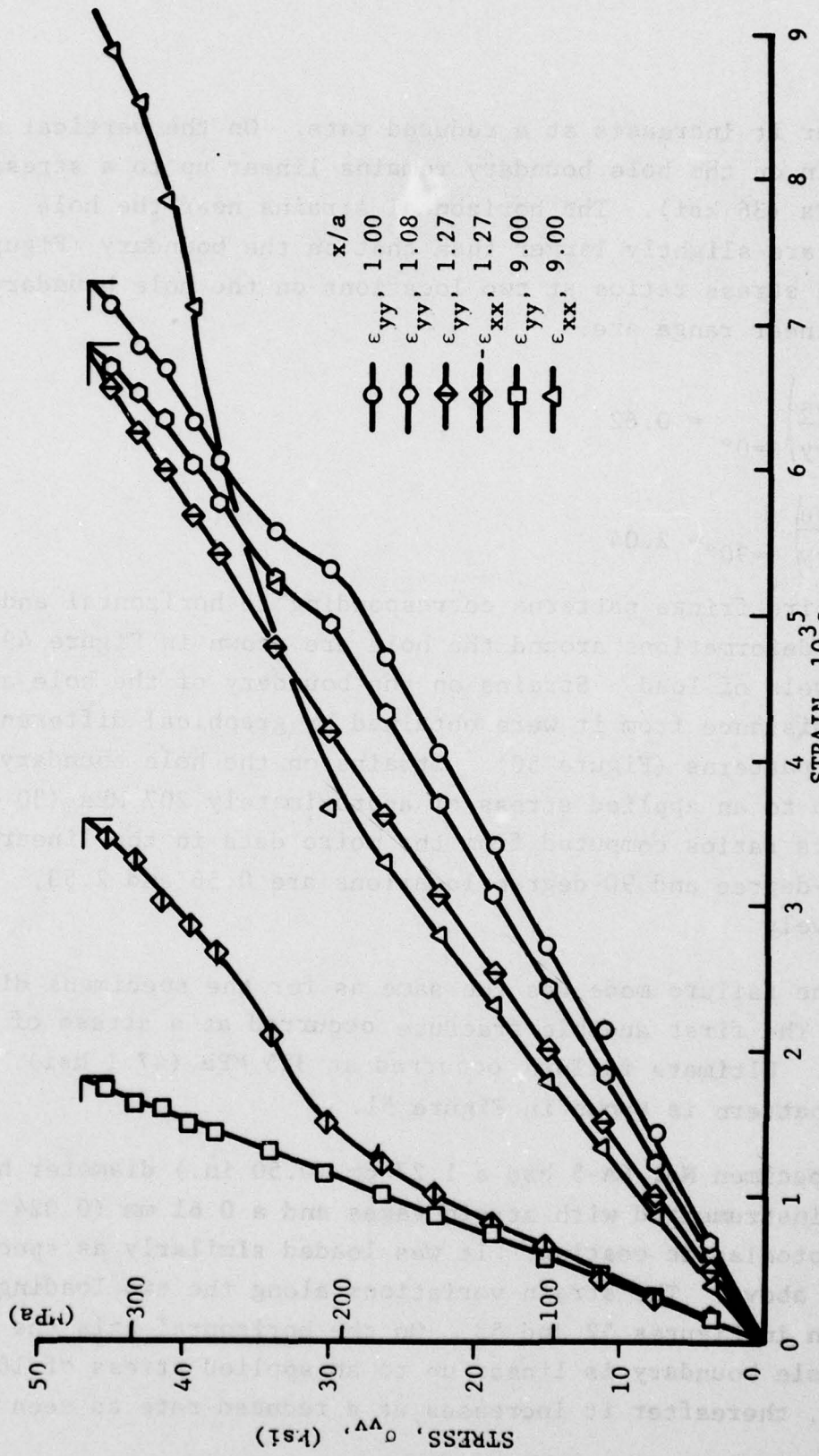


Figure 47. Strains Along Horizontal Axis of [0/±45]_s Graphite/Epoxy Specimen With 1.91 cm (0.75 in.) Diameter Hole Under Biaxial Loading $\sigma_{yy} = 2\sigma_{xx}$ (Spec. No. 6A-4)

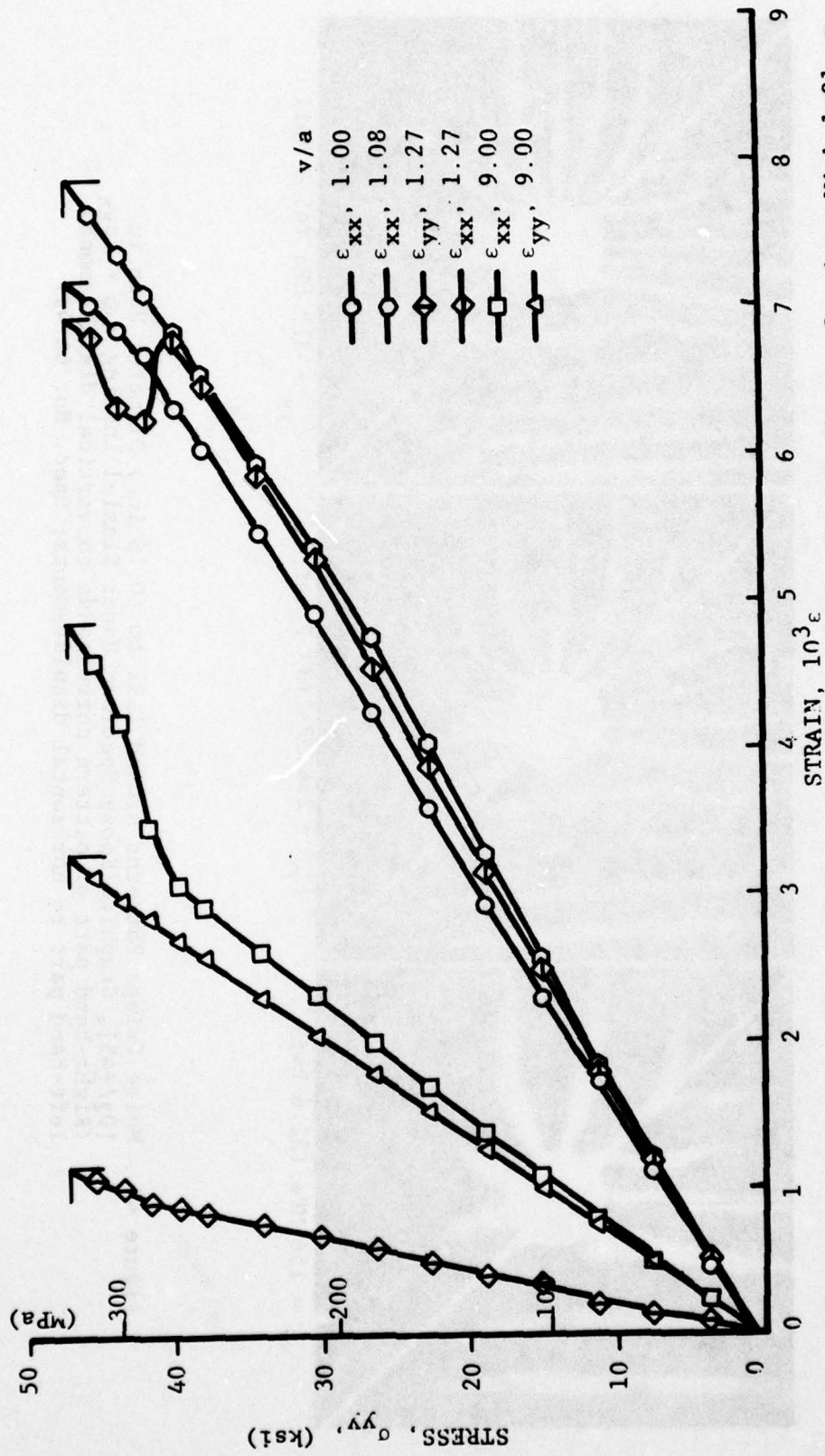


Figure 48. Strains Along Vertical Axis of [02/+45]_s Graphite/Epoxy Specimen With 1.91 cm (0.75 in.) Diameter Hole Under Biaxial Loading $\sigma_{yy} = 2\sigma_{xx}$ (Spec. No. 6A-4)

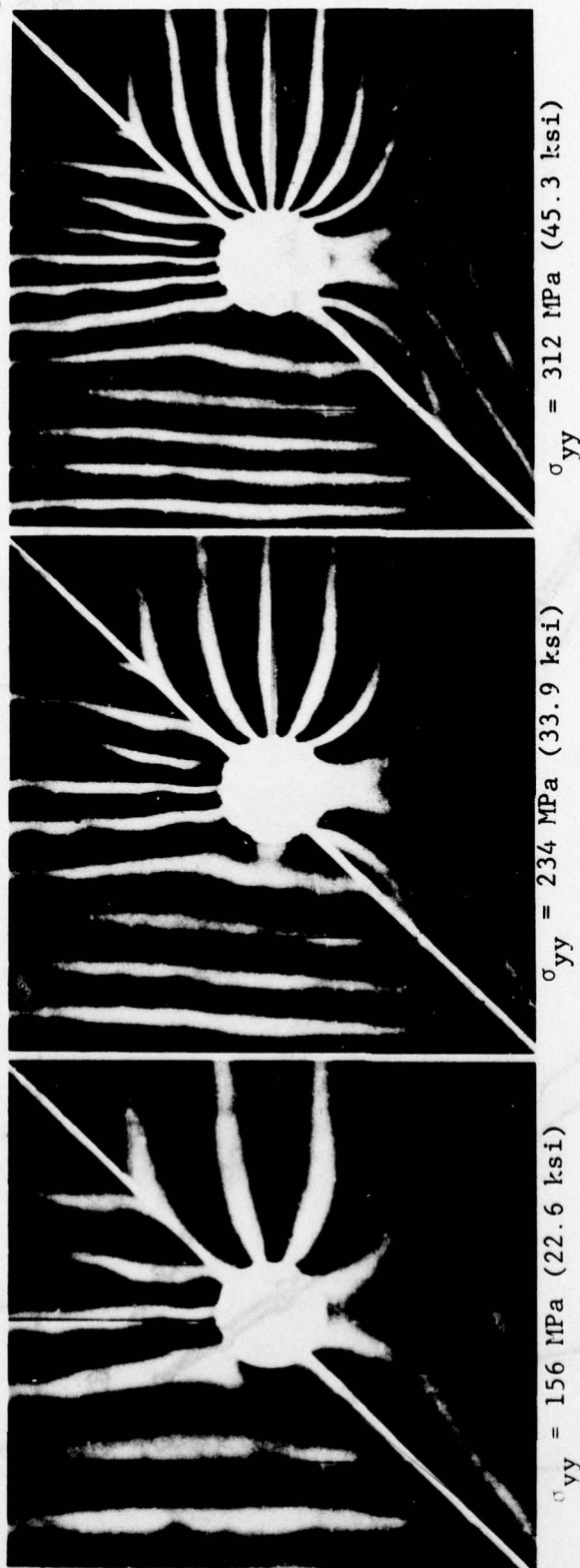


Figure 49. Moiré Fringe Patterns Around 1.91 cm (0.75 in.) Diameter Hole in [0₂/+45]s Graphite/Epoxy Specimen Under Biaxial Loading $\sigma_{yy} = 2\sigma_{xx}$ (Right-hand part of pattern corresponds to vertical displacements, left-hand part to horizontal displacements; Spec. No. 6A-4).

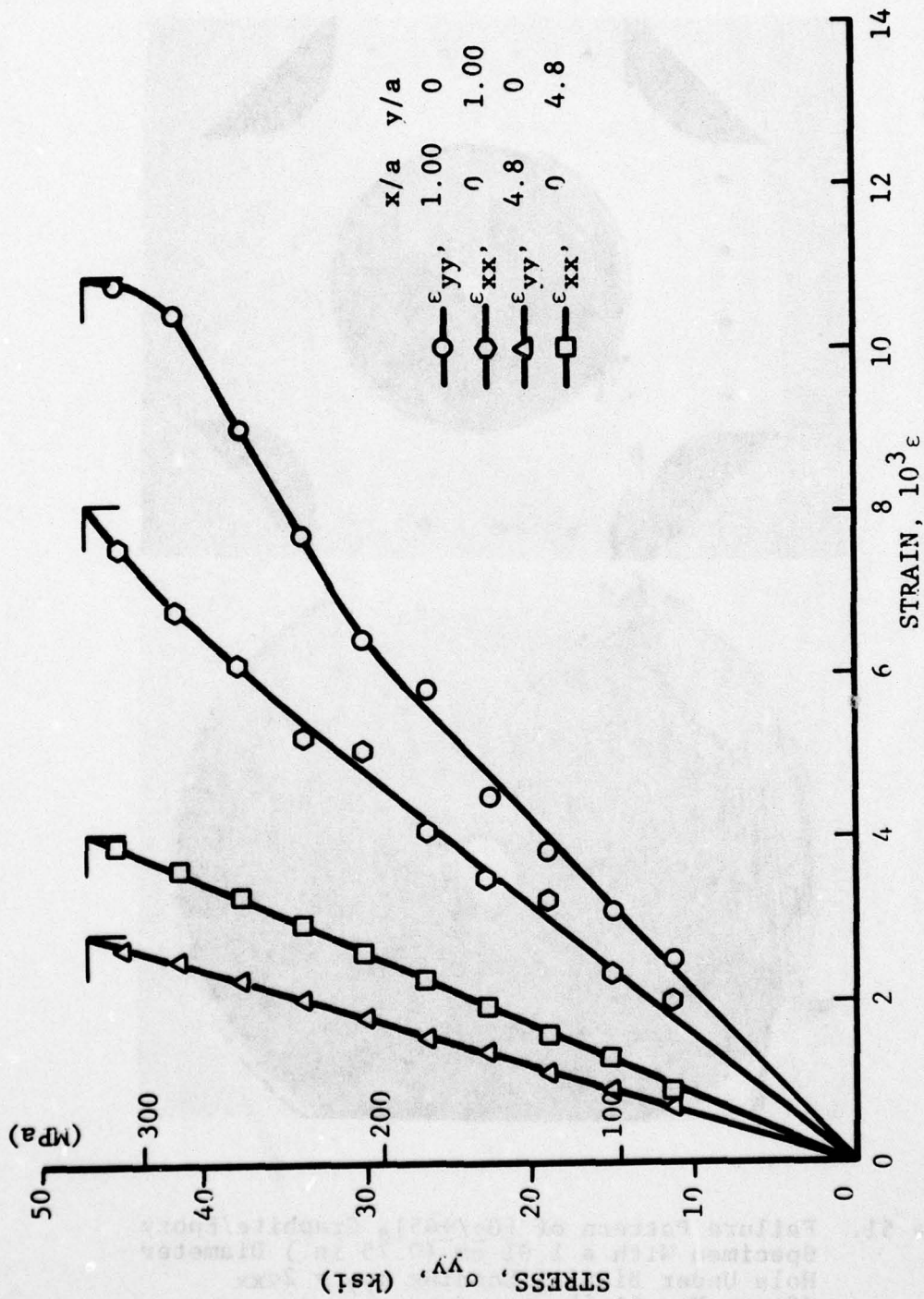


Figure 50. Strains in $[0_2/+45]_s$ Graphite/Epoxy Specimen With 1.91 cm (0.75 in.) Diameter Hole Under Biaxial Loading $\sigma_{yy} = 2\sigma_{xx}$ (Spec. No. 6A-4)

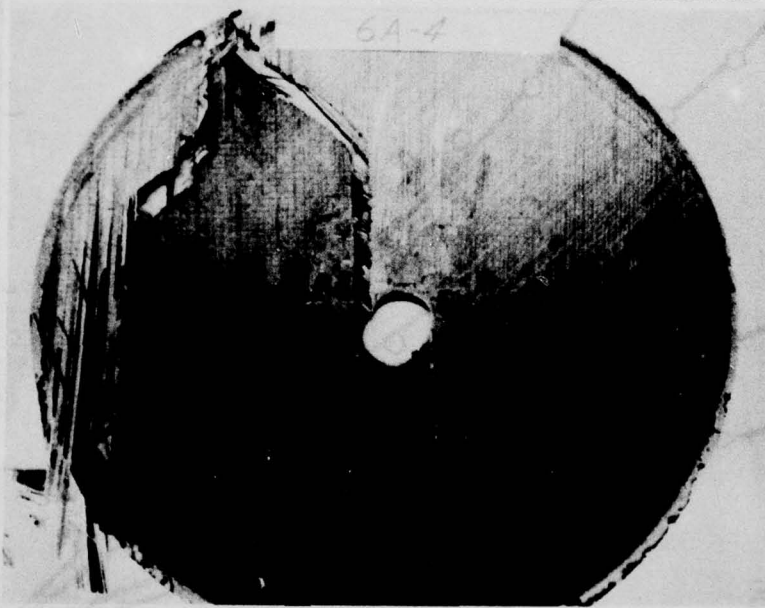
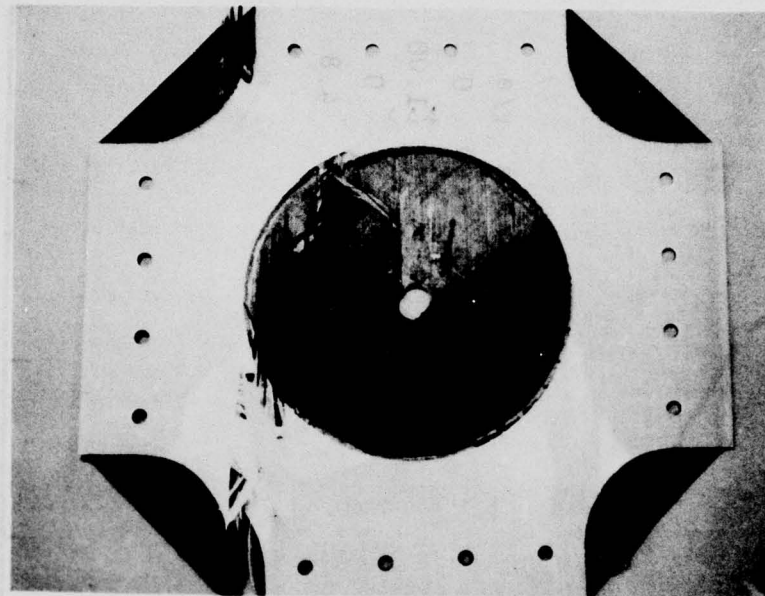


Figure 51. Failure Pattern of $[0_2/+45]_s$ Graphite/Epoxy Specimen With a 1.91 cm (0.75 in.) Diameter Hole Under Biaxial Loading $\sigma_{yy} = 2\sigma_{xx}$ (Spec. No. 6A-4)

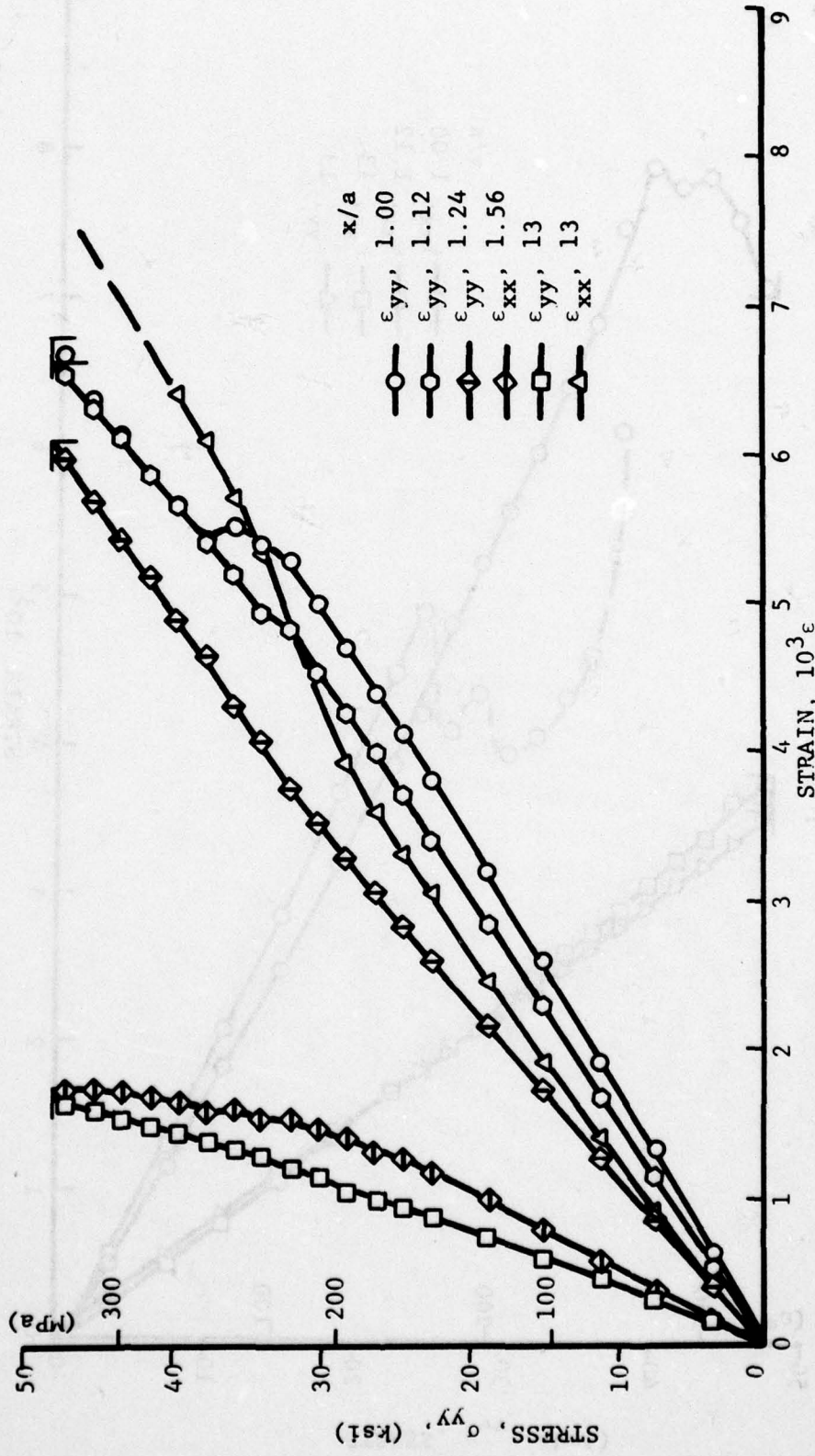


Figure 52. Strains Along Horizontal Axis of [02/+45]_s Graphite/Epoxy Specimen With 1.27 cm (0.50 in.) Diameter Hole Under Biaxial Loading $\sigma_{yy} = 2\sigma_{xx}$ (Spec. No. 6A-5)

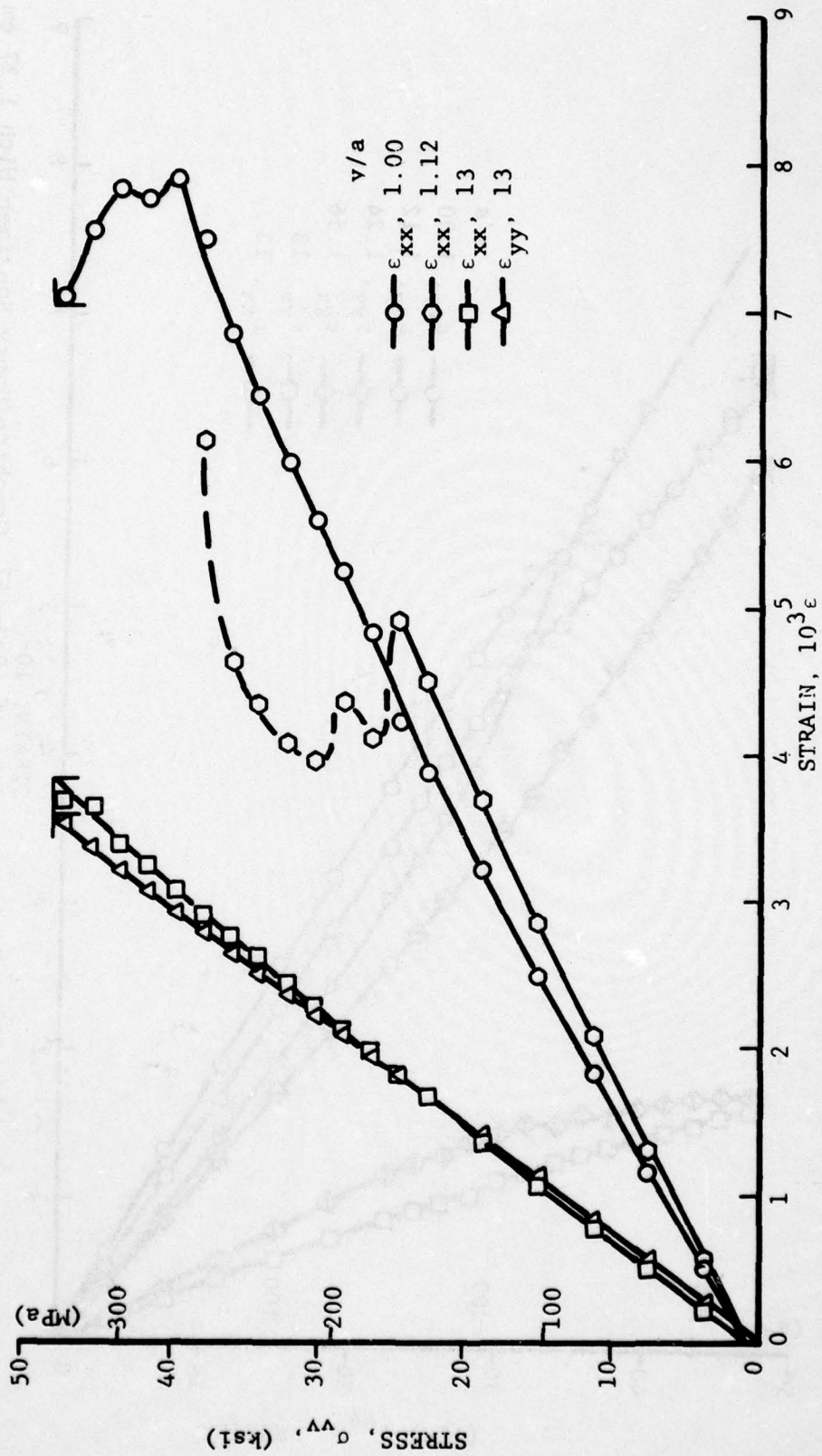


Figure 53. Strains Along Vertical Axis of [02/+45]_s Graphite/Epoxy Specimen With 1.27 (0.50 in.) Diameter Hole Under Biaxial Loading $\sigma_{yy} = 2\sigma_{xx}$ (Spec. No. 6A-5)

AD-A048 659

IIT RESEARCH INST CHICAGO ILL
BIAXIAL TESTING OF GRAPHITE/EPOXY COMPOSITES CONTAINING STRESS --ETC(U)
JUN 77 I M DANIEL

F/G 11/4

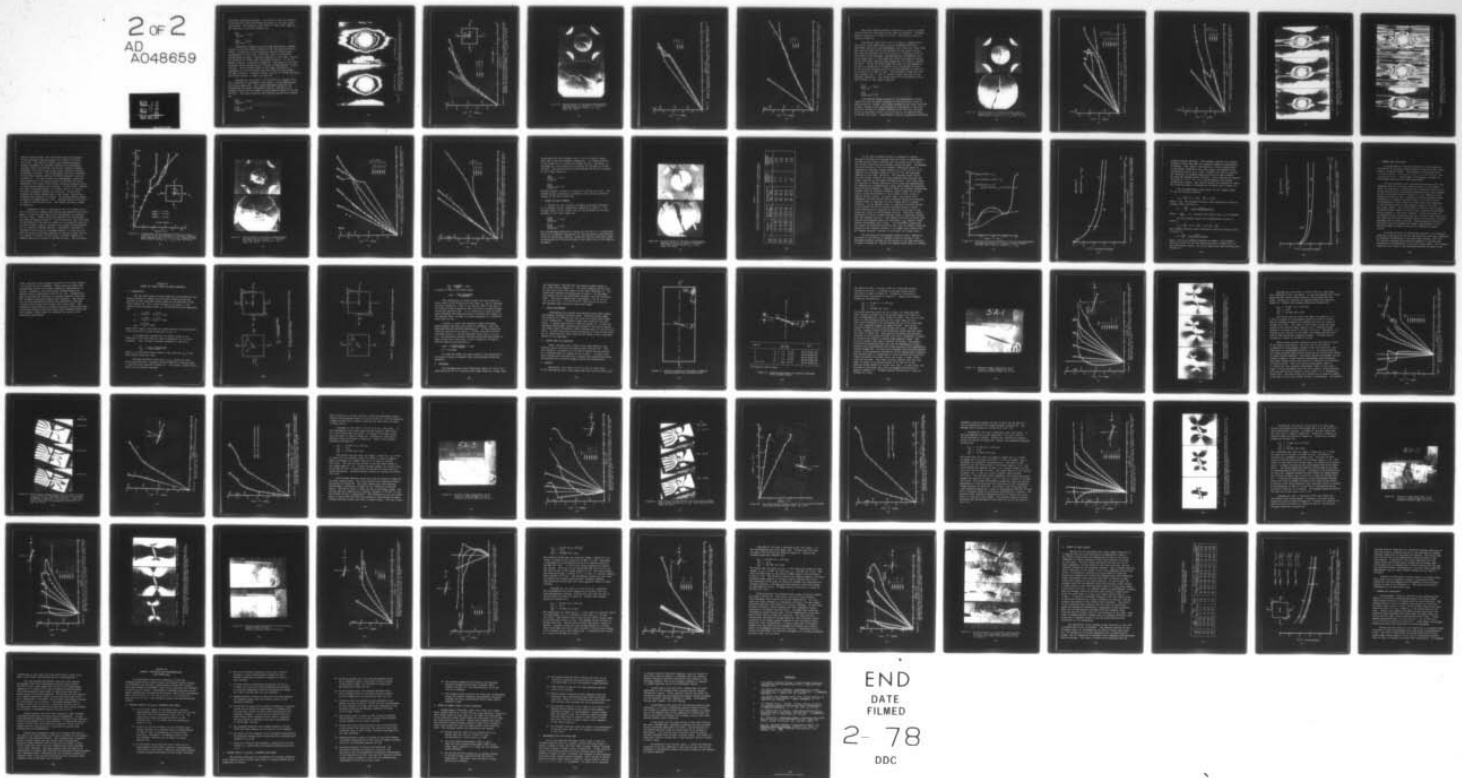
F33615-76-C-5162

UNCLASSIFIED

AFML-TR-76-244-PT-2

NL

2 of 2
AD
A048659



END
DATE
FILMED
2-78
DDC

previously discussed specimens. The strain on the hole boundary on the vertical axis also becomes nonlinear at the same stress level above. The computed stress ratios in the linear range at two locations on the hole boundary are:

$$\left(\frac{\sigma_{\theta\theta}}{\sigma_{yy}} \right)_{\theta=0^\circ} = 0.62$$

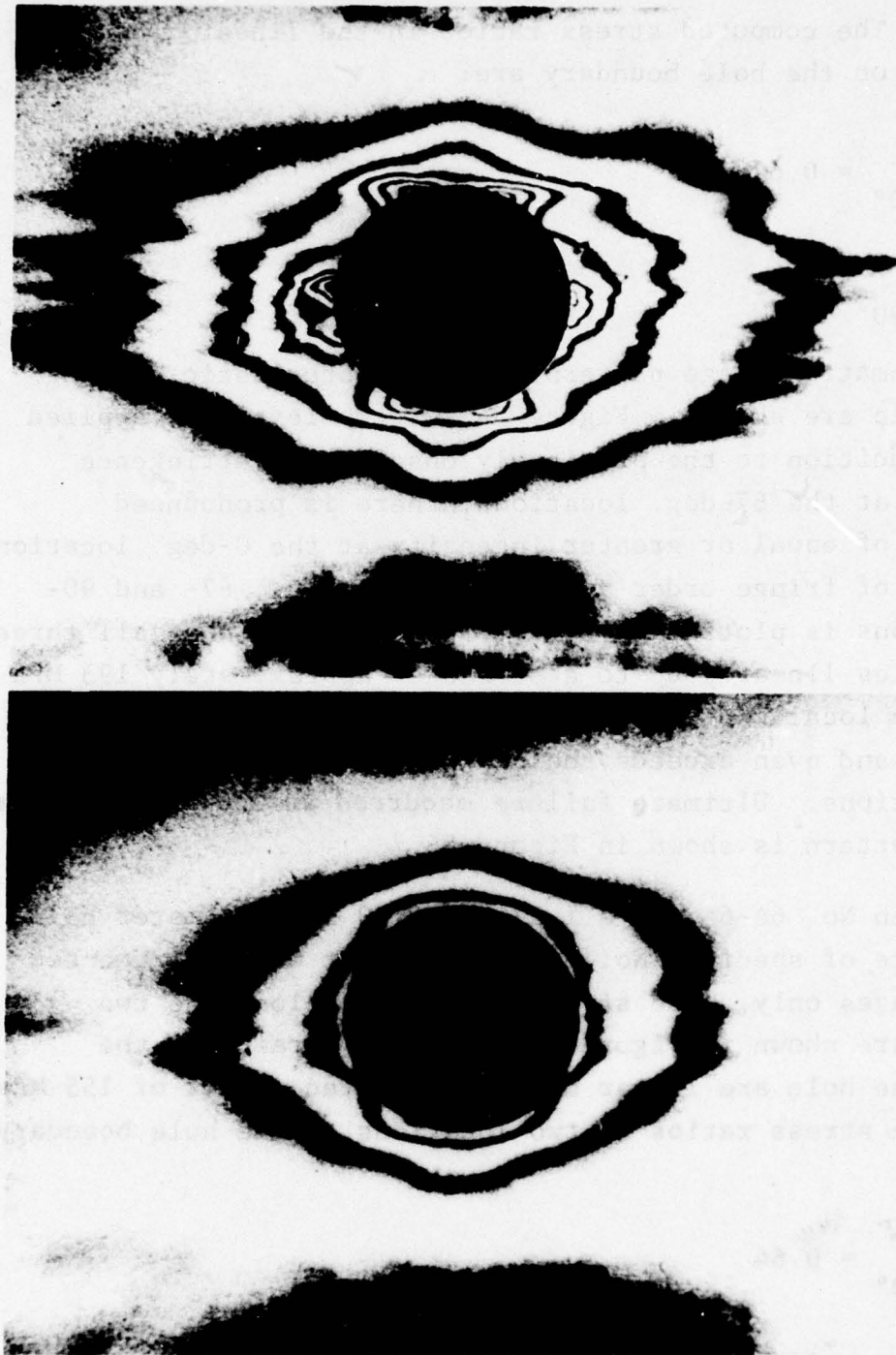
$$\left(\frac{\sigma_{\theta\theta}}{\sigma_{yy}} \right)_{\theta=90^\circ} = 2.02$$

Isochromatic fringe patterns in the photoelastic coating around the hole are shown in Figure 54 for two levels of applied stress. In addition to the previously observed birefringence concentration at the 67-deg. locations, there is pronounced concentration of equal or greater intensity at the 0-deg. location. The variation of fringe order and strain at the 0-, 67- and 90-degree locations is plotted in Figure 55. The strain at all three locations varies linearly up to a stress of approximately 193 MPa (28 ksi). The localized strain at the 0-deg. location is comparable to and even exceeds the peak strains at the 67-deg. off-axis locations. Ultimate failure occurred at 330 MPa (47.9 ksi). The failure pattern is shown in Figure 56.

Specimen No. 6A-6 with a 1.27 cm (0.50 in.) diameter hole was a replicate of specimen No. 6A-5 above. It was instrumented with strain gages only. The strain variations along the two loading axes are shown in Figures 57 and 58. Strains on the boundary of the hole are linear up to an applied stress of 155 MPa (22 ksi). The stress ratios at two locations on the hole boundary are:

$$\left(\frac{\sigma_{\theta\theta}}{\sigma_{yy}} \right)_{\theta=0^\circ} = 0.64$$

$$\left(\frac{\sigma_{\theta\theta}}{\sigma_{yy}} \right)_{\theta=90^\circ} = 2.08$$



$\sigma_{yy} = 208 \text{ MPa (30.2 ksi)}$

$\sigma_{yy} = 325 \text{ MPa (47.1 ksi)}$

Figure 54. Isochromatic Fringe Patterns in Photoelastic Coating Around 1.27 cm (0.50 in.) Diameter Hole in $[0_2/+45]_s$ Graphite/Epoxy Specimen Under Biaxial Loading
 $\sigma_{yy} = 2\sigma_{xx}$ (Spec. No. 6A-5)

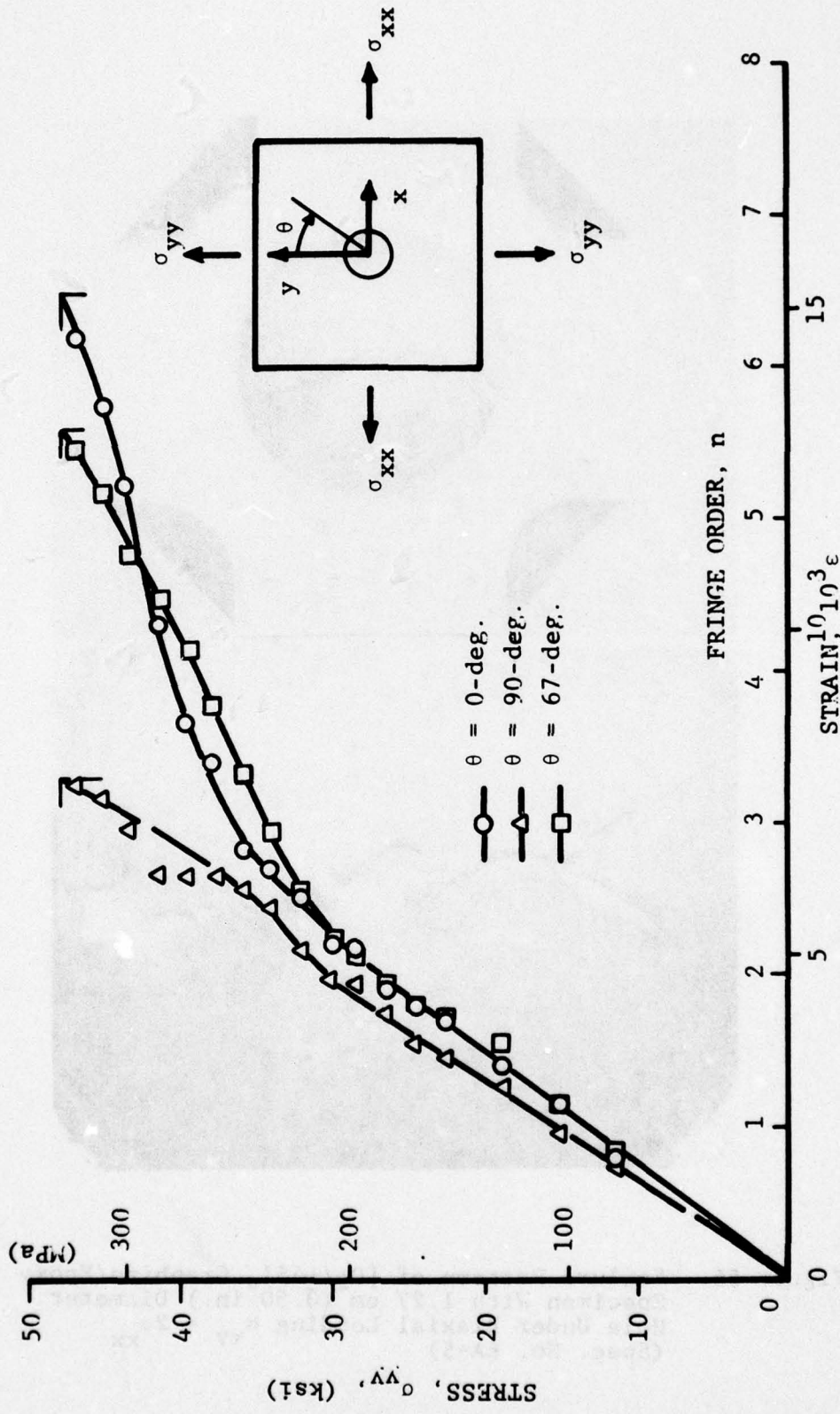


Figure 55. Fringe Order and Circumferential Strain at Three Locations on the Hole Boundary of $[0_2/+45]_s$ Graphite/Epoxy Specimen With 1.27 cm (0.50 in.) Diameter Hole Under Biaxial Loading $\sigma_{yy} = 2\sigma_{xx}$ (Spec. No. 6A-5)

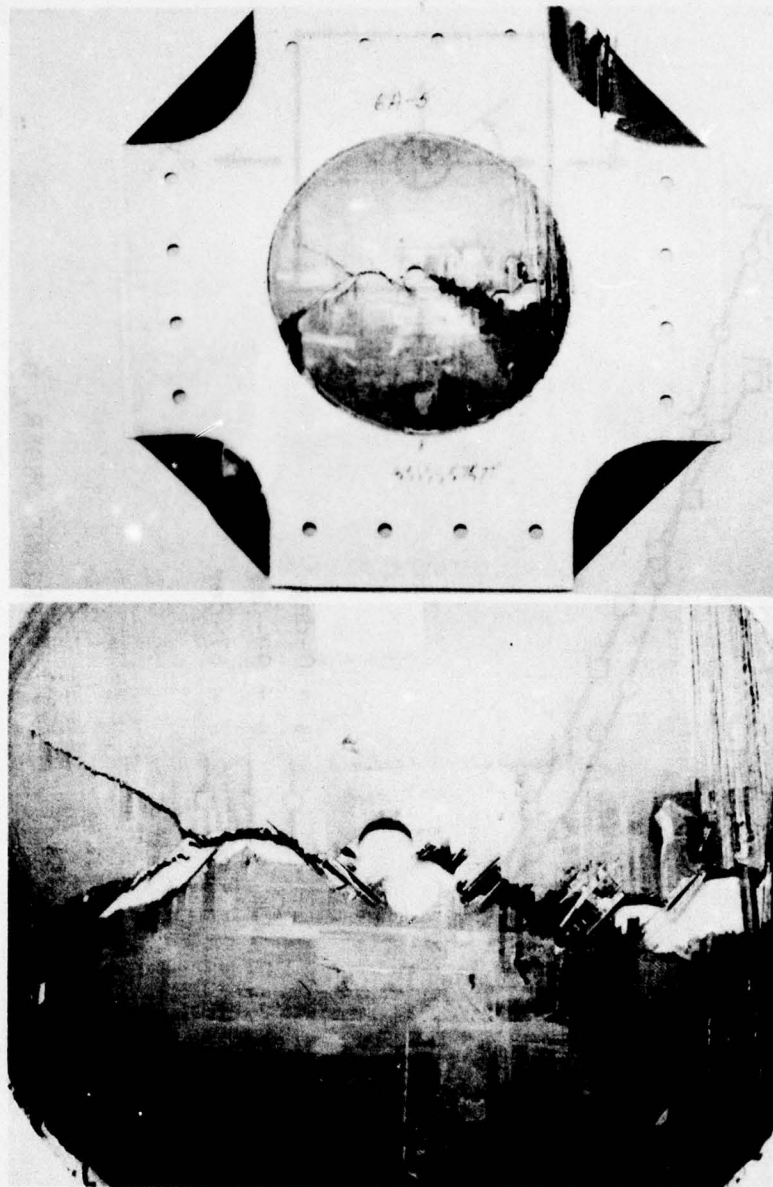


Figure 56. Failure Pattern of $[0_2/+45]_s$ Graphite/Epoxy Specimen With 1.27 cm (0.50 in.) Diameter Hole Under Biaxial Loading $\sigma_{yy} = 2\sigma_{xx}$ (Spec. No. 6A-5)

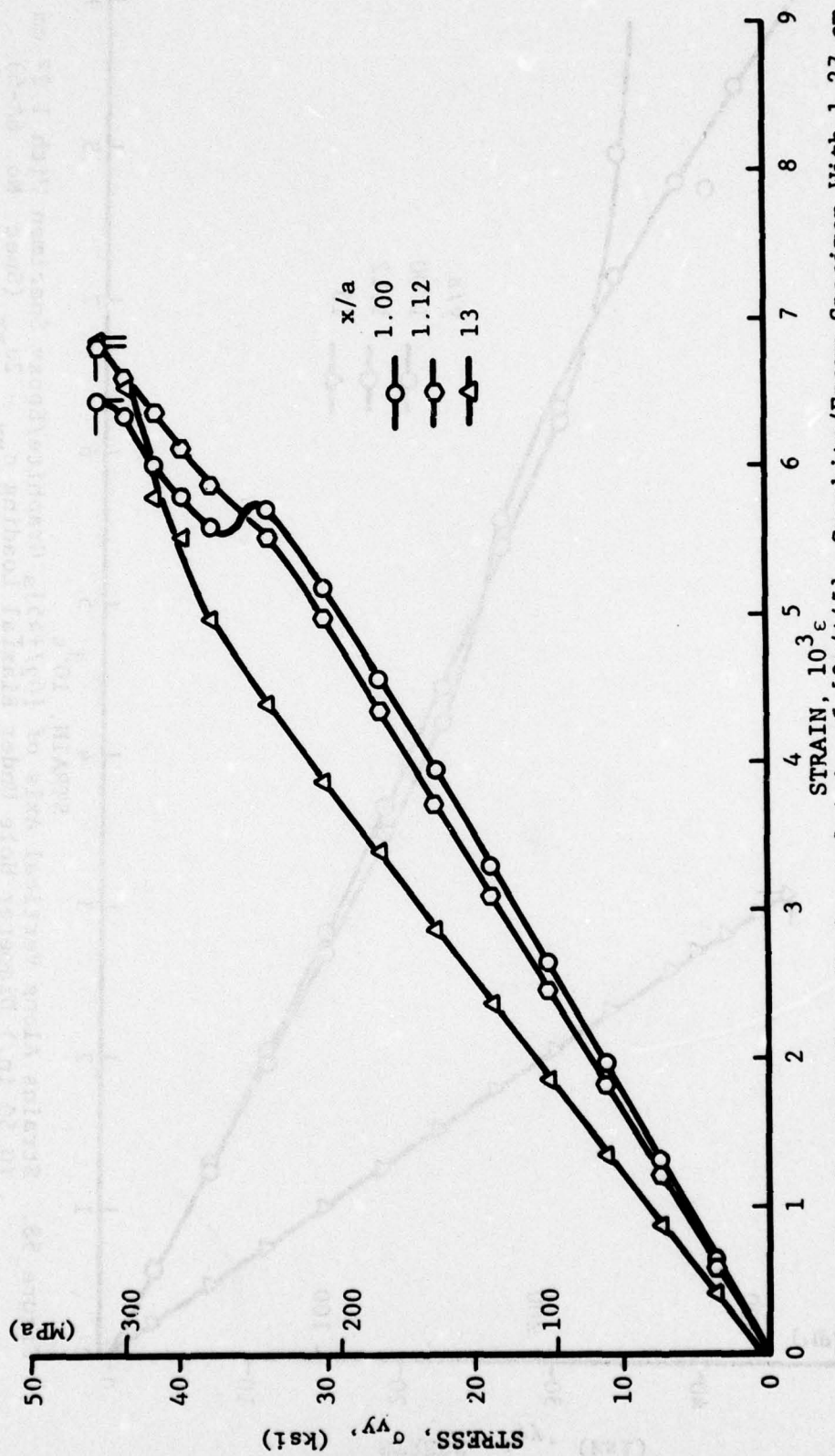


Figure 57. Strains Along Horizontal Axis of [0/±45]s Graphite/Epoxy Specimen With 1.27 cm (0.50 in.) Diameter Hole Under Biaxial Loading $\sigma_{yy} = 2\sigma_{xx}$ (Spec. No. 6A-6)



Figure 58. Strains Along Vertical Axis of $[0_2/+45]_s$ Graphite/Epoxy Specimen With 1.27 cm (0.50 in.) Diameter Hole Under Biaxial Loading $\sigma_{yy} = 2\sigma_{xx}$ (Spec. No. 6A-6)

The first audible fracture occurred at a stress of 156 MPa (23 ksi) which is very close to the limit of linearity. Ultimate failure occurred at 312 MPa (45.3 ksi). The failure pattern is shown in Figure 59.

Specimen No. 6A-7 had a 0.64 cm (0.25 in.) diameter hole. The initial 5-ply glass/epoxy tab was reinforced with three additional layers of resin-impregnated cloth (style No. 1581) which was laid over each side of the original tab and cured in place. This overlay extended up to a 15.2 cm (6 in.) diameter circle in the middle of the specimen. The specimen was instrumented with strain gages and a 0.5 mm (0.020 in.) thick photoelastic coating. Strain variations along the two loading axes are shown in Figures 60 and 61. On the horizontal axis the strain on the boundary of the hole is linear up to an applied stress of 166 MPa (24 ksi). On the vertical axis the strain on the hole boundary is linear up to a stress of 117 MPa (17 ksi). The horizontal strain near the hole boundary ($y/a = 1.24$) is slightly larger than that on the boundary (Figure 61). The stress ratios at two locations on the hole boundary in the linear range are:

$$\left(\frac{\sigma_{\theta\theta}}{\sigma_{yy}} \right)_{\theta=0^\circ} = 0.58$$

$$\left(\frac{\sigma_{\theta\theta}}{\sigma_{yy}} \right)_{\theta=90^\circ} = 2.02$$

Isochromatic fringe patterns in the photoelastic coating around the hole are shown in Figures 62 and 63 for six levels of applied vertical stress. The fringe patterns at low loads indicated a nearly uniform strain distribution on the boundary of the hole. The first evidence of surface cracking in the vertical direction occurs at the 0-deg. points (vertical axis) at an applied stress of 204 MPa (29.5 ksi). Birefringence (strain) concentration develops

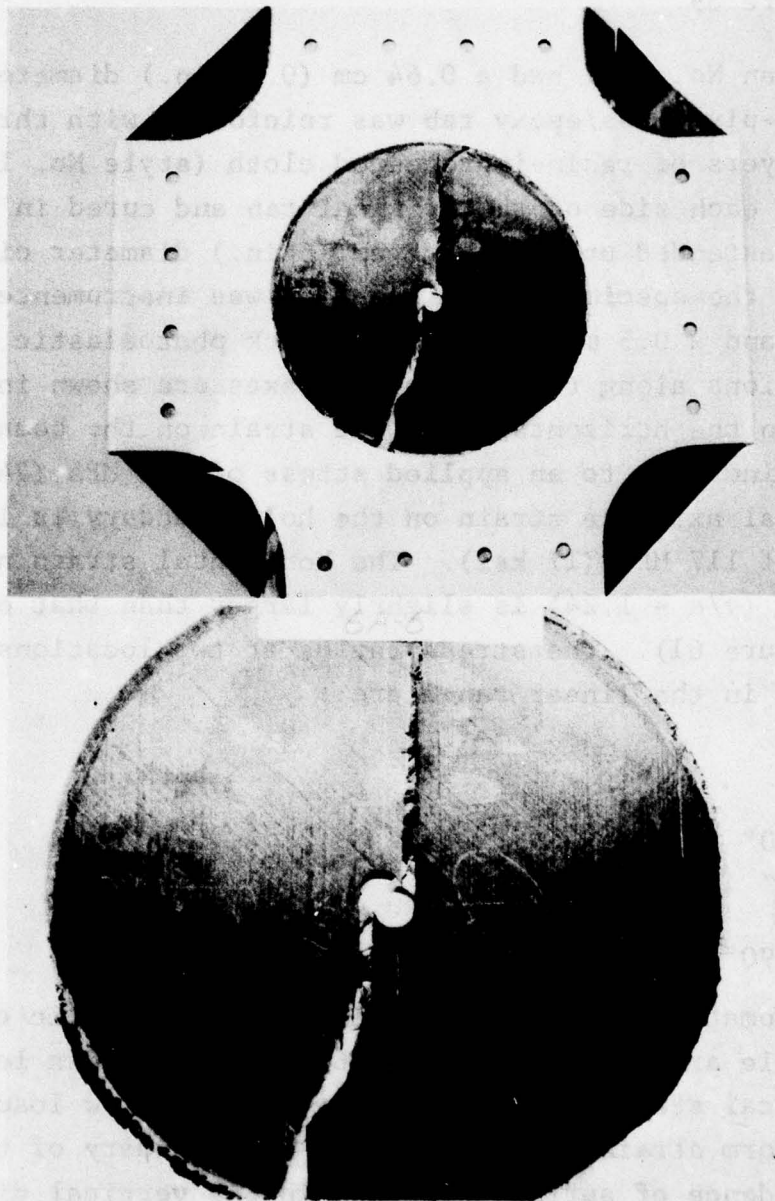


Figure 59. Failure Pattern of $[0_2/+45]_s$ Graphite/Epoxy Specimen With 1.27 cm (0.50 in.) Diameter Hole Under Biaxial Loading $\sigma_{yy} = 2\sigma_{xx}$ (Spec. No. 6A..)

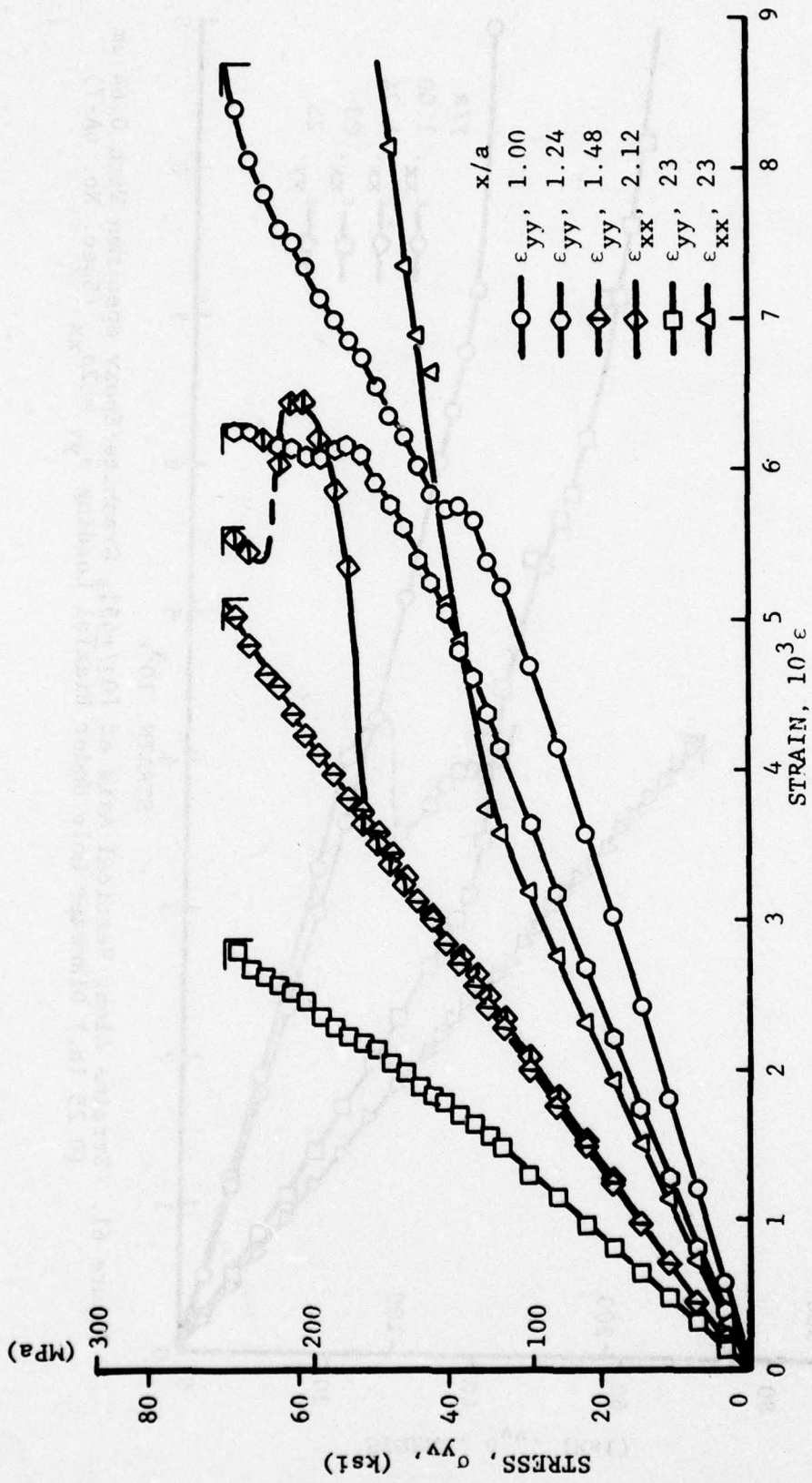


Figure 60. Strains Along Horizontal Axis of $[0_2/+45]_s$ Graphite/Epoxy Specimen With 0.64 cm (0.25 in.) Diameter Hole Under Biaxial Loading $\sigma_{yy} = 2\sigma_{xx}$

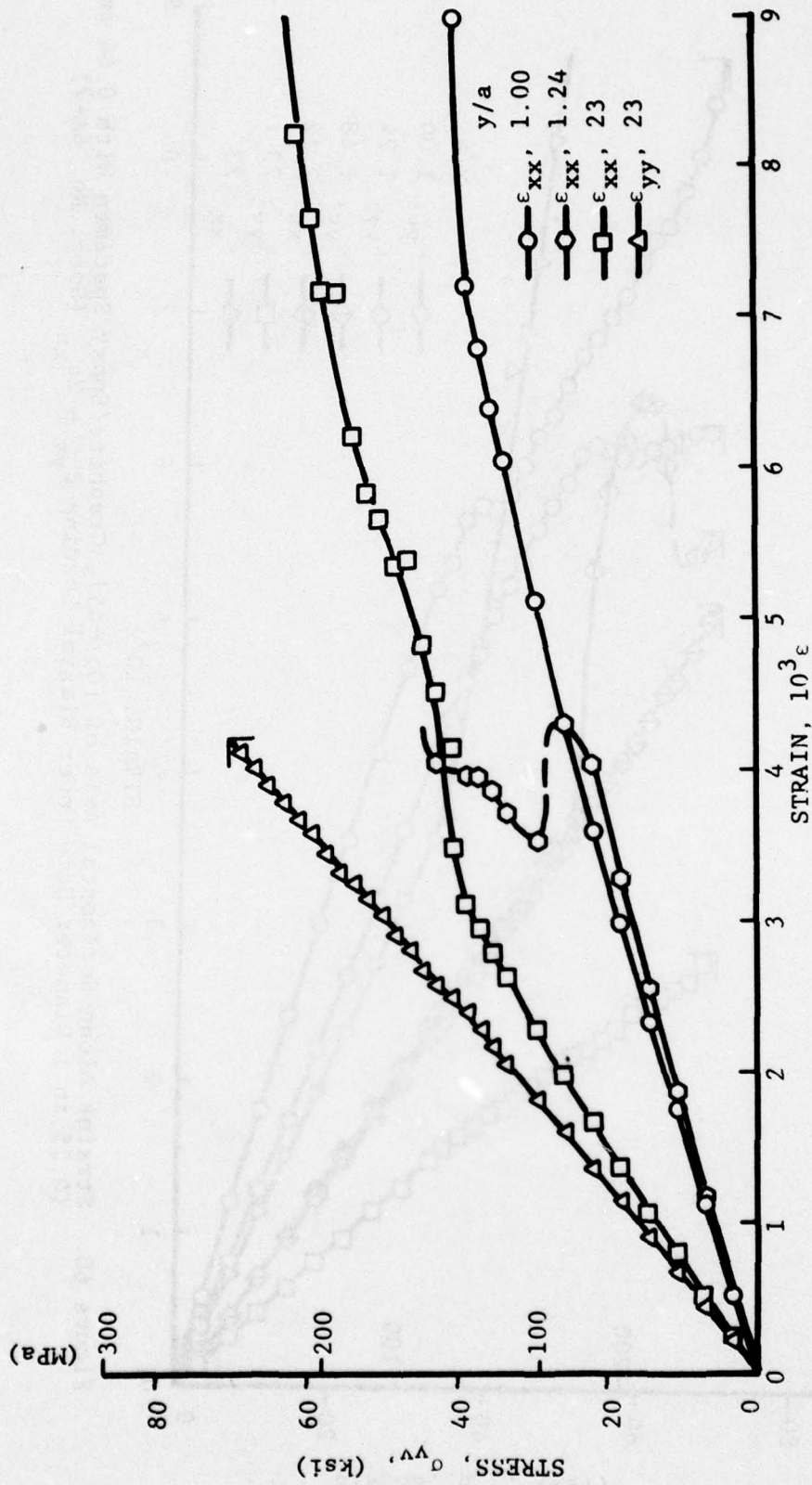
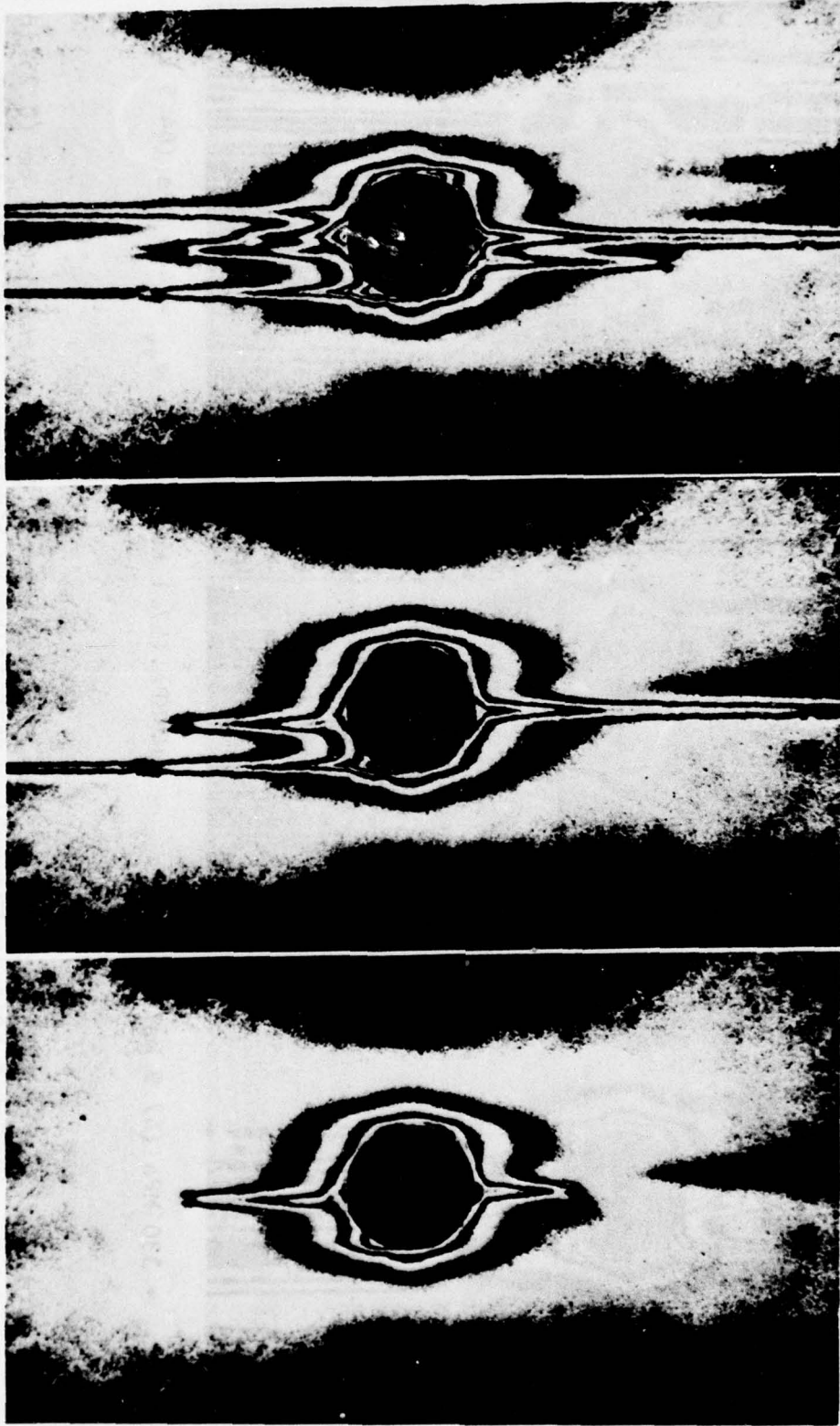
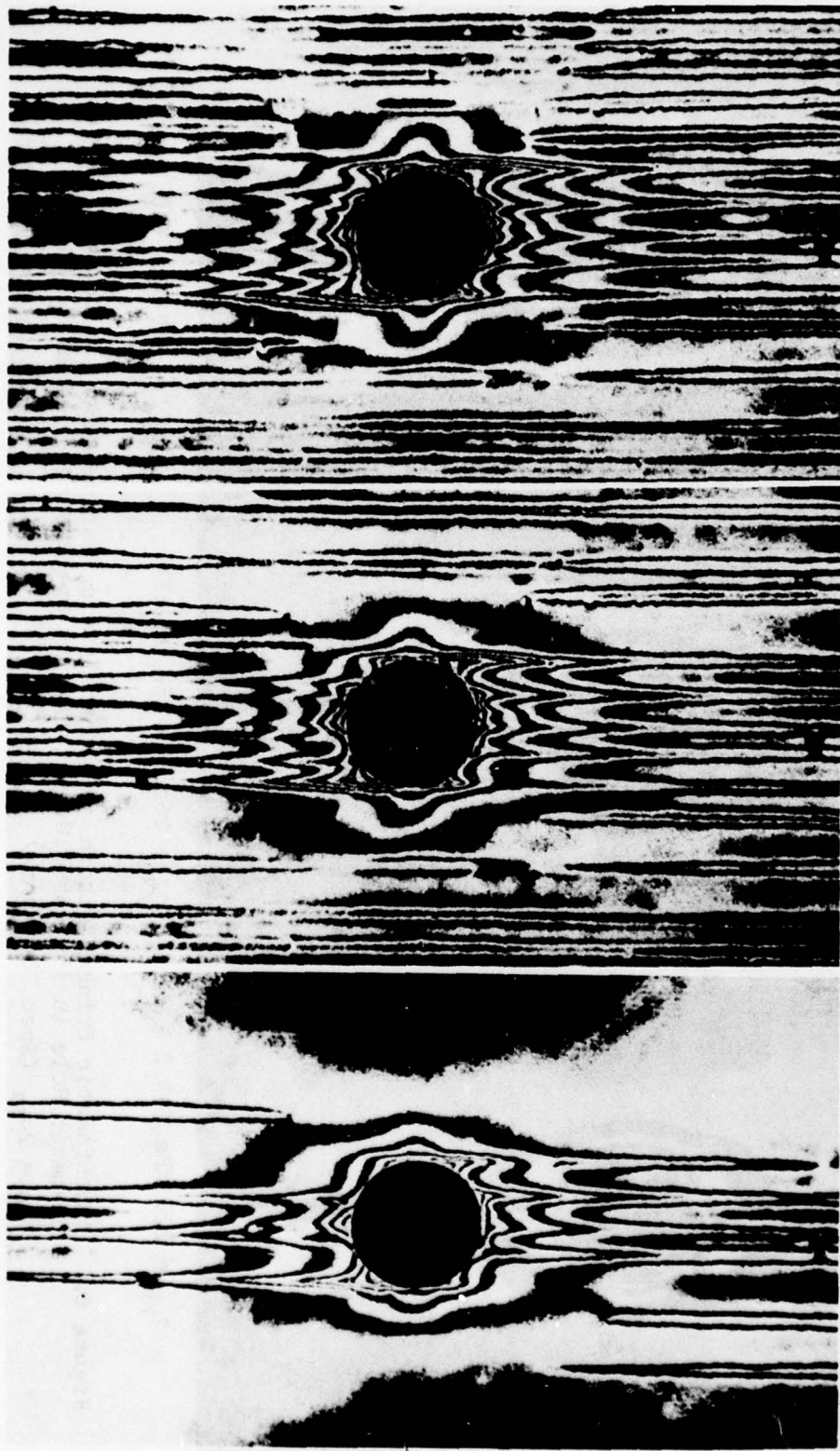


Figure 61. Strains Along Vertical Axis of [02/+45]_s Graphite/Epoxy Specimen With 0.64 cm (0.25 in.) Diameter Hole Under Biaxial Loading $\sigma_{yy} = 2\sigma_{xx}$ (Spec. No. 6A-7)



$\sigma_{yy} = 229 \text{ MPa (33.2 ksi)}$
 $\sigma_{yy} = 255 \text{ MPa (36.9 ksi)}$
 $\sigma_{yy} = 279 \text{ MPa (40.5 ksi)}$

Figure 62. Isochromatic Fringe Patterns in Photoelastic Coating Around 0.64 cm (0.25 in.) Diameter Hole in $[0_2/+45]_s$ Graphite/Epoxy Specimen Under Biaxial Loading
 $\sigma_{yy} = 2\sigma_{xx}$ (Spec. No. 6A-7)



$\sigma_{yy} = 330 \text{ MPa (47.9 ksi)}$
 $\sigma_{yy} = 394 \text{ MPa (57.1 ksi)}$
 $\sigma_{yy} = 445 \text{ MPa (64.5 ksi)}$

Figure 63. Isochromatic Fringe Patterns in Photoelastic Coating Around 0.64 cm (0.25 in.) Diameter Hole in $[0_2/+45]_s$ Graphite/Epoxy Specimen Under Biaxial Loading $\sigma_{yy} = 2\sigma_{xx}$ (Spec. No. 6A-7)

later at points 60-deg. off the vertical axis with vertical cracks initiating from such points at a stress of 255 MPa (36.9 ksi). The vertical surface-crack pattern gradually extends throughout the specimen, whereas the birefringence (strain) level at the 60-deg. and 90-deg. locations remains unchanged. Only the strain at the 0-deg. location continues increasing to failure. The birefringence and strain variation at the three locations above on the hole boundary is plotted in Figure 64. All three strains are approximately equal and vary linearly up to an applied stress of 204 MPa (29.5 ksi). Thereafter, the strain at the 90-deg. location increases little or stays nearly constant up to failure. At the 60-deg. location the strain increases further at a faster rate up to a point and then it remains constant up to failure. At the 0-deg. location the strain exceeds that at the 60-deg. location and continues increasing up to failure. The maximum surface strain at failure is approximately 0.021. Ultimate failure occurred at a stress of 482 MPa (69.8 ksi). The failure pattern is shown in Figure 65.

Specimen No. 6A-8, a replicate of No. 6A-7 above, had a 0.64 cm (0.25 in.) diameter hole and was instrumented with strain gages. It had the same type of tab reinforcement as specimen No. 6A-7 above. Strain variations along the two loading axes are shown in Figures 66 and 67. On the horizontal axis the strain on the boundary of the hole is linear up to an applied stress of 173 MPa (25 ksi), then it continues at a slightly decreased rate up to a stress of 230 MPa (33 ksi). Thereafter, the rate of increase of this strain is decreased sharply. On the vertical axis the strain on the hole boundary is initially linear only up to a stress of 52 MPa (7.5 ksi) then, it varies linearly at a reduced rate up to a stress of 154 MPa (22 ksi). The horizontal

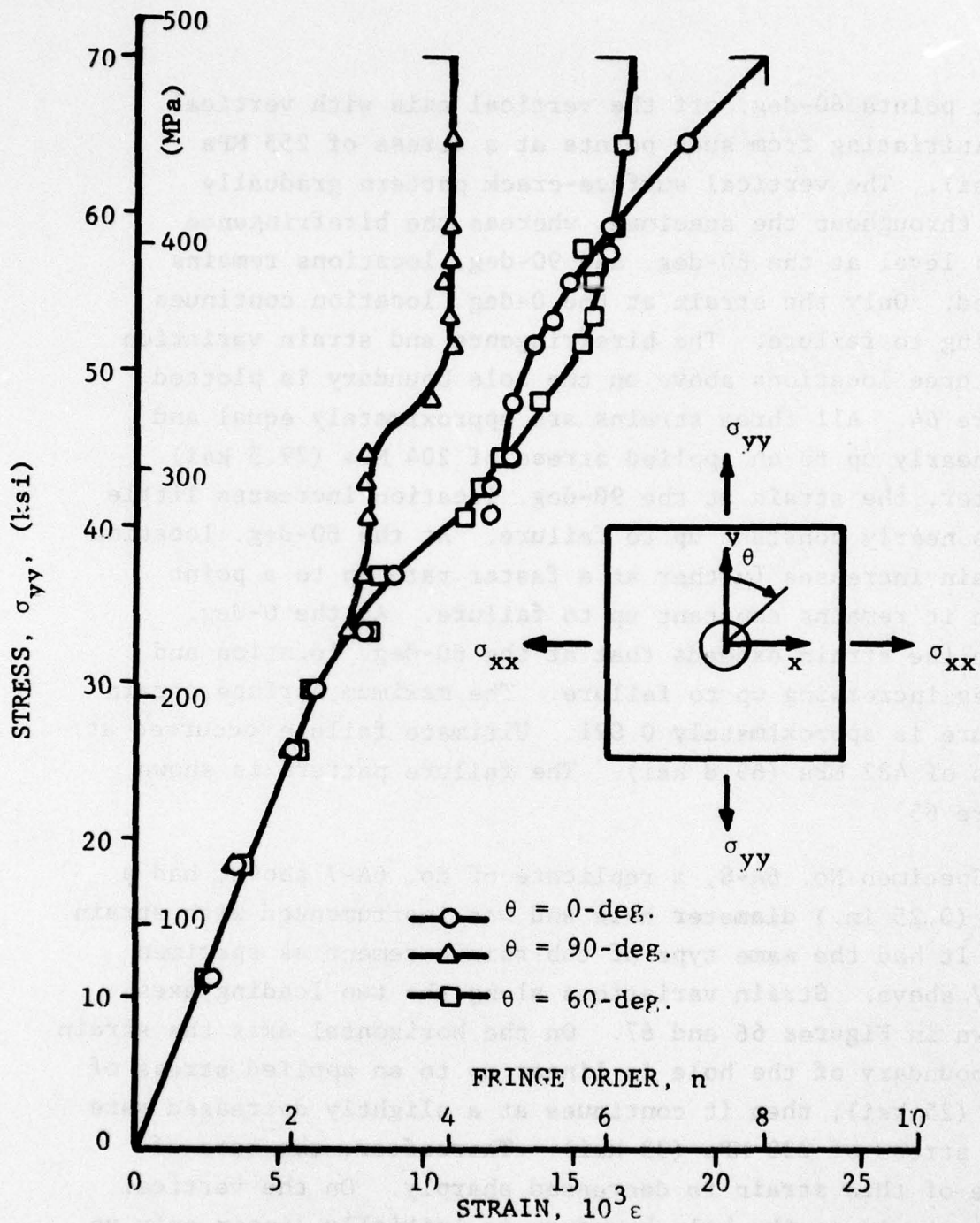


Figure 64. Fringe Order and Circumferential Strain at Three Locations on the Hole Boundary of $[0_2/+45]_S$ Graphite/Epoxy Specimen With 0.64 cm (0.25 in.) Diameter Hole Under Biaxial Loading $\sigma_{yy} = 2\sigma_{xx}$ (Spec. No. 6A-7)

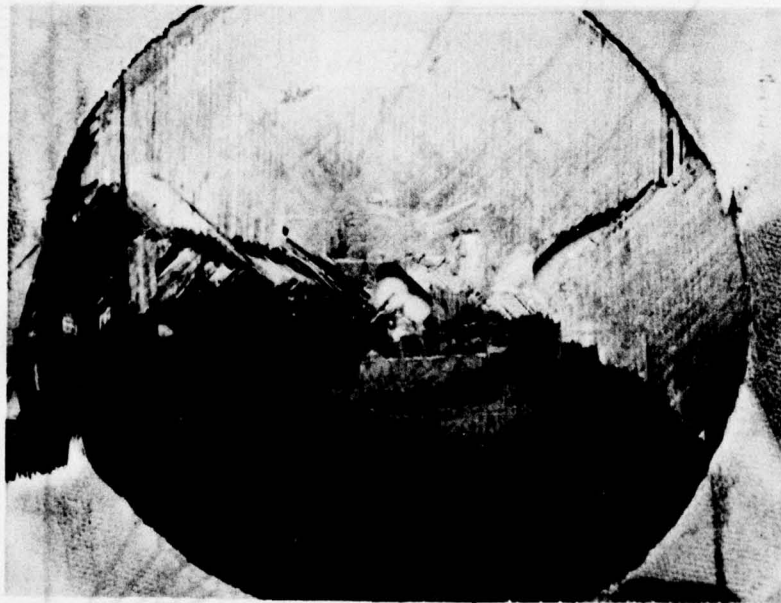
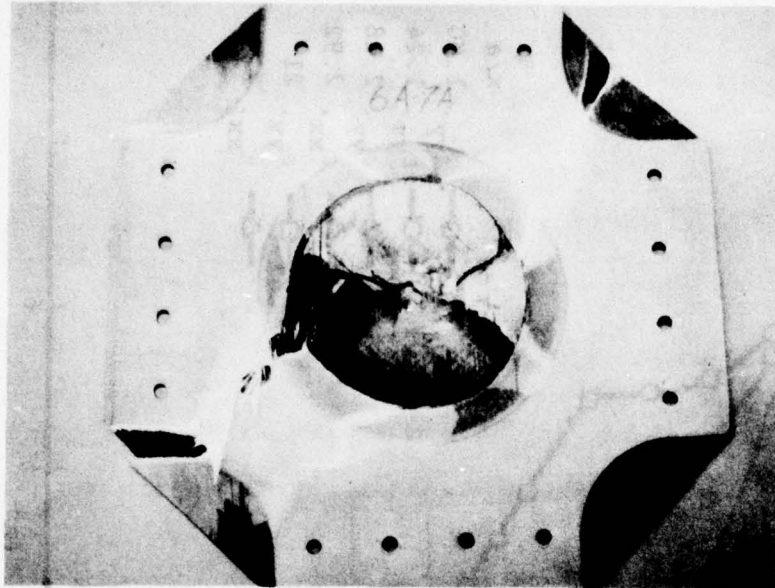


Figure 65. Failure Pattern of $[0_2/+45]_s$ Graphite/Epoxy Specimen With 0.64 cm (0.25 in.) Diameter Hole Under Biaxial Loading $\sigma_{yy} = 2\sigma_{xx}$ (Spec. No. 6A-7)

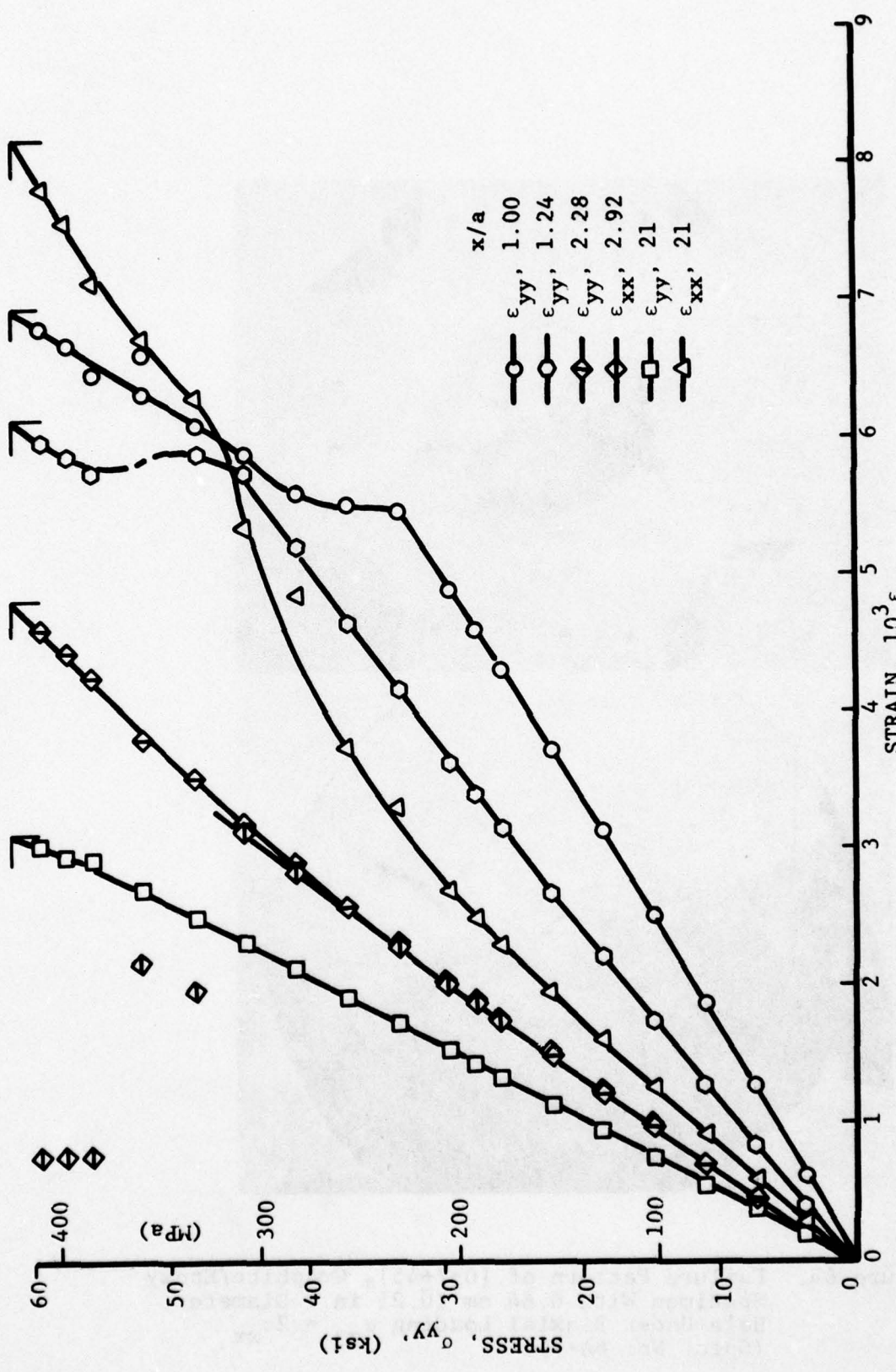


Figure 66. Strains Along Horizontal Axis of [02/+45]_s Graphite/Epoxy Specimen With 0.64 cm (0.25 in.) Diameter Hole Under Biaxial Loading $\sigma_{yy} = 2\sigma_{xx}$ (Spec. No. 6A-8)

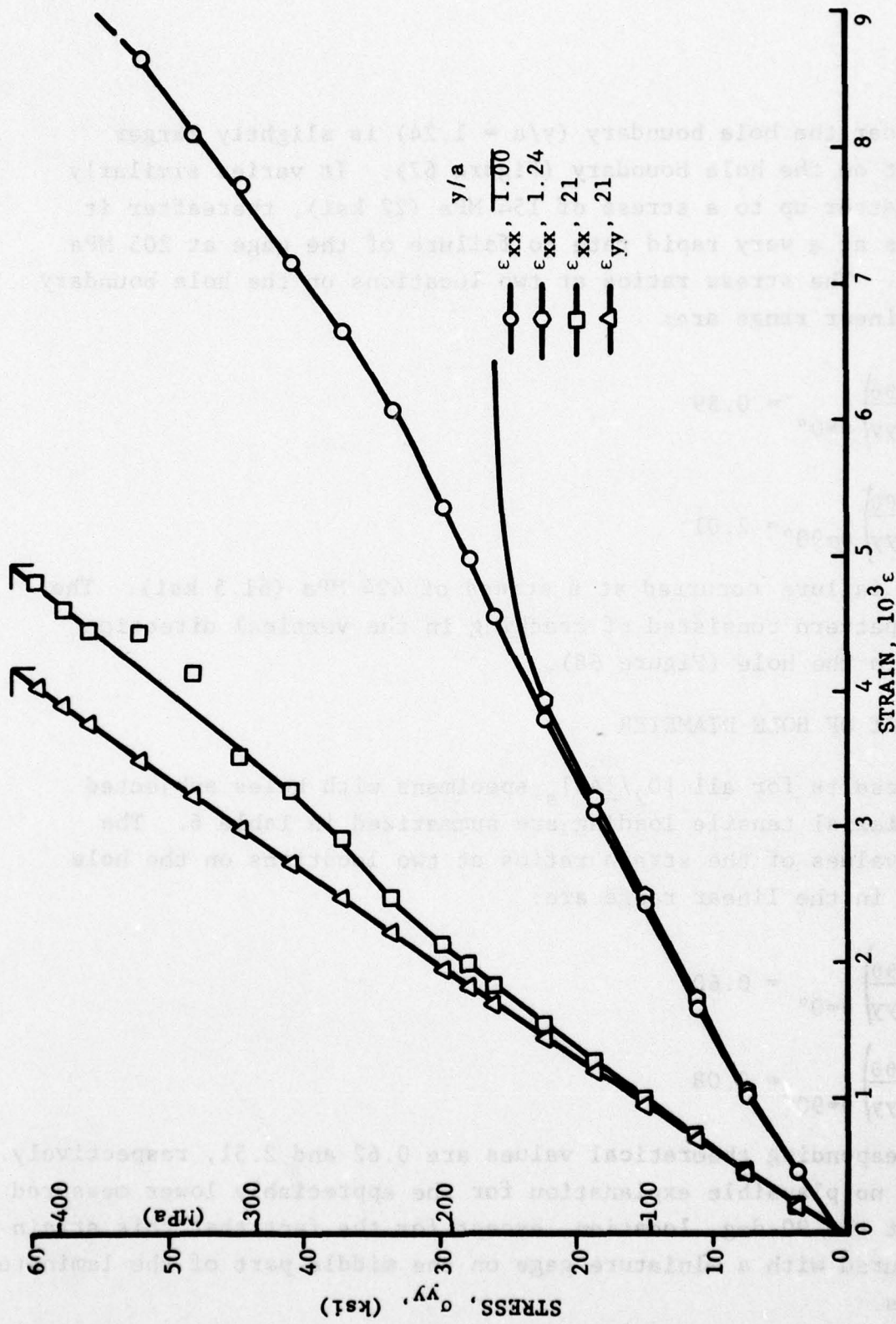


Figure 67. Strains Along Vertical Axis of $[0_2/+45]_s$ Graphite/Epoxy Specimen With 0.64 cm (0.25 in.) Diameter Hole Under Biaxial Loading $\sigma_{yy} = 2\sigma_{xx}$ (Spec. No. 6A-8)

strain near the hole boundary ($y/a = 1.24$) is slightly larger than that on the hole boundary (Figure 67). It varies similarly as the latter up to a stress of 154 MPa (22 ksi), thereafter it increases at a very rapid rate to failure of the gage at 205 MPa (30 ksi). The stress ratios at two locations on the hole boundary in the linear range are:

$$\left(\frac{\sigma_{\theta\theta}}{\sigma_{yy}}\right)_{\theta=0^\circ} = 0.59$$

$$\left(\frac{\sigma_{\theta\theta}}{\sigma_{yy}}\right)_{\theta=90^\circ} = 2.01$$

Ultimate failure occurred at a stress of 424 MPa (61.5 ksi). The failure pattern consisted of cracking in the vertical direction tangent to the hole (Figure 68).

5. EFFECT OF HOLE DIAMETER

Results for all $[0_2/\pm 45]_s$ specimens with holes subjected to 2:1 biaxial tensile loading are summarized in Table 6. The average values of the strain ratios at two locations on the hole boundary in the linear range are:

$$\left(\frac{\sigma_{\theta\theta}}{\sigma_{yy}}\right)_{\theta=0^\circ} = 0.60$$

$$\left(\frac{\sigma_{\theta\theta}}{\sigma_{yy}}\right)_{\theta=90^\circ} = 2.08$$

The corresponding theoretical values are 0.62 and 2.51, respectively. There is no plausible explanation for the appreciably lower measured strain at the 90-deg. location, except for the fact that this strain was measured with a miniature gage on the middle part of the laminate thickness.



Figure 68. Failure Pattern of $[0_2/+45]_s$ Graphite/Epoxy Specimen With 0.64 cm (0.25 in.) Diameter Hole Under Biaxial Loading $\sigma_{yy} = 2\sigma_{xx}$ (Spec. No. 6A-8)

Table 6
 [0₂/+45] _s LAMINATES WITH CIRCULAR HOLES UNDER 2:1 BIAxIAL LOADING

Spec. No.	Hole Dia. 2a cm (in.)	Stress Ratio ($\sigma_{\theta\theta}/\sigma_{yy}$)		Failure Stress $S_{yyT} = 2S_{xxT}$ MPa (ksi)	Maximum Strain at Failure ($10^{-3}\epsilon$)	Strength Reduction Ratio S_{yyT}/S_o
		$\theta=0^\circ$	$\theta=90^\circ$			
6A-1	2.54 (1.00)	0.55	2.12	311 (45.1)	14.5	0.39
6A-2	2.54 (1.00)	0.60	2.09	299 (43.4)		0.37
6A-3	1.91 (0.75)	0.61	2.01	325 (47.1)	16.4	0.41
6A-4	1.91 (0.75)	0.62	2.28	325 (47.1)		0.41
6A-5	1.27 (0.50)	0.62	2.02	330 (47.9)	15.3	0.41
6A-6	1.27 (0.50)	0.64	2.08	312 (45.3)		0.39
6A-7	0.64 (0.25)	0.58	2.02	482 (69.8)	21	0.60
6A-8	0.64 (0.25)	0.59	2.01	424 (61.5)	>12	0.53

In all cases ultimate failure is preceded by audible fractures starting at an applied vertical stress of approximately 172 MPa (25 ksi) which coincides with the stress level at which the strains around the hole boundary become nonlinear. The maximum strain at failure on the hole boundary, measured by means of photoelastic coatings, ranges between 14.5×10^{-3} and 21×10^{-3} compared to an ultimate strain of 10×10^{-3} for the unnotched laminate in the 0-deg. direction. This maximum strain occurs near the 65-deg. location for large diameter holes and near the 0-deg. location for the smaller diameter holes. The stress level and location of failure initiation can be predicted approximately by comparing the circumferential stress and strength distributions around the hole boundary. Figure 69 shows the strength distribution obtained from the unnotched laminate results (Table 4) and the elastic stress distribution at the 152 MPa (22 ksi) level of applied vertical stress. As can be seen, this stress level represents the limit beyond which localized failure and nonlinear response begin to take place at the 0-degree and 67.5-degree locations. As the applied stress is increased localized failure in the vicinity of the 67.5-degree location causes a stress redistribution with a reduction in the rate of increase of the stress and strain at the 90-degree location. Soon after failure initiation at the 67.5-degree location there is localized failure near the 0-degree location. This failure initiates at points away from the hole boundary where the horizontal (σ_{xx}) tensile stress reaches the maximum value $0.68\sigma_{yy}$. The interaction between the two sources of localized failure is such that for smaller holes the strains at the 0-degree location become higher than those at the 67.5-degree location, contrary to the result for larger holes.

The variation of the strength reduction ratio, defined as the ratio of the vertical (0-degree) stress at failure to the unnotched uniaxial strength of the material in the same direction, is shown in Figure 70. Results are compared with those for similar

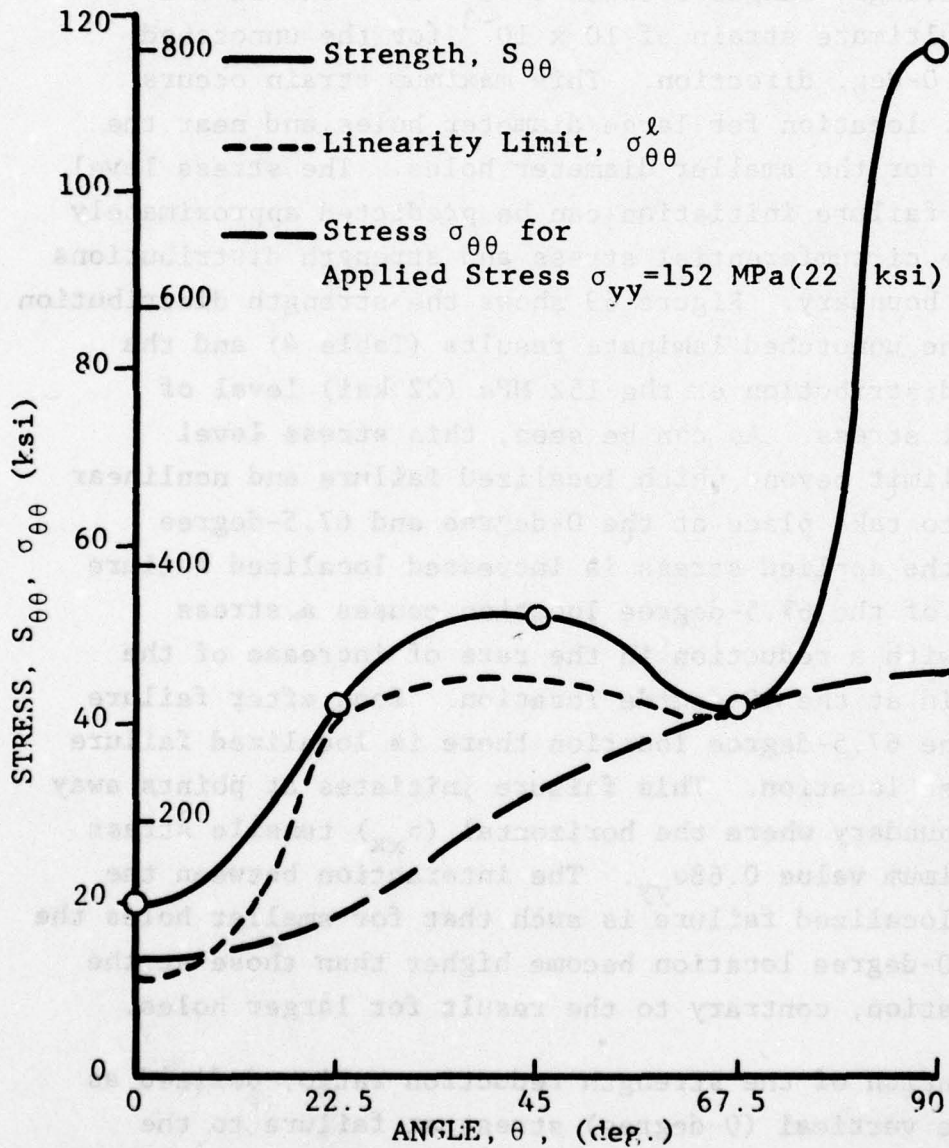


Figure 69. Distribution Around Boundary of Hole of Circumferential Strength and Stress for $[0_2/+45]_s$ Graphite/Epoxy Specimen Under Biaxial Loading $\sigma_{yy} = 2\sigma_{xx}$

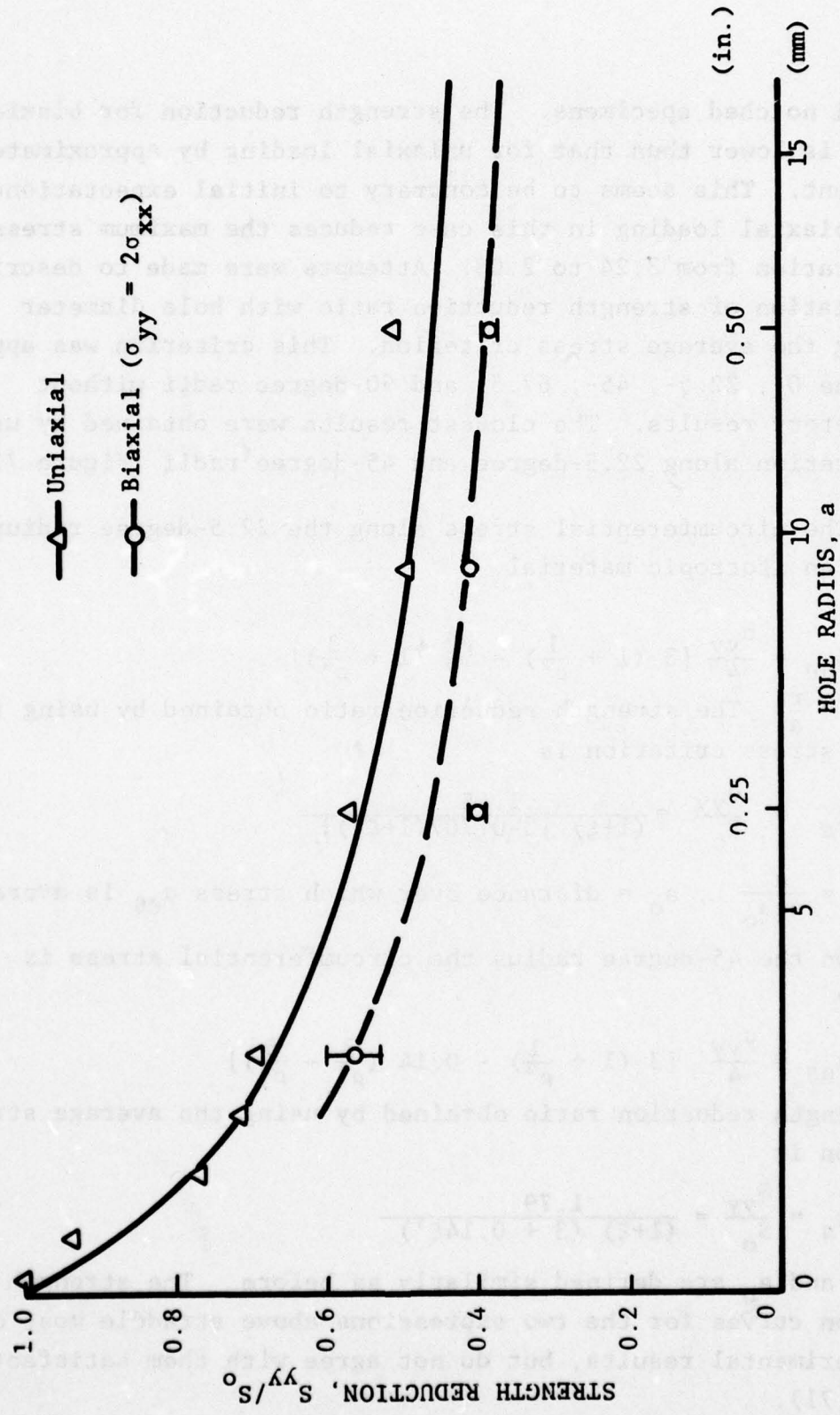


Figure 70. Strength Reduction as a Function of Hole Radius for [02/+45]_s Graphite/Epoxy Plates With Circular Holes Under Uniaxial and 2:1 Biaxial Loading

uniaxial notched specimens. The strength reduction for biaxial loading is lower than that for uniaxial loading by approximately 16 percent. This seems to be contrary to initial expectations as the biaxial loading in this case reduces the maximum stress concentration from 3.24 to 2.08. Attempts were made to describe the variation of strength reduction ratio with hole diameter by using the average stress criterion. This criterion was applied along the 0-, 22.5-, 45-, 67.5- and 90-degree radii without satisfactory results. The closest results were obtained by using the criterion along 22.5-degree and 45-degree radii (Figure 71).

The circumferential stress along the 22.5-degree radius is, for an isotropic material,

$$\sigma_{\theta\theta} = \frac{\sigma_{yy}}{4} \left[3 \left(1 + \frac{1}{\rho^2} \right) - \frac{\sqrt{2}}{2} \left(1 + \frac{3}{\rho^4} \right) \right]$$

where $\rho = \frac{r}{a}$. The strength reduction ratio obtained by using the average stress criterion is

$$k_s = \frac{S_{yy}}{S_o} = \frac{1.45}{(1+\xi) [3 - 0.707(1+\xi^2)]}$$

where $\xi = \frac{a}{a+a_o}$, a_o = distance over which stress $\sigma_{\theta\theta}$ is averaged.

On the 45-degree radius the circumferential stress is given by

$$\sigma_{\theta\theta} \cong \frac{\sigma_{yy}}{4} \left[3 \left(1 + \frac{1}{\rho^2} \right) - 0.14 \left(\frac{3}{\rho^4} - \frac{5}{\rho^6} \right) \right]$$

The strength reduction ratio obtained by using the average stress criterion is

$$k_s = \frac{S_{yy}}{S_o} = \frac{1.79}{(1+\xi) (3 + 0.14\xi^4)}$$

where ξ and a_o are defined similarly as before. The strength reduction curves for the two expressions above straddle most of the experimental results, but do not agree with them satisfactorily (Figure 71).

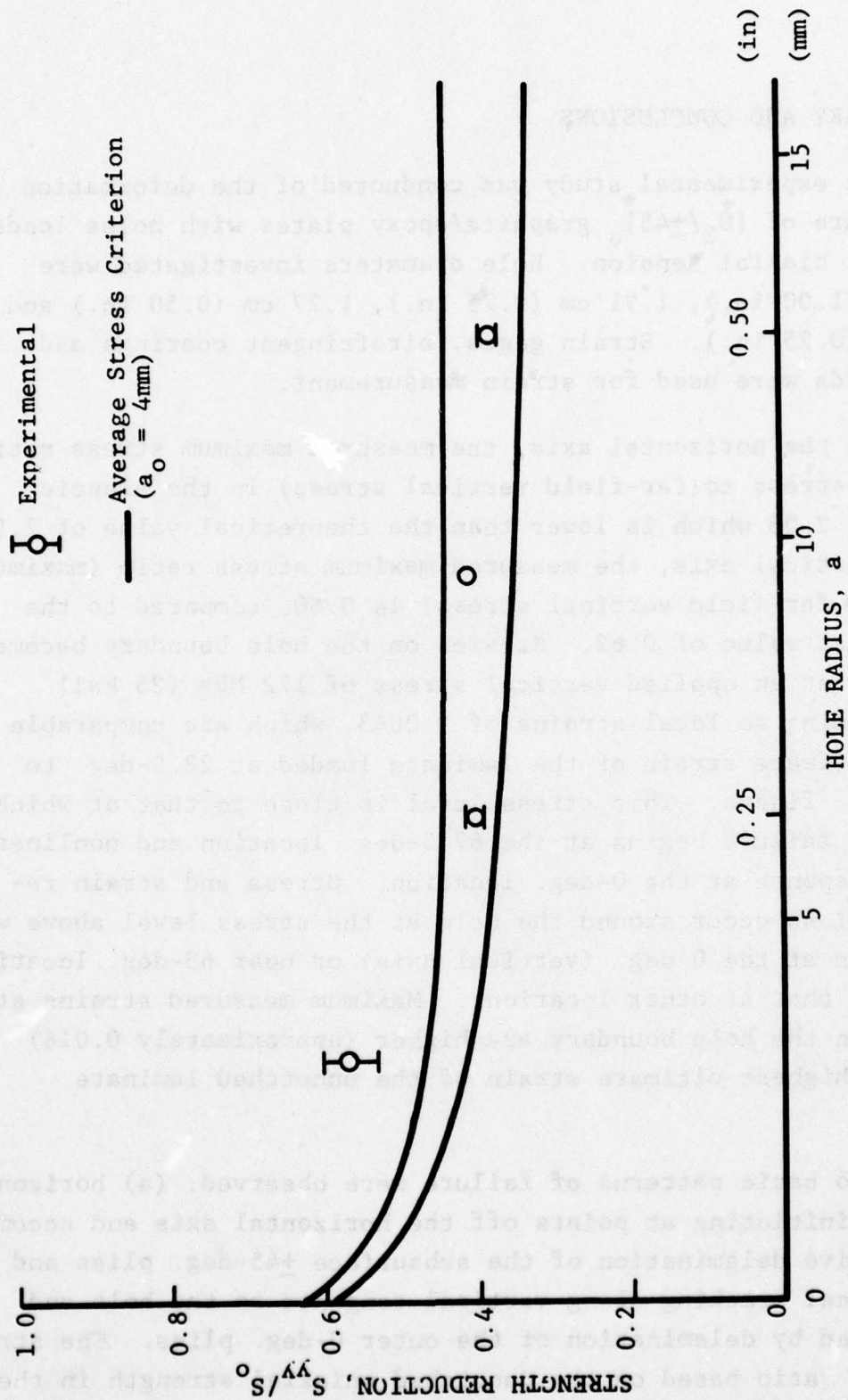


Figure 71. Strength Reduction as a Function of Hole Radius for [0₂/+45]s Graphite/Epoxy Plates With Circular Holes Under 2:1 Biaxial Loading

6. SUMMARY AND CONCLUSIONS

An experimental study was conducted of the deformation and failure of $[0_2/+45]_s$ graphite/epoxy plates with holes loaded under 2:1 biaxial tension. Hole diameters investigated were 2.54 cm (1.00 in.), 1.91 cm (0.75 in.), 1.27 cm (0.50 in.) and 0.64 cm (0.25 in.). Strain gages, birefringent coatings and moire grids were used for strain measurement.

On the horizontal axis, the measured maximum stress ratio (maximum stress to far-field vertical stress) in the elastic range, is 2.08 which is lower than the theoretical value of 2.51. On the vertical axis, the measured maximum stress ratio (maximum stress to far-field vertical stress) is 0.60, compared to the theoretical value of 0.62. Strains on the hole boundary become nonlinear at an applied vertical stress of 172 MPa (25 ksi) corresponding to local strains of 0.0043, which are comparable to the ultimate strain of the laminate loaded at 22.5-deg. to the 0-deg. fibers. This stress level is close to that at which localized failure begins at the 67.5-deg. location and nonlinear strain response at the 0-deg. location. Stress and strain redistributions occur around the hole at the stress level above with the strain at the 0-deg. (vertical axis) or near 65-deg. locations exceeding that at other locations. Maximum measured strains at failure on the hole boundary are higher (approximately 0.016) than the highest ultimate strain of the unnotched laminate (0.010).

Two basic patterns of failure were observed: (a) horizontal cracking initiating at points off the horizontal axis and accompanied by extensive delamination of the subsurface ± 45 -deg. plies and (b) vertical cracking along vertical tangents to the hole and accompanied by delamination of the outer 0-deg. plies. The strength reduction ratio based on the unnotched uniaxial strength in the

0-deg. direction varies between 0.38 and 0.57 for holes between 2.54 cm and 0.64 cm in diameter. These ratios are lower than corresponding values for uniaxial loading by approximately 16 percent, although in this case biaxial loading reduces the maximum stress concentration from 3.24 to 2.08. Attempts were made to describe the variation of strength reduction ratio with hole diameter using the average stress criterion. The closest but not very satisfactory results were obtained by using the criterion above along the 22.5-deg. and 45-deg. radii. The difficulty arises from the localized sources of failure and their interaction causing stress and strain redistributions around the hole boundary, which cannot be accounted for easily in the theoretical description.

SECTION VI
EFFECT OF NORMAL STRESS IN CRACK DIRECTION

1. INTRODUCTION

The far-field state of stress affecting crack extension and failure consists in general of two normal stresses normal and parallel to the crack and a shear stress in the direction of the crack (Figure 72). For a crack inclined at an angle θ with respect to the principal stress σ_1 , the far-field stress components are:

$$\sigma_y = \frac{\sigma_1 (1+k)}{2} - \frac{\sigma_1 (1-k)}{2} \cos 2\theta$$

$$\sigma_x = \frac{\sigma_1 (1+k)}{2} + \frac{\sigma_1 (1-k)}{2} \cos 2\theta$$

$$\tau_{xy} = \frac{\sigma_1 (1-k)}{2} \sin 2\theta$$

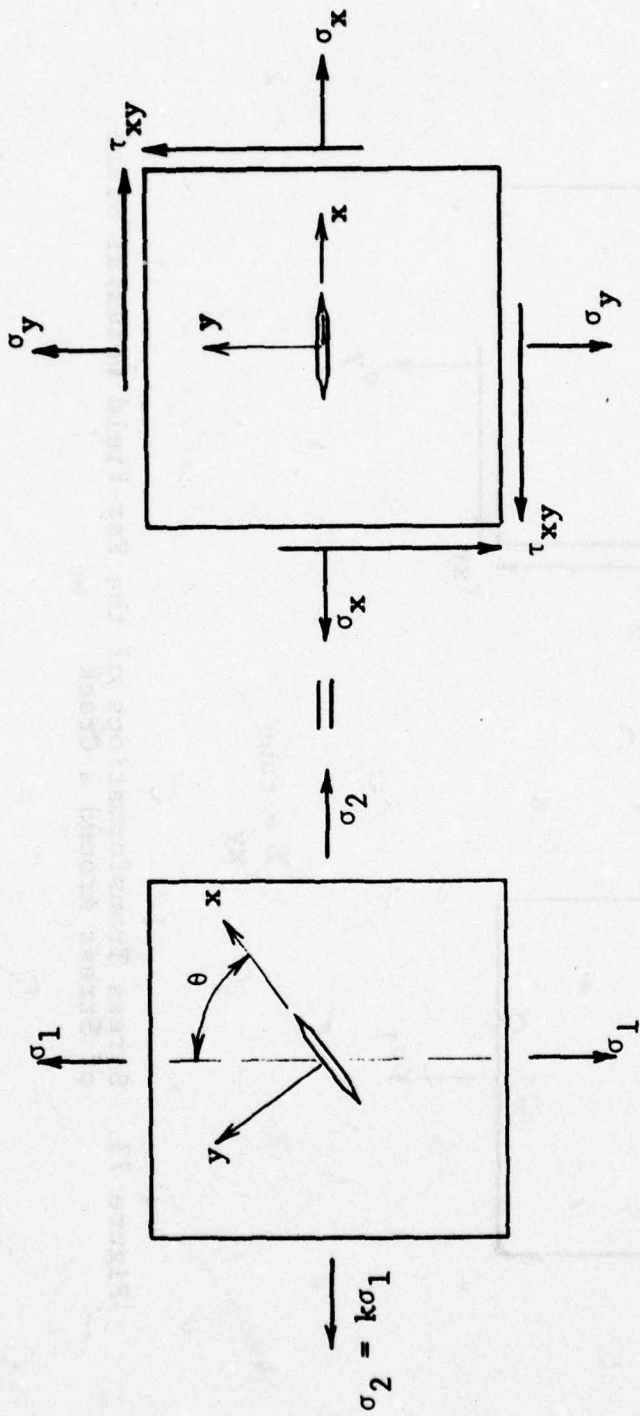
where the x- and y- directions are those parallel and perpendicular to the crack and k is the stress ratio $\sigma_2/\sigma_1 = k$.

It is generally assumed that the normal stress in the direction of the crack does not play an important role in crack extension. Then, the most important parameter is the ratio:

$$\frac{\sigma_y}{\tau_{xy}} = \frac{1+k - (1-k) \cos 2\theta}{(1-k) \sin 2\theta}$$

where σ_y is the normal stress normal to the crack and τ_{xy} is the shear stress along the crack.

The same far-field stress ratio σ_y/τ_{xy} around the crack can be achieved with a specimen loaded uniaxially at another angle θ' with the crack direction (Figure 73). The normal to shear stress ratio for the uniaxial specimen



$$\frac{\sigma_y}{\tau_{xy}} = \frac{1 + k - (1-k)\cos 2\theta}{(1-k)\sin 2\theta}$$

Figure 72. Stress Transformations of the Far-Field Biaxial State of Stress Around a Crack

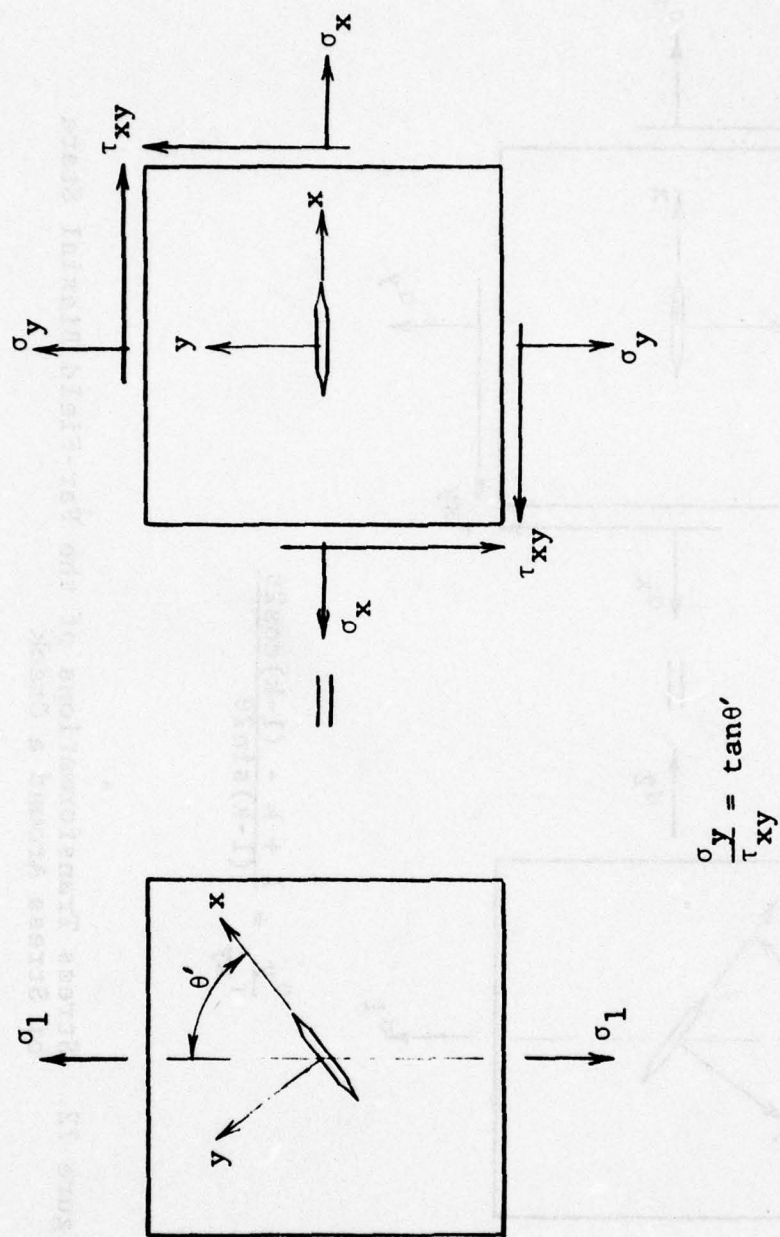


Figure 73. Stress Transformations of the Far-Field Uniaxial State of Stress Around a Crack

$$\frac{\sigma_y}{\tau_{xy}} = \frac{1 - \cos 2\theta'}{\sin 2\theta'} = \tan \theta'$$

is equal to that of the biaxial when

$$\tan \theta' = \frac{1+k - (1-k)\cos 2\theta}{(1-k)\sin 2\theta}$$

This equivalence of course assumes that the normal far-field stress in the direction of the crack, σ_x , has no influence on crack propagation. This is not assured even in the case of self-similar crack propagation when the crack is oriented along a principal material axis. It is certainly not valid in other cases including that when the crack is inclined with respect to the material axis, and when the crack propagates in a direction other than its own.

A series of tests with biaxially loaded $[0/\pm 45/90]_s$ graphite/epoxy specimens with cracks of different sizes has been performed and reported (Reference 1). In this series the crack was inclined at an angle $\theta = 30$ -deg. with the far-field principal stress σ_1 , and the biaxiality ratio was $k = \sigma_2/\sigma_1 = 0.5$. The equivalent uniaxial specimen having the same normal to shear stress ratio would have a crack inclined at an angle θ' with the applied load obtained as

$$\tan \theta' = \frac{1.5 - 0.5 \times 0.5}{0.5 \times 0.866} = 2.887$$

$$\theta' = 70.9\text{-deg.}$$

To study the effect of normal stress in the direction of the crack a series of uniaxial tests with inclined cracks was conducted.

2. SPECIMENS

The specimens were 8-ply $[0/\pm 45/90]_s$ plates 12.7 cm (5 in.) wide and 56 cm (22 in.) long with the 0-deg. fibers at 19-deg. with

the longitudinal (loading) axis and central cracks normal to the 0-deg. fibers (Figure 74). The crack geometry was the same as that used in the first phase of this work (Reference 1). All cracks were machined ultrasonically as before. The specimens were tabbed with 11-ply glass/epoxy crossply tabs (3M, Scotchply 1002). Four crack lengths were investigated, 2.54 cm (1 in.), 1.91 cm (0.75 in.), 1.27 cm (0.50 in.) and 0.64 cm (0.25 in.). Two specimens were tested for each crack length.

3. STRAIN MEASUREMENT

Deformations and strains were measured using strain gages, birefringent coatings and moire grids. Miniature single gages and rosettes were mounted near the crack tips along lines normal to the loading axis. Additional gages were mounted in the far-field. A typical gage layout is shown in Figure 75. In half the specimens birefringent coatings were bonded to one side to obtain full-field strain information. These coatings were 0.25 mm (0.01 in.) thick. In some cases moire grids consisting of arrays of 400 lines per cm (1000 lines per inch) parallel and normal to the crack were applied to the specimens.

4. LOADING AND DATA RECORDING

These specimens were loaded in the same fashion as the uniaxial plates with holes discussed before (Section IV). They were loaded in increments in a 120,000 lb Riehle testing machine at a crosshead rate of 1 mm/min (0.04 in./min.). At every load level strains were recorded with a digital data acquisition system and photoelastic and moire fringes recorded photographically.

5. RESULTS

Specimen No. 5A-1 had a 2.54 cm (1.00 in.) long crack. It was instrumented with strain gages near the crack tip and in the

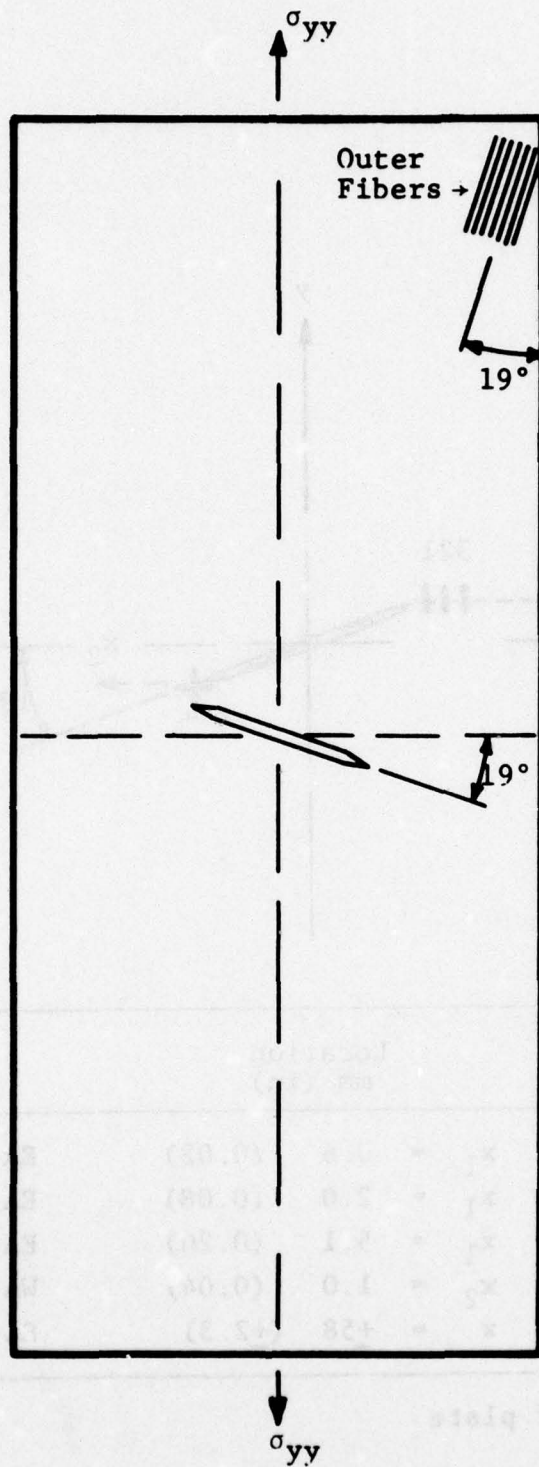
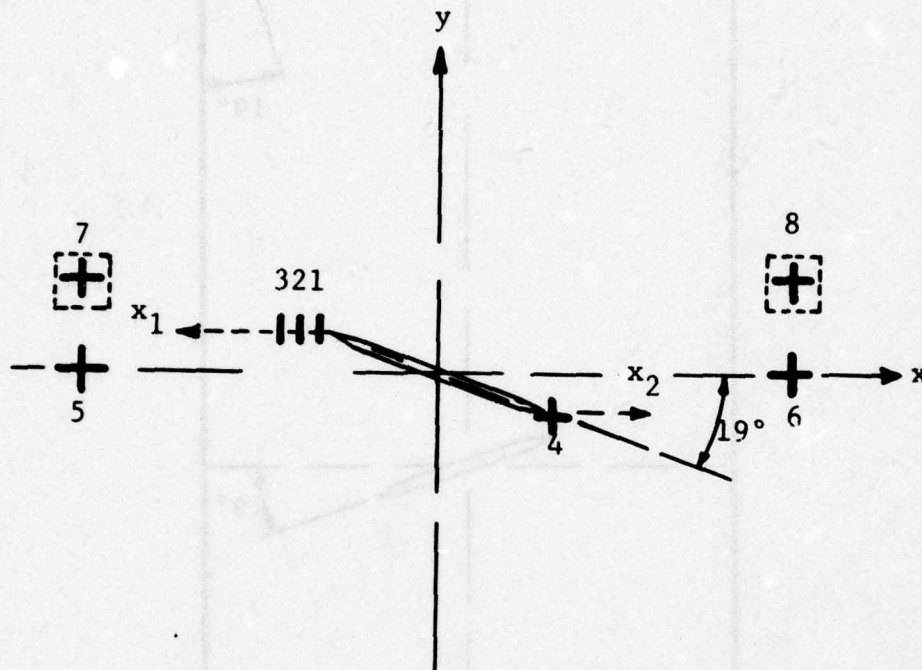


Figure 74. Uniaxial Loading of $[0/+45/90]_s$ Graphite/Epoxy Specimens With Inclined Cracks



Gage No.	Location mm (in)	Type
1	$x_1 = 0.6$ (0.02)	EA-06-015DJ-120
2	$x_1 = 2.0$ (0.08)	EA-06-031DE-120
3	$x_1 = 5.1$ (0.20)	EA-06-031DE-120
4	$x_2 = 1.0$ (0.04)	WA-06-030WT-120
5, 6, 7*, 8*	$x = \pm 58$ (± 2.3)	EA-06-125TM-120

* On opposite side of plate

Figure 75. Typical Gage Layout for Uniaxial Specimens With Inclined Cracks

far-field and with a 0.25 mm (0.010 in.) thick photoelastic coating on one side. A closeup of the gage layout around the crack is shown in Figure 76. Strains as a function of applied stress are plotted in Figure 77. Elastic and strength properties obtained are:

$$\begin{aligned} E_{yy} &= 53 \text{ GPa } (7.7 \times 10^6 \text{ psi}) \\ \nu_{yx} &= 0.30 \\ S_{yy} &= 180 \text{ MPa } (26.1 \text{ ksi}) \end{aligned}$$

The strain near the crack tip ($x_1 = 0.04a$, "a" being the half crack length) is linear up to an applied stress of 52 MPa (7.5 ksi) corresponding to a local strain of 0.0025. The ratio of this strain to the far-field strain in the linear range is 2.72. This strain increases at an increasing rate up to the point when the crack extension reaches the gage location. This occurs between 147 MPa (21.2 ksi) and 155 MPa (22.5 ksi). The most peculiar response occurs in the horizontal strain near the crack tip (Gage 5, Figure 77). The strain is initially positive and increases up to a stress of 86 MPa (12.5 ksi), thereafter it begins to decrease and finally it reaches high negative values. The far-field strains vary nearly linearly to failure. The strain distribution around the crack tips and the phenomenon of crack extension are illustrated by the fringe patterns in the photoelastic coating (Figure 78). In this case it appears that the crack extends clearly in the horizontal (transverse to the loading axis) direction. This pattern bears no resemblance to those obtained from biaxially loaded specimens with cracks, where the normal to shear stress ratio was the same. The fringe patterns indicate that the crack began to extend at an applied stress of 121 MPa (17.5 ksi). Fracture became audible at 129 MPa (18.7 ksi). At this level, the horizontal strain near the crack tip changes from positive to negative (Figure 77). Ultimate failure occurred at a stress of 180 MPa (26.1 ksi).

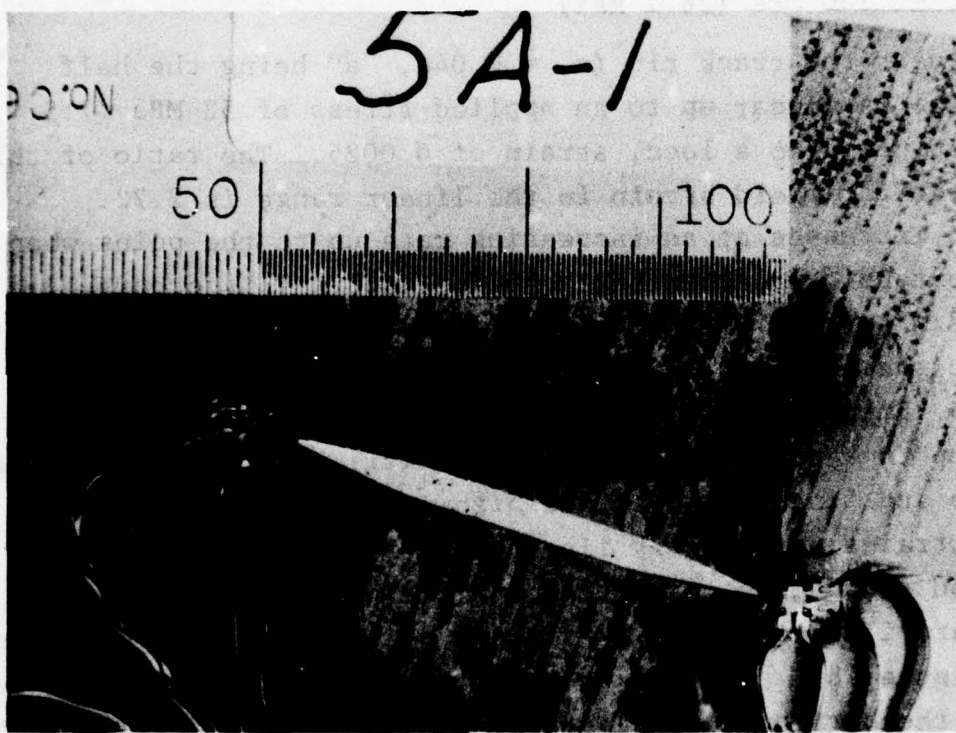


Figure 76. Closeup of Gage Layout Near 2.54 cm
(1.00 in.) Crack of Spec. No. 5A-1
(Smallest Division Shown in 0.01 in.)

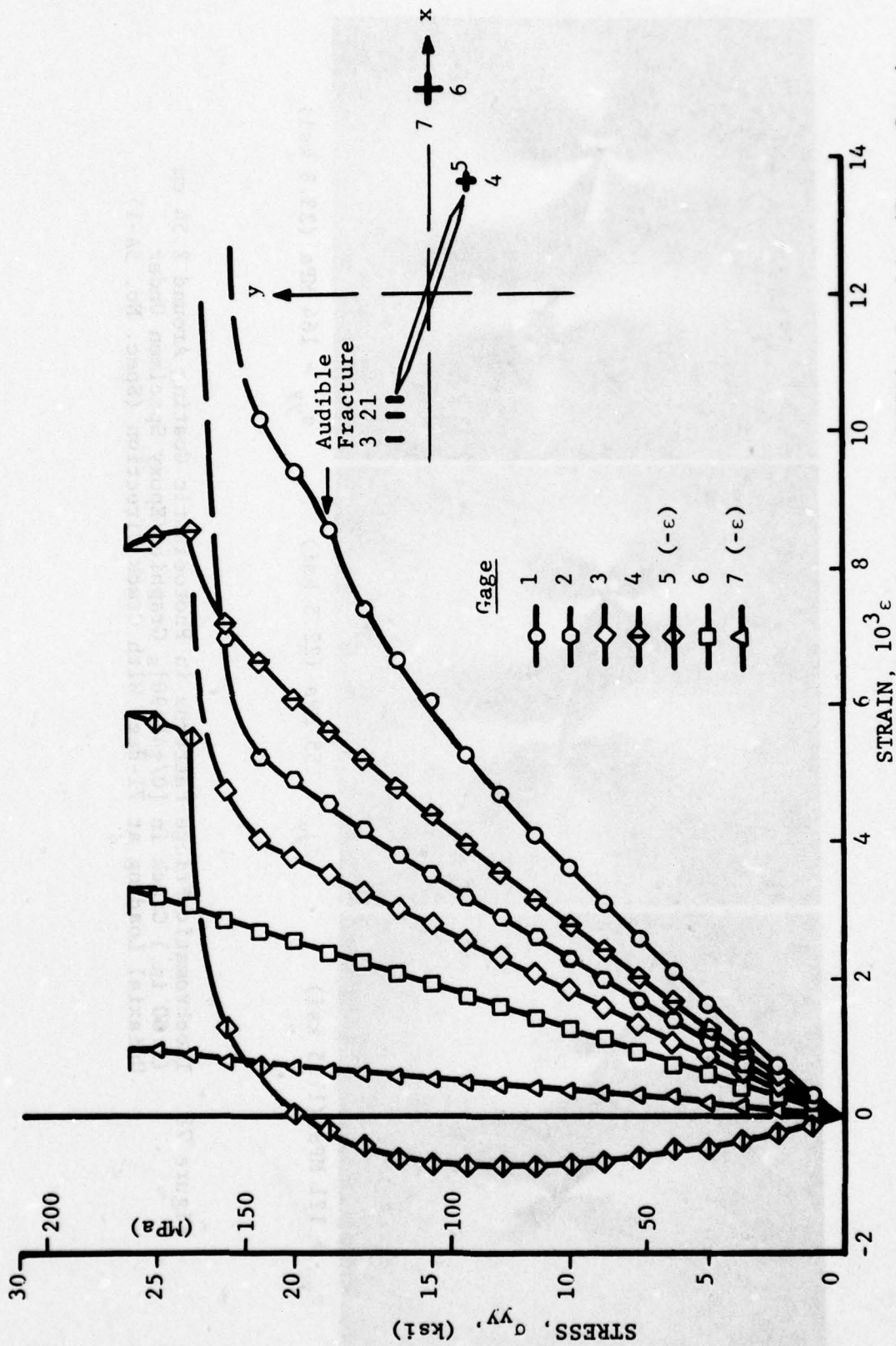
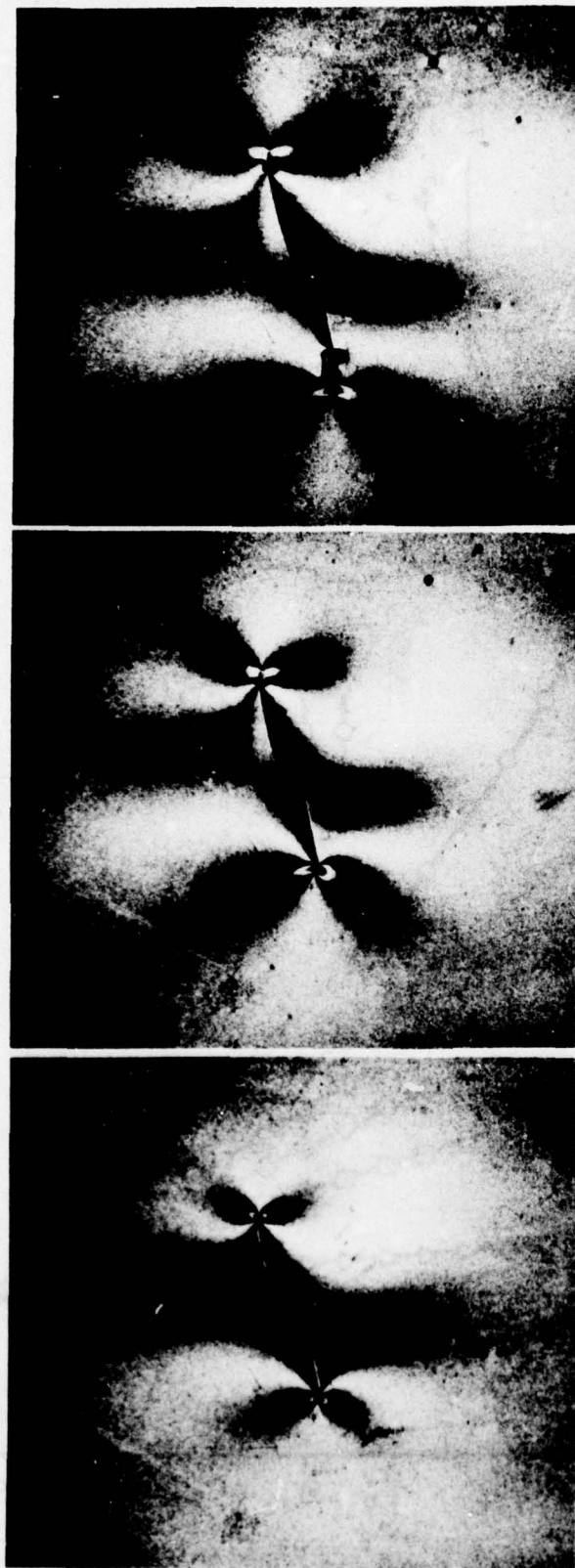


Figure 77. Strains Near Crack Tip and in Far Field in [0/+45/90]s Graphite/Epoxy Specimen With 2.54 cm (1.00 in.) Crack Under Uniaxial Loading at 71-deg. With Crack Direction (Spec. No. 5A-1)



$\sigma_{yy} = 121 \text{ MPa (17.5 ksi)}$

$\sigma_{yy} = 155 \text{ MPa (22.5 ksi)}$

$\sigma_{yy} = 164 \text{ MPa (23.8 ksi)}$

Figure 78. Isochromatic Fringe Patterns in Photoelastic Coating Around 2.54 cm (1.00 in.) Crack in [0/+45/90]s Graphite/Epoxy Specimen Under Uniaxial Loading at 71-deg. With Crack Direction (Spec. No. 5A-1)

Specimen No. 5A-2 with a 2.54 cm (1.00 in.) long crack was a replicate of No. 5A-1 above. It was instrumented with strain gages and 400 lines/cm (1000 lines/in.) moire grids near the crack. Strains as a function of applied stress are plotted in Figure 79. Elastic and strength properties obtained are:

$$\begin{aligned} E_{yy} &= 52 \text{ GPa } (7.5 \times 10^6 \text{ psi}) \\ \nu_{yx} &= 0.30 \\ S_{yy} &= 203 \text{ MPa } (29.4 \text{ ksi}) \end{aligned}$$

The strain near the crack tip (Gage 1 in Figure 79; $x_1 = 0.03a$) is linear up to an applied stress of 52 MPa (7.5 ksi), then it increases linearly at a reduced rate up to a stress of 112 MPa (16.2 ksi). The ratio of this strain to the far field strain in the initial linear range is 3.34. Fracture became audible at a stress level of 121 MPa (17.5 ksi). Thereafter, all strains in the vicinity of the crack tips become nonlinear with some of them exhibiting irregular behavior. Ultimate failure occurred at a stress of 203 MPa (29.4 ksi).

Moire fringe patterns around the crack are shown in Figure 80 for three stress levels. The left part of the pattern corresponds to displacements normal to the crack direction, the right part to displacements parallel to it. By differentiating the fringe patterns away from the crack the far field strains shown in Figure 81 were obtained. The crack opening displacement and the forward sliding or crack shearing displacement were determined from these fringe patterns and plotted in Figure 82 as a function of applied stress. The crack opening displacement (COD) is 4.4 times the crack shearing displacement (CSD) in the linear range. The corresponding ratio for the biaxially loaded specimen with the same ratio of normal to shear stress is 2.5 (Reference 1, Figure 124). The CSD and COD vary linearly up to applied stresses of 104 MPa (15 ksi) and 138 MPa (20 ksi), respectively. The maximum

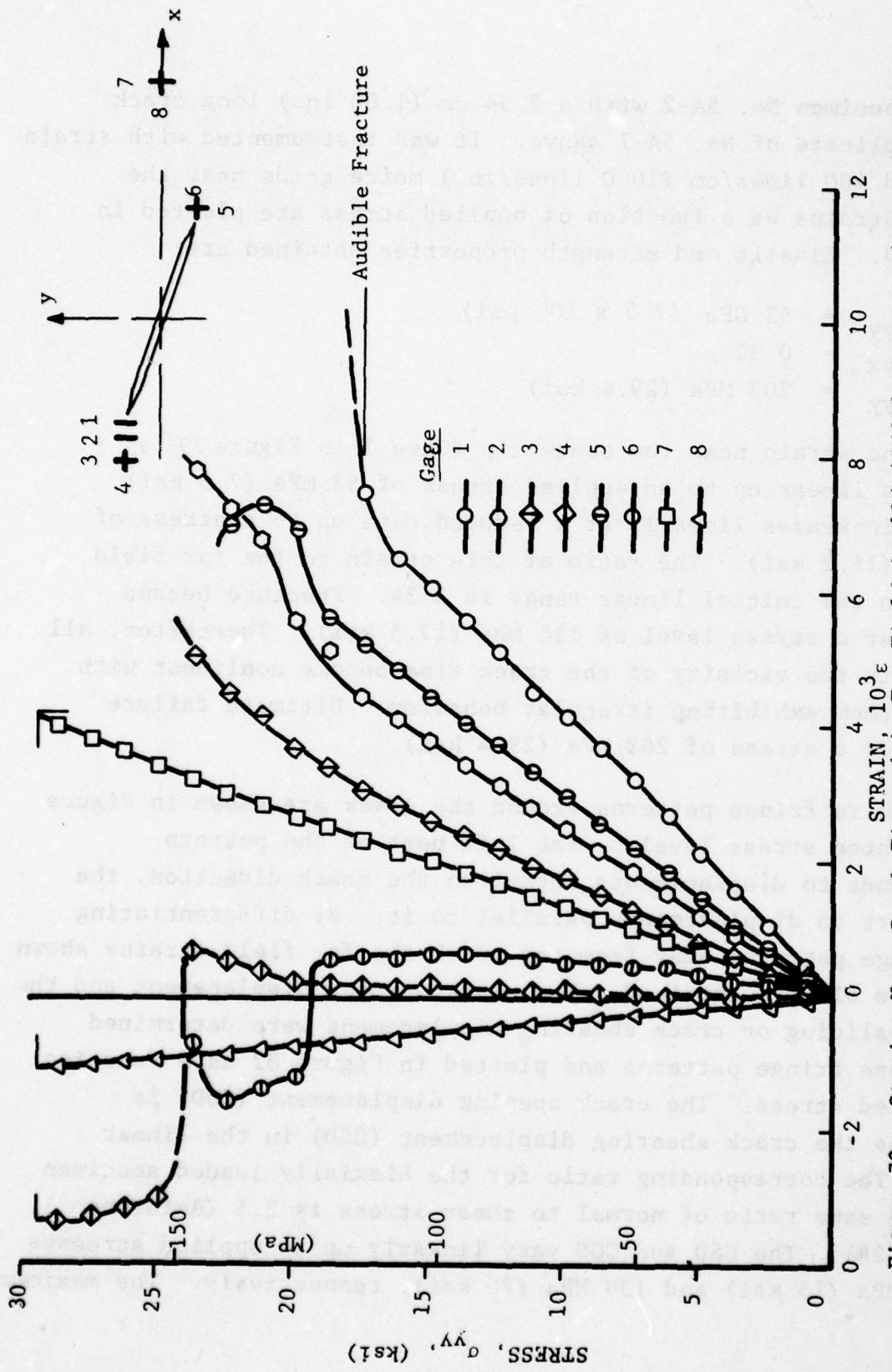
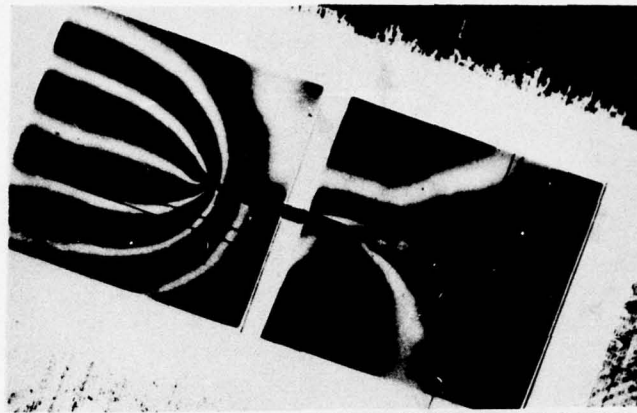
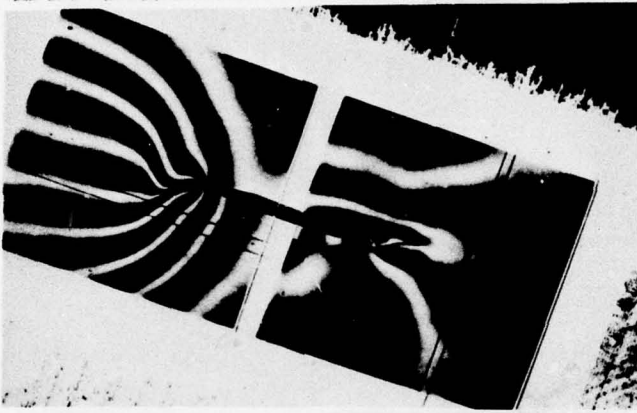


Figure 79. Strains Near Crack Tip and in Far Field in $[0/+45/90]_s$ Graphite/Epoxy Specimen With 2.54 cm (1.00 in.) Crack Under Uniaxial Loading at 71-deg. With Crack Direction (Spec. No. 5A-2)

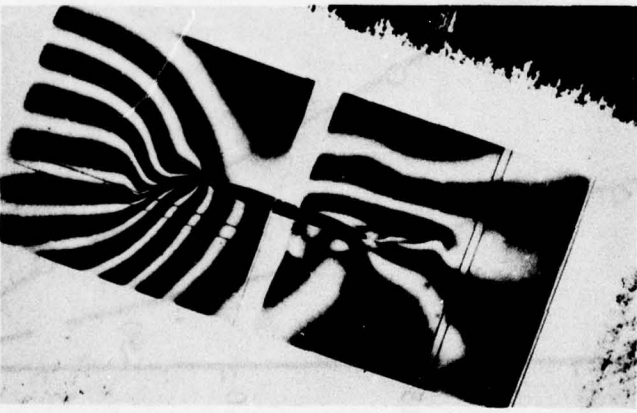
σ_{yy}
MPa (ksi)



164 (23.7)



173 (25.0)



190 (27.5)

Figure 80. Moire Fringe Patterns Around 2.54 cm (1.00 in.) Crack in [0/+45/90] Graphite/Epoxy Specimen Under Uniaxial Loading at 71st deg. with Crack Direction. (Left part of pattern corresponds to displacements normal to the crack, right part to displacements parallel to it, Spec. No. 5A-2).

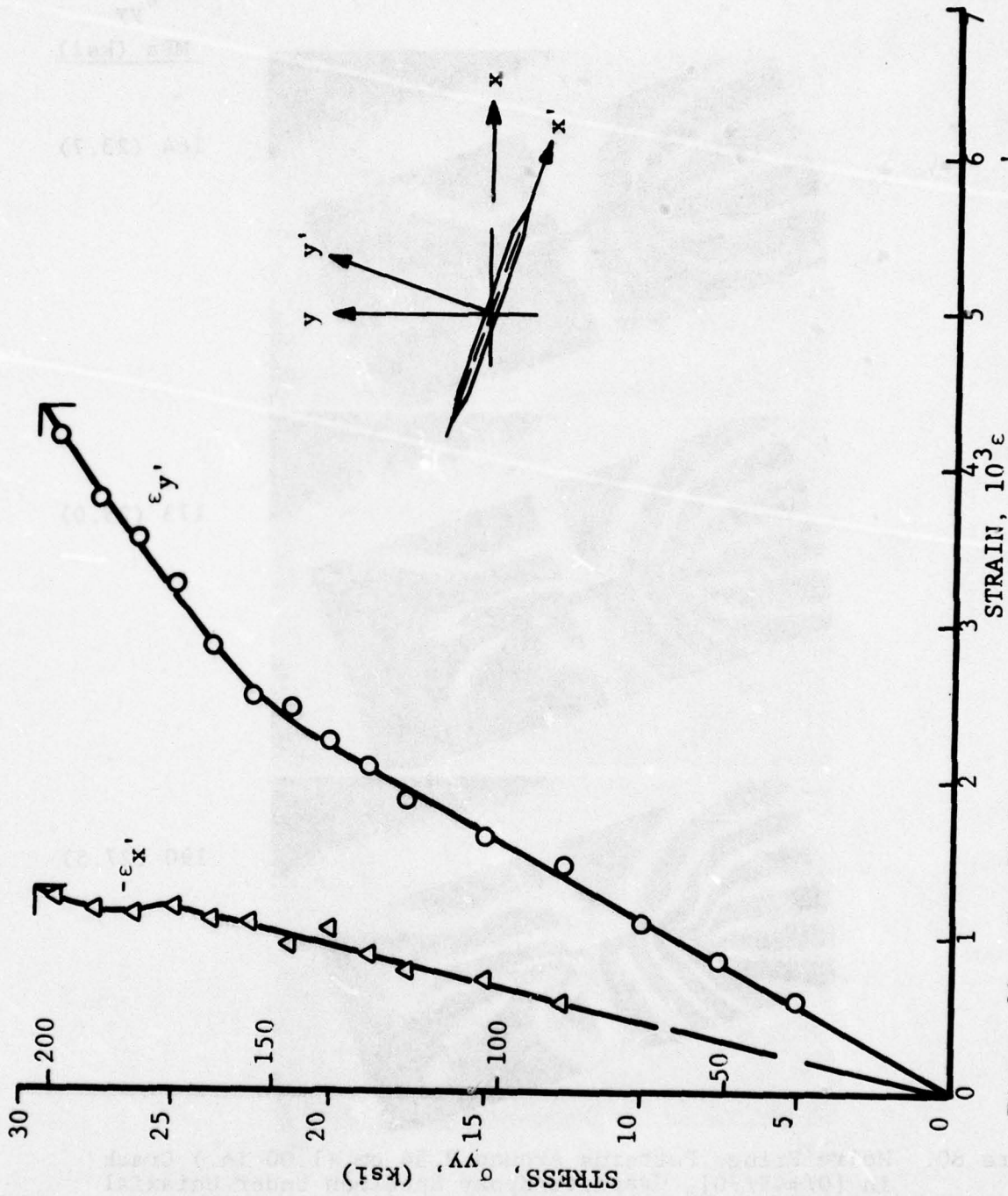


Figure 81. Far Field Strains Around Crack Obtained from Moiré Fringe Patterns (Spec. No. 5A-2)

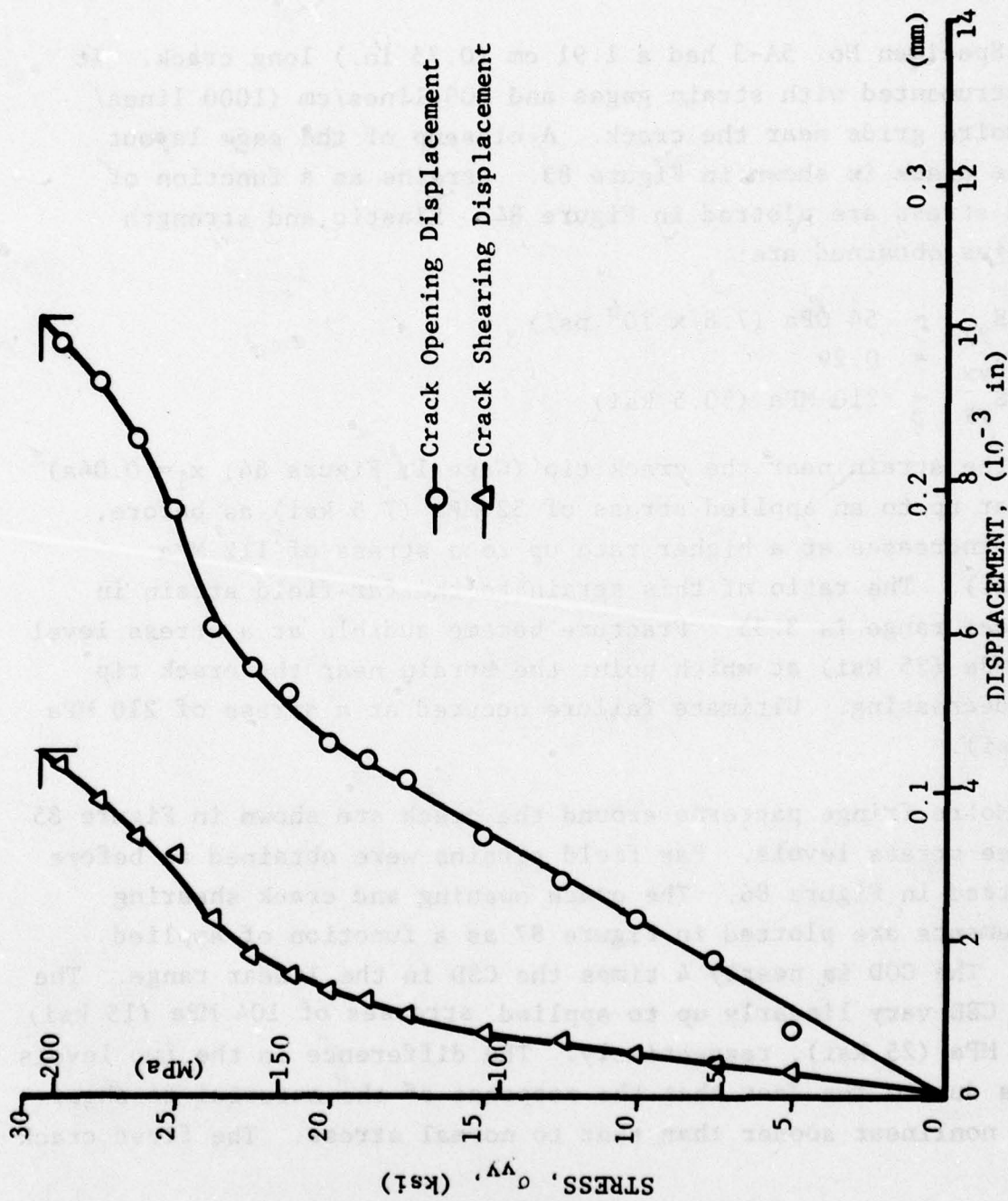


Figure 82. Crack Opening and Crack Shearing Displacement in $[0/+45/90]_s$ Graphite/Epoxy Specimen With 2.54 cm (1.90 in.) Crack Under Uniaxial Loading at 71-deg. With Crack Direction (Spec. No. 5A-2)

COD at failure is 0.25 mm (0.010 in.) which is appreciably larger than the corresponding value of 0.10 mm (0.004 in.) for the biaxially loaded specimen with a similar crack and the same ratio of normal to shear stress.

Specimen No. 5A-3 had a 1.91 cm (0.75 in.) long crack. It was instrumented with strain gages and 400 lines/cm (1000 lines/in.), moire grids near the crack. A closeup of the gage layout near the crack is shown in Figure 83. Strains as a function of applied stress are plotted in Figure 84. Elastic and strength properties obtained are:

$$\begin{aligned} E_{yy} &= 54 \text{ GPa } (7.8 \times 10^6 \text{ psi}) \\ \nu_{yx} &= 0.29 \\ S_{yy} &= 210 \text{ MPa } (30.5 \text{ ksi}) \end{aligned}$$

The strain near the crack tip (Gage 1, Figure 84; $x_1 = 0.04a$) is linear up to an applied stress of 52 MPa (7.5 ksi) as before, then it increases at a higher rate up to a stress of 112 MPa (16.2 ksi). The ratio of this strain to the far-field strain in the linear range is 3.35. Fracture became audible at a stress level of 172 MPa (25 ksi) at which point the strain near the crack tip starts decreasing. Ultimate failure occurred at a stress of 210 MPa (30.5 ksi).

Moire fringe patterns around the crack are shown in Figure 85 for three stress levels. Far field strains were obtained as before and plotted in Figure 86. The crack opening and crack shearing displacements are plotted in Figure 87 as a function of applied stress. The COD is nearly 4 times the CSD in the linear range. The COD and CSD vary linearly up to applied stresses of 104 MPa (15 ksi) and 173 MPa (25 ksi), respectively. The difference in the two levels above is due to the fact that the response of the material to shear becomes nonlinear sooner than that to normal stress. The first crack

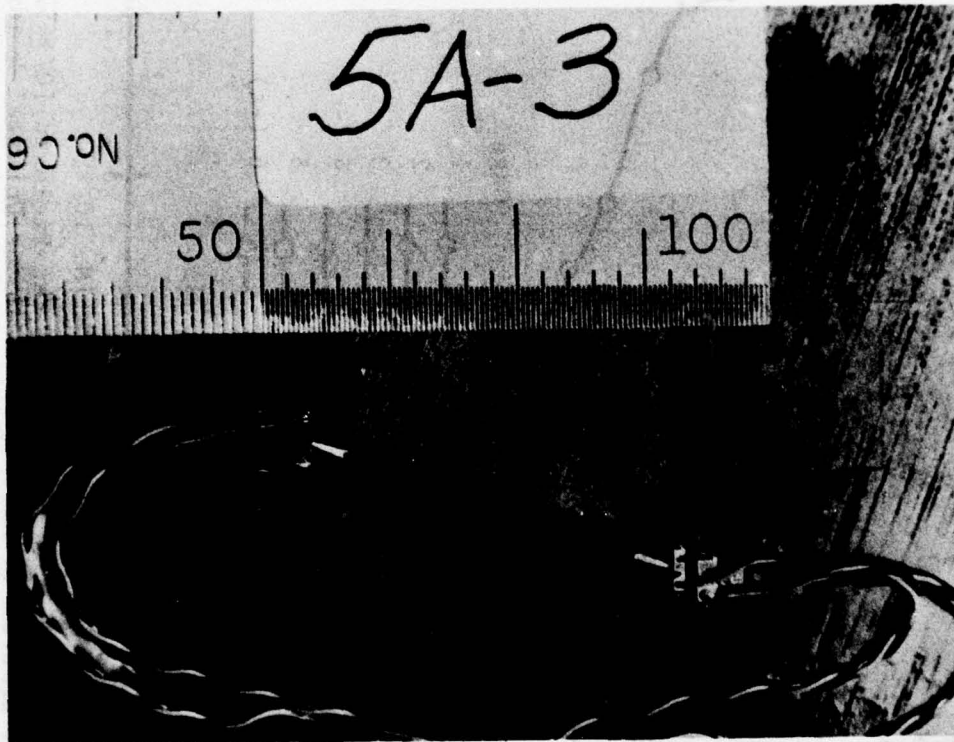


Figure 83. Closeup of Gage Layout Near 1.91 cm
(0.75 in.) Crack of Spec. No. 5A-3
(Smallest Division Shown is 0.01 in.)

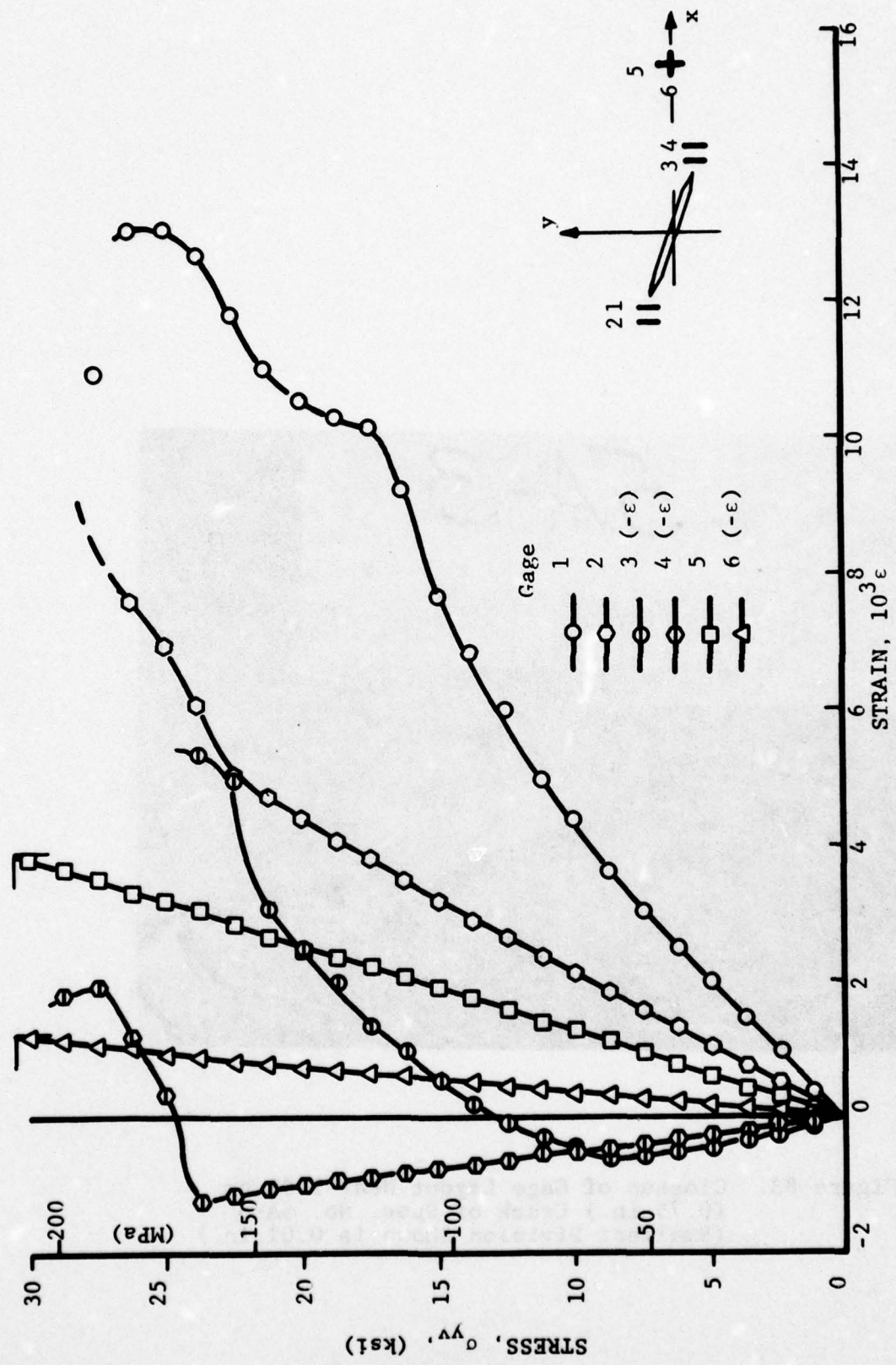


Figure 84. Strains Near Crack Tip and in Far Field in [0/+45/90]s Graphite/Epoxy Specimen With 1.91 cm (0.75 in.) Crack Under Uniaxial Loading at 71-deg. With Crack Direction (Spec. No. 5A-3).

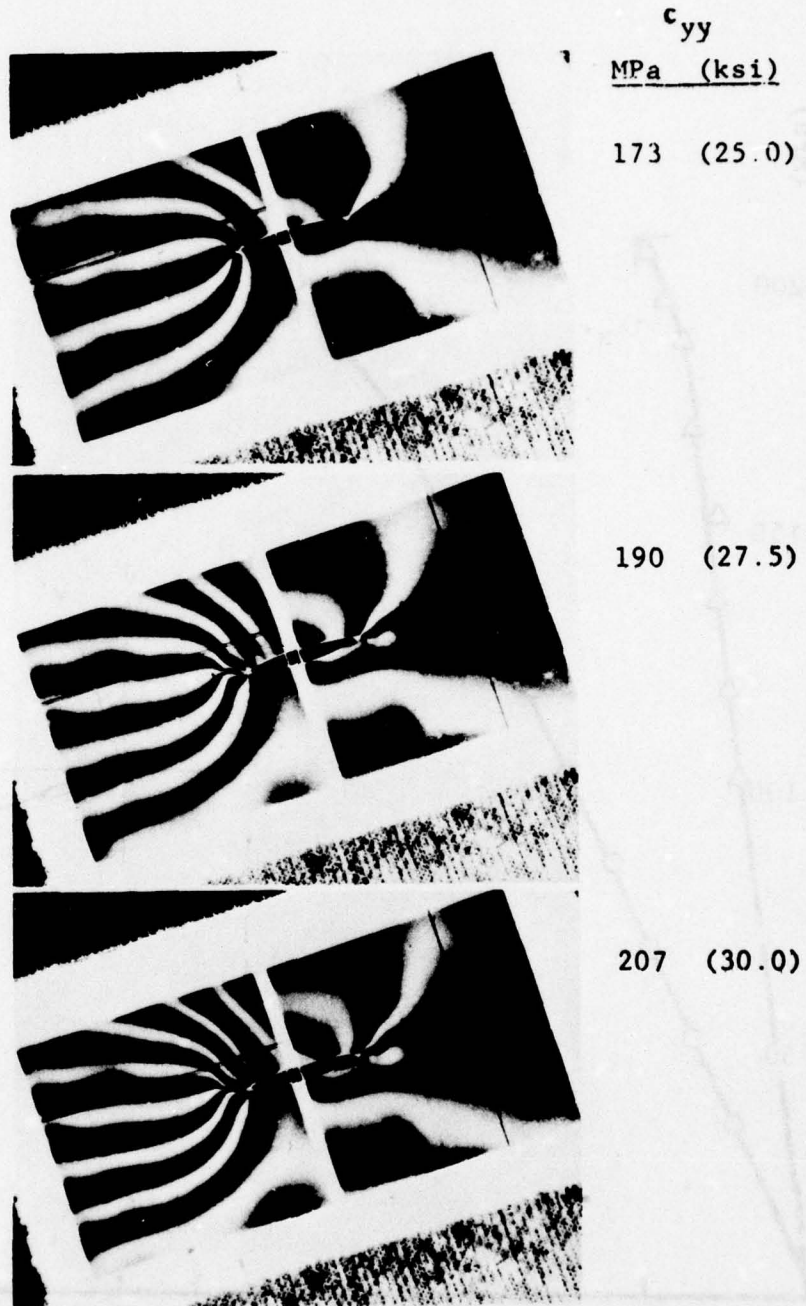


Figure 85. Moiré Fringe Patterns Around 1.91 cm (0.75 in.) Crack Under Uniaxial Loading at 71-deg. with Crack Direction (Spec. No. 5A-3)

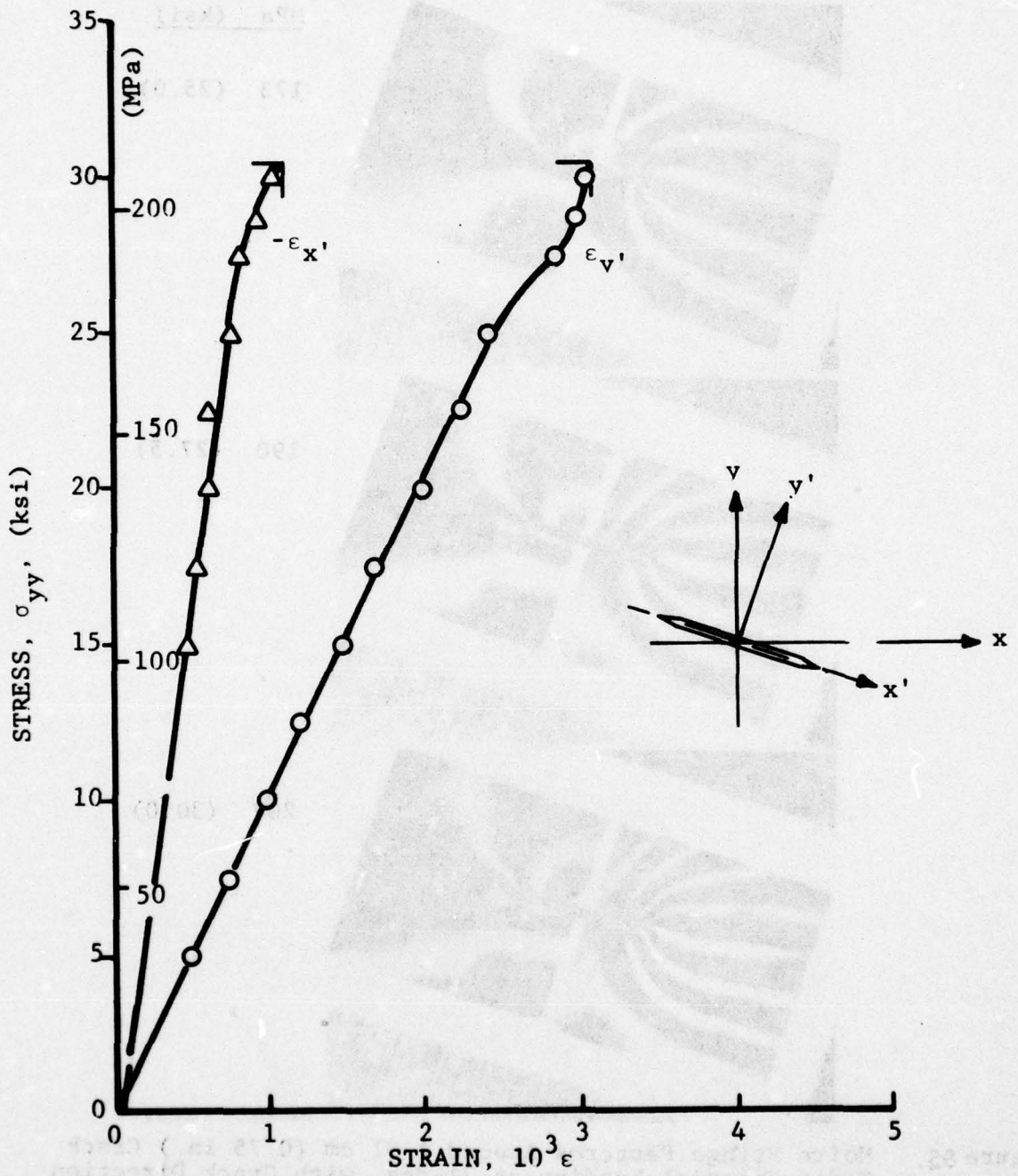


Figure 86. Far Field Strains Around 1.91 cm (0.75 in.) Crack Obtained from Moiré Fringe Patterns (Spec. No. 5A-3)

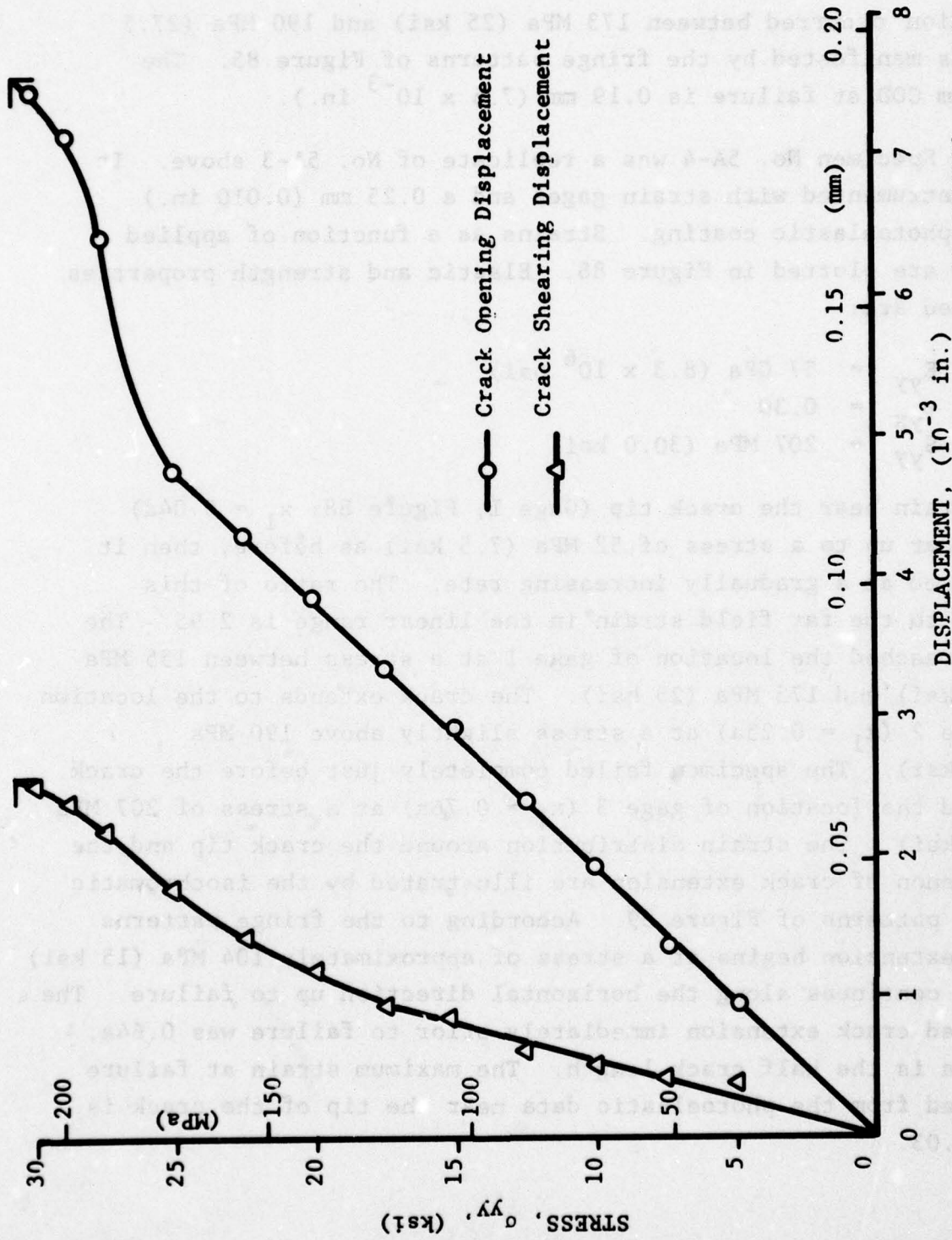


Figure 87. Crack Opening and Crack Shearing Displacements in [0/+45/90]s Graphite/Epoxy Specimen With 1.91 cm (0.75 in.) Crack Under Uniaxial Loading at 71-deg. With Crack Direction (Spec. No. 5A-3)

extension occurred between 173 MPa (25 ksi) and 190 MPa (27.5 ksi) as manifested by the fringe patterns of Figure 85. The maximum COD at failure is 0.19 mm (7.6×10^{-3} in.).

Specimen No. 5A-4 was a replicate of No. 5A-3 above. It was instrumented with strain gages and a 0.25 mm (0.010 in.) thick photoelastic coating. Strains as a function of applied stress are plotted in Figure 88. Elastic and strength properties obtained are:

$$\begin{aligned} E_{yy} &= 57 \text{ GPa } (8.3 \times 10^6 \text{ psi}) \\ \nu_{yx} &= 0.30 \\ S_{yy} &= 207 \text{ MPa } (30.0 \text{ ksi}) \end{aligned}$$

The strain near the crack tip (Gage 1, Figure 88; $x_1 = 0.04a$) is linear up to a stress of 52 MPa (7.5 ksi) as before, then it increased at a gradually increasing rate. The ratio of this strain to the far field strain in the linear range is 2.95. The crack reached the location of gage 1 at a stress between 155 MPa (22.5 ksi) and 173 MPa (25 ksi). The crack extends to the location of gage 2 ($x_1 = 0.25a$) at a stress slightly above 190 MPa (27.5 ksi). The specimen failed completely just before the crack reached the location of gage 3 ($x_1 = 0.76a$) at a stress of 207 MPa (30.0 ksi). The strain distribution around the crack tip and the phenomenon of crack extension are illustrated by the isochromatic fringe patterns of Figure 89. According to the fringe patterns crack extension begins at a stress of approximately 104 MPa (15 ksi) and it continues along the horizontal direction up to failure. The measured crack extension immediately prior to failure was $0.64a$, where a is the half crack length. The maximum strain at failure measured from the photoelastic data near the tip of the crack is over 0.03.

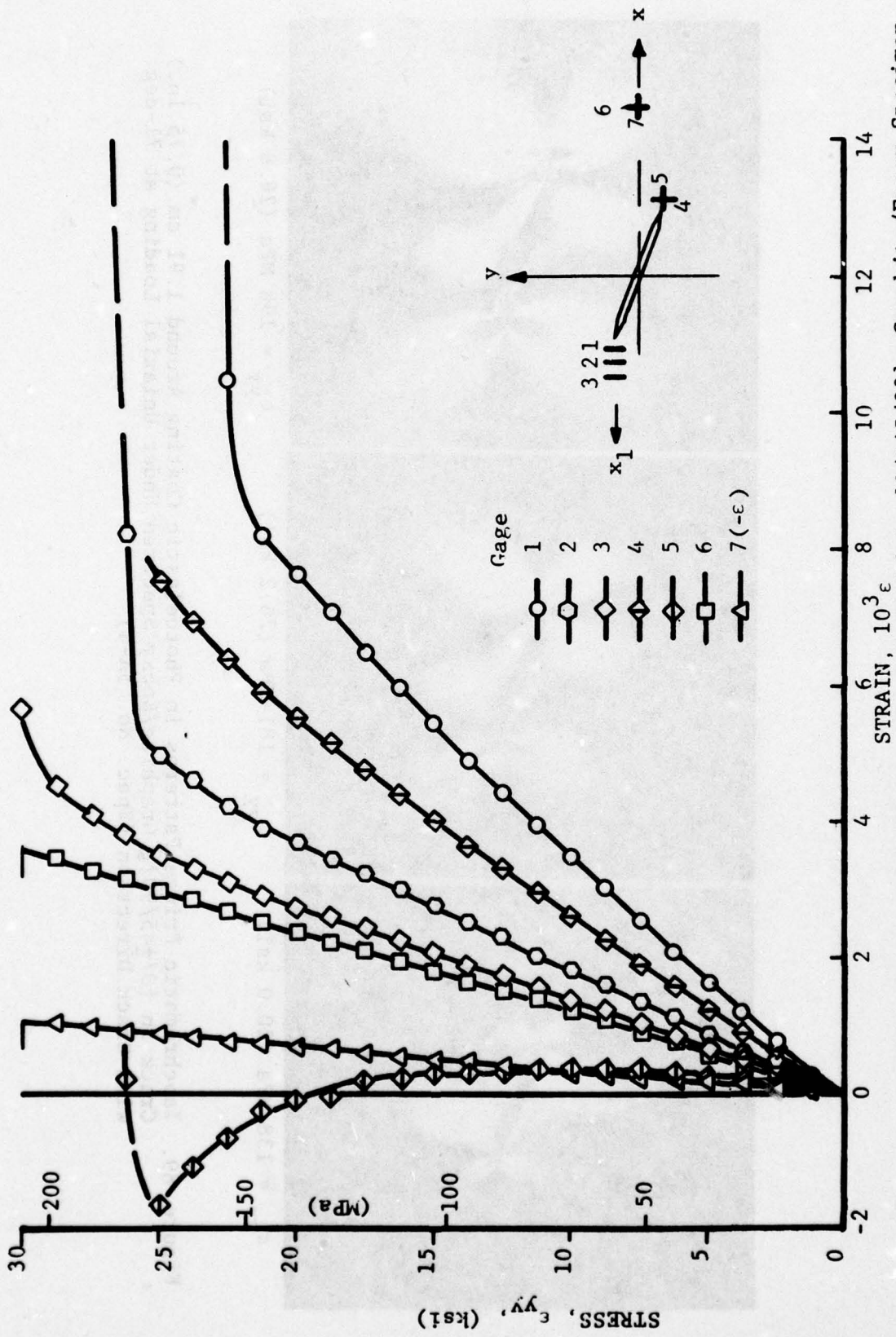
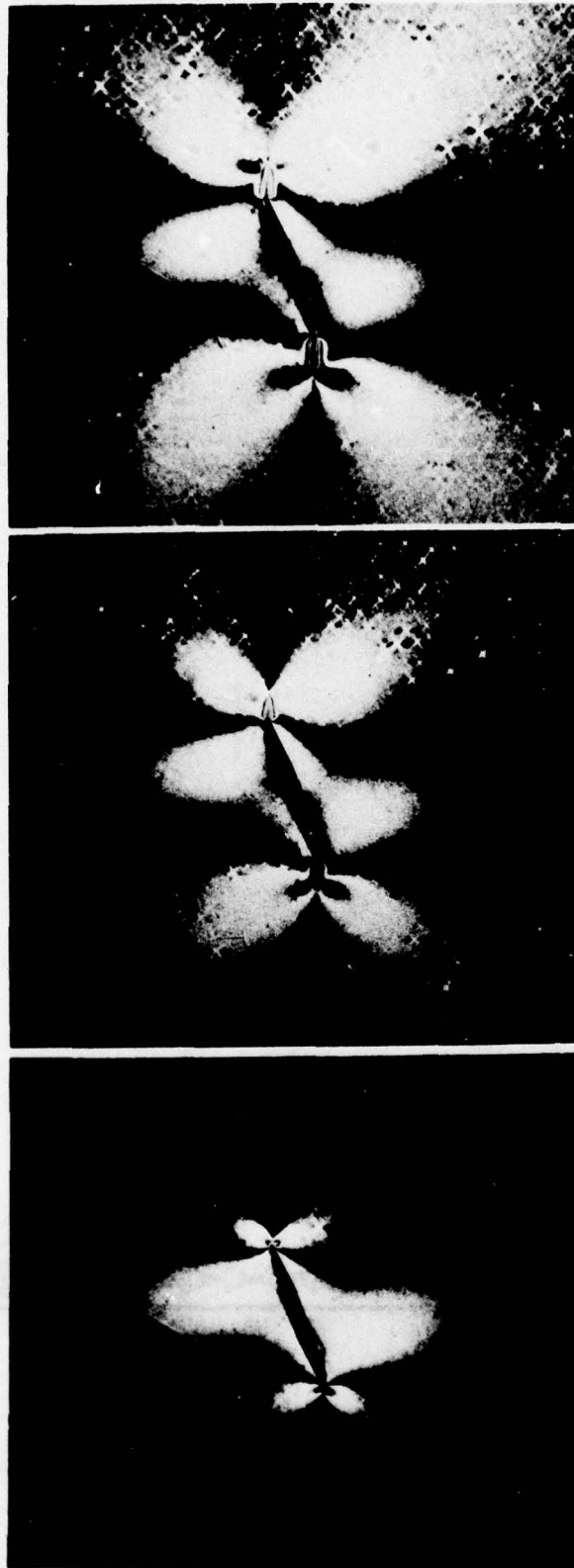


Figure 88. Strains Near Crack Tip and in Far Field in [0/+45/90]_s Graphite/Epoxy Specimen With 1.91 cm (0.75 in.) Crack Under Uniaxial Loading at 71-deg. With Crack Direction (Spec. No. 5A-4)



$\sigma_{yy} = 198 \text{ MPa (28.8 ksi)}$

$\sigma_{yy} = 181 \text{ MPa (26.2 ksi)}$

$\sigma_{yy} = 138 \text{ MPa (20.0 ksi)}$

Figure 89. Isochromatic Fringe Patterns in Photoelastic Coating Around 1.91 cm (0.75 in.) Crack in [0/+45/90]_s Graphite/Epoxy Specimen Under Uniaxial Loading at 71-deg. with Crack Direction (Spec. No. 5A-4)

Specimen No. 5A-5 had a 1.27 cm (0.50 in.) long crack and was instrumented with strain gages and a 0.25 mm (0.010 in.) thick photoelastic coating. A closeup of the gage layout near the crack tips is shown in Figure 90. Strains as a function of applied stress are plotted in Figure 91. Elastic and strength properties obtained are:

$$\begin{aligned} E_{yy} &= 57 \text{ GPa } (8.2 \times 10^6 \text{ psi}) \\ \nu_{yx} &= 0.31 \\ S_{yy} &= 245 \text{ MPa } (35.5 \text{ ksi}) \end{aligned}$$

The strain near the crack tip (Gage 1, Figure 91; $x_1 = 0.06a$) is linear up to a stress of 69 MPa (10 ksi), thereafter it increases at a gradually increasing rate. The ratio of this strain to the far-field strain in the linear range is 2.31. The reason for the lower ratio is that gage 1 is located at a distance equal to a higher fraction of the crack length than in the cases before. The crack reached the location of this gage at a stress of approximately 207 MPa (30 ksi). According to the strain curves of Figure 91, complete failure occurred before the crack reached the location of gage 2 ($x_1 = 0.37a$) at a stress of 245 MPa (35.5 ksi). Isochromatic fringe patterns in the photoelastic coating around the crack are shown in Figure 92 for three stress levels. According to the fringe patterns crack extension starts at a stress of approximately 121 MPa (17.5 ksi) and it continues along the horizontal direction up to failure. The maximum strain at failure near the tip of the crack is over 0.03.

Specimen No. 4A-6, a replicate of No. 5A-5 above, was instrumented with strain gages. A closeup of the gage layout around the crack is shown in Figure 93. Strains as a function of applied stress are plotted in Figures 94 and 95. Elastic and strength properties obtained are:



Figure 90. Closeup of Gage Layout Near 1.27 cm
(0.50 in.) Crack of Spec. No. 5A-5
(Smallest Division Shown is 0.01 in.)

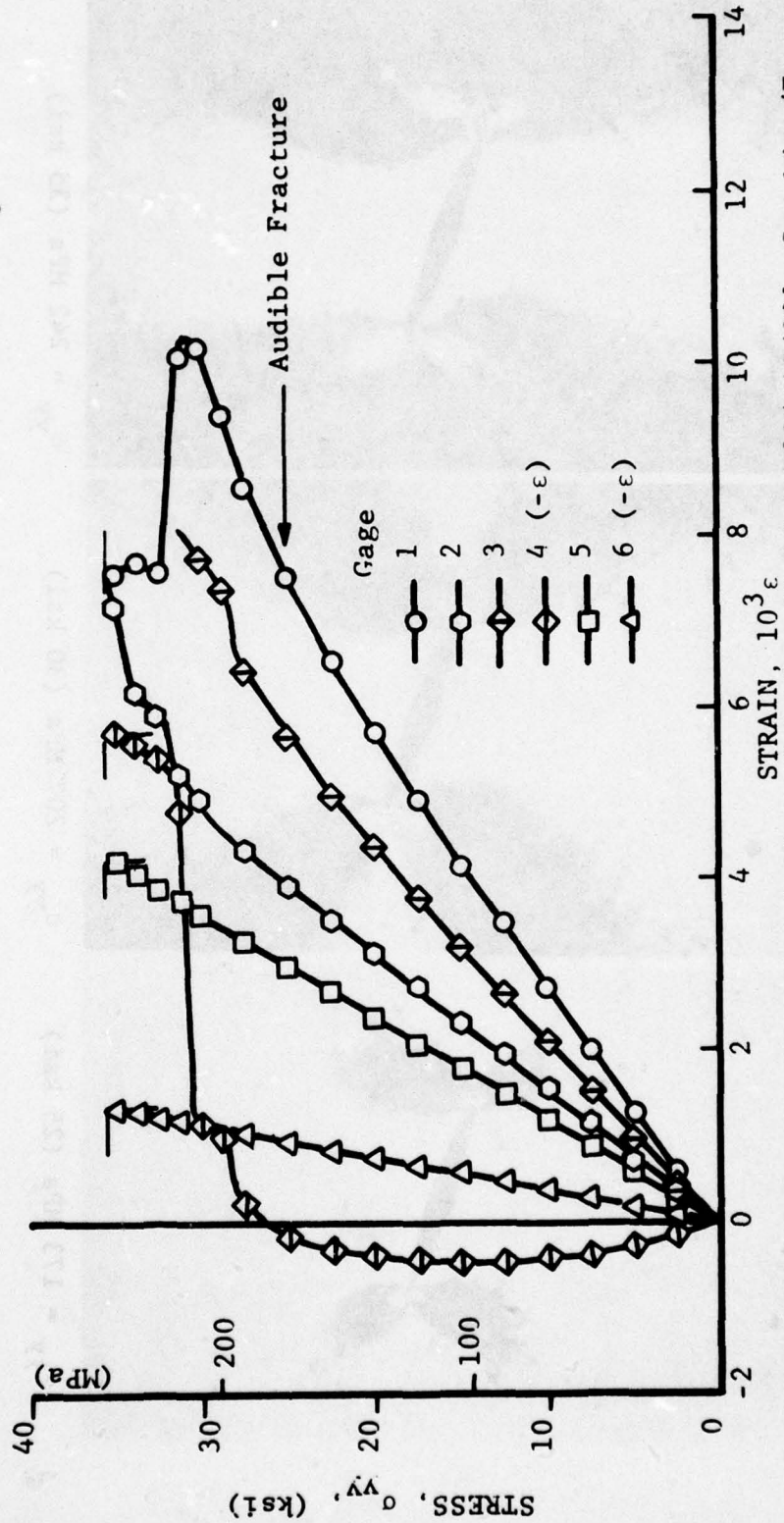
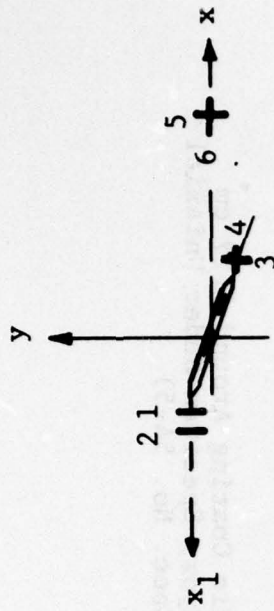


Figure 91. Strains Near Crack Tip and in Far Field in $[0/+45/90]_s$ Graphite/Epoxy Specimen With 1.27 cm (0.50 in.) Crack Under Uniaxial Loading at 71-deg. With Crack Direction (Spec. No. 5A-5)

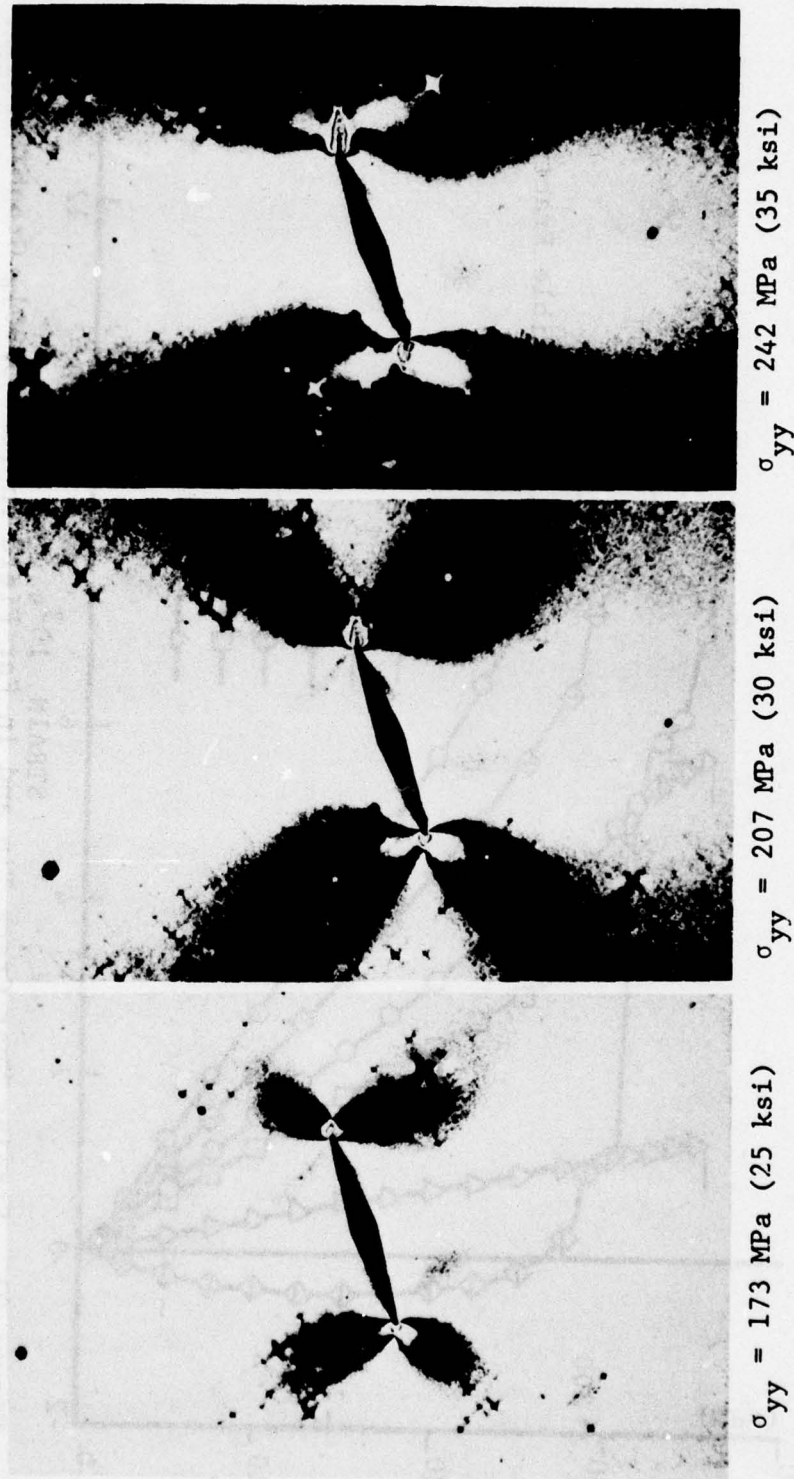


Figure 92. Isochromatic Fringe Patterns in Photoelastic Coating Around 1.27 cm (0.50 in.) Crack in [0/+45/90]_s Graphite/Epoxy Specimen Under Uniaxial Loading at 71-deg. with Crack Direction (Spec. No. 5A-5)

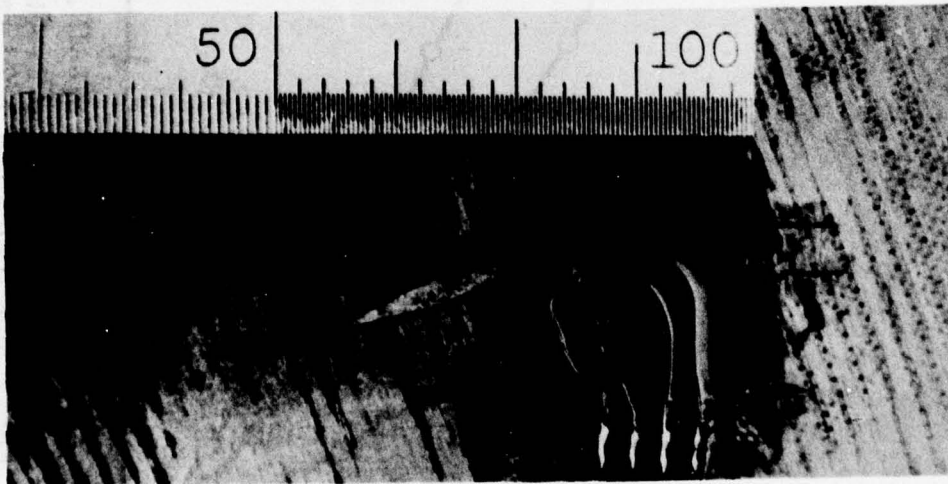
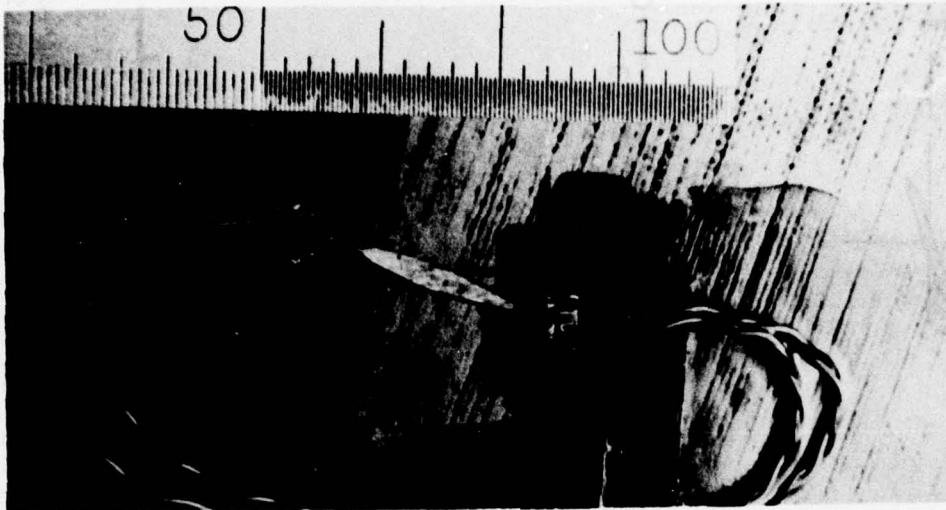


Figure 93. Closeup of Gage Layout Near 1.27 cm (0.50 in.)
Crack of Spec. No. 5A-6
(Smallest Division Shown in 0.01 in.)

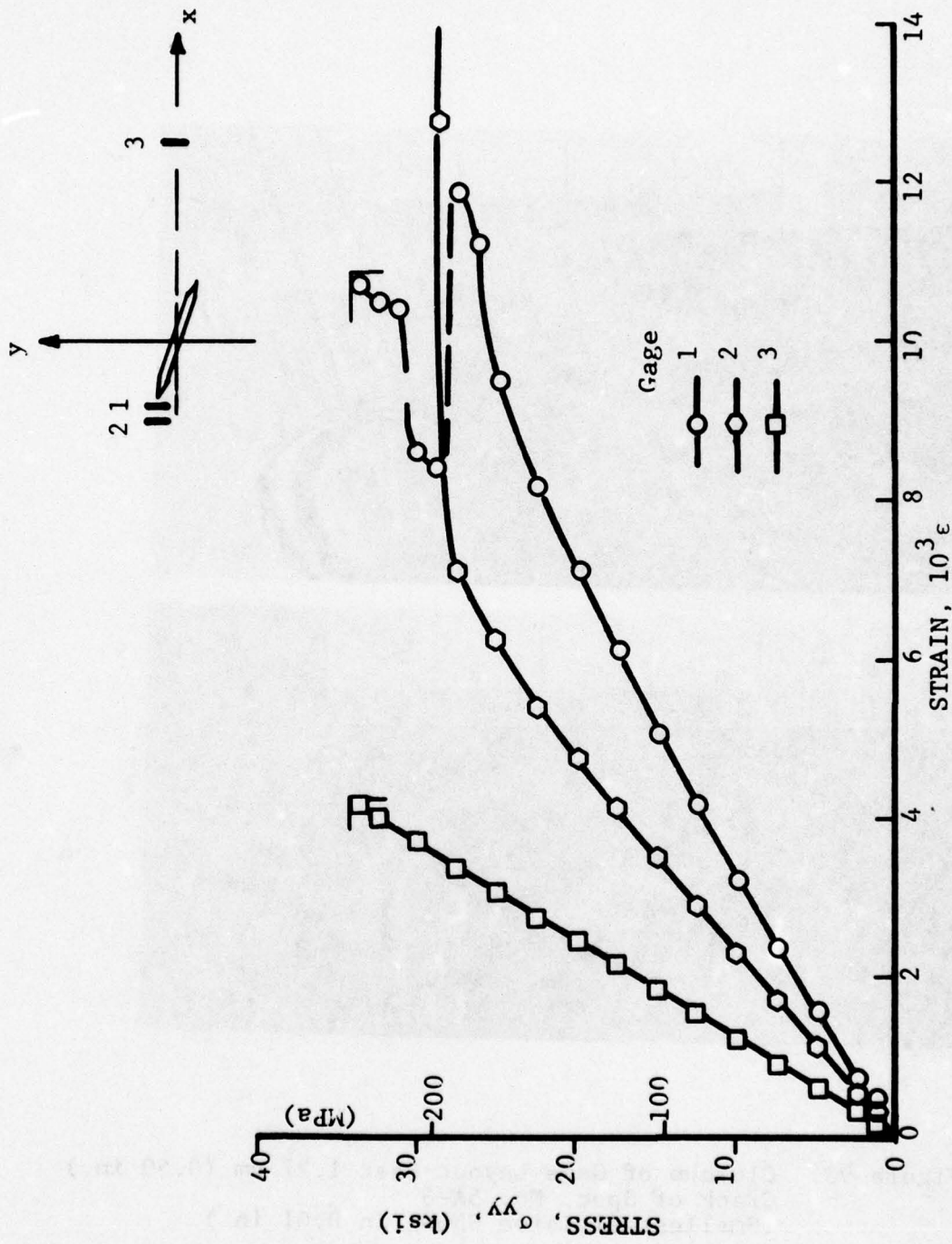


Figure 94. Vertical Strains Near Crack Tip and in Far Field in $[\gamma/+45/90]_s$ Graphite/Epoxy Specimen With 1.27 cm (0.50 in.) Crack Under Uniaxial Loading at 71-deg. With Crack Direction (Spec. No. 5A-6)

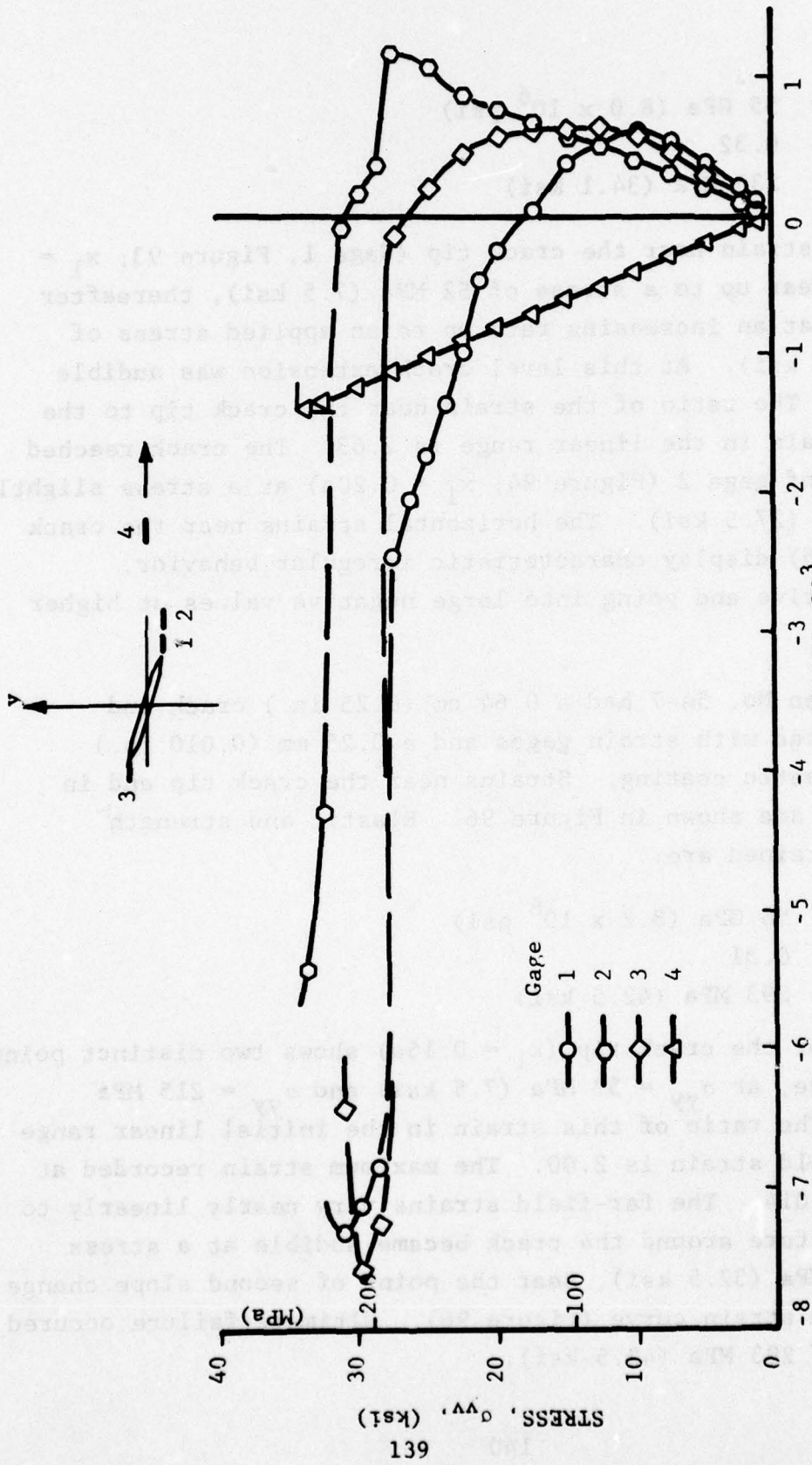


Figure 95. Horizontal Strains Near Crack Tip and in Far Field in [0/+45/90]s Graphite/Epoxy Specimen With 1.27 cm (0.50 in.) Crack Under Uniaxial Loading at 71-deg. With Crack Direction (Spec. No. 5A-6)

$$\begin{aligned}
 E_{yy} &= 55 \text{ GPa } (8.0 \times 10^6 \text{ psi}) \\
 \nu_{yx} &= 0.32 \\
 S_{yy} &= 235 \text{ MPa } (34.1 \text{ ksi})
 \end{aligned}$$

The vertical strain near the crack tip (Gage 1, Figure 93; $x_1 = 0.04a$) is linear up to a stress of 52 MPa (7.5 ksi), thereafter it increases at an increasing rate up to an applied stress of 190 MPa (27.5 ksi). At this level crack extension was audible and visible. The ratio of the strain near the crack tip to the far-field strain in the linear range is 2.63. The crack reached the location of gage 2 (Figure 94; $x_1 = 0.20a$) at a stress slightly above 190 MPa (27.5 ksi). The horizontal strains near the crack tip (Figure 95) display characteristic irregular behavior, starting positive and going into large negative values at higher stresses.

Specimen No. 5A-7 had a 0.64 cm (0.25 in.) crack and was instrumented with strain gages and a 0.25 mm (0.010 in.) thick photoelastic coating. Strains near the crack tip and in the far-field are shown in Figure 96. Elastic and strength properties obtained are:

$$\begin{aligned}
 E_{yy} &= 56 \text{ GPa } (8.2 \times 10^6 \text{ psi}) \\
 \nu_{yx} &= 0.31 \\
 S_{yy} &= 293 \text{ MPa } (42.5 \text{ ksi})
 \end{aligned}$$

The strain near the crack tip ($x_1 = 0.15a$) shows two distinct points of slope change, at $\sigma_{yy} = 52 \text{ MPa } (7.5 \text{ ksi})$ and $\sigma_{yy} = 215 \text{ MPa } (31.2 \text{ ksi})$. The ratio of this strain in the initial linear range to the far-field strain is 2.00. The maximum strain recorded at failure was 0.014. The far-field strains vary nearly linearly to failure. Fracture around the crack became audible at a stress level of 224 MPa (32.5 ksi), near the point of second slope change in the maximum strain curve (Figure 96). Ultimate failure occurred at a stress of 293 MPa (42.5 ksi).

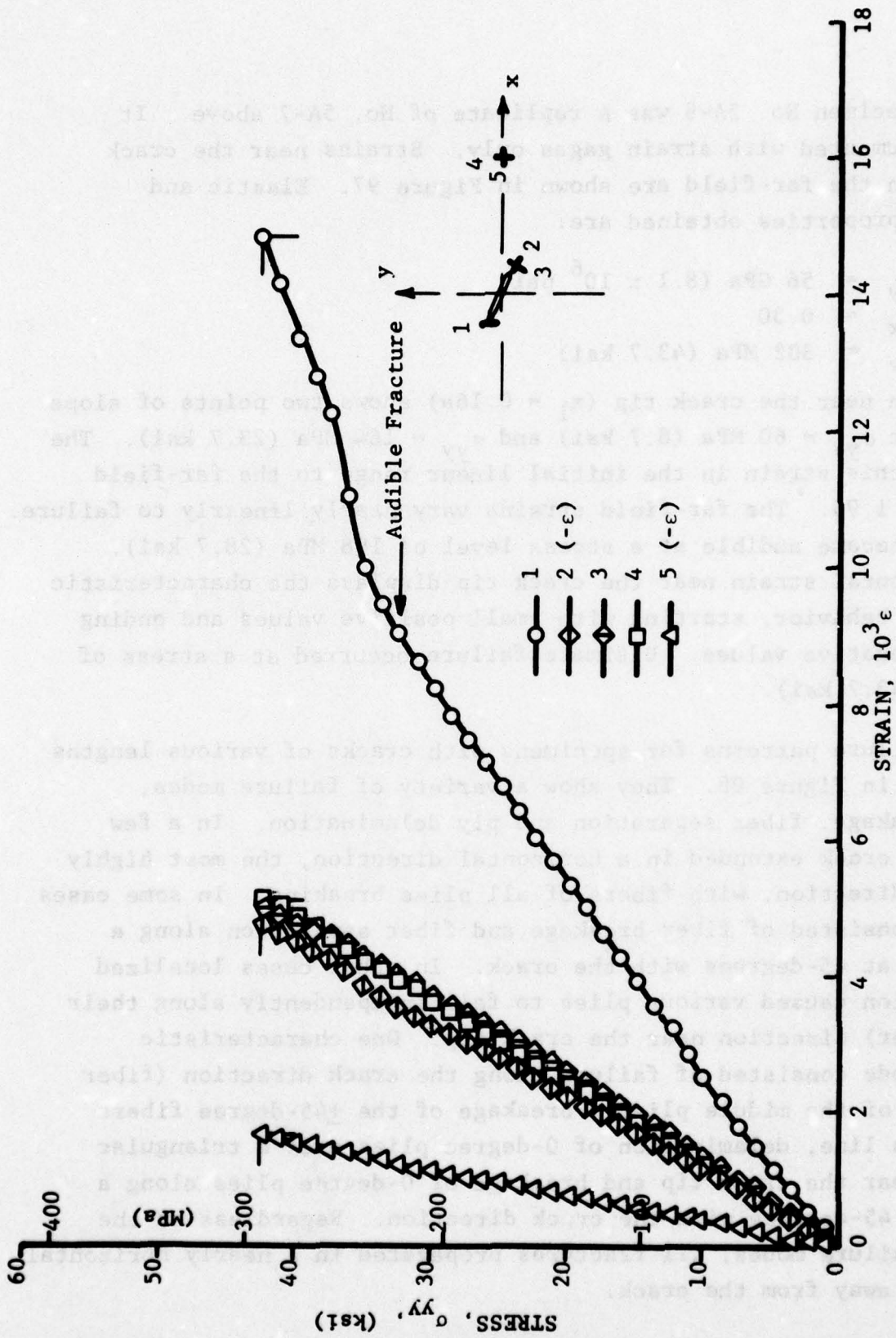


Figure 96. Strains Near Crack Tip and in Far-Field in [0/+45/90]_s Graphite/Epoxy Specimen With 0.64 cm (0.25 in.) Crack Under Uniaxial Loading at 71-deg. With Crack Direction (Spec. No. 5A-7)

Specimen No. 5A-8 was a replicate of No. 5A-7 above. It was instrumented with strain gages only. Strains near the crack tip and in the far-field are shown in Figure 97. Elastic and strength properties obtained are:

$$\begin{aligned} E_{yy} &= 56 \text{ GPa } (8.1 \times 10^6 \text{ psi}) \\ \nu_{yx} &= 0.30 \\ S_{yy} &= 302 \text{ MPa } (43.7 \text{ ksi}) \end{aligned}$$

The strain near the crack tip ($x_1 = 0.16a$) shows two points of slope change, at $\sigma_{yy} = 60 \text{ MPa } (8.7 \text{ ksi})$ and $\sigma_{yy} = 164 \text{ MPa } (23.7 \text{ ksi})$. The ratio of this strain in the initial linear range to the far-field strain is 1.95. The far-field strains vary nearly linearly to failure. Fracture became audible at a stress level of 198 MPa (28.7 ksi). The horizontal strain near the crack tip displays the characteristic irregular behavior, starting with small positive values and ending in high negative values. Ultimate failure occurred at a stress of 302 MPa (43.7 ksi).

Failure patterns for specimens with cracks of various lengths are shown in Figure 98. They show a variety of failure modes, fiber breakage, fiber separation and ply delamination. In a few cases the crack extended in a horizontal direction, the most highly stressed direction, with fibers of all plies breaking. In some cases failure consisted of fiber breakage and fiber separation along a direction at 45-degrees with the crack. In other cases localized delamination caused various plies to fail independently along their weak (fiber) direction near the crack tip. One characteristic failure mode consisted of failure along the crack direction (fiber direction of the middle plies), breakage of the ± 45 -degree fibers along this line, delamination of 0-degree plies over a triangular segment near the crack tip and breakage of 0-degree plies along a radius at 45-degrees with the crack direction. Regardless of the initial failure modes, all fractures propagated in a nearly horizontal direction away from the crack.

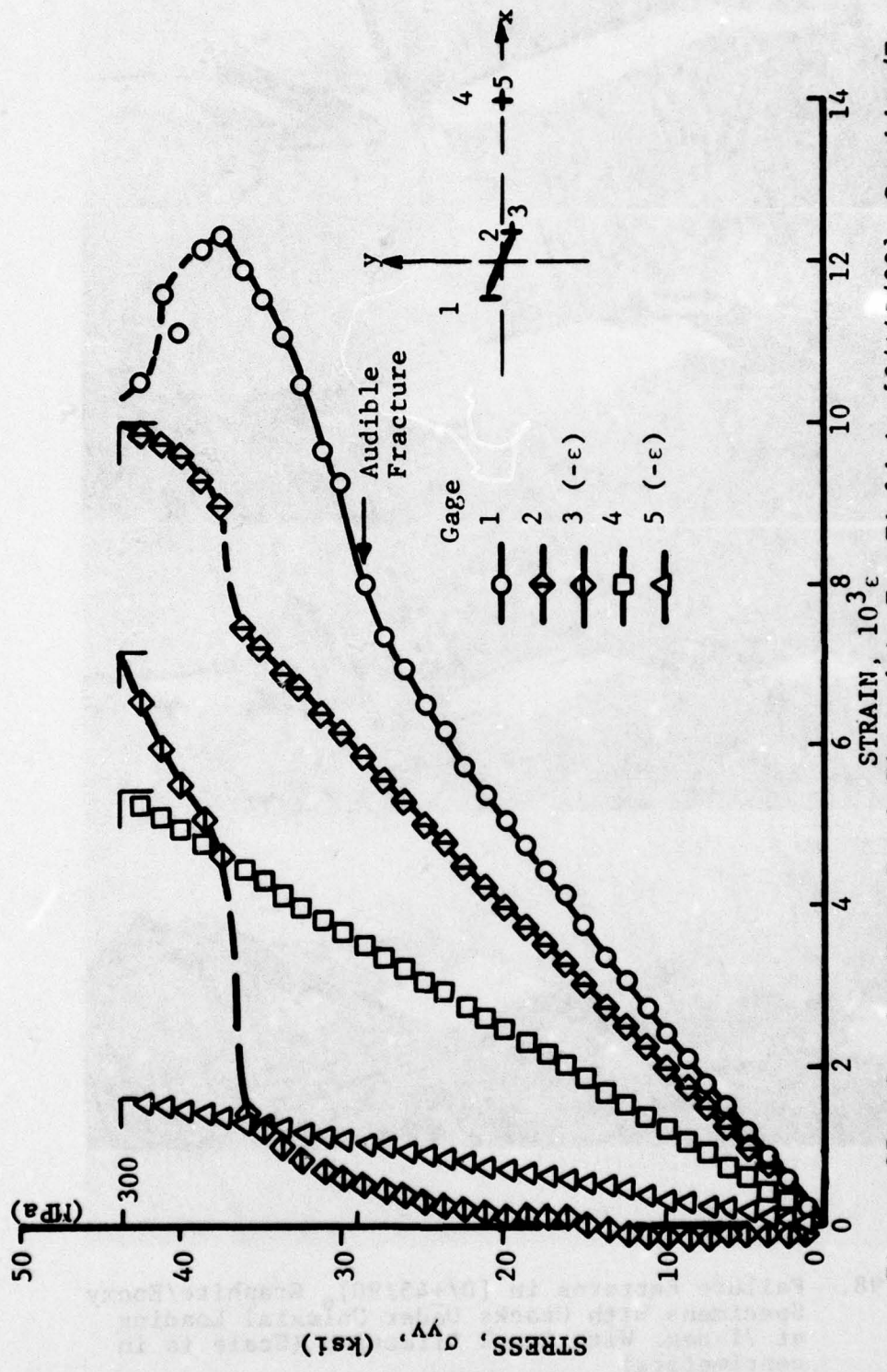


Figure 97. Strains Near Crack Tip and in Far-Field in [0/+45/90]s Graphite/Epoxy Specimen With 0.64 cm (0.25 in.) Crack Under Uniaxial Loading at 71-deg. With Crack Direction (Spec. No. 5A-8)

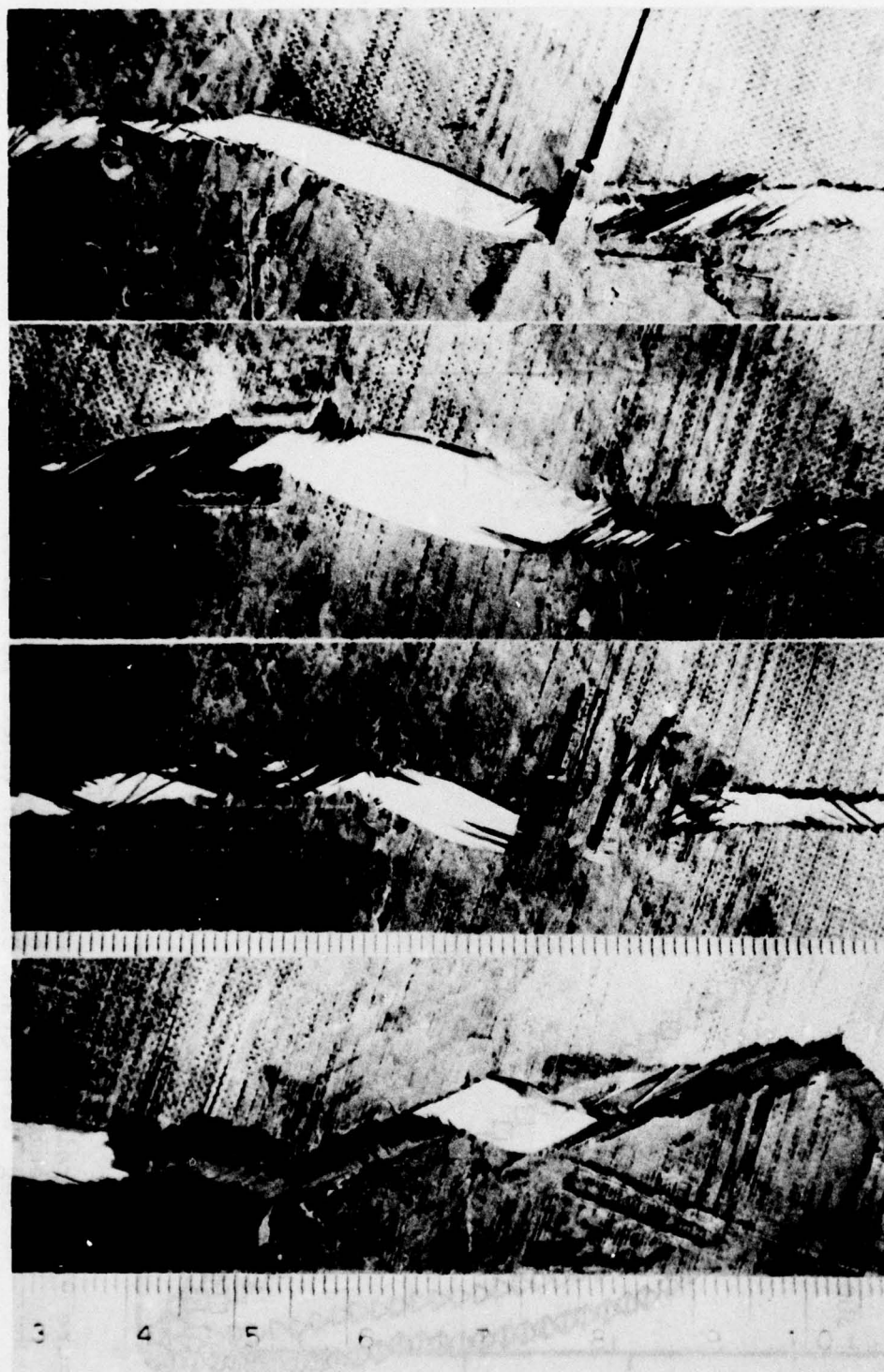


Figure 98. Failure Patterns in $[0/+45/90]_s$ Graphite/Epoxy Specimens With Cracks Under Uniaxial Loading at 71-deg. With Crack Direction (Scale is in centimeters)

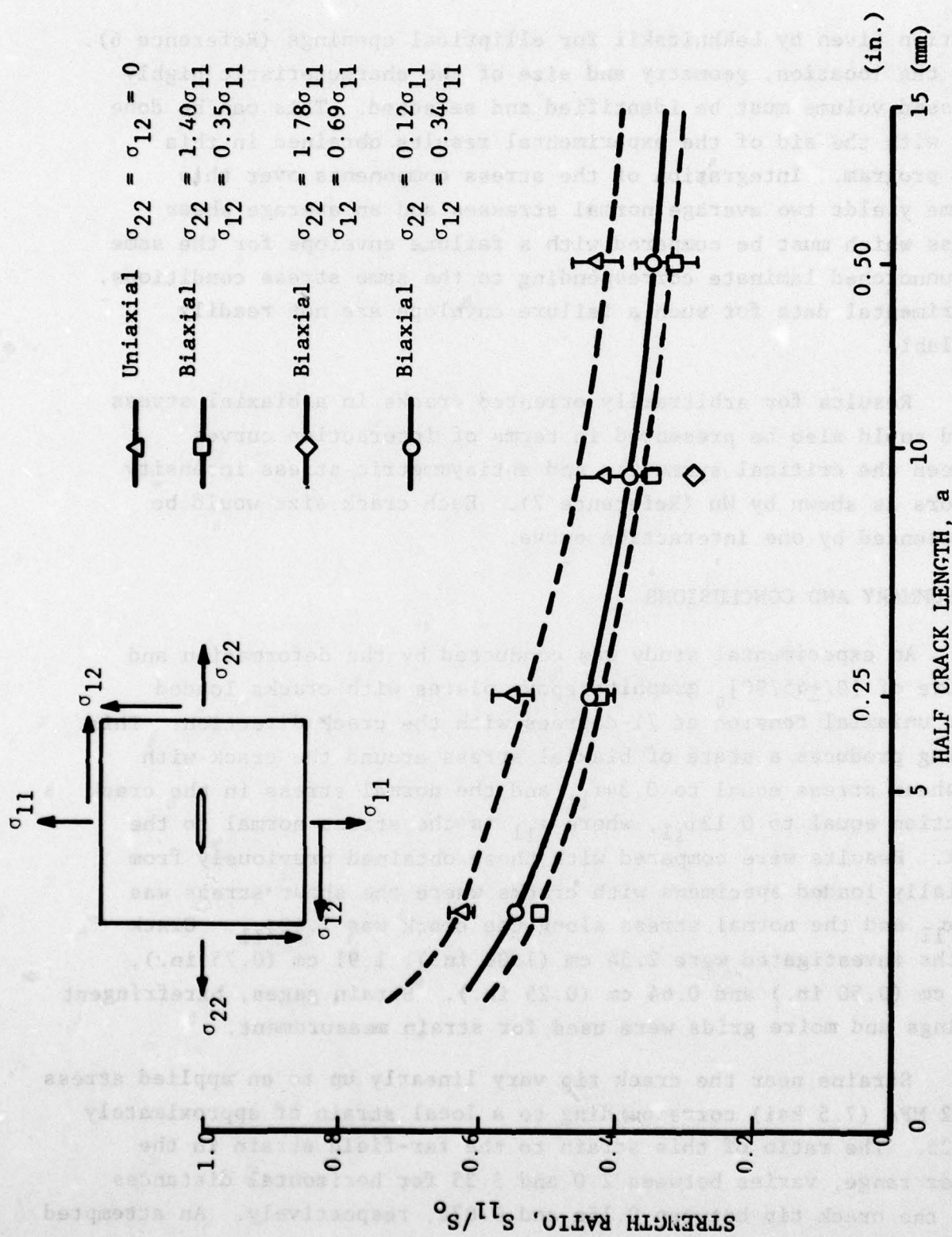
6. EFFECT OF CRACK LENGTH

Results for all specimens with cracks loaded uniaxially at 71-degrees with the crack direction are summarized in Table 7. The failure stress along the loading axis as well as the stress components at failure referred to the crack direction are given in this table. The last column represents the ratio of one of these components, the one normal to the crack direction, and the uniaxial strength of the unnotched laminate. This strength reduction ratio, based only on the normal to the crack component of far-field stress, is plotted as a function of crack length in Figure 99. Results are compared with those from uniaxial tests with transverse cracks and biaxial tests with the same ratio of normal to shear stress with respect to the crack direction. As can be seen, the strength ratio for the uniaxial tests with inclined cracks, having a normal stress in the crack direction equal to $0.12\sigma_{11}$ and a shear stress equal to $0.34\sigma_{11}$, is slightly higher by approximately 7 percent than the strength ratio for biaxial tests having a normal stress along the crack equal to $1.40\sigma_{11}$ and a shear stress equal to $0.35\sigma_{11}$. It could be concluded, therefore, that the normal stress in the crack direction has a small influence on fracture, with the strength decreasing as this normal stress increases. This result is not surprising since failure near the crack tip takes many modes with damage and subcracking propagating in many directions which are not necessarily coincident with the original crack direction and the normal stress in the direction of the crack. Once crack or damage extension changes from its original direction, this stress has a component normal to the new crack direction and contributes to its propagation.

The application of the average stress criterion in this case is complicated but not intractable. The approach consists of the following steps: (1) determination of state of stress near crack tip, (2) integration of stress components over a characteristic volume, and (3) comparison of average stress components with pertinent failure envelope. The state of stress can be obtained from the

Table 7
[0/+45/90]_s GRAPHITE/EPOXY LAMINATES WITH CRACKS UNDER UNIAXIAL
LOADING AT 71-DEG. WITH CRACK DIRECTION

Spec. No.	Crack Length, 2a cm(in.)	Modulus E_{yy} GPa (10^6 psi)	Poisson's Ratio ν_{yx}	Failure Stress, MPa (ksi)				Strength Ratio, S_{11}/S_0
				Along y-axis S_{yy}	Normal to Crack, S_{11}	Parallel to Crack, S_{22}	Shear Along Crack, S_{12}	
5A-1	2.54 (1.00)	53 (7.7)	0.30	180 (26.1)	161 (23.3)	19 (2.8)	55 (8.0)	0.330
5A-2	2.54 (1.00)	52 (7.5)	0.30	203 (29.4)	181 (26.3)	22 (3.1)	62 (9.1)	0.373
5A-3	1.91 (0.75)	54 (7.8)	0.29	210 (30.5)	188 (27.3)	22 (3.2)	65 (9.4)	0.387
5A-4	1.91 (0.75)	57 (8.3)	0.30	207 (30.0)	185 (26.8)	22 (3.2)	64 (9.2)	0.380
5A-5	1.27 (0.50)	57 (8.2)	0.31	245 (35.5)	219 (31.7)	26 (3.8)	75 (10.9)	0.449
5A-6	1.27 (0.50)	55 (8.0)	0.32	235 (34.1)	210 (30.5)	25 (3.6)	72 (10.5)	0.432
5A-7	0.64 (0.25)	56 (8.2)	0.31	293 (42.5)	262 (38.0)	31 (4.5)	90 (13.1)	0.538
5A-8	0.64 (0.25)	56 (8.1)	0.30	302 (43.7)	270 (39.1)	32 (4.6)	93 (13.4)	0.554



solution given by Lekhnitskii for elliptical openings (Reference 6). Then the location, geometry and size of the characteristic highly stressed volume must be identified and selected. This can be done also with the aid of the experimental results obtained in this test program. Integration of the stress components over this volume yields two average normal stresses and an average shear stress which must be compared with a failure envelope for the same but unnotched laminate corresponding to the same stress conditions. Experimental data for such a failure envelope are not readily available.

Results for arbitrarily oriented cracks in a biaxial stress field could also be presented in terms of interaction curves between the critical symmetric and antisymmetric stress intensity factors as shown by Wu (Reference 7). Each crack size would be represented by one interaction curve.

7. SUMMARY AND CONCLUSIONS

An experimental study was conducted by the deformation and failure of $[0/+45/90]_s$ graphite/epoxy plates with cracks loaded under uniaxial tension at 71-degrees with the crack direction. This loading produces a state of biaxial stress around the crack with the shear stress equal to $0.34\sigma_{11}$ and the normal stress in the crack direction equal to $0.12\sigma_{11}$, where σ_{11} is the stress normal to the crack. Results were compared with those obtained previously from biaxially loaded specimens with cracks where the shear stress was $0.35\sigma_{11}$ and the normal stress along the crack was $1.40\sigma_{11}$. Crack lengths investigated were 2.54 cm (1.00 in.), 1.91 cm (0.75 in.), 1.27 cm (0.50 in.) and 0.64 cm (0.25 in.). Strain gages, birefringent coatings and moire grids were used for strain measurement.

Strains near the crack tip vary linearly up to an applied stress of 52 MPa (7.5 ksi) corresponding to a local strain of approximately 0.0025. The ratio of this strain to the far-field strain in the linear range, varies between 2.0 and 3.35 for horizontal distances from the crack tip between $0.15a$ and $0.03a$, respectively. An attempted

extrapolation to the crack tip itself would yield a strain ratio, equal to the stress concentration factor, of approximately 7.

The crack opening displacement (COD) and crack shearing displacement (CSD) were determined from moiré fringe patterns. The COD is over 4 times larger than the CSD in the linear range, compared to 2.5 times for the case of biaxially loaded specimens with cracks having the same normal to shear stress ratio but a higher stress in the crack direction. The CSD and COD vary linearly up to applied stresses of 104MPa (15 ksi) and 138-173 MPa (20-25 ksi), respectively. Thereafter, both of these displacements increase at a much faster rate to failure. The maximum measured COD at failure for the 2.54 cm (1.00 in.) crack was 0.25 mm (0.010 in.). In those cases where the peak strain near the crack tip was recorded up to failure, it exceeded values of the order of 0.03.

Failure modes at the crack tips consisted of fiber breakage, subcracking along fiber directions and ply delamination. In some cases through-the-thickness crack extension occurred in the horizontal direction with fibers of all plies breaking. In other cases partial cracks occurred along fiber directions, parallel, normal or at 45-degrees with the crack direction, accompanied by partial fiber breakage and local delamination.

Results were presented in terms of a strength ratio equal to the ratio of the stress normal to the crack at failure to the uniaxial strength of the unnotched laminate. This strength ratio is approximately 7 percent higher than the similar ratio obtained from biaxially loaded specimens with the same ratio of normal to shear stress around the crack, but with a higher normal stress component in the crack direction. The same strength ratio was found to be approximately 15 percent lower than that for uniaxially loaded specimens with transverse cracks, indicating that the horizontal projection of inclined cracks is not the only criterion and that the shear stress component plays an important role in failure.

SECTION VII
SUMMARY, CONCLUSIONS AND RECOMMENDATIONS
FOR FUTURE WORK

An experimental program was conducted to study the deformation and failure under uniaxial and biaxial tensile loading of $[0/\pm 45/90]_s$ and $[0_2/\pm 45]_s$ graphite/epoxy plates with circular holes and through the thickness cracks and to determine the influence of notch size on failure. Experimental techniques used were strain gages, photoelastic coatings and moiré grids. Notch sizes investigated were 2.54 cm (1.00 in.), 1.91 cm (0.75 in.), 1.27 cm (0.50 in.) and 0.64 cm (0.25 in.). The following results and conclusions were reached:

1. UNIAXIAL TESTS OF $[0_2/\pm 45]_s$ LAMINATES WITH HOLES

- a) In the linear range, the measured stress (strain) concentration factor on the horizontal axis 3.24 is somewhat lower than the theoretical value of 3.44. The compressive strain concentration factor on the vertical axis -2.17 is higher than the theoretical value of -1.85.
- b) Strains on the hole boundary on the horizontal axis become nonlinear at an applied stress of approximately 173 MPa (25 ksi) corresponding to a local strain of 0.0065. Thereafter, the maximum strain on the hole boundary increases nearly nearly at a much reduced rate.
- c) At the stress level above the local strain on the hole boundary at the 0-deg. location is approximately 0.004 which is the level at which the unnotched laminate $[0_2/\pm 45]_s$ behaves nonlinearly in the 90-deg. direction.

- d) The local nonlinear response at the 0-deg. location produces a stress redistribution around the hole boundary resulting in nonlinear response at the 90-deg. location.
- e) A second level of pronounced nonlinearity occurs as a result of stress and strain redistribution produced by localized compressive failure (delamination) around the 0-deg. location near the hole boundary.
- f) Maximum measured strains at failure on the hole boundary are somewhat higher than the ultimate strain of the unnotched laminate.
- g) In the case of larger holes failure initiates at locations around the circumference approximately 72-degrees from the load axis, points of high strain concentration with nonlinear response. In the case of smaller holes the outer 0-deg. plies through the hole tend to separate and thus reduce or eliminate the strain concentration at the 90-deg. location.
- h) The strength reduction ratio ranges between 0.470 and 0.802 for holes between 2.54 cm and 0.64 cm in diameter.
- i) The effect of hole diameter can be described satisfactorily by using the average stress criterion with a characteristic length of $a_0 = 5$ mm.
- j) There is a critical hole diameter, approximately 1.57 mm (0.062 in.), below which the laminate becomes insensitive to it.

2. BIAXIAL TESTS OF $[0_2/\pm 45]_s$ LAMINATES WITH HOLES

The overall conclusions on the behavior of $[0_2/\pm 45]_s$ graphite/epoxy laminates with circular holes under 2:1 biaxial tension can be summarized as follows:

- a) On the horizontal axis, the measured maximum stress ratio (maximum stress to far-field vertical stress) in the elastic range, is 2.08 which is lower than the theoretical value of 2.51.
- b) On the vertical axis, the measured maximum stress ratio (maximum stress to far-field vertical stress) is 0.60, compared to the horizontal value of 0.62.
- c) Strains on the hole boundary become nonlinear at an applied vertical stress of 172 MPa (25 ksi) corresponding to local strains of 0.0043, which are comparable to the ultimate strain of the laminate loaded at 22.5-deg. to the 0-deg. fibers.
- d) This stress level is close to that at which localized failure begins at the 67.5-deg. location and nonlinear strain response at the 0-deg. location.
- e) Stress and strain redistributions occur around the hole at the stress level above with the strain at the 0-deg. (vertical axis) or near 65-deg. locations exceeding that at other locations.
- f) Maximum measured strains at failure on the hole boundary are higher (approximately 0.016) than the highest ultimate strain of the unnotched laminate (0.010).
- g) Two basic patterns of failure were observed: (a) horizontal cracking initiating at points off the horizontal axis and accompanied by extensive delamination of the subsurface ± 45 -deg. plies and (b) vertical cracking along vertical tangents to the hole and accompanied by delamination of the outer 0-deg. plies.

- h) The strength reduction ratio based on the unnotched uniaxial strength in the 0-deg. direction varies between 0.38 and 0.57, for holes between 2.54 cm and 0.64 cm in diameter.
- i) The strength reduction ratios are lower than corresponding values for uniaxial loading by approximately 16 percent, although the stress concentration factor under biaxial loading is lower.

3. EFFECT OF NORMAL STRESS IN CRACK DIRECTION

Graphite/epoxy $[0/+45/90]_s$ plates with cracks were loaded under uniaxial tension at 71-deg. with the crack direction, producing a shear stress along the crack equal to 0.34 times the stress normal to the crack and a normal stress along the crack equal to 0.12 times the stress normal to the crack. Results were compared with those from biaxially loaded specimens having the same ratio of normal to shear stress around the crack but higher normal stress along the crack. The following results and conclusions were reached.

- a) Strains near the crack tip vary linearly up to an applied vertical stress of 52 MPa (7.5 ksi) corresponding to a local strain of 0.0025.
- b) The crack opening displacement (COD) is over 4 times the crack shearing displacement (CSD) in the linear range, compared to 2.5 times for the biaxially loaded specimens.
- c) The CSD and COD vary linearly up to applied stresses of 104 MPa (15 ksi) and 138-173 MPa (20-25 ksi), respectively. Thereafter, they increase at a much faster rate to failure.

- d) The maximum measured COD at failure for the 2.54 cm (1.00 in.) crack was 0.25 mm (0.010 in.) compared to 0.10 mm (0.004 in.) for the biaxially loaded specimen.
- e) Peak strains as high as 0.03 were measured near the crack tip at failure.
- f) Failure modes consisted of fiber breakage along the horizontal axis, subcracking along fiber directions (parallel, normal or at 45-degrees with crack direction) with partial fiber breakage and local delamination.
- g) The strength reduction ratio, equal to the ratio of the failure stress normal to the crack to the uniaxial unnotched strength, is approximately 7 percent higher than the similar ratio for biaxially loaded specimens with the same ratio of normal to shear stress around the crack, but with a higher normal stress component in the crack direction.
- h) The strength reduction ratio was found to be approximately 15 percent lower than that for uniaxial loading normal to the crack.

4. RECOMMENDATIONS FOR FUTURE WORK

One of the important findings of this study is that the strength reduction ratio in $[0_2/+45]_s$ plates with holes under 2:1 tensile loading is lower than that under uniaxial loading, although the latter produces a higher stress concentration. A more detailed study of the failure mode interactions involved under biaxial loading is needed in order to predict the strength of such laminates with holes under varying biaxial loadings. More testing of similar panels with holes under biaxial loading of various ratios, such as 1:1, 3:1, 4:1, 5:1 etc, is recommended. It would not be necessary

to conduct tests for many hole diameters, since all results to date follow similar patterns of variation with hole diameter. Biaxial loading at different orientations with respect to the principal material axes of the $[0_2/+45]_s$ laminate is expected to produce important and not yet predictable results.

It was found in the case of 2:1 loading that the usual application of the average stress criterion did not produce satisfactory results. A more detailed study of the stress distributions around the hole coupled with biaxial failure envelopes for the $[0_2/+45]_s$ unnotched laminate is needed. Such biaxial failure data, however, are still lacking.

As mentioned in the report for the previous phase of work (Reference 1) the task of expressing explicit failure criteria for a crack in a general biaxial stress field remains to be done. This is not hampered only by the complexity of computations but also by the lack of sufficient basic laminate failure data under general biaxial stress conditions.

It was found that the normal stress in the crack direction has some, although small, influence on failure and that the shear stress contributes appreciably to failure. The interaction of the opening and shear modes of failure needs to be studied in more detail. This could be done relatively easily by testing uniaxial specimens with variously inclined cracks. The effects of crack size could be studied only at some discrete ratios of normal to shear stress.

As mentioned in the previous report, a useful and important extension of the work conducted to date would be the study of the influence of environmental effects and cyclic loading on the behavior of notched laminates.

REFERENCES

1. I.M. Daniel, "Biaxial Testing of Graphite/Epoxy Composites Containing Stress Concentrations"-Part I, AFML-TR-76-244, December 1976.
2. I.M. Daniel and R.E. Rowlands, "Determination of Strain Concentration in Composites by Moiré Techniques," J. Composite Materials, Vol. 5, April 1971, pp. 250-254.
3. I.M. Daniel, R.E. Rowlands and D. Post, "Strain Analysis of Composites by Moiré Methods," Exper. Mechanics, Vol. 13, June 1973, pp. 246-252.
4. J.M. Whitney and R.J. Nuismer, "Stress Fracture Criteria for Laminated Composites Containing Stress Concentrations," J. Composite Materials, Vol. 8, July 1974, pp. 253-265.
5. H.J. Konish and J.M. Whitney, "Approximate Stresses in an Orthotropic Plate Containing a Circular Hole," J. Composite Materials, Vol. 9, April 1975, pp. 157-166.
6. S.G. Lekhnitskii, Anisotropic Plates, Translated from second Russian edition by S.W. Tsai and T. Cheron, Gordon and Breach, Science Publishers, Inc., New York, 1968.
7. E.M. Wu, "Fracture Mechanics of Anisotropic Plates," in Composite Materials Workshop, edited by S.W. Tsai, J.C. Halpin and N.J. Pagano, Technomic Publishing Co. Inc., Stamford, Conn., 1968.